e-ISSN : 2320-0847
p-ISSN : 2320-0936

American Journal of Engineering Research (AJER)

Volume 5 Issue 1– January 2016

www.ajer.org ajer.research@gmail.com

Editorial Board

American Journal of Engineering Research (AJER)

CONTENTS

Volume-5 Issue-1

American Journal of Engineering Research (AJER) 2016
American Journal of Engineering Research (AJER)
e-ISSN: 2320-0847 p-ISSN : 2320-0936
Volume-5, Issue-1, pp-01-05
www.ajer.org
Research Paper Open Access

Search Platform Design Based On WSN

Song Jinbo, Duan Zhiwei
College of electrical and Information Engineering, Northeast petroleum university, Daqing Heilongjiang 163318

Abstract: *Based on the advantages of wireless communication, this paper present a search platform used in college to find the number of students in the classroom. Take STC89C52 as the control unit, E18-D50NK IR evading obstacle sensor detect the number of students, take nRF24L01 as the wireless communication module, it works over a range of about 70 meters that meets the requirements. The platform works as follow: the terminal node sensor mounted in each classroom count the number of students in and out of the classroom, then, transmit the number to the relay node which is mounted on the storey of the classroom, at last the relay nodes transmit the number to center node. The center node transmits the data to computer, and then the user can query the number of the students in the classroom from the computer visual interface. The operation shows that the search platform easy to operate and maintenance, has the advantages of high operation reliability, low power consumption, considerable practical value.*

Key words: *wireless communication; microcontroller; wireless sensor networks (WSN); people counting*

I. INTRODUCTION

In college, students always do self-study in the unoccupied classroom. With the increase of the number of students, it is difficult for students to find a classroom with few people. Combined with the develop of microcomputer and wireless sensor network (WSN) [1-3], design a kind of search platform used for indicate the number of students in each classroom, everyone who wants to do self-study in any classroom can see about the number of students in each classroom from the visual interface of the platform. Such a search platform used for students can save time effectively.

II. STRUCTURE AND FUNCTION OF THE SYSTEM

The working principle of the system is as follow: mount the terminal device on the door of each classroom, the system automatically plus one when the IR evading obstacle sensors detect a student coming in; automatically minus one when detect a student out. With the control of the microcomputer STC89C52, the wireless transmitting module nRF24L01 transmit the collected data to the relay node on each storey. The data at the relay node will be transmitted to the center node of the system. The controller of the center node processes all the data. The system connected to the computer via serial communication; display the data on the computer. The user can query the number of student in each classroom. The structure of the system is shown in Fig1.

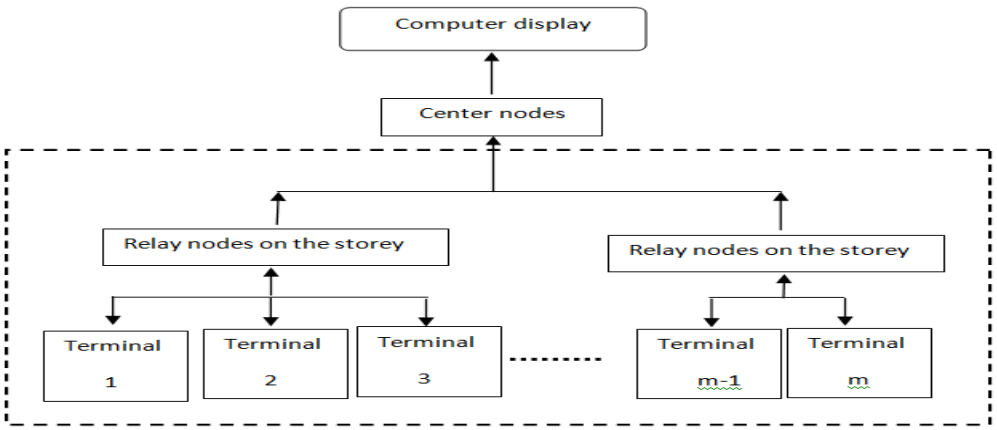

Fig.1. Structure of the system

III. HARDWARE CIRCUIT DESIGN OF THE SYSTEM

3.1 Detection module

The working principle of E18-D50NK is as follow: when an object appears in front of infrared tube, the surface is diffusely emitted, the infrared receiver receives the reflected light, the voltage of the tube will reduces, when the voltage below the comparator threshold voltage of LM324, it outputs a low level. Change the triode static working point by adjusting the size of the resistance potentiometer, thus changing the sensitivity of infrared tube. The connection circuit of the sensor is shown in Fig2.

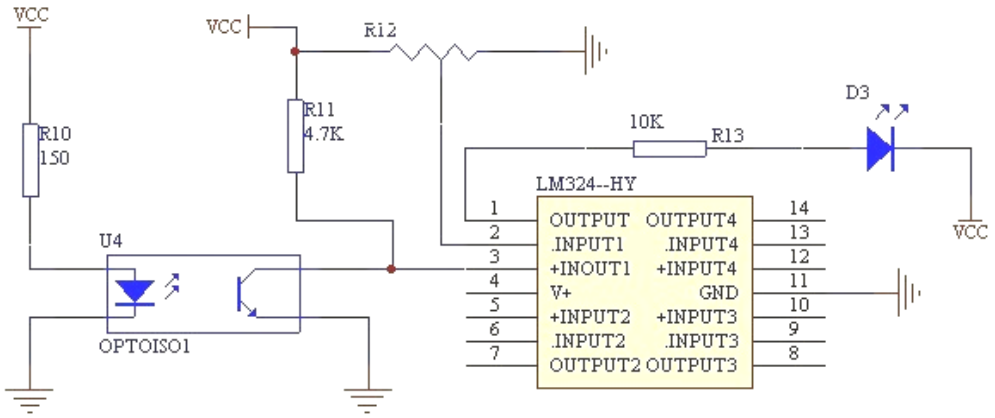

Fig.2. E18-D50NK IR evading obstacle sensor circuit

3.2 Wireless transmission module

nRF24L01 is a kind of wireless communication chip produced by NORDIC, it is a new single chip RF transceiver device, operating at 2.4~2.5GHz ISM band. The wireless communication speed can reach 2 Mb/s. There are two low-power operating mode: power-down mode and standby mode, it makes the energy-saving design more convenient [4-5]. The wireless transmission and reception circuit is shown in Fig3.

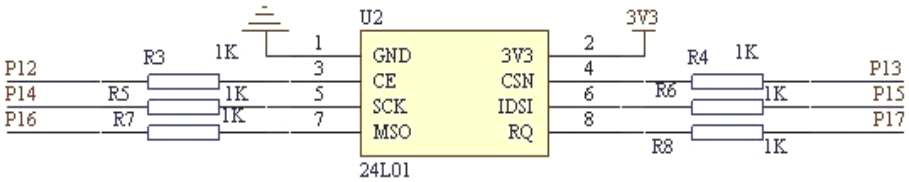

Fig.3. Wireless transmission and reception circuit

3.3 Serial communication module

The data that center node received can be converted by MAX232 so that can realize microcomputer program download and update, at the same time realize microcomputer and PC communication, then the data can be displayed on PC. The circuit connection is shown in Fig 4.

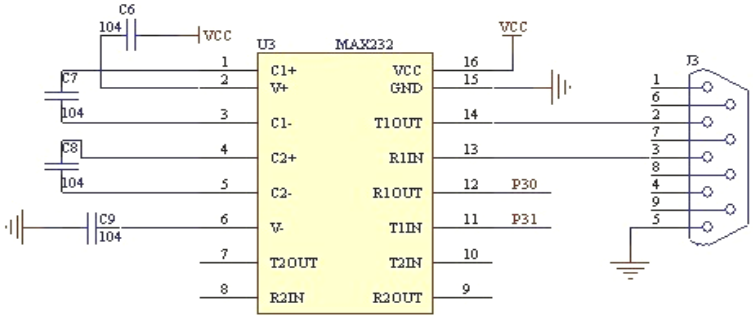

Fig.4. Serial communication circuit

3.4 LED display module LED

The terminal device mounted in each classroom has a display module, used for display the number of students in the classroom at present. The system we designed adopts LED digital tube as the display module, since it has the advantages of clear display and suitable for display in daytime. The LED used in this system adopts common-anode, 4 IO of the SCM are connected through a PNP transistor with 4-bit digital tube. The circuit connection is shown in Fig 5.

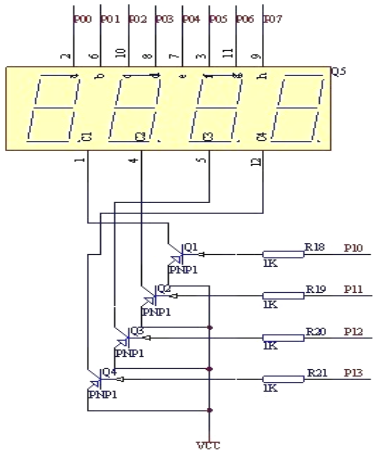

Fig.5. LED digital tube connection circuit

3.5 The power circuit

The power supply circuit design is divided into two parts: one is +5V power used for microcomputer minimum system and IR evading obstacle sensors, another one is +3.3V power used for nRF24L01 wireless communication module.

IV. SOFTWARE DESIGN

4.1 Overall process

The main program flow can be expressed as follow: system initialization after the power supply, include IO port setting initialization and peripheral device control initialization. Then each node transmits the data to center node from the sensor network, and communicates with the computer. The main program flowchart is shown in Fig6.

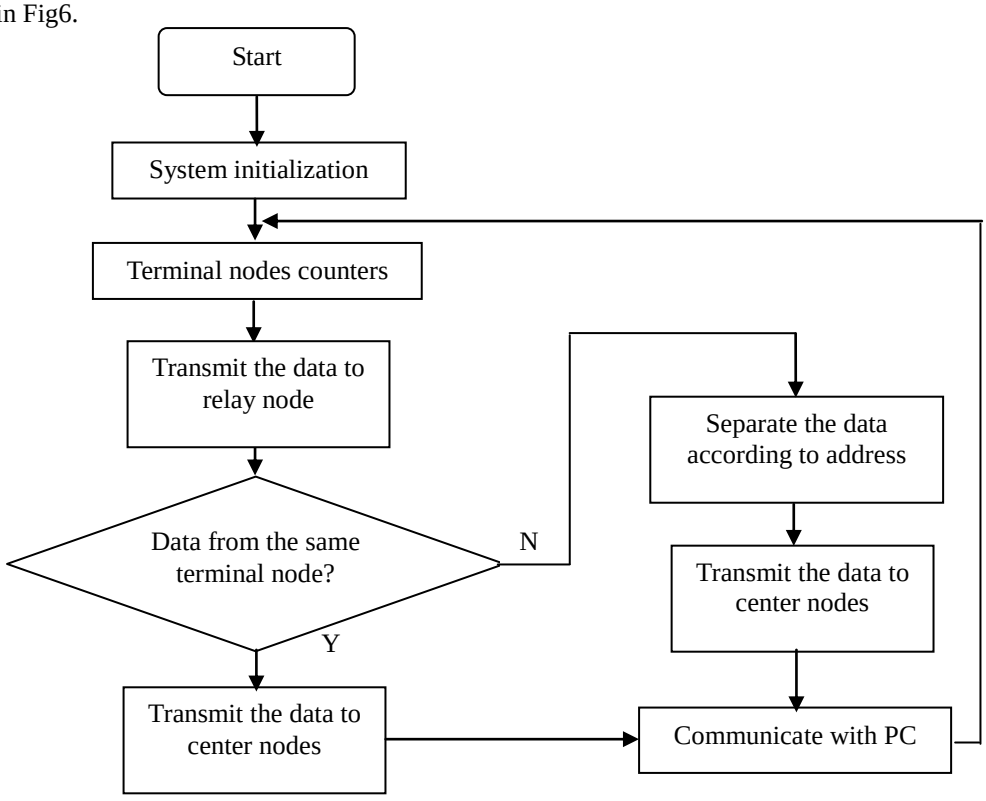

Fig.6. Main program flowchart

4.2 Counting program

The most important in detection program is that the sensor can not only sensing the students but also distinguish between in and out. So, in this system, two inductive probes are used, labeled as probe 1 and probe 2, to judge in and out. Setting a flag in the program, it will be given a different value according to the in and out of the students. The flowchart of the program is shown in Fig7.

The detection process is described as follow: when probe 1 discover there are students, Flag_1 and Flag_2 will be assigned with "1" and "0" respectively, and on this basis, if probe 2 discover there are students, the number of students add 1, that indicate there are a student come in , at the same time, Flag_1 and Flag_2 zero out, prepare for the next counter; similarly, if Probe 2 discover there are students, Flag_1and Flag_2 will be assigned with "0" and "1" respectively, and on this basis, if probe 1 discover there are students, the number of students minus 1, that indicate there are a student out , at the same time, Flag_1 and Flag_2 zero out, prepare the next counter.

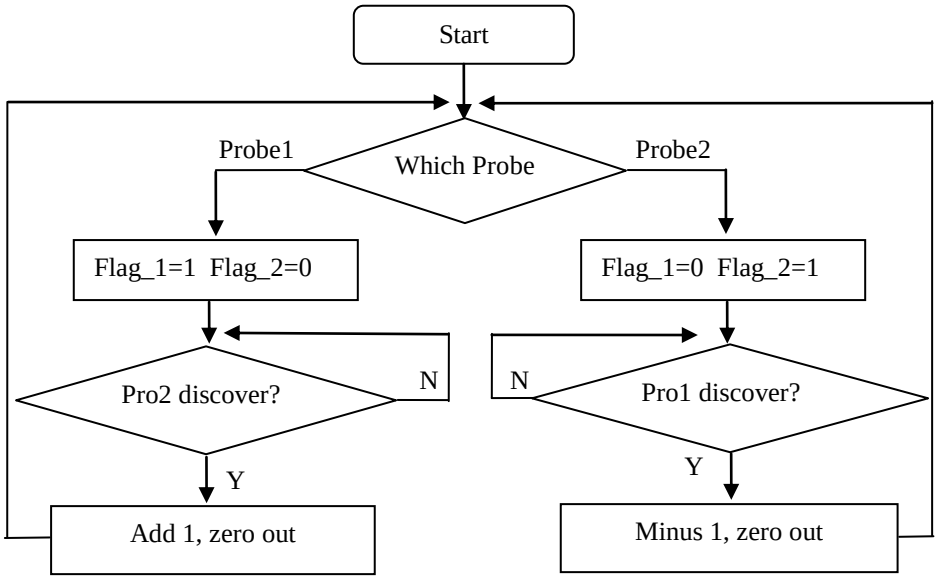

Fig.7. Flowchart of counting program

4.3 Computer display

The display of data on computer use Visual Basic language, Access database. The display interface is shown in Fig8. Current data and time is displayed on top right of the display interface, the upper left is a sent of pull-down menus. Users can select the classroom that they want to go from the pull-down menus, then get the information such as seating capacity and remaining seats etc. Below the interface, there are colorful indicator of the classrooms, red green and yellow indicates the number of students in the classroom respectively, when the number of students less than 1/3 of the number of seats, the color of the classroom is green which indicates few students in the classroom, when the number of students between 1/3 and 2/3 of the number of seats, the color of the classroom is yellow which indicates a number of students in the classroom, and when the number of students more than 2/3 of the number of seats, the color of the classroom is red which indicates many students in the classroom.

Fig.8. Computer display interface

V. EXPERIMENTAL DATA ANALYSIS

Do a test to the system to detecting the stability of the system. Take a classroom as the test room, observe the students in and out situation artificially and then compare with the computer display, check out whether the system correct. The test results are shown in Tab1. There is only one undercount, the system is relatively stable.

Tab.1. Test results

	Door 1				Door 2			
	In		Out		In		Out	
	Actual number In	Test number In	Actual number Out	Test number Out	Actual number In	Test number In	Actual number Out	Test number Out
1	10	10	6	6	10	10	6	6
2	15	15	8	8	15	15	8	8
3	20	20	10	10	20	20	10	10
4	30	29	15	15	30	30	15	15
5	50	50	21	21	50	50	21	21

Terminal node sensors of the system can detect the students accurately, the wireless RF module can transmit the data to the center node real-time exactly, and the computer display interface can show the correct number of students in the classroom, the system works stable.

VI. CONCLUSION

The search platform based on microcomputer and E18-D50NK IR evading obstacle sensor can be used for the students in the college to find suitable classroom do self-study. The system has advantages of low power consumption, simple circuit, easy to use, the computer display visually. Experiments showed that the system could work stable and accurately.

REFERENCES

[1] Yu Jinqian, Yu Bin. Short distance wireless communication break down[M]. Beihang University Press,2009.

[2] Zheng Qichao, Zhou Yuan, Wei Ming. Monitoring System Design of Classroom Usage Condition Based on MCU[J]. Industrial Control Computer, 2015(6):148-151

[3] Huang Ting, Shi Guoliang, Huang Kun. On the Design and Realization of a Microcontroller-Based Wireless Communication System[J]. Microprocessors, 2010 (3):27-31

[4] Shi Zhiyun, Gai Jianping. A New Kind of High Speed Wireless RF Transceiver- nRF24L01 and Its Application[J]. International Electronic Elements,2007(6):18-24

[5] Han Gaining, Zhao Juan, Duan Qun. Implementation of Short Distance Wireless Communication Based on AT89C52[J]. Electronic Design Engineering, 2009(10):23-25

American Journal of Engineering Research (AJER) 2016
American Journal of Engineering Research (AJER)
e-ISSN: 2320-0847 p-ISSN : 2320-0936
Volume-5, Issue-1, pp-06-11
www.ajer.org
Research Paper Open Access

Design of Tapered Riser Using Basic Hydraulic Principles

Melody Chepkoech[1], Ruth Mwongeli Muthoka[1], Charles Kimani[1], Madaraka F Mwema*[1], Japheth Obiko[2]
[1](Department of Mechanical Engineering, Dedan Kimathi University of Technology, Nyeri, Kenya.
[21](Department of Mechanical Engineering, Jomo Kenyatta University of Agriculture &Technology, Nairobi, Kenya)

ABSTRACT: *In sand casting, the design of gating and riser system plays an important role in the quality of the casting. Poor designs of these two parameters lead to major defects such as incomplete filling, porosity, and re-oxidation inclusions. These defects cause the castings to be susceptible to failure during their use. A riser system with high volume to surface area ratio gives a sound casting. The conventional casting setup used in many foundries incorporates the use of cylindrical risers. Improvement of the gating and riser system by use of computational analysis was carried out. Through several computational analyses, it was concluded that a casting with minimal defects could be obtained by modifying a cylindrical riser to form a tapered riser which has a higher volume to surface area ratio.*

Keywords *-Casting defects, Chvorinov's rule, cylindrical riser, hydraulic principles, tapered riser*

I. INTRODUCTION

In spite of the extensive research that has been done in attempts to reduce casting defects, production of a defect free casting still remains a major challenge in the casting industry. The occurrence of most defects is often related to the flow of molten metal (fluid flow phenomena) during pouring and solidification stages [1]. Mechanical properties such as hardness, tensile strength, ease of machinability, fatigue endurance, resistance to fracture and so forth, of cast parts are usually affected by the rate of solidification. Figure 1 shows a typical gating system.

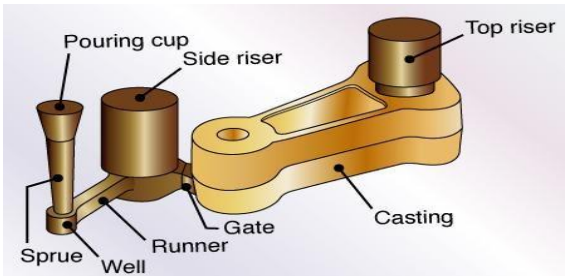

Figure 1: Typical gating system

The design of the gating system and the riser system are critical in the production of quality sand casting products. This research paper focuses on the design and improvement of risers. A riser is a passage made in the cope through which the moltenmetal rises after the mold is filled [2]. Risers serve dual function, they compensate for solidification shrinkage and heat source so that they freeze last and promote directional solidification. Casting process design is important for production quality and efficiency [3].

Most casting designs in the foundries are done on shop floor by trial and error basis [4]. This is time consuming, costly and encourages presence of defects in the final product. This approach makes the design of gating system arduous. The trial and error method can be eliminated by use of a computational approach based on the dimensions of the part to be cast. Up to date, researchers have explored various computational and simulation approaches to minimize the occurrence of these defects. Martin (1953) investigated on the relationship between the dimensions of the gating system with that of the weight of the casting [5]. He concluded that the in-gate area is inversely proportional to the square root of the effective head and the function of the casting weight. He also established that the loss coefficient for molten metal is of the same order to that of the water.

Wallace et al (1957) provided guidelines for the design of the gating system that was meant to be economical [6]. They suggested that selection of optimum pouring rate and time should be made first as closely as practicable with the function of an ideal gating system. Desai and Raghav designed the special gate sticking on the pattern in draining the gas while pouring the molten metal. However, these researches do not provide a suitable gating system to reduce incomplete filling defects in castings. In particular, these experiments used the trial and error method to conduct the solutions hence the experiments wasted a lot of material and took a lot of time [7, 8].

Flemings et al (1960) came up with a functionality of every element of gating system.

This was done with an illustration using the aluminum casting and showed the essence of good gating system. Most of the salient features were discussed systematically but never compared or gave a hint of the best type of the riser or sprue i.e. cylindrical or tapered [9]. Chamber et al (1943) engaged in an investigation on casting and came up with conclusion that a proper riser shape, size and geometry as well as location of the riser inlets should be determined well to minimize the ratio of the gross weight to net weight. The tapper sprue minimizes overtaxing and aspiration as compared to the cylindrical. This helps to stream line the flow of metal hence reducing the effects of the turbulence [10]. The computational analysis presented in this research paper uses basic hydraulic principles in the gating system and Chvorinov's rule for the calculation of the appropriate riser dimensions. This approach has major advantage over the shop floor trial and error method.

II. DESIGN METHODS AND CALCULATIONS

The relationship between volume & area of the part to be cast and the size of risers are important in the entire process of casting. To improve the gating system while focusing on riser design, it is vital to understand certain hydraulic parameters.

Hydraulic Principles Used in the Gating System

2.1.1 Nature of flow

The nature of flow of the molten metal in the gating system can be established by calculating the Reynolds number.

2.1.2 Reynolds number

Reynolds number is the ratio of momentum to viscosity and is usually given as;

$$Re = \frac{density * velocity * diameter}{viscosity}$$

$$Re = \frac{\rho V d}{\mu} (1)$$

Where Re=Reynolds number

ρ= density of the molten metal

V = mean velocity of flow

D = diameter of the tabular flow

μ= viscosity of the molten metal

A Reynolds number below 2000 gives a laminar flow while a number above 2000 leads to a turbulent flow.

Bernoulli's Theorem

To calculate flow velocities, we assumed a steady state and incompressible flow. Using Bernoulli's equation of flow given as

$$h1 + \frac{P1}{\rho} + \frac{V1^2}{2g} + F1 = h2 + \frac{P2}{\rho} + \frac{V2^2}{2g} + F2 \quad (2)$$

Where

h =height of the molten metal (*cm)*

p=static pressure *N/*cm^2

v= velocity of the molten metal *cm/s*

g=acceleration due to gravity

ρ= density of the molten metal g/cm^3

F=head losses due to friction *cm*

Ignoring friction forces, the Bernoulli's equation reduces to;

$$h + \frac{P}{\rho g} + \frac{V^2}{2g} = constant \qquad (3)$$

The velocity of the molten metal at the base of the sprue can be determined from (3). If we take a point 1 at the top of the sprue and point 2 at its base and using point 2 as the reference plane, then the head at that point is zero (h_2=0) andh_1 is the height (length) of the sprue.

When the metal is poured into the pouring cup and overflows down the sprue, its initial velocity at the top is zero (v_1=0) and assuming that atmospheric pressure is maintained, then the equation of velocity reduces to;

$$h_1 = \frac{{v_2}^2}{2g} \qquad (4)$$

Makingv_2 the subject of the formula gives;

$$v_2 = \sqrt{2gh_1} \qquad (5)$$

Continuity Law

Continuity law states that the volume rate of flow remains constant throughout the liquid.

Continuity is expressed as;

$$Q = V_1A_1 = V_2A_2 \quad (6)$$

Where: Q = volumetric flow rate cm^3/s

A= area cm^2

v = velocity

The continuity relationship clearly shows that increase in area results in a decrease in velocity.

Mold Filling Time

Aluminum should be poured at a slow rate in order to avoid turbulence, aspiration and drossing.

Using continuity;

$$Q = V_gA_g = V_2A_2 \qquad (7)$$

And assuming $A_g = A_2$

The velocity of the molten metals in the gating system $V_g = V_2 = \sqrt{2gh_1}$ where h_1 is the height of the sprue.

Therefore,

$$moldfillingtime = \frac{volumeofmold}{A_g * V_g} \quad (8)$$

Calculation of the Solidification Time

Chvorinov's rule

The total solidification time is the time required for the casting to solidify after pouring. This time is dependent on the size and shape of the casting by an empirical relationship known as Chvorinov's rule, which states;

$$T_{TS=C_m\left(\frac{V}{A}\right)^n} (9)$$

Where TS = total solidification time (min)

V = volume of the casting cm^3

A= surface area of the casting cm^2

n = an exponent taken to be 1.5 – 2

C_m = mold constant min/cm^2

The value of C_m depends on the particular conditions of the casting operation, including mold material (e.g. specific heat, thermal conductivity), thermal properties of the cast metal (e.g., heat of fusion, specific heat, thermal conductivity), and pouring temperature relative to the melting point of the metal.

Since Chvorinov's rule indicates that a casting with a higher volume-to-surface area ratio will cool and solidify more slowly than one with a lower ratio. We used this principle in designing the riser in a mold.

Also, since the metal in the riser must remain in the liquid phase longer than the casting, TS_{riser} must exceed$TS_{casting}$.

In our methodology, we designed appropriate risers for casting based in the plate shown below.

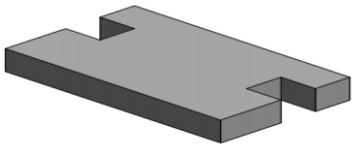

Figure 2:3D view of the sample casting template

Figure 3: Front view of the sample casting plate

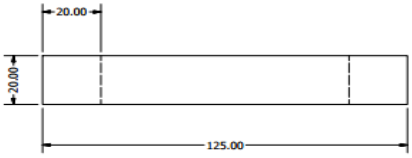

Figure 4: Side view of the sample plate

Volume of the aluminum plate = 171.5 cm^3

Surface area of the plate = 243.5cm^2

Riser Design Requirements

For the aluminum rectangular plate above, we designed both cylindrical and tapered riser that will be able to compensate for shrinkage, and remain molten until after the casing solidifies.

Using Chvorinov's rule, solidification time is given by;

$$T_{TS=C_m\left(\frac{V}{A}\right)^n}$$

The mold constant C_m depends on the material to be cast and for aluminum, $C_m = 3.5\ min/cm^2$

n=2

The total solidification time for the plate is calculated and found to be 1.74 *min.*

Since the solidification time for the riser is 1.25 times that of the casting, the total solidification time for riser is 2.174 *min*

Cylindrical riser

Figure 5: Cylindrical riser

We used chvorinov's rule to get the dimensions of the cylindrical riser. A diameter: height ratio of 1:1 was assumed.

Using the relation

$$T_{TS=C_m\left(\frac{V}{A}\right)^n}$$

We found that the appropriate diameter for the cylindrical riser is *3.94 cm= 4.0 cm.*

The volume to surface area ratio of the cylindrical riser was found to be ***0.79***

Tapered riser

For a sound casting, the volume to area ratio of the cylinder must be as high as possible. To maximize the volume to area ratio, the area of the riser should be minimized. We introduced a taper in the calculated cylindrical riser and investigate if by so doing, the volume to area ratio would be maximized.

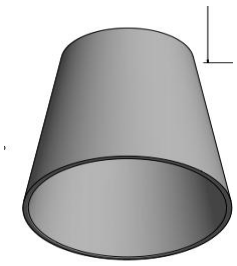

Figure 6: Isometric view of a tapered riser

To find the smaller radius r, we apply a taper at a various angles and calculate the volume to area ratio at each case.

Different angles of taper were applied and the resulting volume to surface area ratio tabulated as shown in the table below.

Table 1: Table indicating taper angles and their respective volume to surface area ratio

Angle of taper(degrees)	Volume to Surface area ratio
5°	1.21
9°	1.21
10°	1.20
11°	1.21
15°	1.21
20°	0.98
30°	Inapplicable
45°	Inapplicable

III. DISCUSIONS

From the above cases of the tapered riser, it can be noted that the volume to area ratio of the riser is higher when the angle of taper is *5° to 15°*giving a volume to surface area ratio of a value around 1.21 as compared to the cylindrical riser of the same dimensions with a volume to surface area ratio of 0.79.This can be concluded that applying a slight taper to the appropriate cylindrical riser to form a riser in the shape of a conical frustum at a taper, preferably *5° to 15°*helps maximize the volume to area ratio hence increasing the chances of producing a sound casting.

IV. CONCLUSION

Through computational approach, tapered as well as cylindrical risers were analyzed. A tapered riser was found to give a more sound casting than a cylindrical riser did. The use of hydraulic principles makes thewhole design process fast, easy to use, and reliable as compared to the shop floor trials. Computational analysis is suitable for all shapes whether complex or simple. It also gives a better yield product within a less time compared to shop floor trials. The defects are decreased by a great percentage meaning the end product is of a higher quality.

V. Acknowledgements

Our sincere acknowledgement goes to the entire Dedan Kimathi University of technology for every contribution and effort they made in this proposal. Special thanks go to our supervisor Mr. Madaraka who spent his precious time to read and justify this document. His continued technical advice, support, and encouragement will not go unmentioned here; may God bless him with more wisdom.

REFERENCES

[1] Campbell J, *casting practice: the ten rules of castings*(Technology and Engineering, 2004).
[2] Armour Research Foundation of Illinois Institute of Technology, *Fluid flow mechanics of molten steel*(Chicago, 1951).
[3] Campbell J, *Castings*(Butterworth-Heinemann, London, 1991).
[4] Lam Y.C, Britton G.A, Liu D.S, Optimization of gate location with design constraints, *International Journal of Advanced Manufacturing Technology, (24)*, 2004, 560-566.
[5] Dr. B Ravi, *casting simulation &optimization, benefits and bottleness & best practices*.
[6] Kannan S, *Computer simulation and water modeling of fluid flow in simple horizontal and vertical gating systems*, Master Thesis, University of Wisconsin-Madison, 1991.
[7] Saxena M, Irani R. K, An Integrated NMT-Based CAE Environment - Part I: Boundary-Based Feature Modeling Utility,*Engineering with Computers*(9), 1993, 210–219.
[8] Saxena M, Irani R.K, Automated Gating Plan Synthesis for Injection Molds,*Computer Engineering ASME*, (1), 1992, 381-389.
[9] Ong S K, Pormbanpong S, Lee K.S, An object-oriented approach to computer aided design of a plastic injection mold, *Journal of Intelligent Manufacturing(6)*,1995, 1–10.
[10] Ravi B, *Metal casting-computer aided design and analysis*, Department of Mechanical engineering IIT Bombay, 2006.

American Journal of Engineering Research (AJER) 2016
American Journal of Engineering Research (AJER)
e-ISSN: 2320-0847 p-ISSN : 2320-0936
Volume-5, Issue-1, pp-12-20
www.ajer.org
Research Paper Open Access

Evaluating the Effect of Various Faults on Transient Stability Using a Single Machine Equivalent (SIME)

Obi, P.I.[1], Iloh, J.P.I.[2] and Nwosu, N.[3]
[1]*Department of Electrical/Electronic Engineering, Michael Okpara University of Agriculture, Umudike, Nigeria*
[2, 3]*Department of Electrical/Electronic Engineering, Chukwuemeka Odumegwu Ojukwu University, Anambra State, Nigeria*

ABSTRACT: *In this work, a single machine equivalent model equipped with static variable compensator in the middle of the transmission line is simulated with simpowersystem. Critical clearing time of this non linear model is estimated with statistical pattern recognition. Classical model of this model is used to compute this critical clearing time using Equal Area Criteria with 4th order Runge Kutta numerical method and simulated in MATLAB 7.5 environment. Different types of faults were introduced at the busbar and were analyzed. The results show that classical critical clearing time estimation for the three-phase-to-ground fault was 0.6308 sec followed by the classical critical clearing time for the double-line-to-ground fault which was 0.8754sec and lastly the single-line-to-ground fault has its classical critical clearing time as 1.89 secs. The three-phase fault was observed to be the severest of all the faults.*

Keywords - *Power System Stability, Transient Stability, Critical Clearing time, Excursion*

I. INTRODUCTION

Power system stability is defined as that property of a power system that enables it to remain in a stable equilibrium state under normal operating conditions and to regain an acceptable equilibrium state after being subjected to a disturbance [1]. Transient stability is a type of power system stability phenomena [2] and the fastest to develop after inception of a disturbance. The planning and maintenance of a secured power system operation depends a lot on its transient satiability, hence transient stability studies play a vital role in providing secured operating configurations in power system networks [3]. Transient stability is defined as the ability of a power system to maintain synchronous operation of the machine when subjected to a large disturbance [4].

The occurrence of a transient instability problem may result to large excursion on the system machine rotor angle. If corrective action fails, loss of synchronism among machines may result in total system collapse [5]. The quality of electricity supply is therefore measured amongst other factors, by the ability of the power system to clear faults before they cause damage to the power system equipment. The time at which fault is cleared before it causes damage on the power system is known as critical clearing time (CCT) [6].

II. MATERIALS AND METHODS

The rotor mechanical dynamics are represented by the Swing equations which were the critical equations used in this analysis [7].

$$2H\frac{d\omega}{dt} = T_m - T_e - D\omega \quad (1)$$

$$\frac{d\delta}{dt} = \omega \quad (2)$$

Where H = per unit inertia constant, D = Damping Coefficient, ω = rotor angle of the generator, δ = angular speed of the generator, T_m = Mechanical torque input, and T_e = Electrical torque output.

$$\delta_c = \frac{\pi f P}{2H} \cdot t_c^2 + \delta_o \quad (3)$$

Where δ_c = Critical clearing angle, H = Machine inertia, t_c = Critical Clearing time, f = frequency, and δ_o = initial corresponding load angle and P = power supplied.

A model of single machine equivalent (SIME) which was used to study the effects of various faults on transient stability of power system is shown in Fig.1

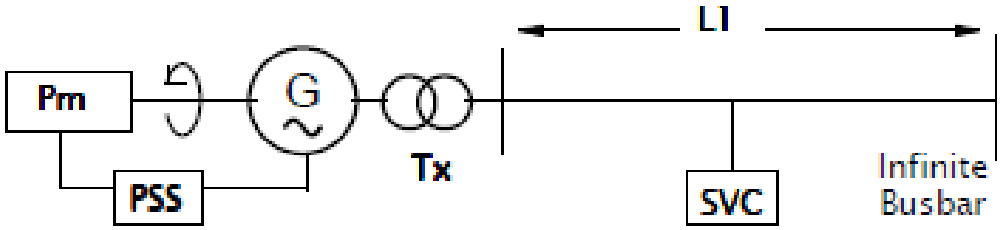

Figure 1: A single line diagram model of single machine equivalent (SIME)

2.1 Simulation of SIME Model with Simpowersystem

Various components of the model of single machine connected to infinite busbar as in Fig. 1 have been modeled in MATLAB under the simpowersystem toolbox. These components include the turbine synchronous generator, the power system stabilizer (PSS), static variable compensator (SVC), the transformer, and the transmission line. This system was configured as shown in Fig. 2. In the configured simpowersystem, the SVC is placed in the middle of the line and fault breaker is connected to the generator busbar to initiate any type of fault and also clear it when required.

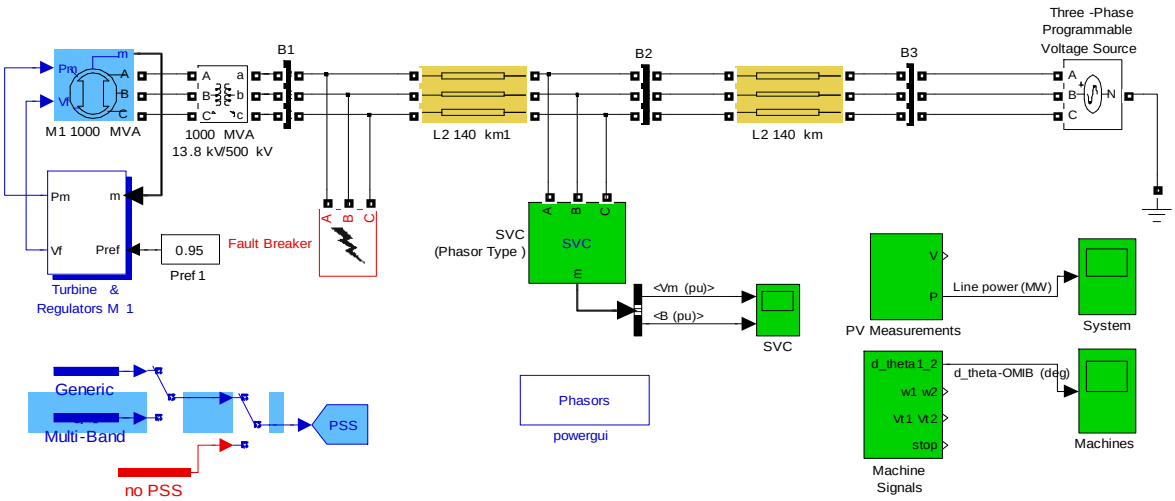

Transient stabilty of a single-machine equivalent with Power System Stabilizers (PSS) and Static Var Compensator (SVC)

Figure 2: single-machine equivalent with Power System Stabilizers (PSS) and Static Var Compensator (SVC)

2.2 Loadflow simulation

The powergui window in the simpowersystem configuration solves the load flow through initial guess of the load flow and then iterates to get the actual load flow values at the machine terminals and buses, other quantities like the machine rotor angle, machine terminal voltage and current flowing in all the phases during steady state are also solved. All the required initialization quantities are then keyed in for transient stability simulation. Some of these calculated quantities like the initial rotor angle, the machine terminal power and voltage are used to calculate the electrical power developed by the generator which will be used to estimate the critical clearing time of faults using classical single machine model.

2.3 Transient stability simulation of faults

The transient stabilities of the following types of faults were simulated to study the effect of the PSS and SVC during fault transient; (i) Single phase to ground fault, (ii) Double Line to Ground fault and (iii) Three-phase to Ground fault. After machine initialization following load flow estimations, these faults are initiated respectively at 0.1 sec. and cleared at 0.2 sec. rotor swing plot and power plot are simulated for three conditions; (a). When neither PSS, nor SVC is ON during fault. (b). When only PSS is ON. (c). When both PSS and SVC are ON.

2.4 Critical clearing time estimation using classical method

In estimating the critical clearing, time the following steps were followed;

i. The load flow solutions from simpowersystem configuration of the test system as in Fig. 2 are used for synchronous internal generated voltage.
ii. The values of V_t, P_t, and Q_t are obtained from the load flow solution in section 2.2 and are used to estimate the synchronous internal generated voltage.

$$I_g = (P_t - jQ_t)/V_t^2 \tag{4}$$

$$E_g = V_t + jX_d^{'}\mathrm{I_g} \tag{5}$$

Where I_g = Generator terminal Currrent, P_t = Scheduled real system power, jQ_t = Scheduled reactive system power, V_t = Generator terminal Voltage, E_g = Transient emf of generator and jX'_d = Transient reactance.

2.5 Transfer impedance for transient stability studies

The transfer impedances of various faults are estimated and these depend on the position of fault and the fault impedance. In this test case, the fault impedance purely resistive and the fault position is at the generator bus and hence the transfer impedances are estimated by applying equation (6)

$$Z_T = \left|Z_a + Z_b + (Z_a Z_b)/(Z_c + Z_{fsh})\right| \tag{6}$$

and the fault shunt for the different faults are as shown in Table I, while Table 2 shows calculated transfer impedance for different types of faults in this study.

Table I: Fault shunt for different types of faults

Types of faults	Fault shunt(Z_{fsh})
L-G	Z_2+Z_0
L-L	Z_2
L-L-G	$Z_2Z_0 / (Z_2+Z_{0)}$
L-L-L(G)	0

Table II: Calculated transfer impedance for different types of faults

L-G(pu)	L-L-G(pu	L-L-L-G(pu)
1.1083	1.501	1.036

2.6 Estimation of maximum electrical power developed by the machine

The maximum electrical power developed by the machine for various faults is estimated substituting the calculated transfer impedances in Table II in equation (7).

$$P_{e(\max)} = \frac{|E_g||V_t|}{Z_t} \tag{7}$$

Transfer impedance Z_t is calculated and shown in Table II.

2.7 Estimation of critical clearing time (CCT) using Runge Kutta.

When this calculated maximum electrical power is used with other variables as required by the Runge-kutta solution of the rotor swing equations (1) and (2), a simulation of the rotor swing response is obtained. The rotor swing response are shown in figs. 10 to 24, while the critical clearing time is read from these graph having calculated the critical clearing angle using equation (3). Compare critical clearing time result with that obtained through statistical pattern recognition in Table III.

Table III: Critical clearing time

H(sec)		24	15	12	7.4	5
Three phase to ground Fault	SPL(SVC NO) CCT	0.5985	0.4910	0.4467	0.3663	0.3142
	SPL(SVC ON) CCT	0.5995	0.4953	0.4516	0.3705	0.3181
	% CCT time gain by SVC	-0.1671	-0.8758	-1.0969	-1.1466	-1.2412
	Classical CCT estimation	0.6308	0.4995	0.4460	0.3514	0.2888
	Classical CCT error	-5.3968	-1.7312	0.1567	4.0677	8.0840
Double phase to ground Fault	SPL(SVC NO) CCT	0.8545	0.6842	0.6124	0.4897	0.4094
	SPL(SVC ON) CCT	0.8600	0.6905	0.6205	0.4952	0.4132
	% CCT time gain by SVC	-0.6437	-0.9208	-1.3227	-1.1231	-0.9282
	Classical CCT estimation	0.8754	0.6921	0.6194	0.4862	0.4000
	Classical CCT error	-2.4459	-1.1546	-1.1430	0.7147	2.2960
Single phase to ground Fault	SPL(SVC NO) CCT	2.115	1.556	1.427	1.001	0.832
	SPL(SVC ON) CCT	—	—	—	—	—
	% CCT time gain by SVC	—	—	—	—	—
	Classical CCT estimation	1.89	1.494	1.336	1.049	0.8625
	Classical CCT error	10.6383	3.9846	6.3770	-4.7952	-3.6659

III. RESULTS AND DISCUSSION

Figures 3 – 5 show plots of rotor angle versus time for single line, double line to ground and three-phase faults respectively. The plots show various transient responses for non presence of PSS and SVC, presence of PSS and no SVC and finally the presence of both PSS and SVC.

Figures 6 – 9 show simulation results plots of only three-phase rotor angle – time response for SIME for different conditions at different clearing times.

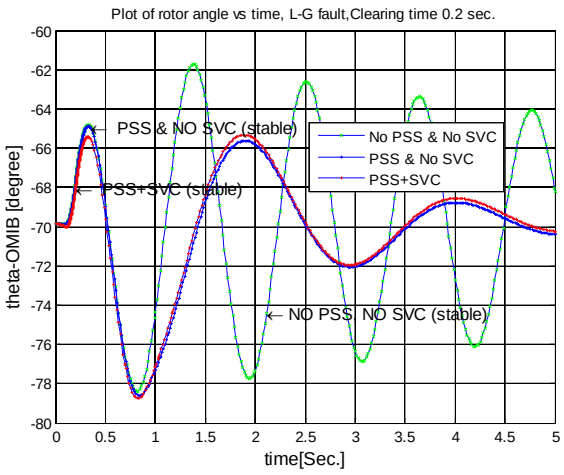

Figure 3: plot of rotor angle versus time for single line to ground fault

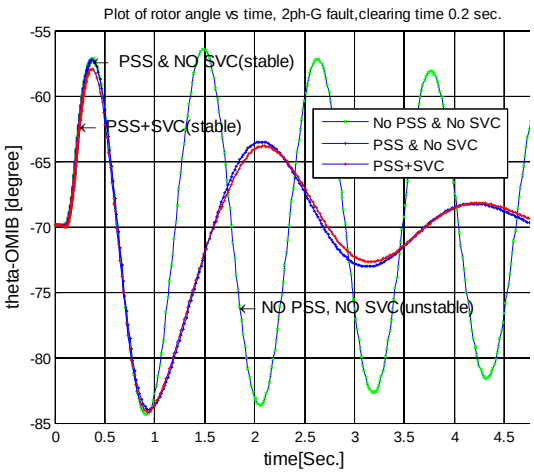

Figure 4: plot of rotor angle versus time for double phase to ground fault

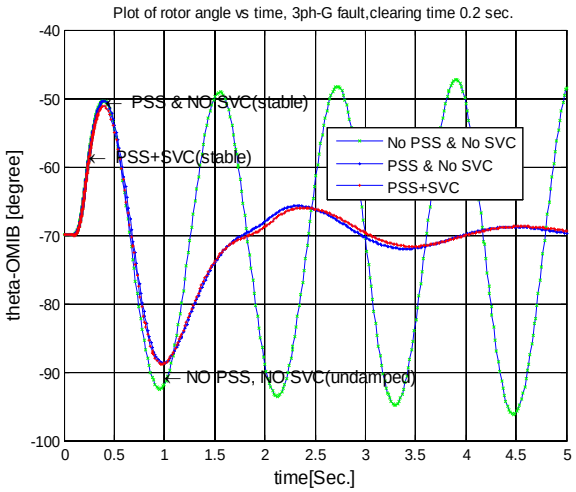

Figure 5: plot of rotor angle versus time for three phase to ground fault

Figure 6: 3Φ-G Rotor angle – time response for SIME, PSS & No SVC at clearing time of 0.36635 Sec

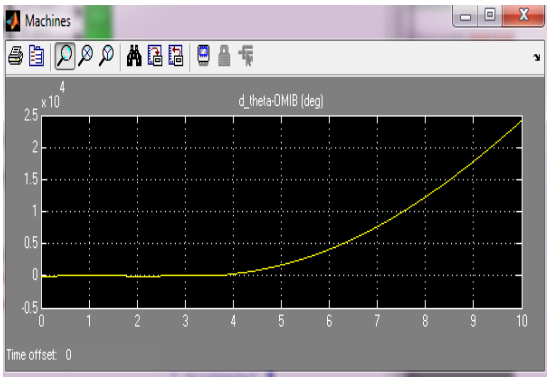

Figure 7: 3Φ-G Rotor angle – time response for SIME, PSS & No SVC at clearing time of 0.3664 Sec.

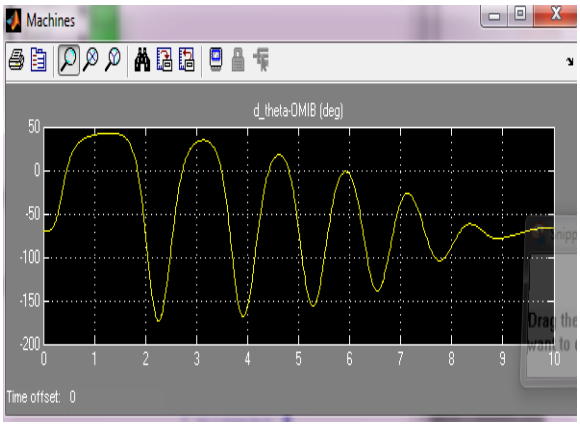

Figure 8: 3Φ-G Rotor angle – time response for SIME, PSS & SVC ON at clearing time of 0.3705 Sec.

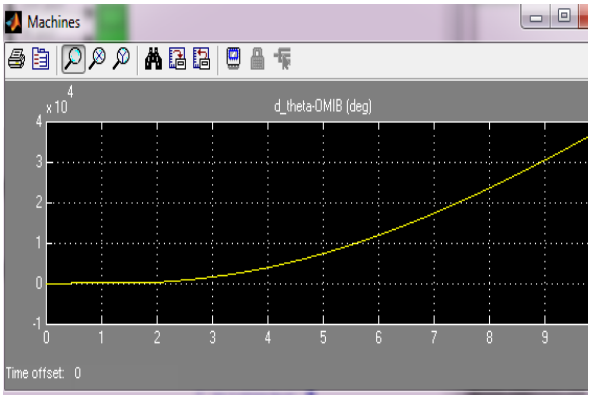

Figure 9: 3Φ-G Rotor angle – time response for SIME, PSS & SVC ON at clearing time of 0.3706 Sec.

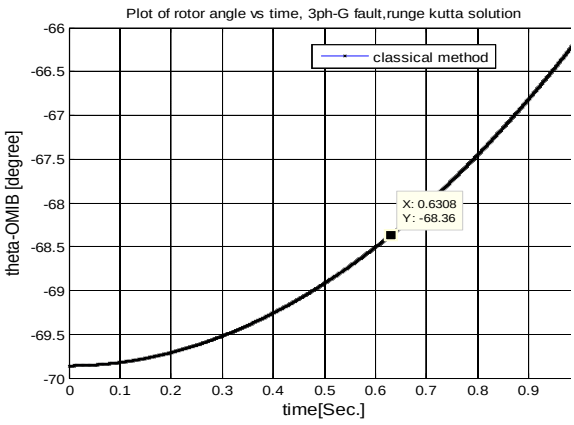

Figure 10: plot of rotor angle versus time (Runge-Kutta solution), 3Ph-G, H=24 sec.

Figures 10 – 24 show plots of rotor angle versus time as calculated using 4th Order Runge-Kutta solution at different inertia values and for various faults.

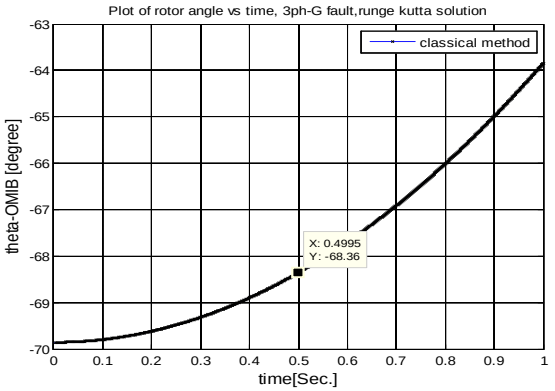

Figure 11: plot of rotor angle versus time (Runge-Kutta solution), 3Ph-G, H=15 sec

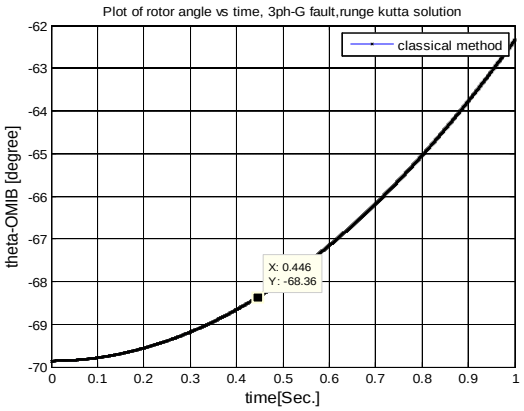

Figure 12: plot of rotor angle versus time (Runge-Kutta solution), 3Ph-G, H=12 sec

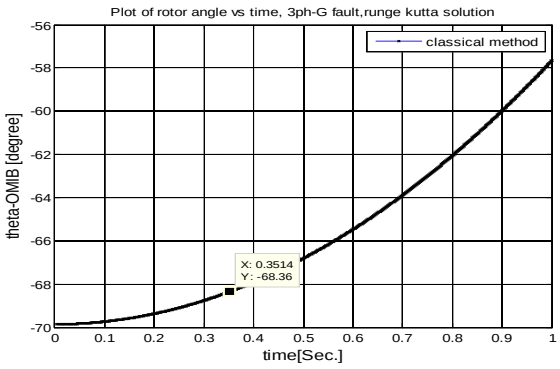

Figure 13: plot of rotor angle versus time (Runge-Kutta solution),3Ph-G, H=7.4 sec.

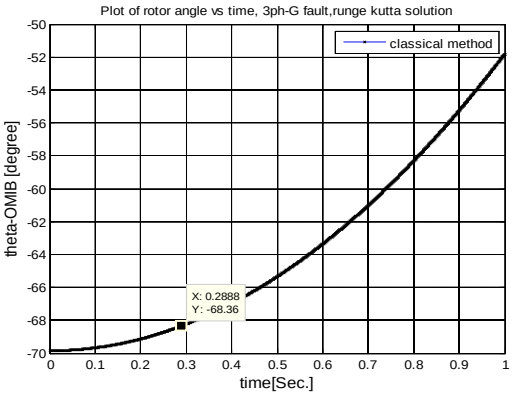

Figure 14: plot of rotor angle versus time (Runge-Kutta solution),3Ph-G, H=5.0 sec.

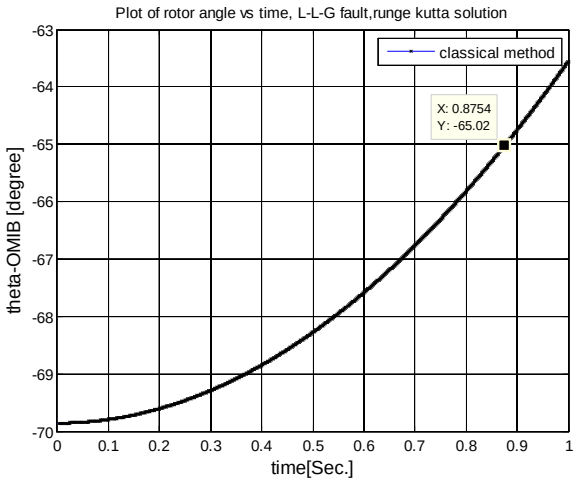

Figure 15: plot of rotor angle versus time (Runge-Kutta solution), L-L-G, H=24 sec

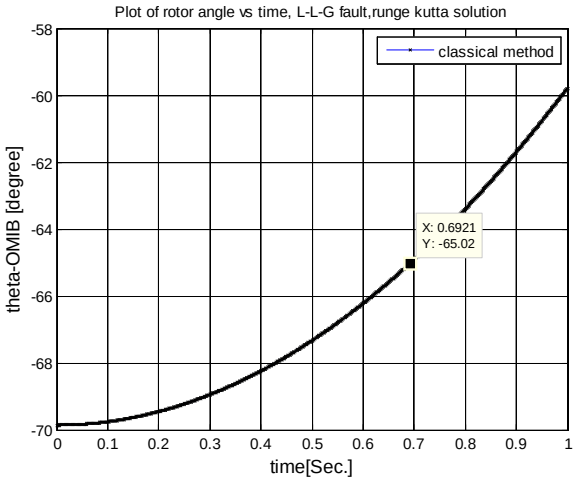

Figure 16: plot of rotor angle versus time (Runge-Kutta solution), L-L-G, H=15 sec

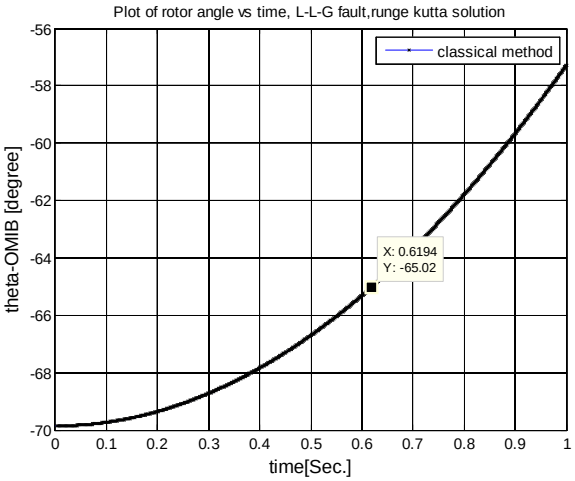

Figure 17: plot of rotor angle versus time (Runge-Kutta solution), L-LG, H=12 sec

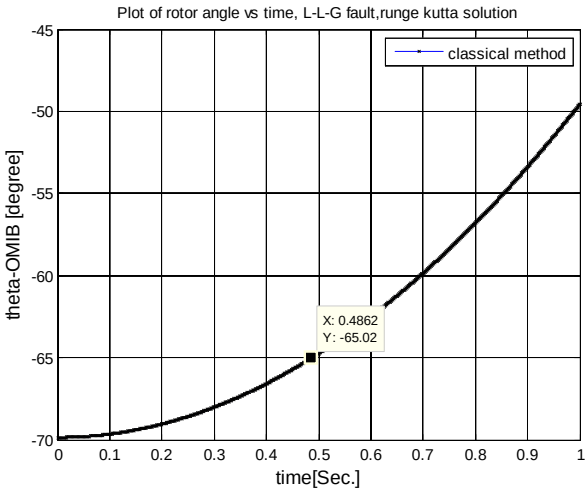

Figure 18: Plot of Rotor Angle versus Time (Runge-Kutta Solution), L-L-G, H=7.4 Sec

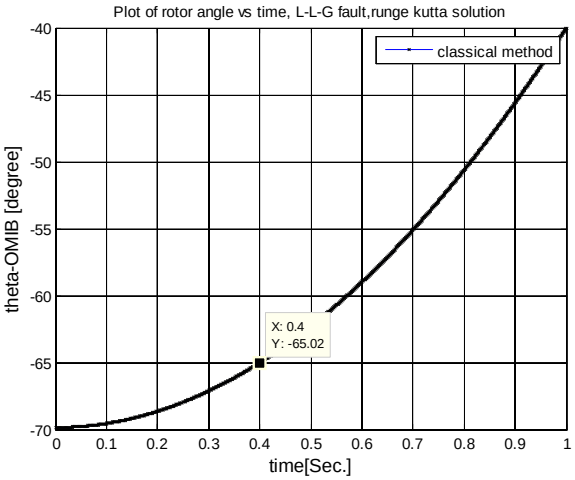

Figure 19: Plot of Rotor Angle Versus Time (Runge-Kutta Solution), L-L-G H=5.0 Sec

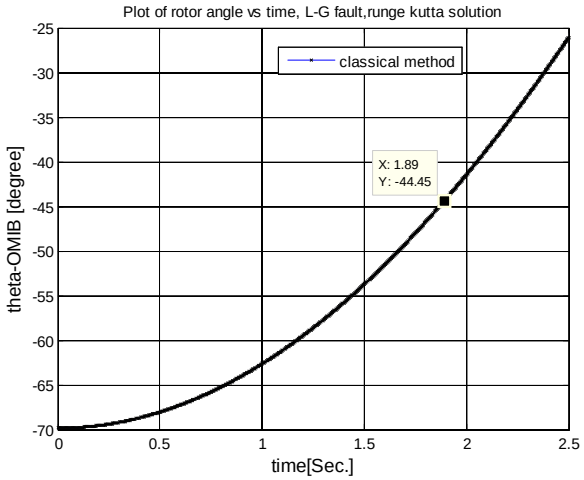

Figure 20: Plot Of Rotor Angle Versus Time (Runge-Kutta Solution), L-G, H=24 Sec

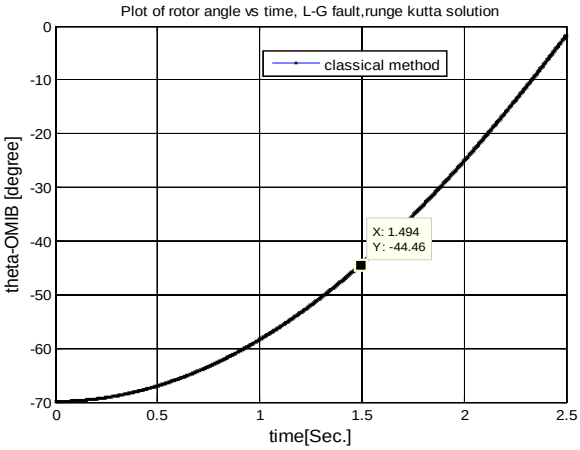

Figure 21: Plot Of Rotor Angle Versus Time (Runge-Kutta Solution), L-G, H=15 Sec

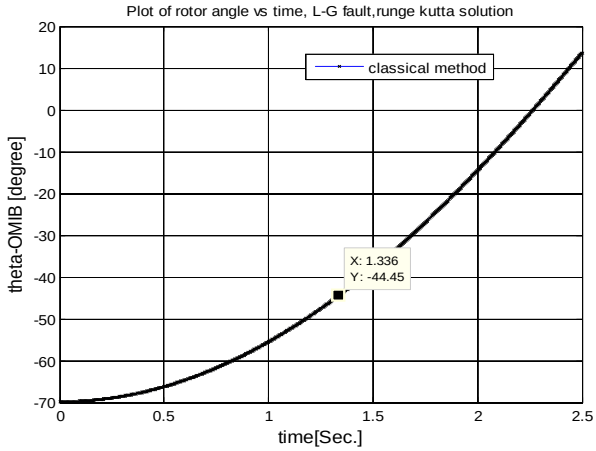

Figure 22: Plot Of Rotor Angle Versus Time (Runge-Kutta Solution), L-G, H=12 Sec

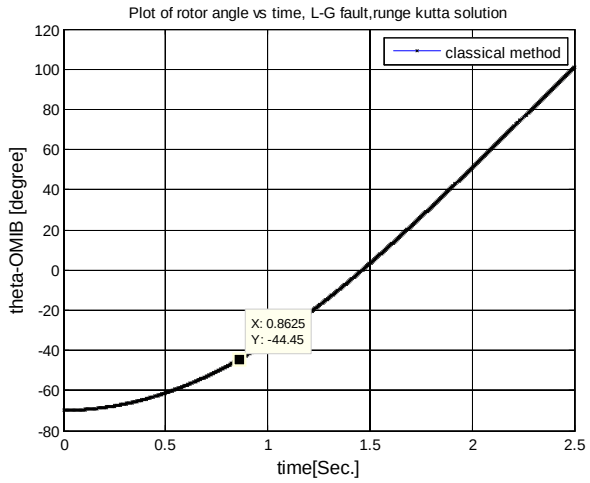

Figure 23: Plot Of Rotor Angle Versus Time (Runge-Kutta Solution), L-G, H=7.4 Sec

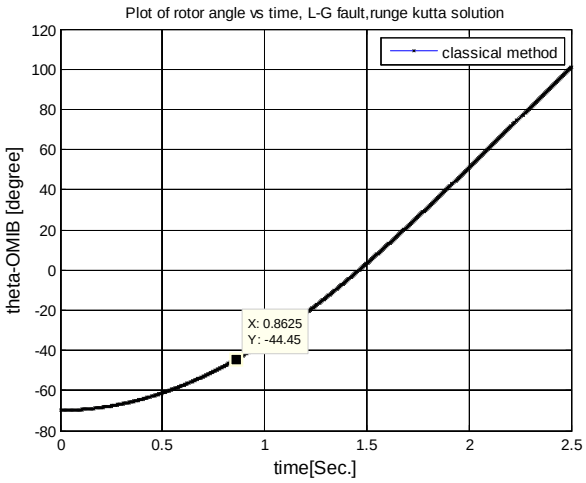

Figure 24: Plot Of Rotor Angle Versus Time (Runge-Kutta Solution), L-G, H=5.0 Sec

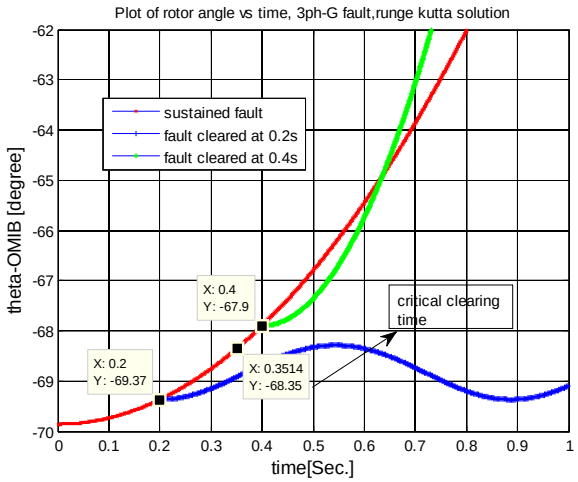

Figure 25: Comparison of Plot of Rotor Angle Versus Time (Runge-Kutta Solution), 3Ph-G, H=7.4 Sec

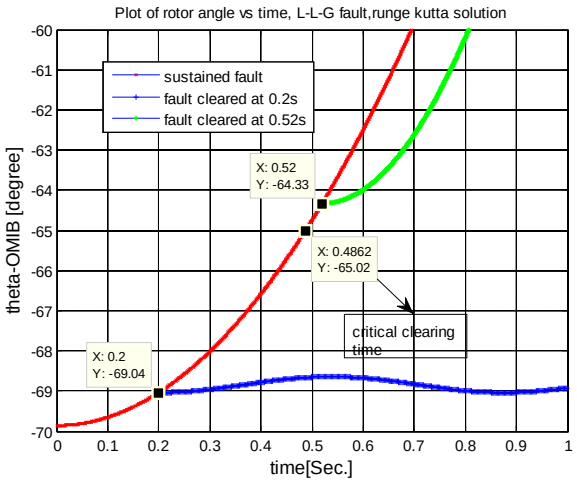

Figure 26: Comparison of Plot Of Rotor Angle Versus Time (Runge-Kutta Solution), L-L-G, H=7.4 Sec

Figure 25 shows comparison of plots of rotor angle versus time using Runge-Kutta 4th Order solution for three-phase to ground fault with inertia constant of 7.4 sec. for (i) Sustained fault, (ii) Fault cleared at 0.2s and (iii) Fault cleared at 0.4s showing Critical clearing time (CCT) of 0.3514sec.

Figure 26 show comparison of plots of rotor angle versus time using Runge-Kutta 4th Order solution for Double line to ground 7.4 sec. inertia constant for (i) Sustained fault, (ii) Fault cleared at 0.2s, and (iii) Fault cleared at 0.52sec with a Critical clearing time (CCT) of 0.4862secs.

IV. CONCLUSION

Transient stability analysis is a critical investigation in power system studies. This work evaluates essential parameters such as critical clearing time (CCT) from transient responses of different faults on a SIME connected to infinite busbar. The model was equipped with static variable compensator in the middle of the transmission line. This was the first stage of enhancement and the line was simulated with simpowersystem for three-phase fault, double line to ground fault and single line to ground fault to assist in drawing a good comparative analysis. . Also the classical model was used to compute the critical clearing time using equal area criteria with the fourth order Runge-Kutta numerical method. The simulation was done in MATLAB 7.5 environment.

In the fault analysis, different types of faults were introduced at the busbar and the faults were analyzed. The results show that during fault voltages and currents, the system is greatly affected by the three phase to ground fault as shown in Table III. Here the classical critical clearing time estimation for the three phase to ground fault was found to be 0.6308 sec followed by the classical critical clearing time for the double line to ground fault which was estimated to be 0.8754sec and lastly the single line to ground fault has its classical critical clearing time to be 1.89 sec. From the above extract, it becomes imperative to say that the three phase to ground fault is the most severe fault on the transmission system followed by the double line to ground fault. The least severe fault is the single line to ground fault.

REFERENCES

[1] P. Kundur, Power system stability and control, McGraw-Hill, 1994.
[2] P. Kundur and G. K. Morison, A review of definitions and classification of stability problems in today's power systems, IEEE-PES Winter Meeting (Panel Session on Stability Terms and Definitions, New York,1997.
[3] J. U. Agber, P. E. Odaba, and C. O Onah, Effect of power system parameters on transient stability studies, American Journal of Engineering Research (AJER), 4(2), 2015, 87-94.
[4] M. Payella, D. Ernest and D. Ruiz-Vega, Transient stability of power systems – a unified approach to assessment and control, Kluwer Academic Publishers, Boston/Dordrecht/London, 2000.
[5] P. I. Obi, J. K. Offor, and G. C. Chidolue, Relative and efficient power supply in Nigeria through National Integrated Power Projects and Independent Power Projects: a case study of Onitsha Metropolis, International Journal of Advancement in Research and Technology, 2(5), 2013, 421-427.
[6] G. A. Adepoju, and M. A. Tijani, Critical clearing time evaluation of Nigeria 330kv transmission system, American Journal of Electrical Power and Energy System. 2(6), 2013, 123-128.
[7] B. Boussahoua and M. Boudour, Critical Clearing time evaluation of power system with UPFC by energetic method, Journal of Electrical Systems, Special Issue. No.1, 2009, 85-88.

American Journal of Engineering Research (AJER) 2016
American Journal of Engineering Research (AJER)
e-ISSN: 2320-0847 p-ISSN : 2320-0936
Volume-5, Issue-1, pp-21-33
www.ajer.org
Research Paper Open Access

HOMER Based Feasibility Study of Off-Grid Biogas Power Generation Model Using Poultry Litter for Rural Bangladesh

Sharmin Sobhan[1], Tanvir Ahmad[2], Md. Jakaria Rahimi[3], Md. Habib Ullah[4], Shaila Arif[5]

[1, 2,3,5](Department of Electrical & Electronic Engineering, Ahsanullah University of Science & Technology, Bangladesh)

[4](Department of Electrical Engineering and Computer Science, South Dakota State University, USA)

ABSTRACT: *Lack of access to electricity is one of the major impediments to the economic growth and development for any developing country. As well as limited reserve of conventional fuel and geo-location of Bangladesh arise the demand to find an effective alternative energy source for rural electrification. This document approaches a poultry-home based power generation model for rural Bangladesh and diagnosis its feasibility through HOMER, a micro power modelling and optimization software. The introduction on renewable energy and its importance is followed by present energy state in Bangladesh and prospect of biogas electrification technology, specially focused on poultry litter base system. Theoretical foundations on formation of biogas and electricity generation process are also presented. Main objective of the study is to diminish energy scarcity and connect rural people with the country's development through electrification*

Keywords - *Biogas , Electricity generation, Poultry litter, Feasibility,HOMER analysis.*

I. INTRODUCTION

Renewable energy comes from natural resources such as sunlight, wind, rain, tides, and geothermal heat, which are renewable (naturally replenished) [1].Mainstream forms of renewable energy: Wind power, Hydro power, Solar energy, Biomass, Biogas, Geothermal energy. Electric energy security is essential, yet the high cost and limited sources of fossil fuels, in addition to the need to reduce greenhouse gasses emission, have made renewable resources attractive in world energy-based economies [2].

Biogas technology, the generation of a combustible gas from anaerobic digestion, is a well-known technology [3]. But producing electricity from biogas is still relatively rare in most developing countries.

To meet the ever-increasing demand of energy, renewable energy can open up new possibilities in developing countries [4]-[5]. Renewable energy resource biogas can be used for off-grid electricity generation as well as it can be added with grid electricity. Due to the abundance of raw materials it is effective for rural electrification in Bangladesh. First part of the paper discusses about biogas related attributes. Afterwards biogas prospect for Bangladesh specially potential of poultry based biogas and bio-electrification technology are perused. This paper aims to propose an off-grid power plant for only home and farm uses in rural Bangladesh using poultry litter as biogas resource. Furthermore HOMER simulated results are disclosed to study economic feasibility of the proposed model.

II. BIOGAS

Biogas is a flammable gas that accrues from the fermentation of biomass in biogas plants. Biogas can be produced utilizing anaerobic digesters. These plants can be fed with energy crops such as maize silage or biodegradable wastes including sewage sludge and food waste [6].

2.1 Biogas Composition

Table -1: Biogas Composition [7]

Typical Composition of Biogas		
Compound	Chemical Properties	%
Methane	CH_4	50-75
Carbon dioxide	CO_2	25-50
Nitrogen	N_2	0-10
Hydrogen	H_2	0-1
Hydrogen sulphide	H_2S	0-3
Oxygen	O_2	0-0

2.2 Biological and Chemical Stages

The overall process can be described by the chemical reaction, where organic material such as glucose is biochemically digested into carbon dioxide (CO_2) and methane (CH_4) by the anaerobic microorganisms [8].

$C_6H_{12}O_6 \rightarrow 3CO_2 + 3CH_4$

There are four key biological and chemical stages of anaerobic digestion [9]:

- Hydrolysis
- Acidogenesis
- Acetogenesis
- Methanogenesis

Depending on temperature, there are two key processes [9]:

- Mesophilic digestion (between 20°C and 40°C).
- Thermophilic digestion(above 40°C)

Types of biogas plants [10]

- Floating cover digester
- Fixed cover digester
- The Balloon or Plastic Cover digester:
- Fiber glass biogas plant

III. PRESENT ENERGY STATE OF BANGLADESH

Natural Gas is used as main fuel for electricity generation in Bangladesh. Alarming issue is that, the country's gas reserves stand at 14.16 trillion cubic feet (tcf) as of June 2015 and 12.96 bcf (billion cubic feet) gases was extracted until May, 2015. If the current rate of extraction remains unchanged, the reserve would last until 2031[11].

Table -2: Installed capacity of BPDB power plants on December 2015[12]

Fuel Type	Capacity(Unit)	Total (%)
Coal	250.00 MW	2.14 %
Gas	7434.00 MW	62.59 %
HFO	2507.00 MW	21.11 %
HSD	956.00 MW	8.05 %
Hydro	230.00 MW	1.94 %
Imported	500.00 MW	4.21 %
Total	11877.00 MW	100 %

On the top of that, country provides electricity to only 74% of its population and maximum people in rural areas are living without electricity. Under this circumstance biogas based technology could be found effective for country's development [13].

Table -3: Bangladesh's power sector at a glance (June 2015) [14]

Generation Capacity	: 11,534 MW* (June, 2015)
Highest Generation	: 8,177 MW (13 August, 2015)
Total Consumers	: 17.5 Million (June, 2015)
Transmission Line	: 9,695 ckt. km
Distribution Line	: 3,26,000 km
Distribution Loss	: 11.36%
Per Capita Generation	: 371 KWh
Access to Electricity	: 74%

IV. BIOGAS PROSPECT IN BANGLADESH

Biogas mainly from animal and MSW (municipal solid waste) may be one of the promising renewable energy resources for Bangladesh. MSW contains an easily biodegradable organic fraction (OF) of up to 40%. It is a potential source to harness basic biogas technology for cooking, rural and urban electrification to provide electricity during periods of power shortfalls[15]-[17].

Table-4: Estimation of total biogas potential in Bangladesh [18]

Cattle Dung • Total cattle population of Bangladesh = 23 million • Dung available = 230 million Kg/day • Gas that may be obtained = 3106 million m3(Mm^3)/year • (1 kg of dung yields = 0.037 m^3 gas, each cow yields = 10 Kg dung/day)
Poultry Litter • Total poultry population (Chickens+ Ducks) of Bangladesh, (234+44) =278million • Total poultry litter that may be obtained = 27.8 million Kg/day • Gas that may be obtained = 750 Mm^3/year • (1 kg litter yields = 0.074 m^3 gas, each bird yields = 0.1 Kg litter/day)
Human Excreta • Total human population of Bangladesh = 140 million • Excreta available = 56 million Kg/day • Gas that may be obtained = 1512 Mm^3/year • (1 kg excreta yields = 0.074 m^3 gas, Excreta per person = 0.4 Kg per day)
Therefore total biogas potential in the country = 53Mm^3/year.

Effectively using this waste, per day approximately 20.5 MWh (mega watt hour) electricity could be generated, which may play a significant role in country's energy situation.

4.1 Prospect of Poultry Based Biogas

Poultry is an emerging and important sector that has been contributing progressively to our economy for the past decade [19]-[22]. It is one of the fastest growing and most promising industries with the brightest of futures for our country.

Along with this, the calorific value of poultry waste is higher than that of cow manure [23]. From "Poultry Business Directory 2015" we find the statistics about poultry farms and number of different types of poultry birds.

Table 5. Number of poultry farms in Bangladesh (Poultry Business Directory 2015) [24]

No of poultry farms	
Grandparent farms	5
Parent stock farms	32
Commercial farms	50,000
Total (approx.)	50,037

Table 6. Number of Different Types of Poultry Birds& their wastes [24]

Total number of poultry birds	
Bird Type	Year 2014
Broiler	8094784
PS Layer	391580
PS Commercial Broiler	502852360
Commercial Layer	20157000
Cock real	20157000
Total (approx.)	550 million
Waste (approx.) -55million kg/day	

Per kg poultry waste may produce 22.5 cft gases as well as if the total poultry waste is used effectively, it may produce approximately 5500 Mwatt electricity which can be used to brighten rural life of Bangladesh with the light of progress.

Bangladesh has now around 75,000 biogas projects built under the Infrastructure Development Company Limited (IDCOL), the Bangladesh Centre for Science and Industrial Research (BCSIR) and the Department of Youth Development (DYD) [25].

V. PROPOSED MODEL

Proposed model is an off-grid power plant for only home and farm uses using poultry litter. Model has three distinct outputs-

- electricity,
- cooking gas and
- fertilizer for agriculture

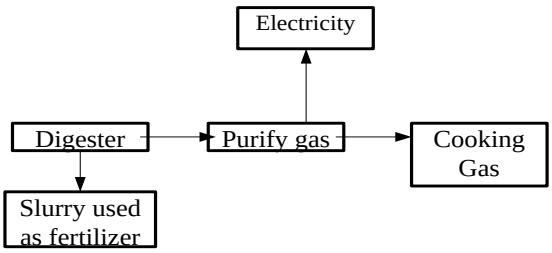

Figure 1: Outputs of Proposed model

Off-grid can be stand-alone power system or mini-grids that desire to provide a smaller community with electricity. Off-grid electrification is an approach to access electricity used in countries and areas with little access to electricity, due to scattered or distant population.

Proposed system is designed to function without the support of remote infrastructure, having 2 generators, each of them has distinct eight working hours. So the off-grid power plant will serve for 16 hours in a day. Generator1 serves only poultry farm demands for 8 a.m. to 4 p.m. whereas generator2 servers 5 families with 5 lights and 5fans according to user demands, as well as also meet up farm demands for 6 p.m. to 2 a.m.

This model proposes co-generation of electricity along with cooking gas for 5 families and slurry of the digester can be used as fertilizer for agriculture.

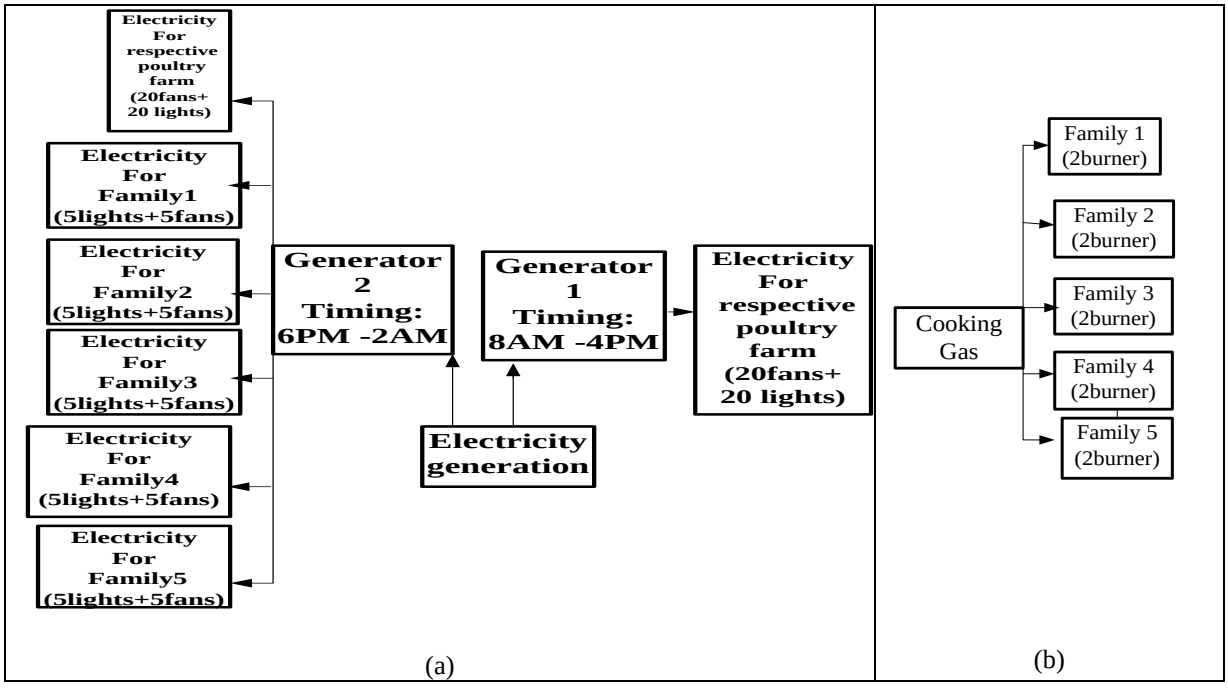

Figure 2: Proposed model (a) electricity distribution (b) gas distribution for cooking purpose

5.1 Methodology for Electricity Generation :

Poultry waste should used as the raw material of biogas digester. Output gas of the digester contains H_2S and moisture components and needs to be purified through H_2S and moisture removal unit. Output of the moisture removal unit should feed as fuel for combustion engines, which convert it to mechanical energy, powering an electric generator to produce electricity and supply it to desired load.

Generator produced heat can be utilized by using it for digester and moisture removal unit [26]-[28]. Also Slurry of the digester can be used as fertilizer, which has two benefits. Thus the overall system acts as an eco friendly system by keeping environment clean [29].

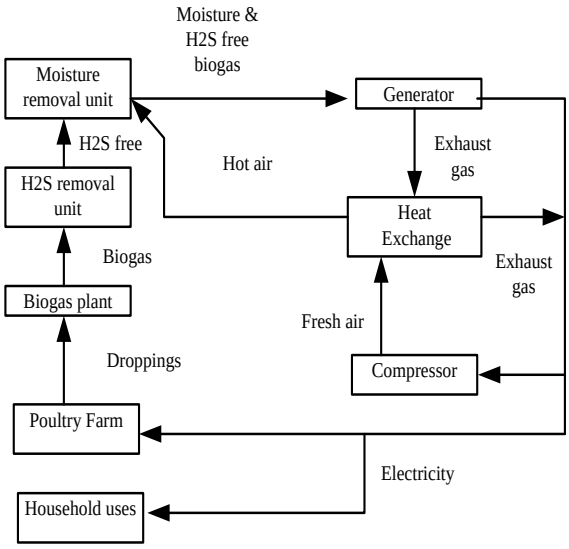

Figure 3: Electricity Generation process

5.2 Control Circuit:

The normal speed of an electric power generator is maintained by a control system that balances the demand on the generator and the steam supplied to the generator, in reference to the power system frequency. In the event when the load voltage fluctuated from the desired value, the control system is designed to simultaneously recover the load voltage to get the desired controlled output from the generator.

Digester produced gas is used as fuel of the DC gas generator. Generated emf of the generator can vary with different changing parameters of prime mover [30].

Generated emf, $Eg = \frac{P\varphi N}{60} \cdot \frac{Z}{A}$

N = rotational speed of armature in revolutions per min. (rpm)

$$\frac{Eg_1}{Eg_2} = \frac{N_1}{N_2} \cdot \frac{I_2}{I_1}$$

Along with changing generated emf, terminal voltage of the generator may also be changed, Fluctuation of gas and voltage are harmful for connected loads. Thus we need to keep the terminal voltage fixed at a desired level.

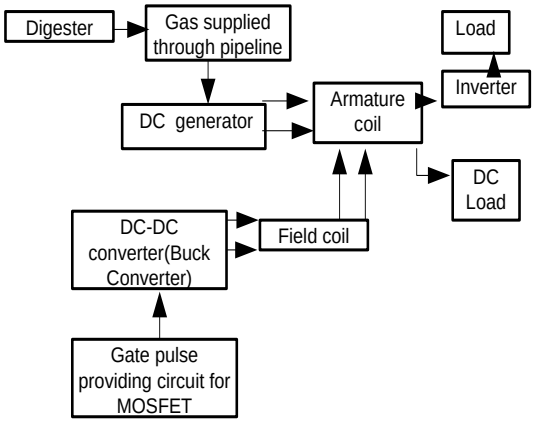

Figure 4: Overall Power generation process

DC-DC converter is a suitable solution to protect the loads from over voltage. Output of the converter can be dominated by controlling duty cycle of the gate pulse of switching device. Output of the converter should connect with the field coil and load should connect with the armature coil. For AC load armature coil output should pass through an inverter before connecting it with load.

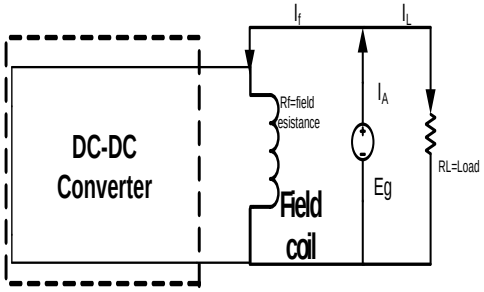

Figure 5: Electrical model of Power generation process

5.3 Estimation

Table-7: Estimation of the proposed Model

Total Birds 4000pcs	Breader 1000pcs	Feeder 3000pcs
Droppings	(1000 X 245g)≈245kg(per day)	(3000 X 98g)≈294kg(per day)
Total Biogas Resource: (245+294)kg =539kg ≈530 kg		
Produced Gas: 530kg x 2.5 cft =1347.5 cft ≈ 1300cft		
Cooking Gas= (5 x 80cft) =400cft		
Electricity = (1Kwh x900cft)/22.5 cft =40kwh ≈38kwh		

Estimation is done considering the farm has 4000 birds. Average amount of poultry droppings are used for calculating biogas. Amount of gas required per kWh electricity = 0.71 m 3 or 25cft (Considering 35% machine efficiency and30% carbon content) [23].

5.4 By products of the Model

- Cooking facility

After purification of the gas, it can also serve cooking purpose. As we all know Bangladesh is facing a gas shortage problem. So rest of the gas that contains methane can be used for household purpose.

- Fertilizer

Bio-slurry may be considered as a good quality organic fertilizer in Bangladesh agriculture. Analysis of representative cow dung and poultry litter slurry samples from biogas plants made at the Bangladesh Agricultural Research Institute (BARI) and Dhaka University (DU) has shown that slurry contains a considerable amount of both macro and micro nutrients besides appreciable quantities of organic matter. Toxic heavy metal concentration in them is minimal [31].

Bio-slurry organic fertilizer is environmental friendly, has no toxic or harmful effects and can easily reduce the use of chemical fertilizers up to 50%. Nutrients from organic sources are more efficient than those from chemical sources.

Table 8. Comparison of Biogas Fertilizer with Chemical Fertilizer

Name	Production with chemical fertilizer[ton/hector]	Production with biogas fertilizer [ton/hector]	percentage
Husk	8.28	9.02	8.93
Corn	7.00	9.5	35.7
Tula	3.13	3.97	26.8
vegetable	less	much	-

VI. HOMER ANALYSIS TO STUDY FEASIBILITY OF PROPOSED MODEL

Hybrid Optimization Model for Electric Renewable (HOMER) software is used to find out the final optimization and sensitive analysis [32]-[36] and to study the economical feasibility of the proposed model by comparing between diesel and biogas resources.

6.1 Resouce inputs:

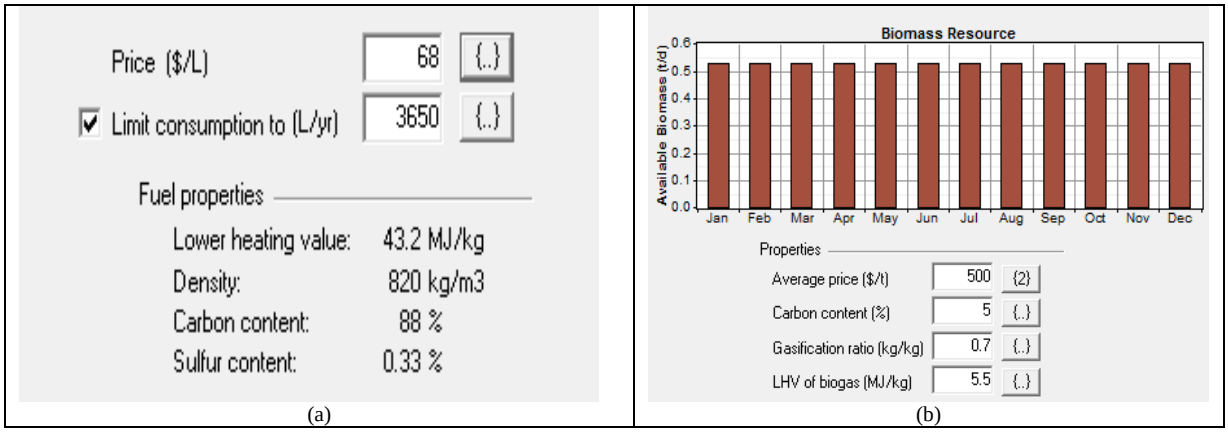

(a) (b)

Figure 6: Resource inputs (a) Diesel inputs (b) Poultry litter inputs

6.2 Analysis for Generator1:

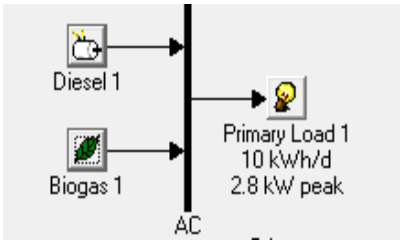

Figure 7: System with biogas generator ,diesel generator and load(for 8 a.m to 4 p.m)

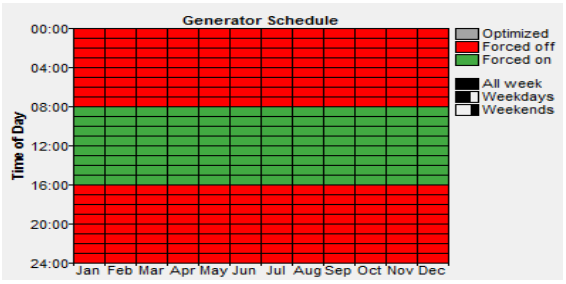

Figure 8: Schedule of generator1

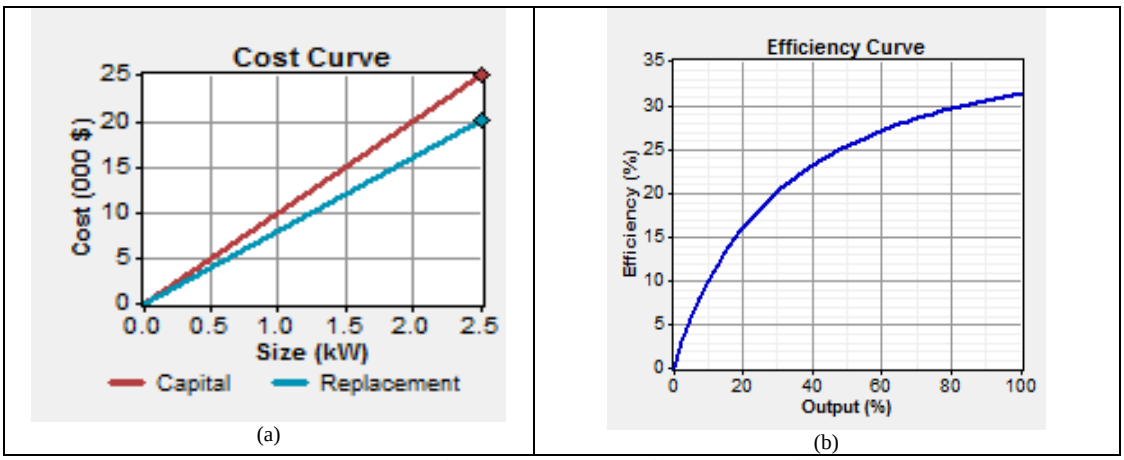

(a) (b)

Figure 9: (a) Cost curve of diesel generator1 (b) Efficiency curve of diesel generator1

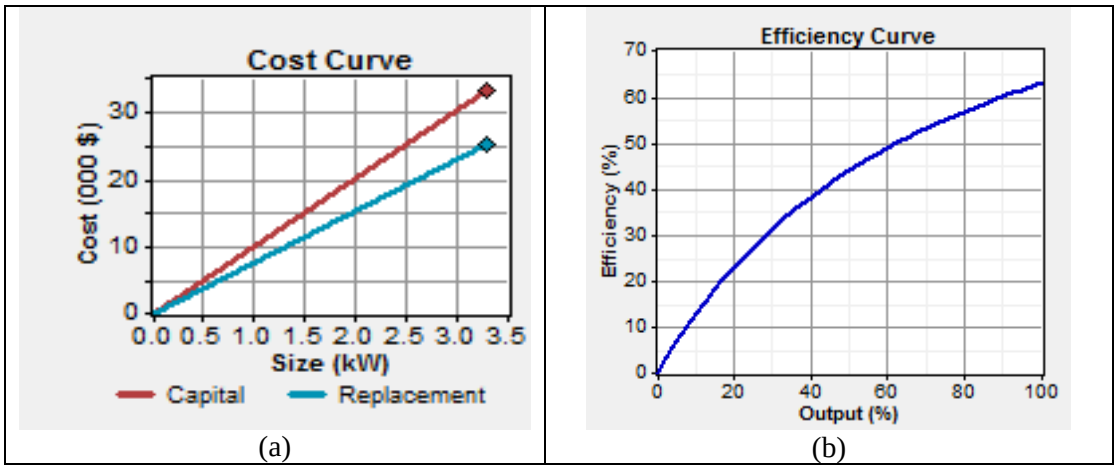

(a) (b)

Figure 10: (a) Cost curve of biogas generator1 (b) Efficiency curve of biogas generator1

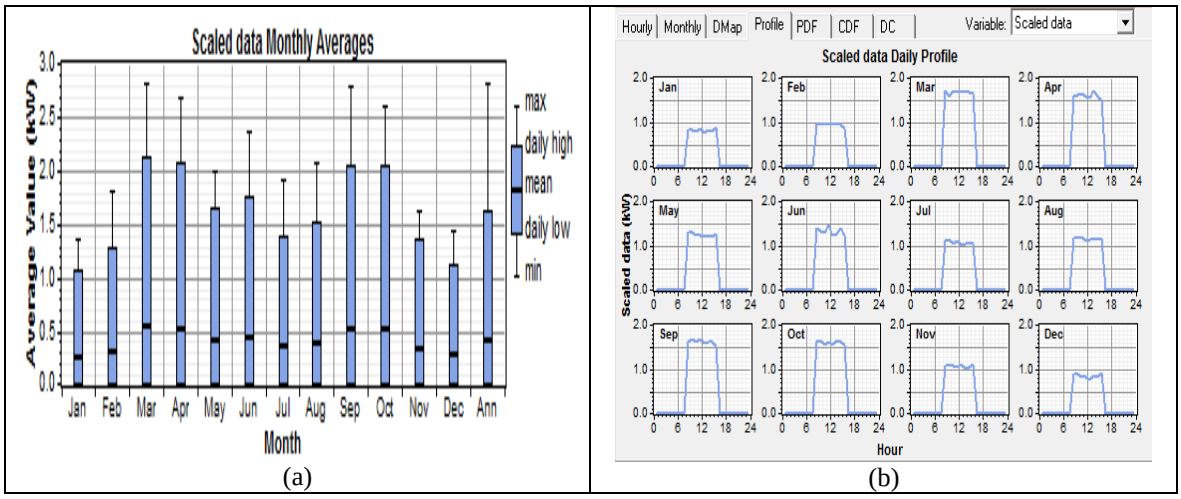

(a) (b)

Figure 11: Load profile for generator 1 (a) Scaled data monthly average load profile (b) Scaled data daily load profile

Sensitivity Results | Optimization Results

Double click on a system below for simulation results.

	D1 (kW)	B1 (kW)	Initial Capital	Operating Cost ($/yr)	Total NPC	COE ($/kWh)	Ren. Frac.	Diesel (L)	Biomass (t)	D1 (hrs)	B1 (hrs)
		3.3	$ 33,000	23,166	$ 329,145	7.054	1.00		9		2,920
	2.5	3.3	$ 58,000	115,846	$ 1,538,903	32.982	0.40	1,108	9	2,920	2,920

Figure 12: Optimization results of biogas generator and diesel generator

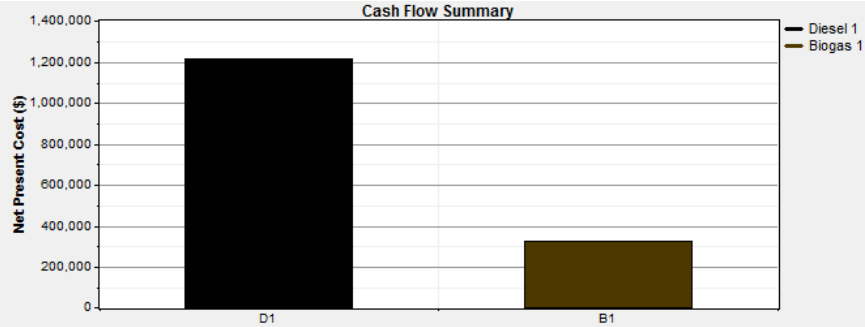

Component	Capital ($)	Replacement ($)	O&M ($)	Fuel ($)	Salvage ($)	Total ($)
Diesel 1	25,000	40,005	186,637	963,287	-621	1,214,308
Biogas 1	33,000	50,007	186,637	55,729	-777	324,596
System	58,000	90,012	373,274	1,019,016	-1,398	1,538,904

Figure 13: Cost comparison between biogas generator and diesel generator

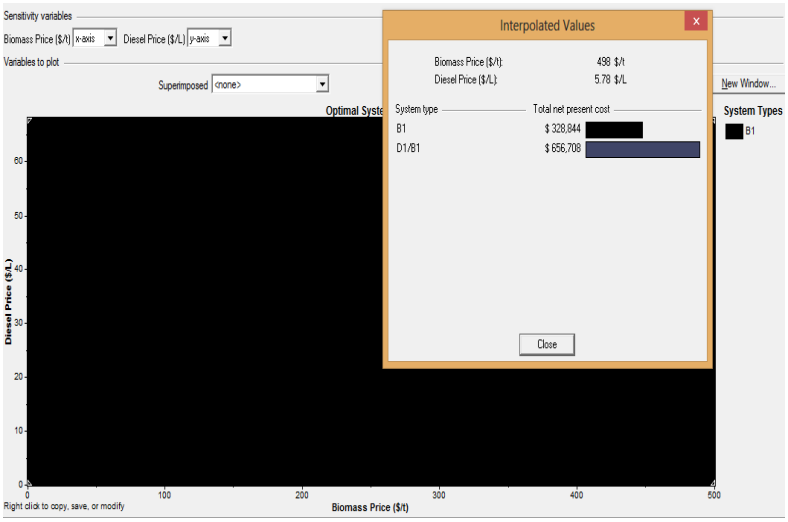

Figure 14: Sensitivity results of diesel generator1 Vs biogas generator1 (optimal system type)

6.3 Analysis for Generator 2:

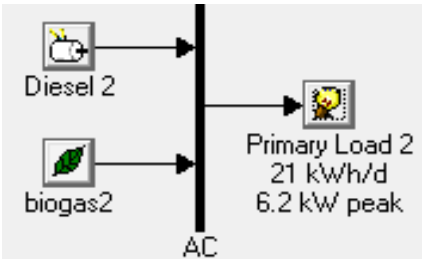

Figure 15: System with biogas generator ,diesel generator and load(for 6 p.m to 2 a.m)

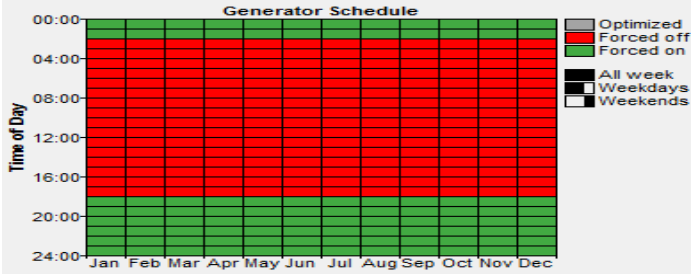

Figure 16: Schedule of generator2

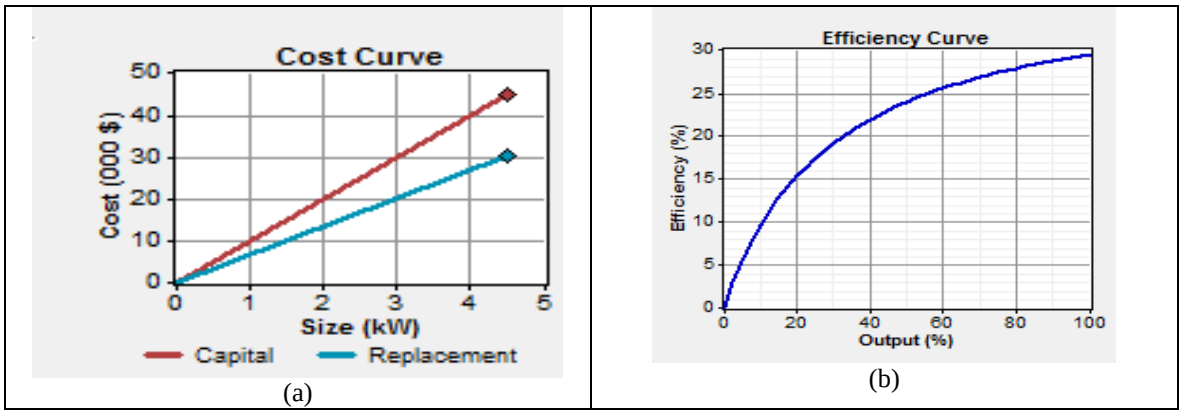

Figure 17: (a) Cost curve of diesel generator2 (b) Efficiency curve of diesel generator2

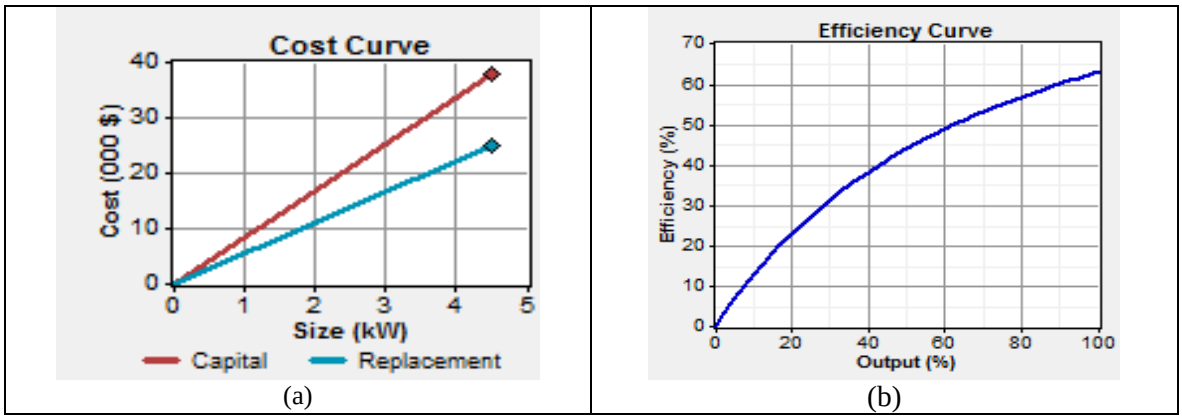

Figure 18: (a) Cost curve of biogas generator2 (b) Efficiency curve of biogas generator

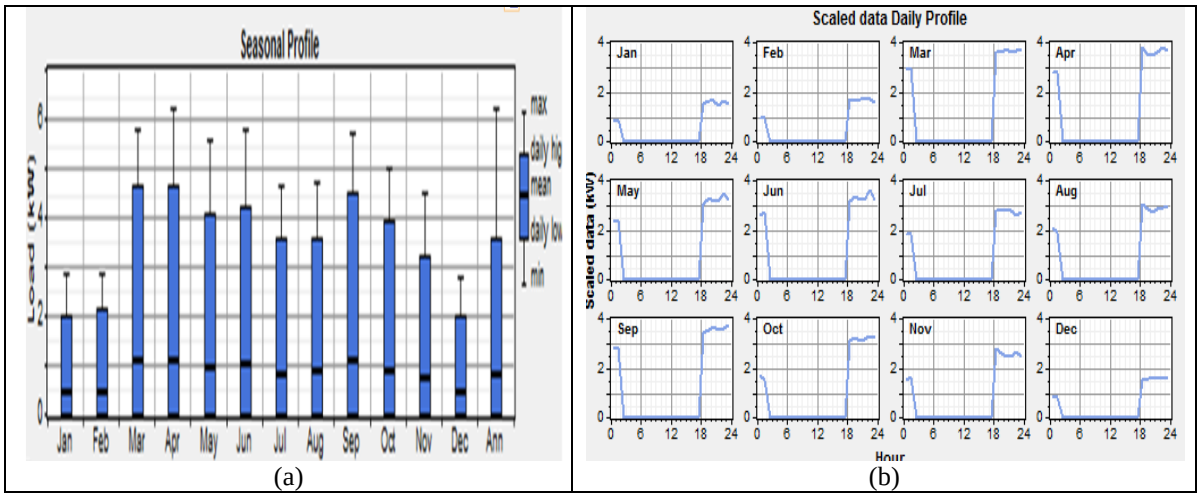

Figure 19: Load profile for generator2 (a) Scaled data daily load profile (b) Scaled data monthly average load profile

Double click on a system below for optimization results.

Biomass Price ($/t)	Diesel ($/L)	D2 (kW)	B2 (kW)	Initial Capital	Operating Cost ($/yr)	Total NPC	COE ($/kWh)	Ren. Frac.	Diesel (L)	Biomass (t)	D2 (hrs)	B2 (hrs)
500.000	68....	4.5	4.5	$ 83,000	186,555	$ 2,467,801	25.428	0.48	2,096	13	2,920	2,920
500.000	0.000	4.5	4.5	$ 83,000	43,557	$ 639,808	6.592	0.33	2,408	12	2,920	2,920
0.000	68....	4.5	4.5	$ 83,000	180,173	$ 2,386,214	24.587	0.48	2,096	13	2,920	2,920
0.000	0.000	4.5	4.5	$ 83,000	37,672	$ 564,580	5.817	0.33	2,408	12	2,920	2,920

Figure 20: Optimization results of biogas generator and diesel generator

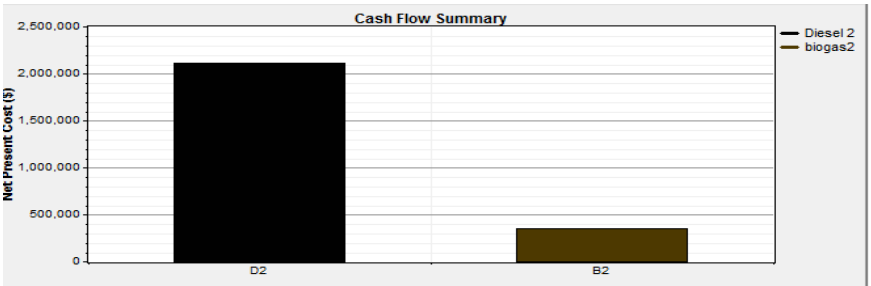

Component	Capital ($)	Replacement ($)	O&M ($)	Fuel ($)	Salvage ($)	Total ($)
Diesel 2	45,000	60,008	186,637	1,821,635	-932	2,112,348
biogas2	38,000	50,007	186,637	81,587	-777	355,454
System	83,000	110,015	373,274	1,903,222	-1,709	2,467,802

Figure 21: Cost comparison between biogas generator and diesel generator

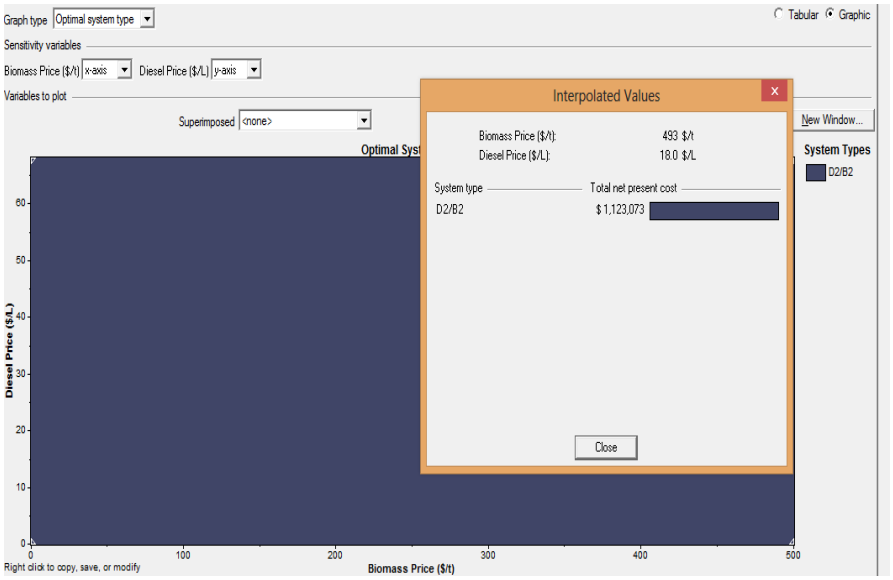

Figure 22: Sensitivity results of diesel generator Vs biogas generator (optimal system type)

6.4 Observation

Assessment is carried out in the HOMER environment to observe the feasibility of proposed model for an off-grid home-farm system for rural Bangladesh.

Fig-6 shows resource input parameters those are used for simulation. Analysis is done for two generators separately. For generator1, Fig- 9 & Fig-10 display cost curve and efficiency curve for diesel and gas generator respectively. Fig-17 and Fig-18 exhibit same parameters for generator 2. It is clearly observe in both cases that biogas generator provide much better efficiency than diesel generator.

System overview, generator on-off schedule and load profiles for generator1 are shown in Fig-7, Fig-8 and Fig-11 accordingly. For generator 2, mentioned parameters are exposed in Fig-15, Fig-16 and Fig-19 subsequently.

Fig-13 and Fig-21 illustrates cost effective feature of biogas for both cases separately showing a huge difference between biogas and conventional fuel cost.

The levelized COE (cost of energy) is the average cost per kWh of useful electrical energy produced by the system. HOMER uses the total net present cost (NPC) to represent the life-cycle cost of a system. Costs may include capital costs, replacement costs, operating and maintenance costs, fuel costs, the cost of buying electricity from the grid, and miscellaneous costs such as penalties resulting from pollutant emissions. Optimization results of generator 1 and generator 2 are presented in Fig-12 and Fig-20 respectively. Both figures demonstrate that NPC and COE are much less for biogas based system compared to diesel based system.

Optimization and sensitivity results of the proposed model clearly portrait the feasibility of poultry litter based bio-electrification technology.

VII. CONCLUDING REMARKS

Along with rest of the world, Bangladesh is also facing an accelerating crisis of the globally established fossil fuels, therefore immediate different breakthroughs for renewable energy is necessity to reach our electricity goal. Off-grid renewable energy systems are not only urgently needed to connect a vast number of people with a source of electricity, but are also most appropriate due to geographical constraints and costs for grid extension. In developed countries, minigrids are increasingly considered an option to improve energy security, power quality and reliability. In this document, an off-grid, poultry litter based power generation model is proposed and HOMER based assessment demonstrate the feasibility of the model for rural Bangladesh. Declining cost and increased performance of off-grid biogas based renewable energy systems are gradually rendering them more cost-competitive compared to alternatives.

REFERENCES

[1] El Bassam, Nasir, Preben Maegaard, and Marcia Lawton Schlichting.*Distributed Renewable Energies for Off-grid Communities: Planning, Technologies, and Applications*. Newnes, 2013.

[2] Ellabban, Omar, Haitham Abu-Rub, and Frede Blaabjerg. "Renewable energy resources: Current status, future prospects and their enabling technology."*Renewable and Sustainable Energy Reviews* 39 (2014)-Elsevier: 748-764.

[3] Weiland, Peter. "Biogas production: current state and perspectives." *Applied microbiology and biotechnology* 85.4 (2010): 849-860.

[4] S. R. Bull, "Renewable energy today and tomorrow," *Proceedings of the IEEE*, vol. 89, no. 8, pp. 1216-1226, Aug. 2001

[5] J. M. Guerrero, F. Blaabjerg, T. Zhelev, K. Hemmes, E. Monmasson, S.Jemei, M. P. Comech, R. Granadino, and J .I. Frau, "Distributed generation: toward a new energy paradigm," *IEEE Industrial Electronics Magazine*, vol. 4, no. 1, pp. 52-64, Mar. 2010.

[6] "Biology project on Biogas plant,An unique approach to alternative energy source in rural india". Internet: http://www.slideshare.net/TulikaGhosh1/biogas-plant-project-47375752, April24,2015.

[7] "Basic Information on Biogas" , www.kolumbus.fi. Retrieved 2.11.07

[8] Agrawal, Karan M., B. R. Barve, and Shareena S. Khan. "Biogas From Press mud." *IOSR journal of mechanical and civil engineering (IOSR-JMCE) ISSN* (2010): 2278-1684.

[9] Ziemiński, Krzysztof, and Magdalena Frąc. "Methane fermentation process as anaerobic digestion of biomass: Transformations, stages and microorganisms." *African Journal of Biotechnology* 11.18 (2014): 4127-4139.

[10] Bond, Tom, and Michael R. Templeton. "History and future of domestic biogas plants in the developing world." *Energy for Sustainable development*15.4 (2011): 347-354.

[11] The Daily Star. "Bangladesh's gas reserve to last until 2031". Internet: http://www.thedailystar.net/backpage/gas-reserve-last-until-2031-104479, June 29, 2015

[12] Bangladesh Power Development Board. Internet: http://www.bpdb.gov.bd/bpdb/index.php?option=com_content&view=article&id=150&Itemid=16

[13] A.Jamil. "Biogas and Cattle Organs- An Alternative Significant Source of Energy for Sustainable Development in Rural Bangladesh." M.Sc. Thesis, Södertorns Högskola, Stockholm, Sweden, 2006-07

[14] Power Cell. Internet: http://www.powercell.gov.bd/index.php?page_id=267

[15] Biswas, Wahidul K., Paul Bryce, and Mark Diesendorf. "Model for empowering rural poor through renewable energy technologies in Bangladesh." *Environmental Science & Policy* 4.6 (2001): 333-344.

[16] Biswas, Wahidul K., and N. J. D. Lucas. "Economic viability of biogas technology in a Bangladesh village." *Energy* 22.8 (1997): 763-770.

[17] Hossain, A. K., and O. Badr. "Prospects of renewable energy utilisation for electricity generation in Bangladesh." *Renewable and Sustainable Energy Reviews* 11.8 (2007): 1617-1649.

[18] Salma A. Iqbal, Shahinur Rahaman, Abu Yousuf, "Present Scenario of Biogas Technology in Bangladesh-Prospects, Potentials and Barriers,"Proceedings of the 15th Annual paper Meet, "APM 2013", At Dhaka,Bangladesh,Pages: 1-9

[19] Islam, Mohammad Shariful, Asif Islam, and Md Islam. "Variation of biogas production with different factors in poultry farms of Bangladesh."*Developments in Renewable Energy Technology (ICDRET), 2014 3rd International Conference on the*. IEEE, 2014.

[20] Islam, M. Rofiqul, M. Rabiul Islam, and M. Rafiqul Alam Beg. "Renewable energy resources and technologies practice in Bangladesh." *Renewable and Sustainable Energy Reviews* 12.2 (2008): 299-343.

[21] Shamsuddoha, Mohammad. "A sustainable supply chain process model for Bangladeshi poultry industry." *Curtin Business School, Doctoral Students' Colloquium*. 2010.

[22] Huda, A. S. N., S. Mekhilef, and A. Ahsan. "Biomass energy in Bangladesh: Current status and prospects." *Renewable and Sustainable Energy Reviews*30 (2014): 504-517.

[23] A.S.M.Hasan,M.F.Khan, R.Mostafa;A.Kaium "Feasibility study on electricity generation from poultry litter based biogas in Bangladesh." *Developments in Renewable Energy Technology (ICDRET), 2014 3rd International Conference on the*. IEEE, 2014.

[24] Poultry business directory 2015 - Poultry Khamar Bichitra. Internet: http://www.poultrykhamarbichitra.com/mg/Directory-2015-Part-A.pdf

[25] BSS News Dhaka. "Plan to install 'Bio-Socket' in 35,000 biogas plants forelectricity".Internet: http://www.bssnews.net/newsDetails.php?cat=0&id=388242&date=2014-02-09, Feb 9, 2014

[26] Kelleher, B. P., et al. "Advances in poultry litter disposal technology–a review." *Bioresource technology* 83.1 (2002): 27-36.

[27] Rao, P. Venkateswara, et al. "Biogas generation potential by anaerobic digestion for sustainable energy development in India." *Renewable and Sustainable Energy Reviews* 14.7 (2010): 2086-2094.

[28] Watkins, Pete, and Peter McKendry. "Assessment of waste derived gases as a renewable energy source–Part 1." *Sustainable Energy Technologies and Assessments* 10 (2015): 102-113.

[29] X. Fan, Z. Li, T. Wang; F. Yin; X. Jin, "Introduction to a Large-Scale Biogas Plant in a Dairy Farm," *Digital Manufacturing and Automation (ICDMA), 2010 International Conference* onYear: 2010, Volume:1Pages: 863 - 866, DOI: 10.1109/ICDMA.2010.271

[30] Sharmin Sobhan, Tanvir Ahmad, "Modeling and Analysis of Control Circuit for Biogas Electrification Technology," *International Journal of Research in Engineering and Technology*, vol. 4, issue 10, pp. 06–11, Oct 2015

[31] Islam, M. S. "Use of bioslurry as organic fertilizer in Bangladesh agriculture."*Prepared for the presentation at the International Workshop on the Use of Bioslurry Domestic Biogas Programme. Bangkok, Thailand*. 2006.

[32] Sen, Rohit, and Subhes C. Bhattacharyya. "Off-grid electricity generation with renewable energy technologies in India: an application of HOMER."*Renewable Energy* 62 (2014): 388-398.

[33] Mondal, Md Alam Hossain, and Manfred Denich. "Assessment of renewable energy resources potential for electricity generation in Bangladesh."*Renewable and Sustainable Energy Reviews* 14.8 (2010): 2401-2413.

[34] Dalton, G. J., D. A. Lockington, and T. E. Baldock. "Case study feasibility analysis of renewable energy supply options for small to medium-sized tourist accommodations." *Renewable Energy* 34.4 (2009): 1134-1144.

[35] Sureshkumar, U., P. S. Manoharan, and A. P. S. Ramalakshmi. "Economic cost analysis of hybrid renewable energy system using HOMER." *Advances in Engineering, Science and Management (ICAESM), 2012 International Conference on*. IEEE, 2012.

[36] Zoulias, E. I., and N. Lymberopoulos. "Techno-economic analysis of the integration of hydrogen energy technologies in renewable energy-based stand-alone power systems." *Renewable Energy* 32.4 (2007): 680-696.

American Journal of Engineering Research (AJER) 2016
American Journal of Engineering Research (AJER)
e-ISSN: 2320-0847 p-ISSN : 2320-0936
Volume-5, Issue-1, pp-34-41
www.ajer.org
Research Paper Open Access

Evaluation of the Strength Properties of Soil Bricks Produced with Processed African Locust Bean Waste water as Stabiliser

*Zievie[1], P. and Yalley[2], P. P.
[1]*Department of Building Technology and Estate Management, Wa Polytechnic, Post Office Box 553, Wa, Ghana,*
[2]*College of Technology Education, University of Education, Winneba, Ghana*

ABSTRACT : *A newly proposed concept of soil bricks as masonry units for low-cost environmentally friendly construction is proposed using agro-based waste water obtained from the processing of the African locust bean into local food condiments. Laboratory test system was designed to perform strength and durability test on four types of soil brick mixed with African locust bean waste water (ALBWW) as replacement of portable water and also as soil stabiliser for bricks production. Tests were conducted on strength and durability properties of the specimens. There was an increase of 66% over unstabilised specimens when the soil was fully mixed with ALBWW. The density of the bricks increased from 2120kg/m^3 for the soil bricks without ALBWW to 2167kg/m^3 when the soil was mixed with ALBWW. The resistance to wear for bricks increased steadily from 6.45cm^2/g for bricks without ALBWW as stabilisation to 9.45cm^2/g for bricks with ALBWW. The presence of ALBWW reduced the amount of water absorbed by the bricks. The study concluded that ALBWW which is an environmental nuisance can be used to replace portable water and also as stabiliser for masonry units in construction. This then implies that effective utilization of ALBWW as soil stabiliser would reduce the cost of relative durable houses for the rural and peri-urban areas in Northern part of Ghana where locust beans are prevalent.*

Keywords: *abrasion resistance, compressive strength locust bean, water absorption,*

I. INTRODUCTION

Building with soil materials is one of the ancient technology which still remains as the cheapest means of providing accommodation needs to a large number of people. Despite popular misconception that soil is a walling material for low income earners, soil-built houses, according to [1] portray cultural diversity and will continue to be a major integral part of modern housing needs. The most tangible proof of this is the continued use and existence of many thousands of new and historic traditional houses such as rammed, cob, wattle and daub, etc, soil-built houses dotted across both developed and developing countries. Using soil for housing projects offers a number of advantages to human life. Firstly, it is eco-friendly due to its low embodied energy content and low environmental impact. This is because soil is locally obtained with minimal transportation costs and used in its natural state; hence no fossil fuel is needed for processing. Secondly, soil-built houses can boast of excellent sustainability credentials and this is combined with good thermal and acoustic properties. It has also been indicated that earth buildings are cost effective, when compared with other materials. (Dobson, 2000; as cited in [2].

Historically, primitive man in his attempt to use soil to provide comfortable shelter, did little more than sticking lumps of wet soil on poles woven closely together. Though in modern times, the traditional methods of erecting soil houses in the past have improved. It has been found that soil-built houses are vulnerable to the hazards of the weather elements causing early development of erosion, cracks and collapse [1]. To address these and many other problems associated with the use of soil, several experimental investigators have studied the stabilising effect of conventional additives such as cement, lime, bitumen and the like on soil to improve strength and durability properties [3].

Even though research findings have shown that small addition of cement, lime, bitumen, etc, in the soil enhances its performance properties, the Ghana Business News [4] reported that the over dependence on these materials for housing is responsible for the continuous increase in housing cost in developing countries, often beyond the means of the poor. The report added that the importation of clinker and gypsum alone for the

production of Portland cement, use extensively in Ghana cost the nation not less than 180 million dollars annually. It is in the light of this that the United Nations Habitat [5] advised that, for developing countries to be able to provide affordable housing, they should take cost of imported materials into consideration and develop new technologies that would employ the use of local materials through research. In response to this, some local additives derived from industrial and agricultural sources have been studied as potential substitutes [1], [6], [5] and [7]. However, most published works have focused on pulverized and ash wastes because of their pozzolanic activity towards lime [8] and [9]. The main drawbacks of using soil block as a building material is the need for continuous maintenance due to its low durability and poor resistance to water [10] and [11]. Soil blocks have also been found to suffer from shrinkage cracking and most importantly low strength making them unsuitable for homes of more than two-storeys high.

Stabilization of soil is the process of modifying the soil properties in relation to its strength, texture, voids and water resisting properties, so as to obtain permanent properties compatible with a particular application. Research findings indicate that, stabilizing soil leads to irreversible change in the physical properties of soil depending on the quality of building design, materials employed, economic aspects of the project, or on issues of durability [11]. The use and adoption of the right stabilisation method can improve the compressive strength of a soil by as much as 400% to 500% with other supplementary characteristics such as increased cohesion, reduced permeability, improved water repellent, increased durability and minimal shrinkage and expansion of soil during dry and wet conditions [10]. The stabilisation mechanism may vary widely from the formation of new compounds binding the finer soil particles to coating particle surfaces by the additive to limit the moisture sensitivity. Therefore, a basic understanding of the stabilization mechanisms involved with each additive is required before selecting an effective stabilizer suited for a specific application. Chemical stabilization involves mixing or injecting the soil with chemically active compounds such as Portland cement, lime, fly ash, calcium or sodium chloride or with visco-elastic materials such as bitumen the process of chemical modification or stabilization with calcium-based chemicals, like African locust bean waste water requires a basic understanding of the mechanisms of reaction. Each calcium-based stabilizer contains some amount of free lime (CaO or $Ca(OH)_2$) that reacts pozzolanically with the fine particles [12].

The savanna belt across west and central Africa leads in the production of the African locust bean (Parkia biglobosa), commonly known in Hausa as ‘dawadawa’, which is traditionally used in a fermented state [13]. The fermentation process involves the bean seeds being sorted and soaked in hot water for seven days or boiled for eight hours to de-hull and the water poured away as waste. This waste water has been found to contain chemicals such as calcium, iron, potassium, sodium and magnesium [14] which are equally present in cement, lime and bitumen. Such binders and certain locally specific plant-based materials such as gum arabic, other specific resins and the sap, latexes and juices from specific trees and are a [6] aimed to improving water proofing or wear resistance properties of vulnerable earth based construction. These materials can make a particular contribution in conserving energy in the manufacture of cementitious materials and of lightweight aggregates. A study on the reuse of paper de-inking sludge, undertaken in Spain, showed that, it has the potential as raw material for producing a binding material with pozzolanic properties [6]. Research findings showed that calcination paper sludge has higher pozzolanic characteristics as compared to other industrial pozzolanic by-products, such as fly ashes normally used in cements [9].

Therefore the purpose of this study is to evaluate the strength characteristics of soil bricks stabilised with African locust bean waste water. To realize this objective, soil stabilisation techniques already in use were studied and references made to other relevant studies.

II. MATERIALS AND TESTING METHODS

Materials

Soil

The soil material used for the study was taken from a depth of 300mm below ground level after removing the top soil from a local construction site closed to Wa Polytechnic in the Upper west region of Ghana. This Local construction site is where the indigenes fetch soil for construction of mud houses; hence the research deemed it fit to use samples from this site for soil test and brick moulding

African Locust Bean Waste Water (ALBWW)

African locust bean waste water was used in the study as the stabiliser. It is an agro-based waste water obtained from the processing of the African locust bean into local food condiments popularly called ‘dawadawa’ in the Hausa language. It was sourced from a local ‘dawadawa’ processing set-up in Kpaguri in the Wa Municipality in the Upper west region of Ghana.

Testing Methods and Procedures

Classification of Soil

Laboratory quality identification tests were performed on the soil used for the study. To ensure that stones and other foreign matter were removed, the soil was firstly passed through a 5mm network of sieves before it was characterized to assess its index properties. Sieve analysis was performed in accordance with Clause 7.4.5 of BS 1377 – 1: 1990 [15] to determine the grade of soil used through the proportion by mass of various sizes of particles present in the sample. This was followed by sedimentation test, using the jar method, to assess the silt, clay and sand/gravel fractions for the determination of the soil type.

The Casagrande Apparatus method was used in Atterberg Limits test and was conducted in accordance with Clause 7.4.3 of BS 1377 – 1: 1990 [15] to determine the plasticity range of the soil sample. To assess the amount of organic compounds present in the soil that may have an effect on the strength characteristics, the organic matter content test by ignition was performed. For the assessment of the soil's linear shrinkage, Clause 6.5 of BS 1377 – 2: 1990 [15] procedures were followed whiles the specific gravity was determined in accordance with BS 1377: 1990 [15]. Soil compaction test was conducted to determine the optimum water content for moulding of the soil bricks. This was done in accordance with BS 1377 – 1: 1990 [15].

Soil Bricks Production using African Locust Bean Waste Water

A BREPAK earth block press (see Fig. 1) that could deliver pressures of up to 35 MPa for brick production was available at the Wa Polytechnic Civil Engineering laboratory. The soil and water with or without locust bean waste water were thoroughly mixed manually. With four different batches (0%, 25%, 50%, 100 %,), fifteen (15) soil bricks with dimensions 200mm × 150mm × 100mm were produced from each batch (five bricks for compression test, five for abrasion resistance test and five for water absorption test).

Figure 1 BREPAK brick mould

The soil bricks were initially covered with damp plastic sheets and sacks for the first 7 days, according to the shrinkage test results. This was to prevent surface shrinkage cracking due to rapid evaporation which tends to promote undesirable loss and uneven distribution of moisture in the bricks. The plastic sheets were then removed after which the soil bricks were air dried at room temperature of 25°C for the remaining twenty-one (21) curing days.

Testing Methods and Procedures

Experimental tests such as dry density, compressive strength, water absorption and abrasion resistance were conducted on the bricks specimens. Three soil bricks which had no surface cracks visible to the naked eye were selected from each batch for these tests. The bricks were wiped of any dust or loose dirt stuck to them before being tested and the means and standard deviations reported.

Compressive Strength

The compressive strength test was performed in accordance with BS 3921: 1990 [15]. The test was done at the Wa Polytechnic, Civil Engineering Departments laboratory using the compression test machine.

Water Absorption by Capillary

The water absorption by capillary test was conducted according to BS 3921 [15]. The water absorption was measured by the increase in weight for bricks immersed in 5mm depth of water for ten minutes and subsequently the absorption coefficients (C_b) using the equation;

$$C_b = \frac{100 \times (M_1 - M_2)}{S\sqrt{t}} = g/cm^2/min.$$

Source: Centre for Development of Enterprise Guides [16]

Where, $M_1 - M_2$ is the mass of absorbed water in grams, S is the submerged surface area in centimetre square, and t duration of immersion in minutes.

Abrasion Resistance

For the abrasion strength test, BS 3921: 1921 [15] procedures were followed. The test was used to determine the surface hardness of the soil bricks and thus their resistance to wear. The abrasion coefficient (C_u) given by CDEG [16] expresses the ratio of the brushed surface, S (in cm^2) to the mass of the material detach by brushing ($M_1 - M_2$). The bricks were subjected to mechanical erosion applied by brushing with a metal brush in turns at forward and backward motions per about a second for 60 cycles. The mass of the detached (loose) matter was collected and weighed from which the abrasion coefficients (C_u) were calculated

$$C_u = \frac{S}{M_1 - M_2} = cm^2/g$$

III. RESULT AND DISCUSSION

Soil Characteristics

Various laboratory and field tests were conducted on the soil sample used in accordance with BS 1377-1990 [15] so as to determine it characteristics. The tests conducted were sieve analysis, sedimentation test, Atterberg limits, organic matter test, linear shrinkage test and specific gravity test. Table 1 presents the summary of characteristics of the soil used.

Sieve analysis

The results indicated that the soil is well graded with small amount of fine particles. The soil's coefficient of uniformity (C_u) and coefficient of gradation (C_g) were 6.4 and 1.2 respectively. Previous studies found that soil having C_u greater than 6 and C_g between 1 and 3 has its grain size distribution being at the optimum [17]. Thus, in terms of particle size grading, the soil used was well graded (Table 1).

Table 1: Characteristics of the Soil used

S/N	Soil Properties	Results
1	Sieve analysis	C_u = 6.4 and C_g = 1.2
2	Soil grade	Well graded
3	Silt fraction (%)	9
4	Clay fraction (%)	22
5	Sand/gravel fraction (%)	69
6	Soil type	Sandy clay loam
7	Liquid limit (%)	26
8	Plastic limit (%)	15
9	Plasticity index (%)	11
10	Plasticity range	Low plastic clay
11	Organic matter content (%)	1.7
12	Linear shrinkage (%)	3.8
13	Specific gravity	2.8

Sedimentation test

From the sedimentation test results, the soil was found to have a silt content of 9%, clay content of 22% and sand/gravel content of 69% (Table 1).This satisfies the recommendations made by previous studies that, for soil material to be suitable for brick production, the optimum fine content should be about 25% of which more than 10% should be clay [17].

Organic content

The amount of organic compounds present in the soil tested by ignition was 1.7% (Table 1). Past studies have shown that up to 2% organic compound in the soil does not have any significant influence on strength and durability [18].

Linear shrinkage

The linear shrinkage test was to establish the extent to which the soil can shrink and to help the curing regime. The soil recorded a maximum of 3.8% linear shrinkage after 5 days (Table 1). Previous studies showed that soil mixture with a maximum shrinkage of 6% is satisfactory for building purposes [16].

Specific gravity

The specific gravity of the soil tested was 2.8 (Table 1). It has been established that soils with specific gravities between 2.5 and 3.2 are suitable for building purposes [3]. In general, the soil sample used for the experimental studies was suitable for building purposes.

Atterberg limit

The result from the Atterberg limit test indicates that the soil has a liquid limit of 26%, plastic limit of 15% and plasticity index of 11% (Table 1). According to the Commonwealth Experimental Building Station [19] the preferred plasticity index for a soil for bricks, the mixture of gravel, sandy clays and clay loams should be between 10% and 20%. Thus the soil used could be classified as intermediate sandy clay loam as indicated in Figure 2.

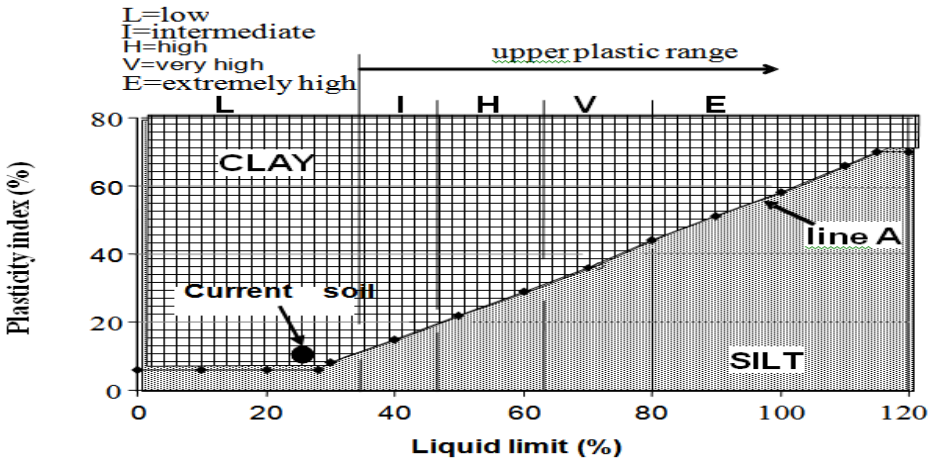

Figure 2: Plasticity Chart for Soil Classification

Soil Bricks Properties

Density

The mean densities of the bricks presented in Table 2, range from 2120kg/m^3 for soil bricks without ALBW content to 2167kg/m^3 for soil bricks with hundred percent ALBW content stabilisation. Previous studies had found that juicy liquid stabilisers enhance compressed soil density more than ash and pulverized stabilisers, hence the results was expected [21]. These values obtained fall within the ranges of 1200kg/m^3 and 2400kg/m^3 recommended by [20] as being suitable for masonry units.

Compressive Strength

From the results presented in Table 2, it is noticed that compressive strength steadily increased as the African locust bean waste water content increases. A compressive strength of 2.38N/mm^2, 3.29N/mm^2, 3.53N/mm^2, and 3.95N/mm^2, were obtained for the specimens A_o, $B_{25,}$ $B_{50,}$ and B_{100} respectively. The compressive strength of stabilised specimens' increased by 66% over the un-stabilised specimens when the soil was fully mixed with African locust bean waste water for bricks production.

This steady increased in compressive strength was expected as previous studies have found that soils stabilised with juicy liquid stabilisers improve the compressive strength more than with ash, pulverized and greasy stabilisers [18] and [21]. It has been found that the compressive strength of soil materials adequate for walls in low-rise and low-cost buildings is between 2N/mm^{2}and 4N/mm^2 [6]. Hence, these bricks compressive strength is within the recommended range and therefore is adequate in terms of strength for low rise buildings.

The compressive strength values and the African locust bean waste water percentage additions were highly correlated with a correlation coefficient, R^2 = 0.851 and this implies that the compressive strength of the soil bricks was highly influenced by the juicy liquid of the ALBWW by 85%. Again, from the regression equation, Y = 0.014 (X) + 2.12 0; where Y = compressive strength (dependent variable) and X = ALBWW content, (independent variable) it is clear that the compressive strength of the soil bricks has positive but weak relationship with the ALBW content. A percentage increase in the ALBWW content would increase the compressive strength of the soil bricks by 1. 4 N/mm^2

Table 2: Dry Density and Compressive Strength of Soil Bricks

ALBWW Content (%)	n	Dry Density (kg)		Compressive Strength (N/mm^2)	
		Mean	**Std. Deviation**	**Mean**	**Std. Deviation**
A_O	5	2120	9.165	2.38	0.234
B_{25}	5	2135	6.083	3.29	0.195
B_{50}	5	2161	11.080	3.53	0.081
B_{100}	5	2167	14.502	3.95	0.262

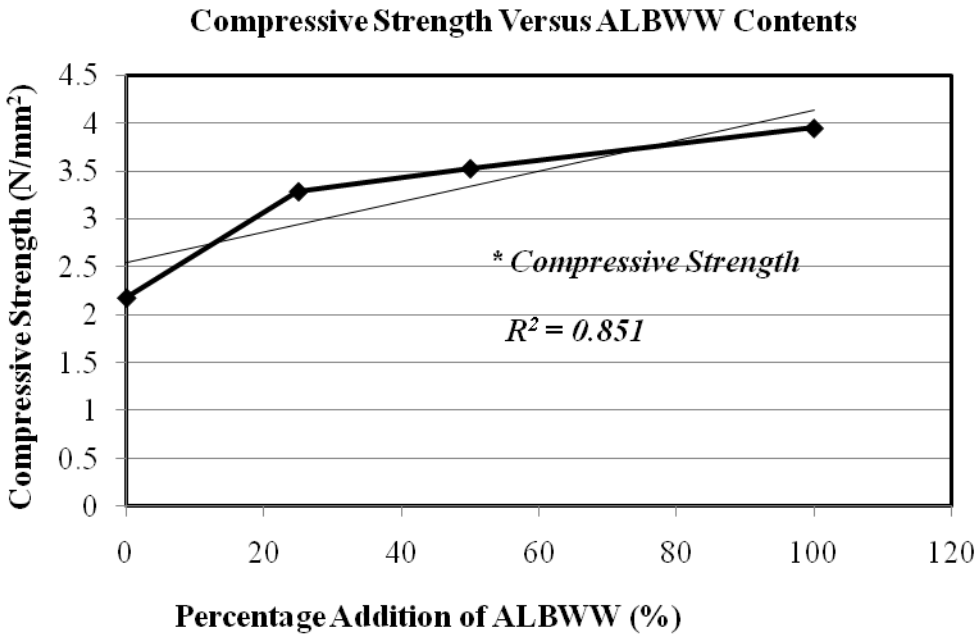

Figure 3: Relationship Between Compressive Strength and

Water Absorption by Capillary

The results given in Table 3, indicates that increasing levels of ALBWW has a steady declining effect on the amount of water absorbed by the bricks, that is, the higher the ALBWW content the less the absorption. The R-square value (0.643) shows that the low ingression of water into the soil bricks is about 64% influenced by the addition of the ALBWW content. From the regression equation obtained, Y = -0.086 (X) + 10.22, it is observed that a fairly negative relationship exists between the ALBW percentage additions and the water absorption coefficients. Hence, a percentage increase in ALBWW content would reduce the water permeating into the soil bricks by 8.6%.

The results confirms previous works that reported that soil with optimum clay content stabilised with agro-based juicy liquids has an increasing effect on density and compressive strength and decreasing effect on water absorption [22], [23] and [21].

Table 3: Water Absorption Coefficients of Soil Bricks

ALBWW Content (%)	Sample 1 (g/cm^2min)	Sample 2 (g/cm^2min)	Sample 3 (g/cm^2min)	Mean (g/cm^2min)	Std Dev.
A_O	7.906	15.969	15.811	13.229	4.610
B_{25}	6.541	5.060	3.004	4.902	1.824
B_{50}	6.166	4.427	3.320	4.638	1.435
B_{100}	3.472	2.842	2.688	3.004	0.418

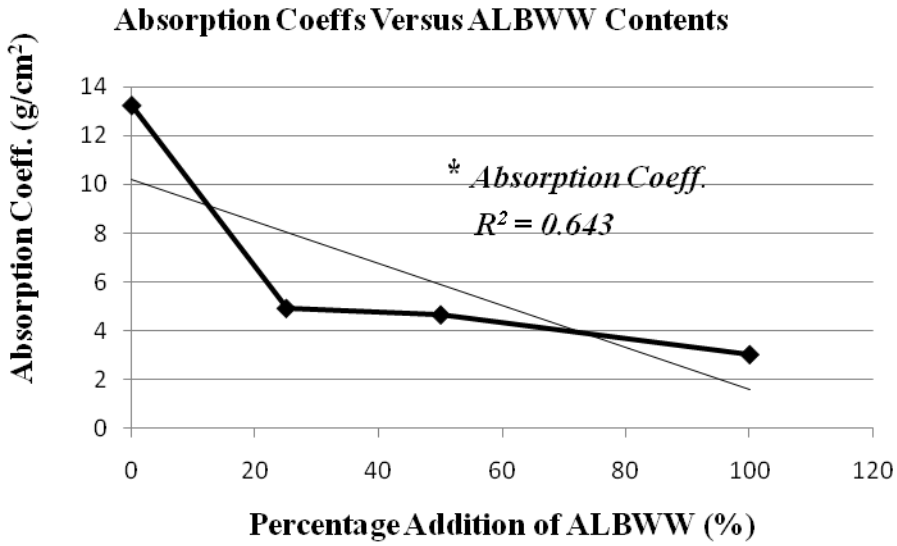

Fig. 4.0: Relationship Between Absorption Coeffs and ALBWW

Abrasion Resistance

The abrasion coefficient for bricks without ALBWW content was $6.45cm^2/g$. This increased steadily to $9.45cm^2/g$ for bricks stabilised with 100% ALBWW (Table 4). A high abrasion coefficient shows that a large brushing area is required to yield a certain amount of discarded material. This then implies that the increase in the ALBWW contents increased the bricks resistance to wear and tear by cutting and erosive agents such as wind, rain, snow, etc. These findings are similar to those of [24] and [21] who observed that agro-based juicy liquid wastes stabilizers increase compacted/compressed soil weight thereby improving its abrasion resistance.

Table 4: Weights and Abrasion Resistance Coefficients of Soil Bricks

ALBWW Contents (%)	Weight Before Brushing		Abrasion Coefficients	
	Mean (g)	Std Dev.	Mean (cm^2/g)	Std Dev.
A_O	2108	0.009	6.45	1. 229
B_{25}	2123	0.006	7.44	1.688
B_{50}	2148	0.010	8.84	1.817
B_{100}	2154	0.014	9.45	1.797

IV. CONCLUSION AND RECOMMENDATION

The results of the study support the conclusion that, the addition of the African locust bean waste water in the soil bricks has steadily improved its strength and durability. Even though the maximum values were achieved at the 100% ALBWW content, the results obtained at the 25% and 50 % ALBWW content met the required recommendations for earth housing. The ALBWW which is environmentally nuisance can be used to replace portable water and also as a stabiliser for masonry units in construction

The study recommended that, to produce cheap and environmentally-friendly stabilised soil specifically for rammed, cob, and wattle and daub walling, the soil type and its suitability must be established before using ALWW as mixing water.

LIMITATION

Hand mixed was used for mixing of the bricks ingredients. It would have been better if concrete mixer was used for the mixing to reduce possible evaporation of both mixing water and the juice stabiliser.

Soil sample was taken from one site near the Wa Polytechnic, it would have been appropriate if samples were taken from different site within the Wa Municipality to ascertain the suitability of the soil in the municipality.

ACKNOWLEDGEMENT

This paper was first published by the West Africa Built Environment Research (WABER) as part of the Conference Proceedings of the 6th WABER Conference, 10 – 12 August, 2015, Accra, Ghana, 373 – 385. The authors are therefore grateful to members of the review panel and scientific committee of WABER for the evaluation and re-evaluation of this paper to ensure quality of content.

REFERENCES

[1] R. Stulz and K. Mukerji, *Appropriate building material: A catalogue of potential solutions 2nd edition* (Swiss Centre for Appropriate Technology Publications St. Gallen, Swertzerland, 1988)

[2] M. Hall, P. Damms and Y. Djerbib, Stabilized rammed earth and the building regulations, 2000' Part A – Structural Stability. *Association of Building Engineers, Building engineer,* 2004, 18 – 21

[3] E. Amsterdam, *Construction materials for civil engineering* (Juta and Co. Limited, Tandym print, Cape Town, South Africa, 2012)

[4] Ghana Business News, *Ghana has 60% housing deficit.* Retrieved on 2/3/2013. Ghanabusinessnews.com/2009/10/08

[5] United Nations Habitat, *Human settlement in crises interlocking stabilised soil block* (Appropriate earth technology in Uganda. SSPP, Nairobi, Kenya, 2009)

[6] G. Browne, *Stabilised interlocking rammed earth blocks:* Alternative to cement stabilisation, Southampton Solent University. Retrieved on 3/3/2013. www.sheltercentre.org/2009

[7] P. P. Yalley and P. Zievie, Stabilization of bricks with shea butter residue for housing. *International Journal of Civil Engineering Research. ISSN 2278 – 3652, Volume 4, Number 3*, 2013, 213 – 222. Research India Publications

[8] M. Alhassan, Potentials of rice husks ash for soil stabilization. Assumption University *Journal of Technology, Volume 11(4),* 2008, 246 – 250

[9] P. P. Yalley and J. Bentle, Stabilisation of soil blocks using ash from sugarcane waste. *Journal of Ghana Institution of Engineers. Volume 6 & 7, Number 1*, 2009, 67 – 76

[10] E. Adam and A. R. A. Agip, *Compressed stabilised earth blocks manufactured in Sudan.* United Nations Education and Cultural Organization. 7 place de fontenoy, 75352 Paris 07 SP, France, 2001, 4 – 27

[11] P. P. Yalley and E. Asiedu, Enhancing the properties of soil bricks by stabilising with corn husks ash. *Civil and Environmental Research, ISSN 2224 – 5790 (paper) ISSN 22250514*

[12] *(Online) Volume 3, Number 11*, 2013

[13] D. Little and S. Nair, Background for development of standard practice for modification and stabilisation of subgrade soils and base courses. *NCHRP 20 – 07*, 2008

[14] R. Akinoso and N. E. El-alawa, Some engineering and chemical properties of cooked locust bean seed (parkia biglobosa). *The West Indian Journal of Engineering, Volume 35, Number 2*, January 2013. ISSN 0511 – 5728, 51 – 57

[15] H. M. Bot, *Evaluation of African locust bean (parkia biglobosa0 pulp for broiler chicken as an energy source* (Department of Animal Science, Faculty of Agriculture, Ahmadu Bello University, Zaria, Nigeria, 2007)

[16] British Standards, *Methods of testing soils for civil engineering purposes, part 1:* General requirements and sample preparation, 1377, 1990

[17] Centre for Development of Enterprise Guides, *Compressed earth blocks testing procedure.*

[18] *A joint Centre for Development of Enterprise* (National Engineering Institute for Public Works of Lyon and CRATerre-EAG Publication, Belgium/France, 2000)

A. Aysen, Soil mechanics; *Basic concepts and engineering applications* (Taylor and Francis groups plc, London, UK, 2005)

[19] H. Houben and H. Guillaud, *Earth construction, CRATerre* (Primer Brussels,CRATerre/PGC/CRA/UNCHS/AGCD, 1984)

[20] Commonwealth Experimental Building Station, *Silicone water-repellents for masonry,Notes on science of building* (NSB 76, Australia, 1970)

[21] T. Morton, *Earth masonry-Design and construction guidelines* (Willoughby road,Bracknell. Published by HIS BRE Press, 2008)

[22] E. Obonyo, Optimising the physical, mechanical and hydrothermal performance ofcompressed earth bricks. *Journal of Sustainability, Volume 3*, 2011, 596 – 604

[23] G. P. McHenry, *Adobe and rammed earth buildings, design and construction* (John Wiley and Sons, Toronto, Canada, 1984)

[24] P. Walker, Performance of stabilised soil blocks masonry under uniform and concentrated compressive loading. *British Masonry Society, Number 7*, London, 1997

[25] G. Minke, *Building with earth: Design and technology of a sustainable architecture* (Birkhauser Publications for Architecture, Boston, 2006)

American Journal of Engineering Research (AJER) 2016
American Journal of Engineering Research (AJER)
e-ISSN: 2320-0847 p-ISSN : 2320-0936
Volume-5, Issue-1, pp-42-48
www.ajer.org
Research Paper Open Access

Two-Part Tariff Model Formulation for Bulk Sale of Energy by Depreciating the Plant Using Declining Value Method

Osita Oputa
Department of Electrical/Electronic Engineering Michael Okpara University of Agriculture, Umudike, Nigeria.

ABSTRACT: *The electric power sector may be aimed at making life meaningful and comfortable for man, but making profit while this is been done cannot be exempted. However, the supplier must keep his tariff at competitive prices to keep his costumers while he makes profit especially in a competitive market. It is important for the bulk seller of electric energy to know the best tariff that can guarantee this from the very start of the business. This paper shall develop a mathematical model the bulk electricity seller can use in fixing a two-part tariff that will be both profitable to himself and affordable to his customers. This model will be developed on the basis of depreciating the power generating plant by the diminishing value method of calculating depreciation. This model reveal how a 490MW power generating plant of $480 million installation cost with a life span of 42 years and a targeted $24 million profit at the end of the investment (the end of the plant useful lifetime) can be archived by using a two-port tariff. Testing of the developed model revealed tariffs of $6.4385/kWh and $0.0018/kWh as variable and fixed tariff respectively for the first to three years of plant life time. At the plant's last three years of existence, the energy bulk seller sells energy at variable energy tariff as $5.4882/kWh and $0.00882/kWh as fix energy tariff. With this, the investor can know how to set and vary energy tariff that can generate his expected profit at the end of the investment.*

Key word: *Model fixing two-port tariff.*

NOMENCLATURE

IC	Installation cost of the Plant ($).
S	Salvage value of plant after m years ($).
m	Lifetime of the plant (years)
CD_g^h	Cash deposit to be made for between year 'g' and 'h' ($).
x	Rate of depreciation per annum.
n, g, h	1, 2, 3 ……. year.
V_n	Value of plant after n^{th} year.
TI	Cash paid for tax and insurance per annum($).
r	Interest rate (% of IC).
I	Interest paid on capital per annum ($).
MC	Expected/estimated maintenance cost per annum ($).
MPD	Maximum power delivered (MW)
K	Fix tariff ($/kWh).
t_g^h	Variable tariff for 'g' to 'h' year ($/kWh).
SW	Expected salaries/wages per annum ($).
M	Expected Miscellaneous expensive per annum ($).
P_T	Expected total profit to be made in the investment ($).
P	Expected profit to be made per annum ($).
a	% of installation cost to be made as profit by investor
FC	Annual Cost of fuel burnt ($)
Lf	Load factor

I. INTRODUCTION

The rate at which electric energy is sold to consumers is known as tariff. Fixing tariff for bulk sale of electricity especially in a competitive market shall be examined in this paper; a two-part tariff plan shall be considered in this paper. This two-part tariff consists of the fix and variable tariffs. The bulk sellers of electricity are the generation companies selling energy to transmission companies. For a market with many sellers and buyers of this commodity, the tariff of the electricity sold by these generation companies should be done considering among others the following.

(i) Ability/Willingness of the consumer to pay
(ii) Cost of generating and transmitting of the electric energy (which comprise of the fixing and running cost);
(iii) Quality of Services rendered.

Out of the above three factors, the second factor is the only factor that is quantifiable [1].

At the end of the useful life time of the power plant, it should be replaced so as to keep the supplier in business; hence, cash allocation for the replacement of the plant should be in considered while the plant running healthy. Inflation and interest rates should also be strongly considered when fixing tariff. This is because these monies set aside for the replacement of the power plant will have appreciated by the time the replacement is due. Also, inflation may catch up with the monies reserved for the plant replacement.

In this paper, the plant will be depreciated using the declining value method. In this method, the value or worth of the plant at the end of the first year is taken as the worth of the plant at the beginning of the second year and so on.

1.1 ADVANTAGES OF THE DEPRECIATING THE PLANT BY DECLINING VALUE METHOD

1. The value of the plant at the beginning of every year is not taken as the initial or installation cost but as the value of the worth at the end of the preceding year.
2. This method gives higher tariffs at the initial stage of the business when the plant efficiency is high and encouraging to costumers.

1.2 DISADVANTAGES OF THE DEPRECIATING THE PLANT BY DECLINING VALUE METHOD

1. The method does not take appreciation of deposit made at early stages of the plant into consideration at the time when the plant will be salvaged.
2. This method is associated with high tariff at the initial stage of the business. It is bad to give more financial obligations to a new business with little customers by setting high initial tariff.
3. The early stage encounter the challenge from the manufacturer's error which may cause reduced reliability; hence, setting high tariff at this stage may not be fair.

II. MODEL FOMULATION FACTORS

The formulation of the model to be used to determine electric energy bulk sale will depend on a number of parameters. These among others include

1. Cost of fuel source to be burnt during the period under analysis.
2. Taxation and Insurance.
3. Depreciation of the power plant over its expected useful life time.
4. Interest payable on invested capital.
5. Expected profit (a percentage of the invested capital).
6. Expected energy to be generated in the period under analysis.
7. Estimated maintenance cost during the period under analysis.
8. Estimated salaries and wages of staffs throughout the period under analysis.
9. Load factor.

2.1 Expected Annual Cost of Fuel Source

This is the cost of the primary source of fuel burnt annually for the generation of the expected power. The actual quantity of fuel will not be constant for the entire life time of the plant. As the plant is ageing, the expected fuel cost per annum of running the power will be increasing as long as the net output power of the plant will be unchanged. To compensate for this increase, 2% rise in fuel consumption will be adopted at the end of every ten years of the plant's life time.

For first three years of the plant (0-3 years), annual cost of fuel burnt is $FC.

The plant life of 04 -06 years, annual cost of fuel burnt is $1.02FC.

Between 07-09 years, annual cost of fuel burnt is $1.04FC and so on.

2.2 Cash reservation due to depreciation

They say nothing last forever; so, the plant that is commissioned for use today that is expected to run for a useful life time of 'm' years will surely be uneconomical in the power generation business after its useful life time. Hence, a good businessman will make reservation to replace the power generating plant be the end of its useful life. The cash reservation should be made during the useful life time of the plant.

In this paper, the declining balance depreciation method will be used for computing monies to be set aside for cash reservation for the replacement of the plant at the end of its useful working years.

Using the declining balance depreciation method, the value of the plant at the end of the n^{th} year is

$$V_n = (1-x)^n IC \quad (1)$$

Where $x = 1 - \left[\frac{s}{IC}\right]^{\frac{1}{m}}$ (2)

Hence, the cash deposit to be made at the end of each year is

$$CD = V_k - V_{k-1} \quad (3)$$

The deposited cash for any 3 consecutive years is,

$$CD_{k-3}^{k} = [V_k - V_{k-1}] + [V_{k-1} - V_{k-2}] + [V_{k-2} - V_{k-3}] \quad (4)$$

2.3 Servicing of interest due to collected loan

Most businessmen will never invest with their own capital; they will rather take loans from the banks. These loans will have to be serviced and the servicing must be included in the model formulation for fixing of the tariff.

2.4 Estimated maintenance cost

This includes all expected daily, weekly, monthly and annual maintenance expenditures that will be made during the period under analysis for the running of the plant. It include expected rotten plant inspection and maintenance cost. This will not be constant all through the life time of the plant, as the plant is aging, maintenance activities on the plant will be more frequent; hence, the maintenance cost of the plant per annum should increase by a percentage, say 10% in every 3 years.

2.5 Expected Profit

The profit the investor should want to make is a major determinate of the tariff of the power that will be generated. No doubt, the profit should be such as to encourage investment in the power sector; but the investor should place his profit margin in such a way that consumers will be willing to buy his power (especially in a competitive market). The profit should be a very small percentage of the investment cost and should be spread throughout the lifetime of the plant.

$$P_T = a\%\ of\ IC = \frac{a(IC)}{100} \quad (5)$$

As this will be spread throughout the lifetime of the plant, a profit of

$P = \frac{a \times IC}{100m}$ will be made each year.

2.6 Load factor

In the running of the power plant during the period under analysis, it is certain that the plant maximum power (plant capacity) will not be demanded throughout this period; at some times, an average load will be demanded from the plant. The load factor is the ratio of the expected average load demanded from the plant to the expected maximum load demanded during this period.

$$Lf = \frac{expected\ average\ power\ demanded}{expected\ maximu\ power\ demanded} \quad (6)$$

In actual fact, the Lf decreases as the plant is aging.

2.7 Period Under analysis

Cost of fuel throughout the life time of the plant cannot be the same; this can be due to inflation and increase of fuel cost, ageing of the plant among others. This period could vary from plant to plant depending on the source of fuel (most importantly). For example, a gas turbine plant uses natural gas whose price is control by the international market and could change easily, analysis of such plant should not exceed three to five years at a time. In this paper, a three-year analysis period shall be used.

2.8 Wages and salaries (SW)

An estimate of what should be spent annually on salaries and wages should be known from the start of the business.

2.9 Fixed Charge or Tariff (K)

The electric power supplied by any plant is not constant; hence, it will be beneficial for any generation company to charge his client by using a two part tariff – the fix and variable charges. The fix charge is the amount paid by the client when ever power is supplied to the client irrespective of the power supplied; i.e, this tariff does not varies with the power supplied. In this paper, the fix tariff will be slightly increased by +0.3 at the beginning of a new the period of analysis from the preceding one (say 3 years as will be used in this paper).

III. MODEL FORMULATION

As stated earlier, a 3-year analysis period shall be used in this paper. However, using a smaller time frame will result more number of equations but will give more accurate results. Now combining all the expensive incurred in running the plant for a 3-year interval plus 3 times the expected annual profit; should be equal to the total money realized from sale of energy for the 3 years.

Considering the first 3 years of the plant,

$$CD_1^3 + 3TI + 3MC + \frac{3r1C}{100} + 3FC + 3M + 3SW + \frac{3a1C}{100m} = Lf \times MPD \times 3 \times t_1^3 \times 8.76 \times 10^3 + 3 \times 8.76 \times 10^3 K \quad (7)$$

The nest 3 years,

$$CD_4^6 + 3TI + 3.1MC + \frac{3r1C}{100} + 3.02FC + 3.1M + 3SW + \frac{3a1C}{100m} = Lf \times MPD \times 3 \times t_4^6 \times 8.76 \times 10^3 + 3 \times 1.3 \times 8.76 \times 10^3 \times K \quad (8)$$

.

.

.

.

The last (k^{th}) three years

$$CD_{k-2}^k + 3TI + 3MC + \frac{3x1C}{100} + 3 \ldots FC + 3 \ldots M + 3SW + \frac{3a1C}{100m} = Lf \times MPD \times 3 \times t_{k-2}^k \times 8.76 \times 10^3 + 8.76 \times 10^3 \times 3 \ldots \times K \quad (k)$$

.

The sum of the RHS of equations (7) to (k) is the sum of the present worth of the installation cost and the total profit to be made at the end of the investment by the investor.

$$Lf \times 3 \times MPD \times 8.76 \times 10^3 \times \left[t_1^3 + t_4^6 + \cdots + t_{k-2}^k\right] + 3 \times 8.76 \times 10^3 \times [K + 0.3K + \cdots + .. \times K] = IC + P_T \quad (9)$$

IV. ASSUPTIONS MADE IN MODEL

DEVELOPMENT

1. It was assumed that the maximum output power delivered by the plant will be constant throughout its useful lifetime.
2. The system is free from inflation.

V. MODEL TESTING

The model developed in this paper shall be tested with Nigeria's first ever Independent Power Plant (IPP), capable of generating 490MW of electricity, commissioned by Former Nigerian President Olusegun Obasanjo at Okpai in Delta State. This plant has a capital cost of $480million and uses 75 million standard cubic feet of gas per day (scfd) for its operation.

The parameters of the power plant are given below

TABLE 1: PLANT'S DATA (Source: [5])

ITEM	VALUE	ITEM	VALUE
IC	$480M	S	$30M
TI	$25,000	MC	$50,000
M	$100,000	SW	$200,000
Lf (0-70% of lifetime)	0.896	Lf (71-100% of lifetime)	0.850
FC	$1,200	MPD	460MW
r	5%	m	30 years
x	8%	a	5%
P_T	$24M		

Using these data,

$$x = 1 - \left[\frac{s}{IC}\right]^{\frac{1}{m}} = 0.064 \qquad (10)$$

The cash deposits for every three years is given below

TABLE 2: COMPUTED CASH DEPOSIT TO BE MADE IN STATED PERIODS

PERIOD (YEAR)	CASH DEPOSIT ($)
1 – 3	86.39
4 – 6	70.83
7 – 9	58.10
10 – 12	47.63
13 – 15	39.07
16 – 18	32.03
19 – 21	26.27
22 – 24	21.54
25 – 27	17.66
28 – 30	14.12
31 – 33	11.88
34 – 36	9.74
37 – 39	7.99
40 – 42	6.55

The plant tariff model for first to three years is

$$CD_1^3 + 3 \times 25{,}000 + 3 \times 50{,}000 + \frac{3 \times 0.08 \times 480 \times 10^6}{100} + 3 \times 1{,}200 + 3 \times 100{,}000 + 3 \times 200{,}000 + \frac{3 \times 0.05 \times 480 \times 10^6}{100 \times 42} = 0.896 \times 460 \times 10^3 \times 3 \times t_1^3 \times 8.76 \times 10^3 + 3 \times 8.76 \times 10^3 \times K$$

(11)

Tariff model for 4^{th} to 7^{th} years is

$$CD_4^7 + 3 \times 25{,}000 + 3 \times 1.2 \times 50{,}000 + \frac{3 \times 0.08 \times 480 \times 10^6}{100} + 3 \times 1{,}200 + 3 \times 1.2 \times 100{,}000 + 3 \times 1.05 \times 200{,}000 + \frac{3 \times 0.05 \times 480 \times 10^6}{100 \times 42} = 0.896 \times 460 \times 10^3 \times 3 \times t_4^6 \times 8.76 \times 10^3 + 3 \times 8.76 \times 10^3 \times 1.3 \times K \quad (12)$$

.

.

.

$$CD_{40}^{42} + 3 \times 25{,}000 + 3 \times 3.6 \times 50{,}000 + \frac{3 \times 0.08 \times 480 \times 10^6}{100} + 3 \times 1{,}200 + 3 \times 3.6 \times 100{,}000 + 3 \times 1.65 \times 200{,}000 + \frac{3 \times 0.05 \times 480 \times 10^6}{100 \times 42} = 0.850 \times 460 \times 10^3 \times 3 \times t_{40}^{42} \times 8.76 \times 10^3 + 3 \times 8.76 \times 10^3 \times 4.9 \times K \quad (24)$$

and

$$460 \times 10^3 \times 8.76 \times 10^3 \times [0.896 \times (t_1^3 + t_4^6 + t_7^9 + \ldots . + t_{28}^{30}) + 0.850 \times (t_{31}^{33} + \cdots + t_{40}^{42})] + 10 \times 8.76 \times 10^4 \times K[1 + 1.3 + 1.6 + 1.9 + \ldots . 4.9] = IC + P_T \quad (25)$$

Finding the solution to these fifteen set of equations (11 – 25) using MATLAB gives the following values:

TABLE 3: OBTAINED VARIABLE AND FIX TARIFFS FOR STAGES OF PLANT

t_1^3	6.4385
t_4^6	6.2925
t_7^9	6.1752
t_{10}^{12}	6.0809
t_{13}^{15}	6.0061
t_{16}^{18}	5.9467
t_{19}^{21}	5.9003
t_{22}^{24}	5.8644
t_{25}^{27}	5.8371
t_{28}^{30}	5.8133
t_{31}^{33}	5.5048
t_{34}^{36}	5.4958
t_{37}^{39}	5.4905
t_{40}^{42}	5.4882
K	0.0018

Using these results, the tariffs for the respective periods can be formulated as given in table 4.

TABLE 4: TARIFF FOR PERIODS UNDER ANALYSIS

S/N	PERIOD (YEAR)	VARIABLE TARIFF ($/kWh)	FIX TARIFF ($/kWh)	TOTAL TARIFF ($/kWh)
1	1 – 3	6.4385	0.00180	6.4403
2	4 – 6	6.2925	0.00234	6.2948
3	7 – 9	6.1752	0.00288	6.1781
4	10 – 12	6.0809	0.00342	6.0843
5	13 – 15	6.0061	0.00396	6.0101
6	16 – 18	5.9467	0.00450	5.9512
7	19 – 21	5.9003	0.00504	5.9053

8	22 – 24	5.8644	0.00558	5.8700
9	25 – 27	5.8371	0.00612	5.8432
10	28 – 30	5.8133	0.00666	5.8200
11	31 – 33	5.5048	0.00720	5.5120
12	34 – 36	5.4958	0.00774	5.5035
13	37 – 39	5.4905	0.00828	5.4988
14	40 – 42	5.4882	0.00882	5.4970

VI. ASSUMPTIONS MADE IN THE SYSTEM ANALYSIS.

1. Dollar rate of 2003 was used in the analysis.
2. An assumed Interest rate of 8% of the capital was used for the analysis.
3. A life span of 42 years was used as the actual 30 years was for when the plant 24 hours per day for its entire life time which is practically impossible as a result of shunt down during maintenance, e.t.c.
4. The fuel here is a by-product of petroleum exploration; hence, no increase over the years was taken into account as most part of the fuel cost is the capital cost of the gas line from the flow station where the petroleum exploration is taking place to the gas plant.
5. A profit of 5% of capital cost of the project was assumed to be targeted by investor.
6. It was assumed that the fixed tariff will be increasing at a rate of 30% at the end of every 10 years.

VII. DISCUSSION OF RESULTS

As observed, the energy tariff at the first three years was highest with total tariff at \$6.4403/kWh (\$6.4385/kWh and \$0.0018/kWh for variable and fix charges respectively). The investor's plant operates at its highest efficiency at this stage and therefore provides the best services to energy buyers; his product will therefore be highly demanded and will get good patronage at that price. As time goes on, say between sixteen to eighteen years, the efficiency of the plant will not be as in the first three years, there will be more frequent turn around maintenance resulting to frequent outage. The investor tries to keep his business and costumers by crashing his energy tariff to a total of \$5.9512/kWh (\$5.9467/kWh and \$0.0045/kWh for variable and fix charges respectively). The tariff continue declining as systematically planed until the last three years of the plant when the tariff becomes a total of \$5.4970/kWh consisting of variable energy tariff as \$5.4882/kWh and \$0.00882/kWh as fix energy tariff. With this, the investor is fully aware that at the end of the 42-year period, he will make a total profit of 5% of the installation cost of the project. He also knows how to place his tariff at any particular time throughout the plants so as to make his desired profit.

VIII. SUMMARY

By using this model, a proper plan can be made by any investor of how he can fix his energy tariff from the start of the power plant working life to the end its end that will generate the extract or desired profit the investor wishes to make. The implication of using this model in a country like Nigeria is that energy tariff may rise unless governments will as usual subsidence it for her citizens.

REFERENCES

[1] Fred Espen Benth, Valery A Kholodnyi and Peter Laurence. Quantitative Energy Finance Modeling, Pricing and Hedging in Energy and Commodity Markets. Springer new York Heidelberg Dordrecht, London, pp 41 – 80. 2014

[2] Gupta J. B. Generation and Economic Considerations. S. K. Kataria and Sons, Delhi – 110006, India, pp 245 - 306. 2009.

[3] S. L. Uppal and S. Rao. Electrical Power Systems. Khanna Publishers, New Delhi – 110002, pp 234 – 248. 2009.

[4] B. L. Theraja and A.K. Theraja. A Textbook of Electrical Technology. S. Chand and Company Ltd. Ram Nagar, New Delhi – 110 055, pp 1567 – 1616. 2000.

[5] Nigeria Independent Power Plant (NIPP) Okpai, Kwalle, Delta State Data book (2003), pp 349 – 356).

[6] Rick Tidball, Joel Bluestein, Nick Rodriguez, and Stu Knoke. Cost and Performance Assumptions for Modeling Electricity Generation Technologies. National Renewable Energy Laboratory 1617 Cole Boulevard Golden, Colorado. 2010.

[7] Pavla MANDATOVA, Gunnar LORENZ,. Network tariff structure for a smart energy system. A EURELECTRIC paper. 2013.

[8] Seth B. Darling, Fengqi You, Thomas Veselka and Alfonso Velosa. Assumptions and the Levelized Cost of Energy for Photovoltaics.

[9] Gupta J. B. A Course in Power Systems. S. K. Kataria and Sons, Delhi – 110006, India, pp 280 – 314. 2007.

[10] Richard G. Newell and Juha Siikamäki. Nudging Energy Efficiency Behavior -The Role of Information Labels. Discussion Paper, RFF DP 13 – 17. 2013.

[11] Samantha DeMartino, David Le Blanc. Estimating the Amount of a Global Feed-in Tariff for Renewable Electricity. DESA Working Paper No. 95. 2010.

[12] Rudra Pratap. Getting Started with MatLab, A Quick Introduction for Scientists and Engineers. Indian Edition. Oxford University Press. Pp 15 – 73. 2000.

American Journal of Engineering Research (AJER) 2016
American Journal of Engineering Research (AJER)
e-ISSN: 2320-0847 p-ISSN : 2320-0936
Volume-5, Issue-1, pp-49-61
www.ajer.org
Research Paper Open Access

Characterization and assessment of heavy metal pollution levels in soils of Dana steel limited dumpsite, Katsina state, Nigeria using geo-accumulation, ecological risk and hazard indices.

S. Bello[1], Y. I Zakari[2], I.G.E Ibeanu[3] and B.G Muhammad[1]
[1] *Department of Physics, Umaru Musa Yaradua University Katsina. Katsina state, Nigeria*
[2] *Department of Physics, Ahmadu Bello University Zaria. Kaduna State, Nigeria.*
[3] *Center for energy research and training, Ahmadu Bello University Zaria. Kaduna State, Nigeria.*

ABSTRACT: *This study was carried out to quantitatively assess the heavy metal pollution level of soils collected from Dana steel limited dumpsite, katsina state, Nigeria using Potential ecological risk index, Hazard quotient and geochemical accumulation index.. Soil samples were collected from the dumpsite and control site at depths ranges 0- <20cm,20- <40cm,40-<60cm and 60-<80cm.Flame Atomic Absorption spectrophotometry (FAAS) was used to obtain the composition and Concentration(mg/kg) of the eight studied heavy metals (Zn, Cu, Cd, Co, Ni, Cr, Pb and As).the obtained concentrations(mg/kg) were compared with the WHO and Romanian guidelines for the legal permissible heavy metal concentration in soils. Based on these guidelines, it has been established that all the observed heavy metals in the dumpsite soils have concentrations above the WHO limit except Cobolt, world median and the Romanian threshold values. The concentrations of the heavy metals analyzed were subjected to computations of ecological risk index (ERI), geochemical accumulation index (I-geo) and hazard quotient. The obtained results were subjected to Univariate descriptive statistics. The mean geochemical accumulation index characterizes Zn and Cu in the moderate category, while Ni, Co, Cd and As in the unpolluted category. The mean Ecological risk index characterizes Zn, Ni and Cd in low potential ecological risk and Cu in considerable ecological risk. The mean Hazard quotient classifies all the studied metals in the polluted category. Inter-element correlation was observed among the concentrations of the studied heavy metals in the dumpsite and in the control area. The results reveal the pollution potential of the industrial waste dumping which suggested that the dumpsite was seriously contaminated with all the observed heavy metals and the need for proper waste management and immediate implementation of remediation measures by the relevant authority to avert the consequences that it can pose on public health and environment.*

KEY WORDS: *Heavy metals, flame AAS, pollution, ERF, HQ, I-geo*

I. INTRODUCTION

Heavy metal is term used to describe a wide group of metallic elements with density equal or greater than 5g/cm3.such metals include Cadmium, Copper, Chromium, Lead, Nickel, Iron etc. they are trace elements when their occurrences in the environment is less than 0.2ppm.they are generally associated with pollution and toxicity (Knight et al,1997).Trace metals occur naturally in soils (but rarely at toxic levels),sedimentary deposits and water bodies; therefore, there are normal background concentrations of these metals. These metals also find their way into soils, vegetation, water bodies and sediments through airborne particulate matter in the form of dust and vehicular emission. The pace and scale of environmental contamination by industrial activities have steadily increased in the last two centuries due to the pronounced industrial revolution (Stigliani et al.,1991).hence 40% of the USEPA's national priority list involved heavy metal contamination associated with industrial activities (Fostner,1995) and 70% of all the metal contaminated sites involve two or more heavy metals.

Anthropogenic activities usually create wastes which constitute risks to the environment and public health, as a result of the way these wastes are handled, stored, collected and disposed off .in the urban areas, especially a rapidly urbanizing city like katsina, problems and issues of solid waste management are of immediate importance. the rapid population growth presents serious challenge to the authorities, so much that when wastes are collected they are disposed off in uncontrolled dumpsites and/or burnt, polluting water resources and air (Onibokun A.G et al, 2000: Srivastava, 2012).Dana steel limited is not an exception since the steel rolling activity has been known to be one of the most anthropogenic source of heavy metals in soil.

The Dana steel limited dumpsite has been densely engaged with various industrial wastes (see plate1 and 2) which can consequently introduce some traces of heavy metals in to the environment. These wastes may expose near-by residents, scavengers, passers-by, staff and suppliers of raw materials to undue burden of heavy metals and may affect lots of people if it succeeds in polluting ground water which is extensively used in katsina for various purposes or are washed by rain and carried into the water channels or transported by wind.

The aim of the present work is to characterize Dana steel limited dumpsite soil samples for Zinc, Copper, Cadmium, Chromium, Lead, Cobolt, Arsenic and Nickel composition and concentration so as to characterize their pollution level using geo-accumulation index, ecological risk index and hazard quotient.

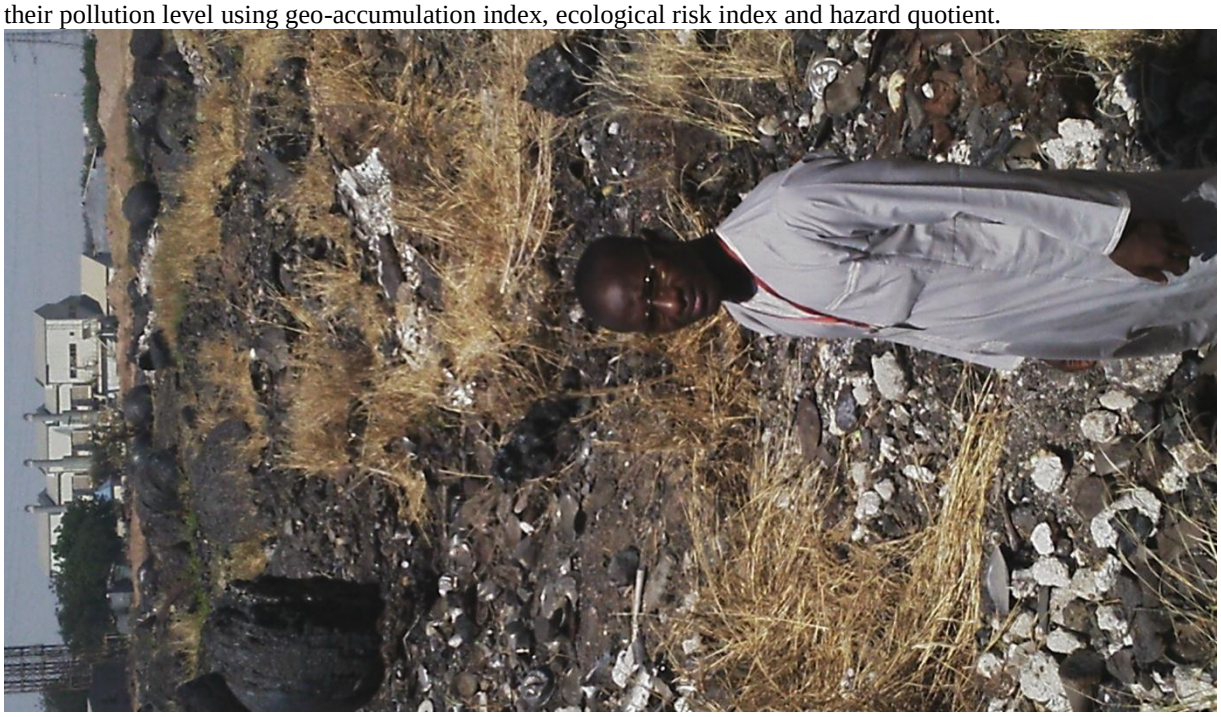

Plate 1: Dumpsite Studied showing the discarded waste generated by the steel rolling activity.

Plate2: the plate showing the dumpsite and the water way that link to river Ginzo .Note the dumpsite in higher altitude than the water way

II. MATERIALS AND METHODS

2.1 Study Area: (Description and sampling techniques)

Dana steel limited dumpsite is located in latitude 12º 57¹ 43¹¹N to 12º 58¹ 7¹¹N, Longitude 7º 37¹11¹¹E to 7º 37¹ 16¹¹E and altitude 522.5m to 616.6m in Katsina state of Nigeria. The dumpsite was partitioned into nine (9) grid points labeled A-I. Soil samples were collected from each grid according to depth using hand auger. The depths were designated 1, 2, 3 and 4 which stands for 0- <20cm, 20- <40cm, 40-<60cm and 60-<80cm respectively. Nine (9) soil samples were collected from each depth making a total of 36 samples. Samples 1-9, 10-18, 19-27 and 28-36 were collected from depths 1, 2, 3 and 4 respectively. Control samples were collected at a distance of 3km away from the dumpsite. After removal of stones and some metal scraps, each soil sample was packed into its own secure water tight polythene bag to prevent cross contamination.

2.2 Sample preparation and analysis

All soil samples were air-dried at ambient laboratory temperature. Soil samples were grounded using mortar and pestle and sieved to pass through 2 mm sieve and stored for chemical analysis. With the aid of spatula and weighing bottle, 0.5g of each soil sample was obtained. This was placed in a Teflon beaker and transferred to a fume-cupboard for digestion. The digestion was carried out using concentrated nitric (10mL) and concentrated perchloric (5 mL) acids in the ratio of 2:1 and the oven was maintained at 200 ^{o}C. After one hour, the mixture was allowed to cool before leaching the residue with 5 cm3 of 20% HNO3. Digested samples were then filtered and made up to 100 mL with deionized water. A blank determination was treated in the Atomic Absorption Spectrometer but without sample. Solution of samples were then taken and aspirated into Atomic Adsorption Spectrophotometer (Unicam Solar A.A.S 969 model) for analyzing metals. Blank determination was also carried out as in a similar way as described above except for the omission of the sample. A calibration graph was plotted for each element using measured absorbance and the corresponding concentration. The calibration curve was used to determine the concentration of the metal.

2.3 Heavy metal pollution characterization

2.3.1 Maximum permissible heavy metal concentration in soil.

The maximum threshold heavy metal concentration (mg/kg) in soil designated by the world health organization (WHO) and the Romanian guideline is tabulated in table 1 and 2 respectively.

Table1: Maximum Allowed concentration limits of some toxic metals in soil (mg/kg) (WHO, 1996)

TOXIC METAL	WHO Maximum Allowed limits(mg/kg)
Nickel(Ni)	80
Copper(Cu)	30
Cadmium(Cd)	3.00
Chromium(Cr)	100.00
Lead(Pb)	100.00
Zinc(Zn)	300

Table2: Romanian guidelines on toxic metals level permitted in soil for pollution assessment (Romanian, 1997).

Element	Literature values		Romanian norms				
	European median in soil	World median	NV*	ALS*	ALLS*	ITS*	ITLS*
As	7.03	6	5	15	25	25	50
Cd	0.145	0.35	1	3	5	5	10
Cr	60	70	30	100	300	300	600
Cu	13	30	20	100	250	200	500
Ni	18	50	20	75	200	150	500
Pb	22.6	35	20	50	250	100	1000
Zn	52	90	100	300	700	600	1500

*: NV=normal value; ALS and ITS=Alert level and Intervention threshold in the sensitive area: ALLS and ITLS=Alert level and Intervention threshold in the less sensitive area.

2.3.2 Geo-accumulation index

Geo-accumulation index is used to quantify the degree of anthropogenic or geogenic accumulated pollutant loads in soil and can be determined through the following formula:

$$I_{geo} = log_2(C_n/1.5B_n) \quad \text{.....(1)}$$

Where, C_n and B_n are the determined concentration of metals in the target and reference areas respectively. The factor1.5 is possible anthropogenic variations of contaminants in reference areas (Lokeshwari and Chandrappa 2006; Fagbote and Olanipekun 2010).The classification of the index is tabulated below

Table3: Classification of geo-accumulation Index (after: Hakanson, 1980)

Geo accumulation Index	Classification	Level of Contamination
5＜I geo≤10	6	Extremely Serious
4＜I geo≤5	5	Strong to Extremely Serious
3＜I geo≤4	4	Strong
2＜I geo≤3	3	Moderate to Strong
1＜I geo≤2	2	Moderate
0＜I geo≤1	1	Light to Moderate
I geo≤0	0	Non Contamination

2.3.3 Ecological risk factor

Ecological risk index (ERI) is critical to measure both risk factor and metals concentrations in soil. The potential ecological risk index can be determined through the following formula:

$$ERI = CF * TRF \quad \text{.....(2)}$$

Where ERI is the potential ecological risk factor/index, TRF represents the toxic-response factor, and CF represents contamination factor. The toxic response values for some of the toxic and trace elements are As=10, Cr=2, Cd=30, Cu=5, Pb=5, Ni=5, and Zn=1 as suggested by Hakanson (1980).

The Potential ecological risk assessment PERI as established by Hakanson (1980) is made using the following components.

(a)Contamination Factor (CF)

Contamination factor (CF) is also called single pollution index (PI).Contamination factor is the quotient obtained by dividing the concentration of metals related to the target area by reference area. Their results are mostly associated with single pollution load, while their n-root was used for integrated pollution load index. The contamination factor can be calculated through the following formula as suggested by Harikumar et al. (2009).

$$CF = C_n/B_n \quad \text{.....(3)}$$

In the above equation, C_n is the concentration of metals in the target area, and B_n is the metals concentration of the reference area. the classification is tabulated below:

Table4: Classification of contamination factor (Hakanson, 1980)

Contamination factor	Classification
CF<1	Low
1≤CF<3	Moderate
3≤CF<6	Considerable
CF≥6	Very high

The degree of contamination (DC) of one determined area is the sum of all Contamination factors:

$$DC = \sum CF \quad \text{.....(4)}$$

Table5: Classification of degree of contamination (Hakanson, 1980)

Degree of Contamination	Classification
DC<1	Low
1≤DC<3	Moderate
3≤DC<6	Considerable
DC≥6	Very high

(b) Potential ecological risk (PER): is given by

$$PER = TRF * CF \ldots\ldots\ldots\ldots\ldots\ldots\ldots\ldots (5)$$

This is calculated separately for each metal. The results classifications are as follows:

Table6: Classification of Potential ecological Risk factor (Hakanson, 1980)

Potential Ecological Risk	Classification
PER<40	Low
40≤PER<80	Moderate
80≤PER≤160	Considerable
160≤PER≤320	High
PER≥320	Very high

2.3.4 Hazard Quotient

The soil Hazard Quotient (HQ) is the ratio of the heavy metal concentration of surveyed soil samples to reference permissible limit and is computed using the relation;

HQ=Cc/Cp …….(6)

Where, Cp and Cc = reference maximum permissible limit of heavy metal concentration and the concentration obtained in the sampled area respectively.

III RESULTS AND DISCUSSION

3.1 Heavy metals concentration in soils

Table 7 and 8 presented the average concentrations of each of the studied heavy metals in the target and control area respectively. The average concentrations observed in the target area were seriously higher than that in the control area for all the studied heavy metals except Co. The Average concentrations in the target and control area were compared with the world health organization guideline on the maximum limits of toxic metals in the soils (WHO, 1996) as provided in table1.All the observed toxic metals in the target area were found to have concentrations above the WHO limit, while in the control area the concentrations were below the WHO limit. Zn, Cu, Cd, and Cr were found to have concentrations greater than 3 times the recommended WHO limit ,Pb was 2 times greater and Ni was Slightly(7%) above the WHO limit. The obtained concentrations of the toxic metals (mg/kg) in the dumpsite and in the control area were compared with the Romanian guideline for the allowed maximum normal legal concentration values in soils and the world median value as presented in table 2. Base on this guideline and the obtained concentrations in the target area, it could be deduced that (i) Zn, Pb, Cr and Cd concentrations (mg/kg) in the target area exceeded the world median and Intervention threshold for sensitive area. (ii) Ni and Cu exceeded the world median and the Alert level in the sensitive area. (iii) As was below the world wide median. While the concentrations in the control area were (i) Zn, Cu, As, and Pb were within the normal value (ii) Ni, Cd and Cr where above the normal legal value.

Table7: Univariate descriptive Statistics of the concentration of the heavy metals in the dumpsite (mg/kg) (n=36)

Toxic metal	Mean	Minimum	Maximum	Standard deviation
Zn	646.228	108.200	1189.400	340.562
Cu	175.278	0.800	841.000	206.6223
Ni	85.844	10.600	337.400	77.450
Cd	15.022	0.400	31.400	7.314
Co	62.361	6.800	82.200	18.590
Cr	1096.296	800.000	4800.00	912.090
As	0.564	0.430	0.740	0.081
Pb	202.100	91.000	818.200	208.116

Table8: Univariate descriptive statistics of the toxic metals concentrations (mg/kg) in the control area(n=4).

Statistical parameter	Zn	Cd	Co	As	Cu	Ni	Cr	Pb
Mean	91.1	12.6	80.15	0.61	11.9	27.45	800	N/d
Minimum	59.6	10.4	72.8	0.59	7.6	20.4	N/A	N/A
Maximum	132.2	14.4	83.6	0.63	15.4	39.2	N/A	N/A
Standard deviation	30.320	1.657	5.1	0.018	3.994	8.628	N/A	N/A

N/A means not available

3.2 Geochemical accumulation index

The geochemical accumulation indices were computed for all the concentrations of the sample points using equation1.the results of this indices were presented in a scatter plot(Fig 1(a-f)) for some of the analyzed toxic metals whose background values were available. The index was not computed for Pb and Cr because their background concentration was not available as it was below detection limit. Table9 presented the summary statistics of the computed geo-chemical accumulation indices from which the mean elemental concentration in the studied soil samples could be categorized as follows (i) Zn and Cu in Moderately polluted Category. (2) Ni, Cd, Co and As in Unpolluted Category.

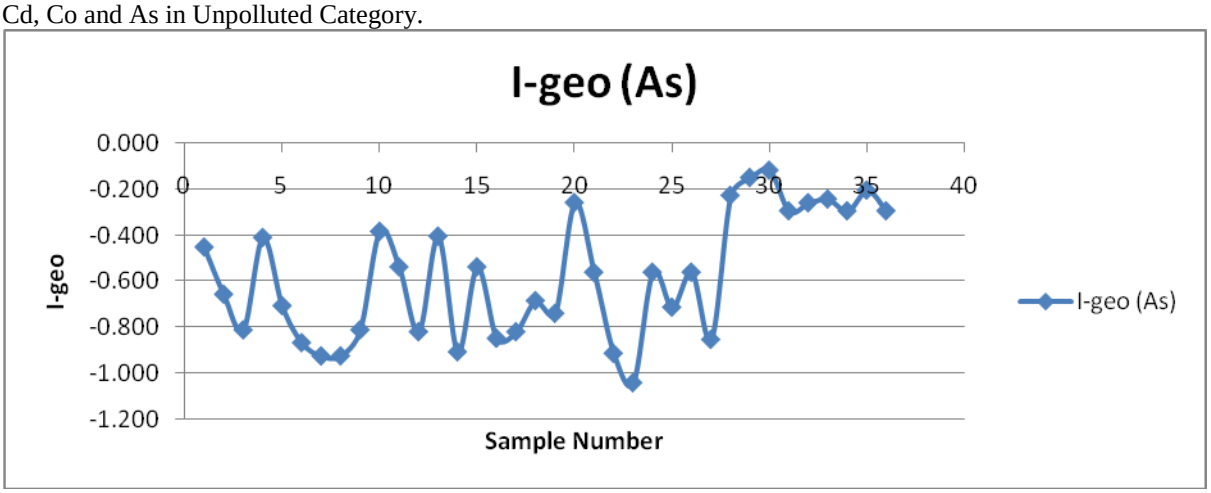

(a)

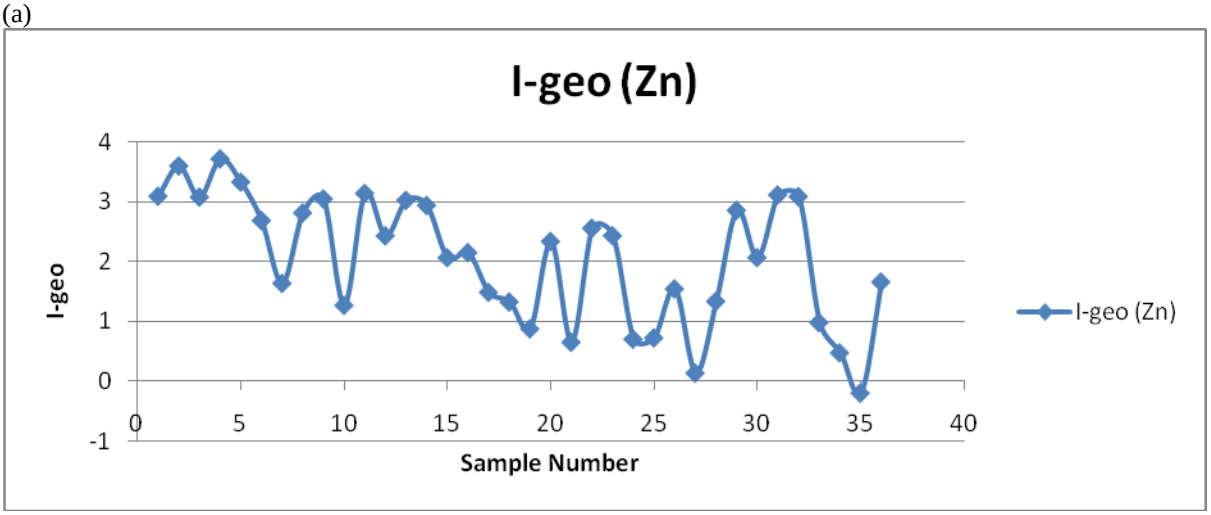

(b)

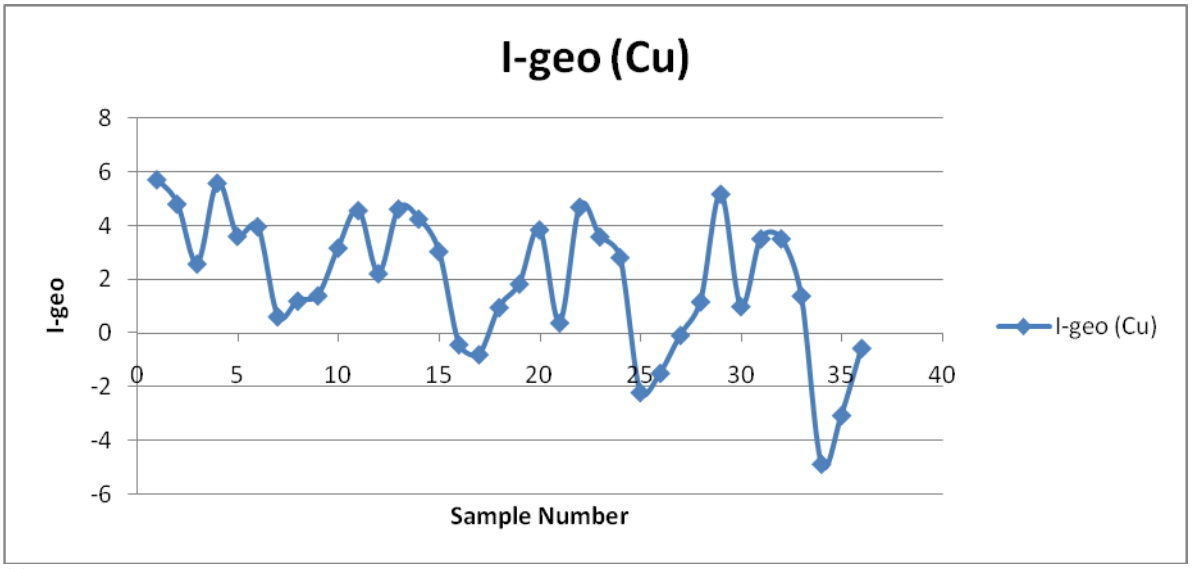
I-geo (Cu)
I-geo
Sample Number
I-geo (Cu)

(c)

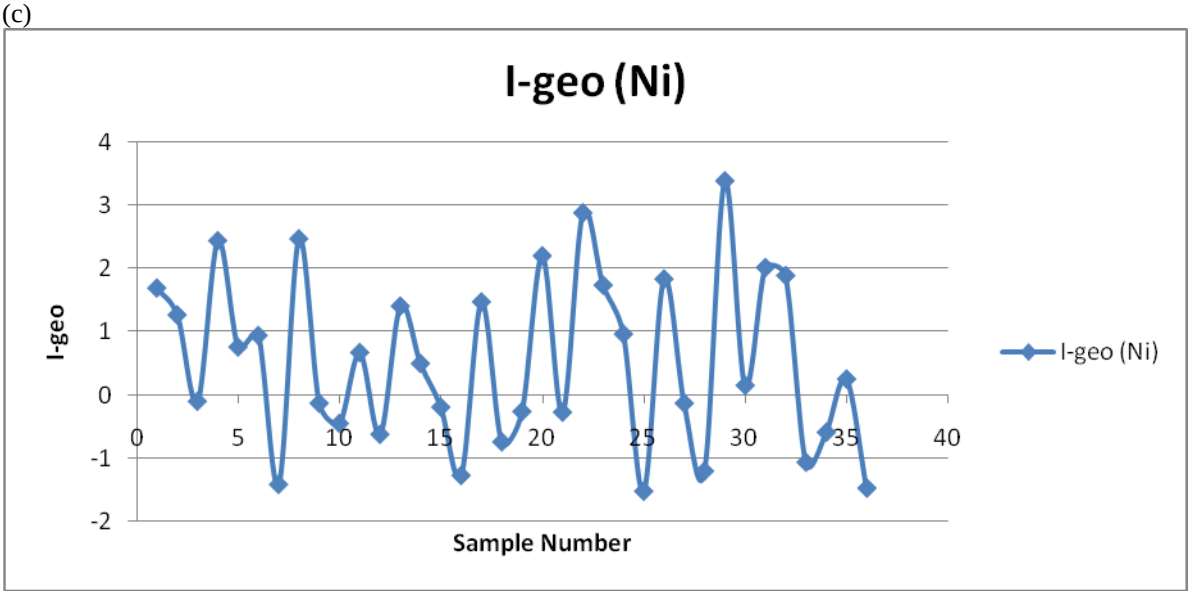
I-geo (Ni)
I-geo
Sample Number
I-geo (Ni)

(d)

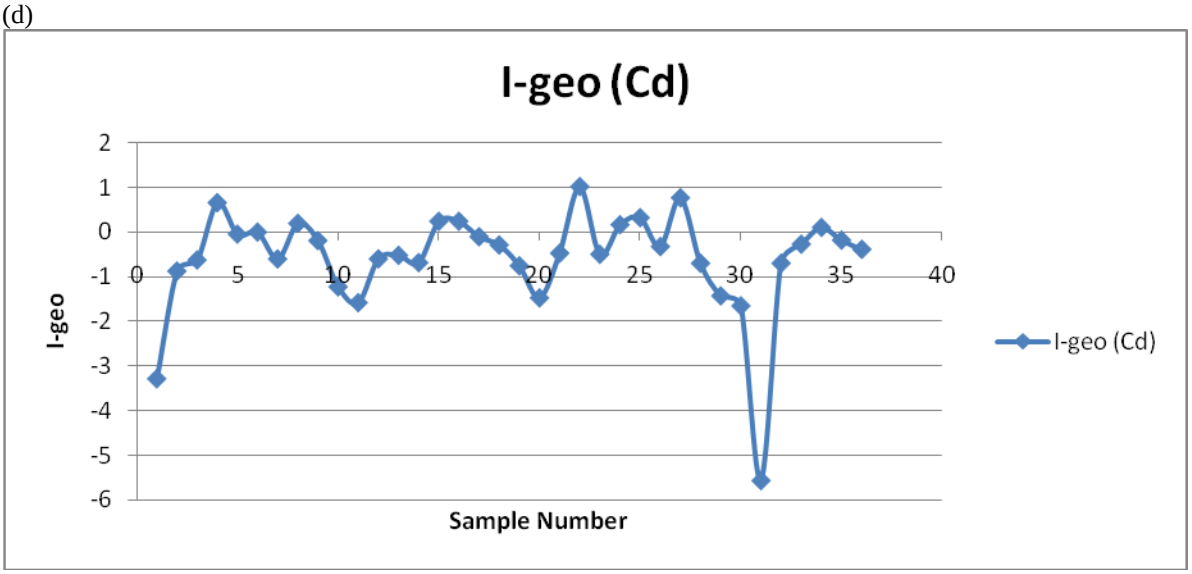
I-geo (Cd)
I-geo
Sample Number
I-geo (Cd)

(e)

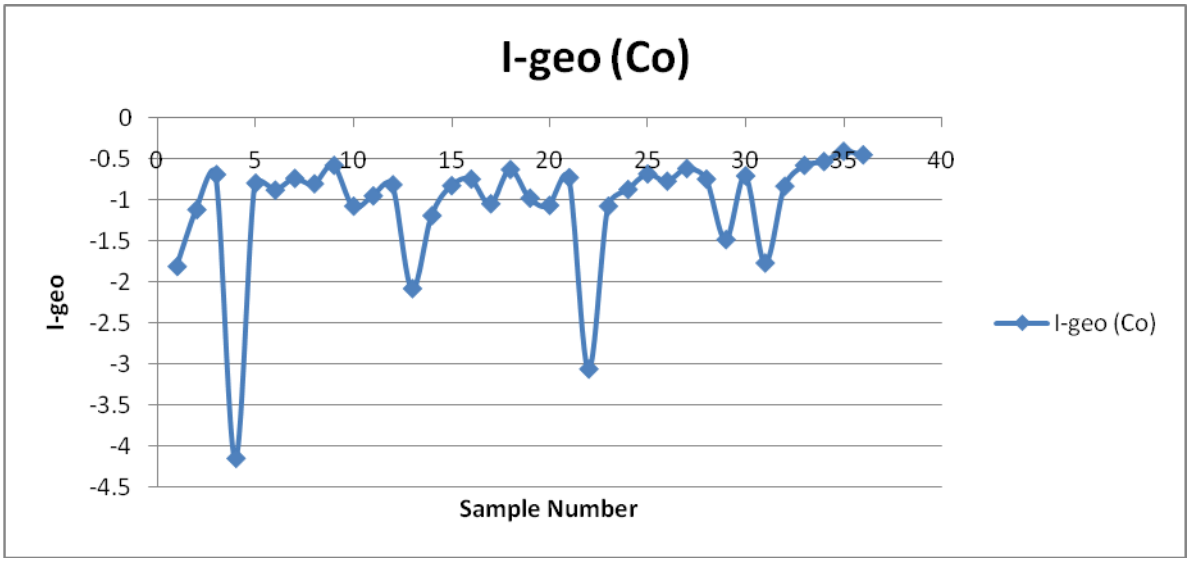

(f)

Fig1 (a-f): Scatter Plot of geochemical accumulation Index for Some elements in the analyzed dumpsite soil samples.

Table9: Univariate Descriptive statistics of the geochemical accumulation Indices of the analyzed dumpsite soil samples.

Geochemical accumulation index	mean	minimum	maximum	Standard deviation
I(Zn)	2.060	-0.192	3.711	1.054
I(Cu)	2.004	-4.852	5.722	2.544
I(Ni)	0.534	-1.530	3.381	1.357
I(Cd)	-0.598	-5.563	1.009	1.164
I(Co)	-1.066	-4.153	-0.410	0.738
I(As)	-0.577	-1.041	-0.118	0.270

3.3 Ecological Risk Factor

The Ecological risk Factors (ERF) was calculated for some metals studied in each of the samples utilizing equation5. Fig 3(a-d) displayed the calculated values of this index in a scatter plot. The Ecological risk factors of the other heavy metals studied were not computed due unavailability of their toxic response factors in literatures The Summary Statistics of this Index for some of the studied metals (those whose toxic response factor is in literatures and the contamination factor has been calculated) were presented in table. The mean elemental concentration could be categorized base on this index into (i)Cu in considerable Ecological risk category (ii) Zn, Ni and Cd in Low potential ecological risk.

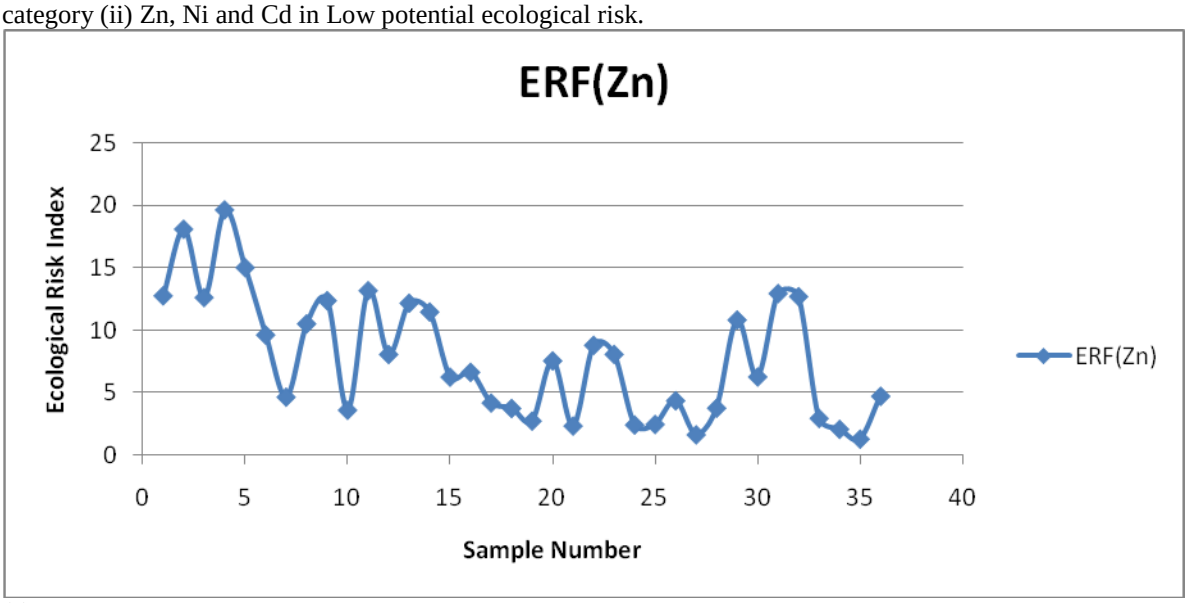

(a)

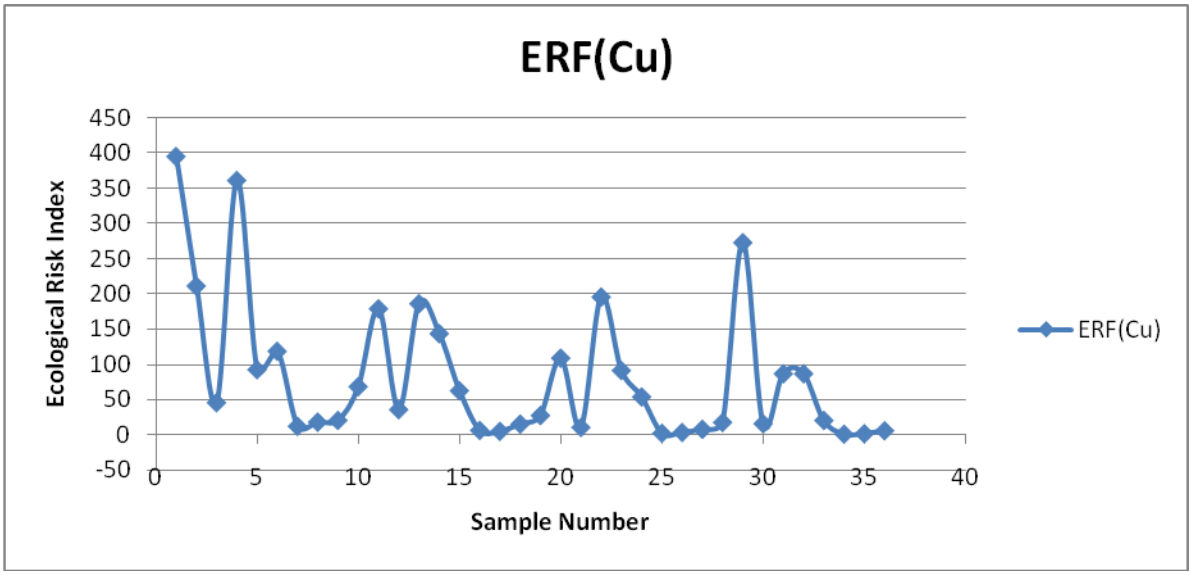

(b)

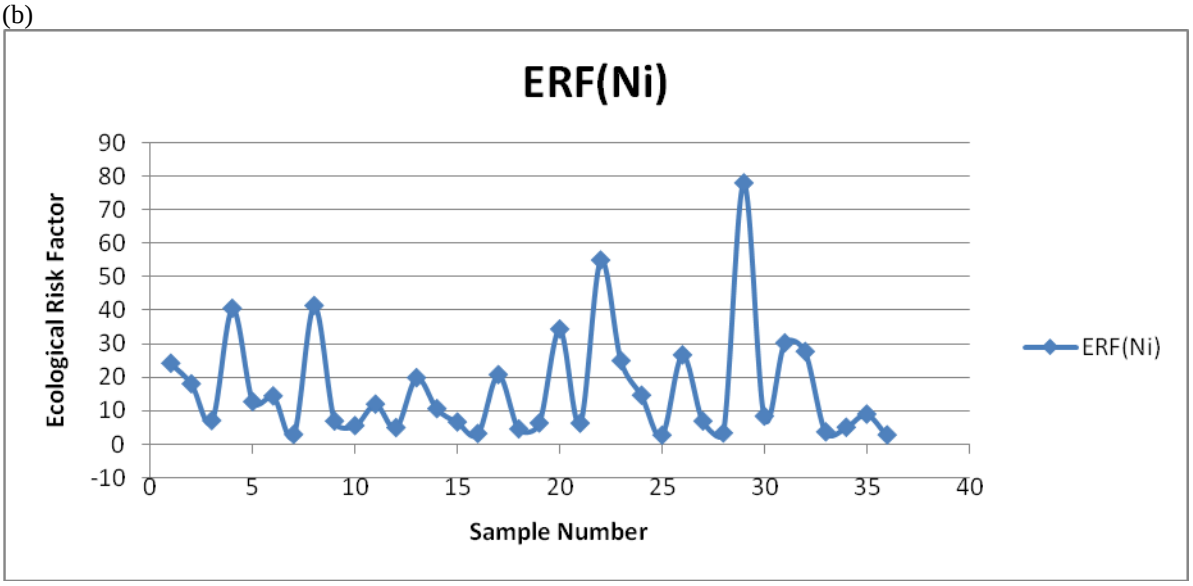

(c)

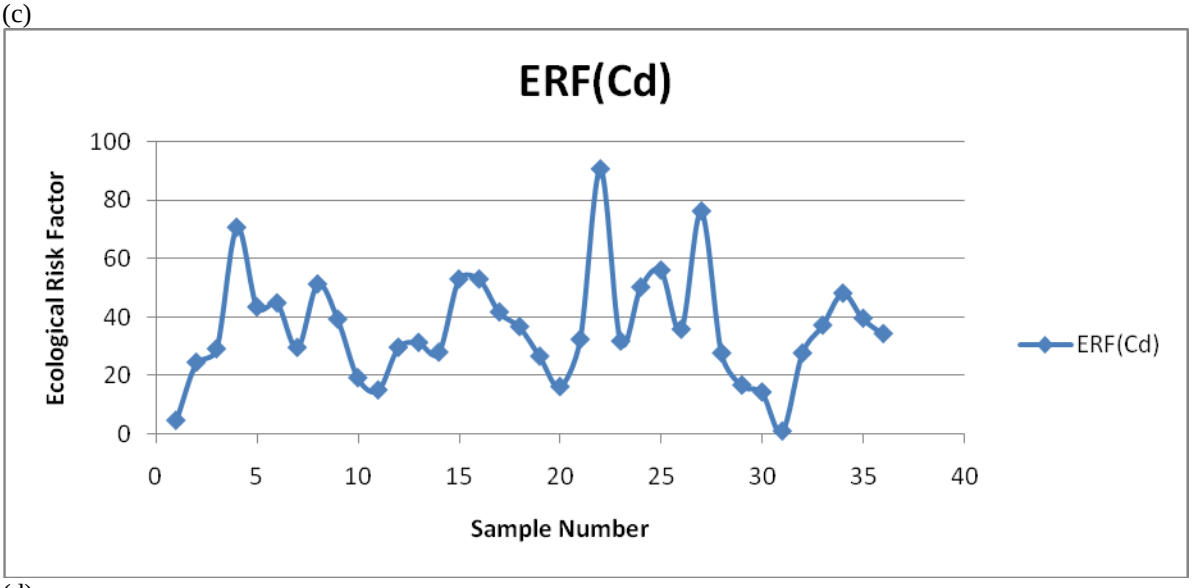

(d)

Fig3 (a-d): Scatter Plot showing the values of the calculated Ecological risk factors for the determined toxic metals in the dumpsite soil samples analyzed.

Table10: Univariate Descriptive Statistics of the determined Ecological risk Factors

Ecological Risk Factor	mean	Minimum	Maximum	Standard deviation
ERF(Zn)	7.866	1.313	19.644	4.925
ERF(Cu)	82.558	0.26	395.789	101.661
ERF(Ni)	16.660	2.598	78.102	16.729
ERF(Cd)	36.266	0.952	90.577	18.761

3.4 Hazard Quotient

The Hazard Quotient for each heavy metal in each of the samples in the target area was calculated using equation6 and WHO recommended threshold limit for concentrations of metals in soils (provided in table1). The results of the calculated Hazard quotient were presented in a scatter plot (Fig4 (a-e)) in the case of Zn, Cu and Ni and in Histogram in the case of Pb, Cr and Cd. the Base line (maximum permitted hazard quotient for the soil to be unpolluted) was plotted along the hazard quotients of the samples for comparison sake. The hazard quotients of the samples were subjected to Univariate descriptive statistics and the summary was presented in Table11.the mean Hazard quotients for all the toxic metals studied (Zn, Cu, Ni. Pb, Cr and Cd) were far greater than unity except Ni which was slightly greater indicating that the dumpsite has been heavily polluted by the disposed wastes and may pose significant risk to occupants of the site and the nearby ecosystem.

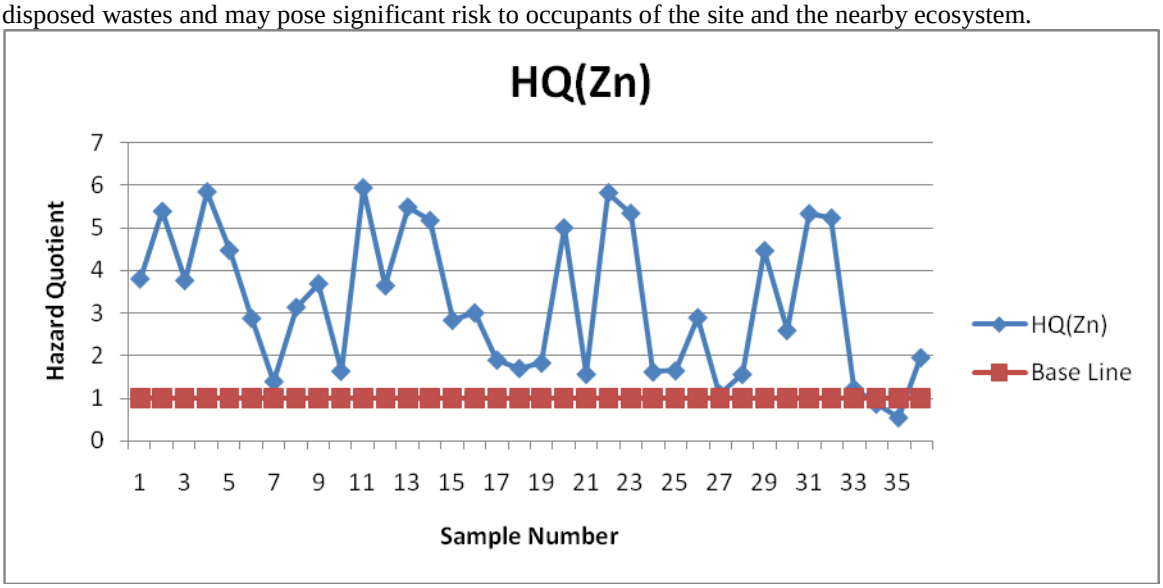

(a)

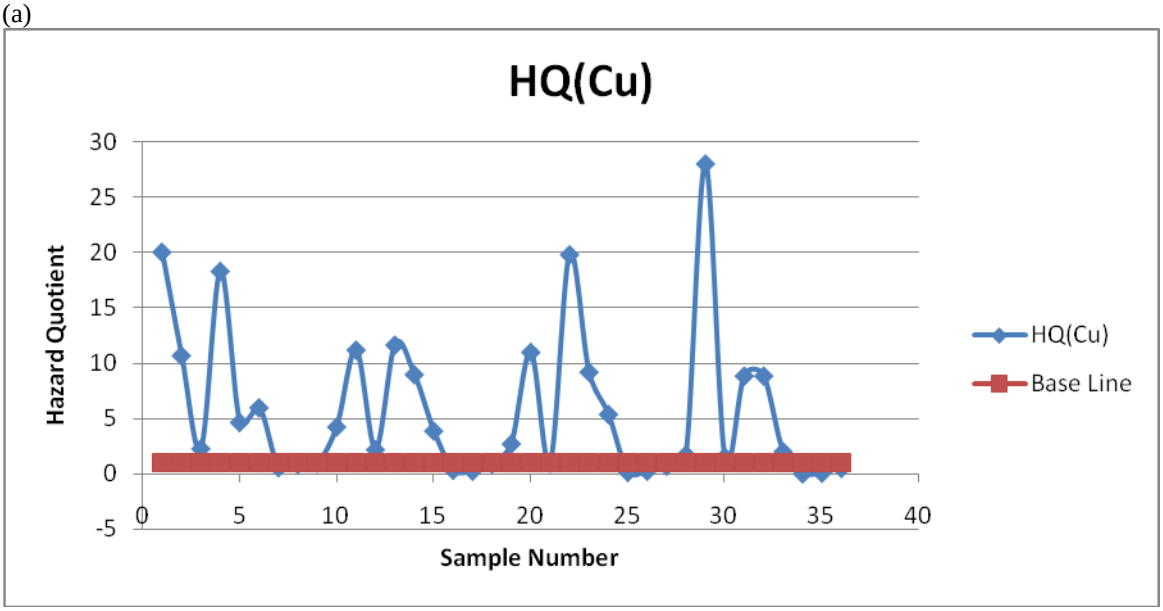

(b)

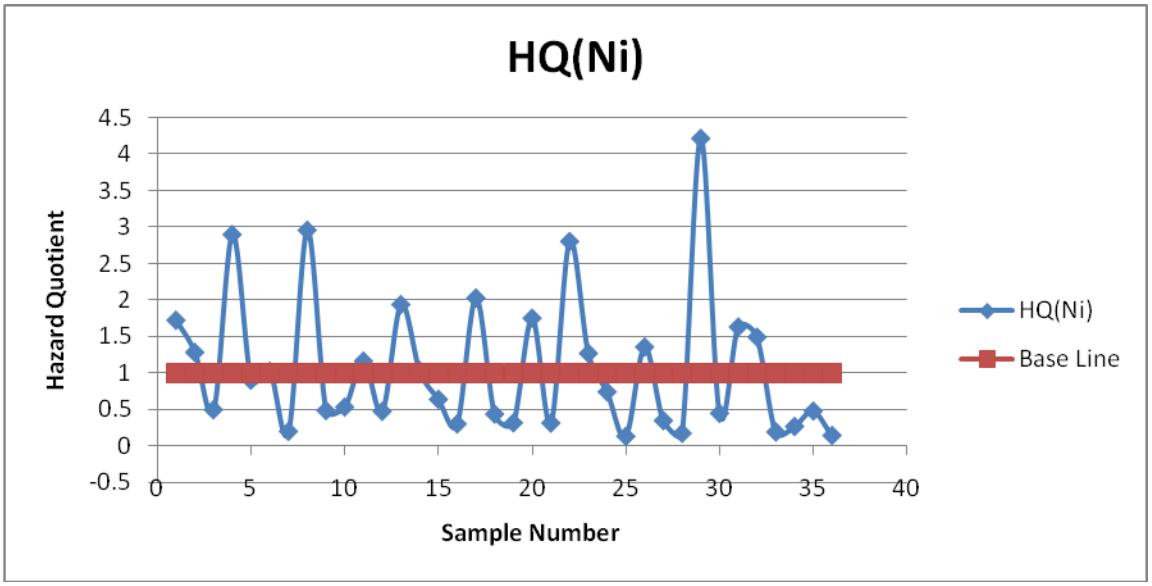
HQ(Ni)
Hazard Quotient
4.5
4
3.5
3
2.5
2
1.5
1
0.5
0
-0.5
0
5
10
15
20
25
30
35
40
Sample Number
HQ(Ni)
Base Line

(c)

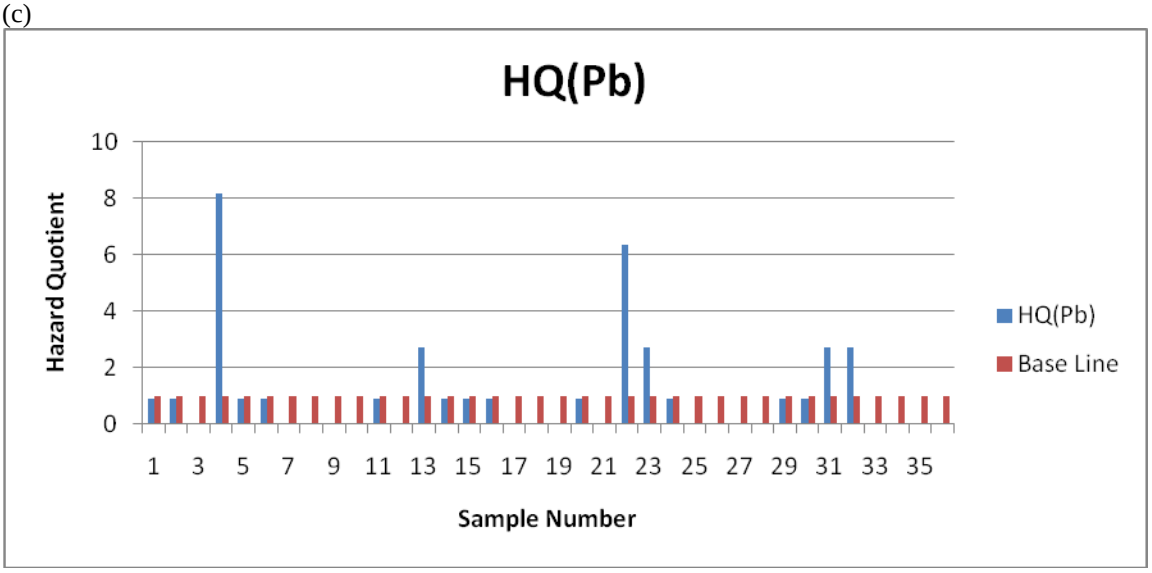
HQ(Pb)
Hazard Quotient
10
8
6
4
2
0
1 3 5 7 9 11 13 15 17 19 21 23 25 27 29 31 33 35
Sample Number
HQ(Pb)
Base Line

(d)

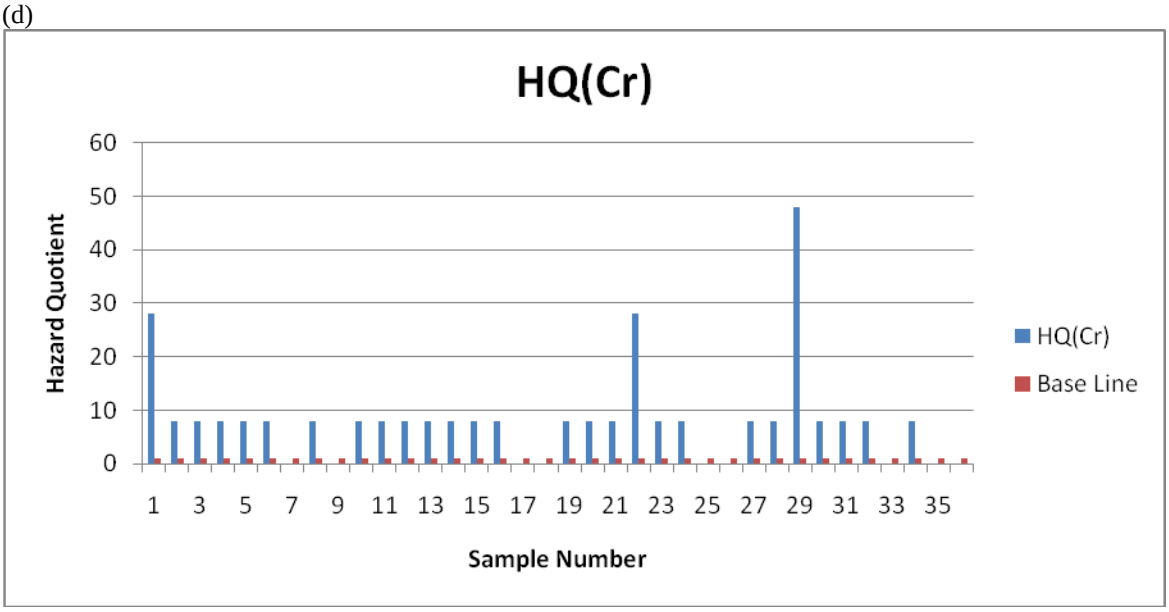
HQ(Cr)
Hazard Quotient
60
50
40
30
20
10
0
1 3 5 7 9 11 13 15 17 19 21 23 25 27 29 31 33 35
Sample Number
HQ(Cr)
Base Line

(e)

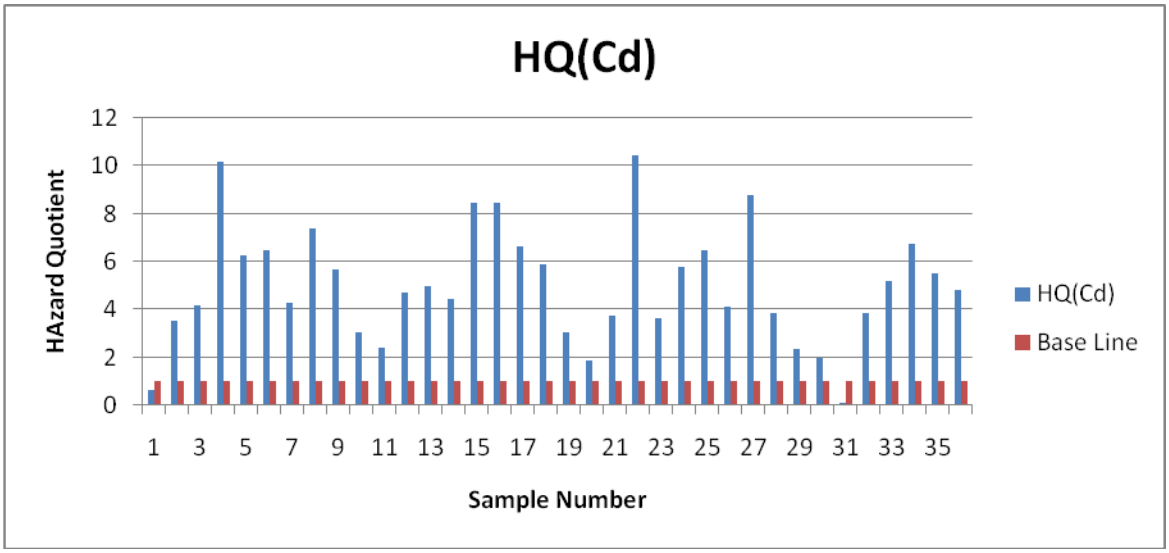

(f)

Fig 4 (a-e): Histogram showing the calculated Hazard quotient for the sampled points in the site and the base line provided by world health organization.

Table11: Univariate descriptive Statistics for the Calculated Hazard Quotient in the determined toxic metals in the dumpsite soil samples.

Hazard Quotient	Mean	Minimum	Maximum	Standard deviation
HQ(Zn)	3.231	0.541	5.947	1.703
HQ(Cu)	5.843	0.027	28.033	6.887
HQ(Ni)	1.073	0.133	4.218	0.968
HQ(Pb)	2.021	0.910	8.182	2.081
HQ(Cr)	10.963	8.000	48.000	9.121
HQ(Cd)	5.007	0.133	10.467	2.438

3.5 Correlation

The trend in the concentration of the toxic metals in the dumpsite soil samples indicated a certain measure of similarity between the different sets of samples. This similarity is expected since these concentrations could be influenced by the same steel rolling industrial activity. In an attempt to unravel the relationship between the toxic metals concentrations in the dumpsite, the concentrations of the elements (mg/kg) were subjected to Correlation Analysis using Microsoft office 2007.the correlation coefficients were displayed in Tables 12 1nd 13 for the dumpsite and the control area respectively.

The results of this correlation in the control area indicated a significant Positive correlation between the pairs depth/Cu, Zn/Cu, Ni/Cd and Significant negative Correlation between depth/Ni, Cu/Ni, Zn/Cd, Cu/Cd and Depth/Co. The results of Pearson correlation in the target area showed a significant positive correlation between Zn/Cu, Zn/Ni, Cu/Ni and Significant negative correlation between Zn/Co, Cu/Co, and Ni/Co.

Table12: correlation matrix for concentration (mg/kg) of pairs of elements in the dumpsite Area.

	Zn	*Cu*	*Ni*	*Cd*	*Co*
Zn	1				
Cu	**0.70301**	1			
Ni	**0.6113**	**0.78075**	1		
Cd	-0.133	-0.1573	0.04392	1	
Co	**-0.6734**	**-0.8295**	**-0.7322**	0.00305	1

Table13: Pearson correlation matrix for concentration of pairs of elements (mg/kg) in control samples with depth

	Depth	*Zn*	*Cu*	*Ni*	*Cd*	*Co*
Depth	1					
Zn	0.47007	1				

Cu	**0.94361**	**0.66838**	1			
Ni	**-0.5955**	-0.364	**-0.7549**	1		
Cd	-0.4051	**-0.6941**	**-0.6787**	**0.86535**	1	
Co	**-0.5923**	0.40625	-0.4074	0.45249	-0.0473	1

IV. CONCLUSION

Flame Atomic absorption spectrometry technique has been employed in order to evaluate pollution of Dana steel limited dumpsites soils with heavy metals. from the experimental results presented in this work it can be seen that the concentrations of heavy metals studied in the target area exceeded the world health organization limit of heavy metals in soils, the maximum values admitted by the Romanian guidelines as well as the concentrations of all the heavy metals in the control area except cobalt. The calculated indices used in this characterization reveal the pollution potential of some of these metals. Based on the results of this work it must be stressed that pollution impact on the environment by this heavy metals is present. The situation can be labeled as "potentially significant pollution". in this case, the competent authorities should take actions to reduce the pollutants emission in to the air as well as excessive dumping of metal slags and scraps in the dumpsite so as to diminish the possibilities of contaminating the underground water and the ecosystem around the area.

REFERENCES

[1] Fagbote EO, Olanipekun EO (2010).,Evaluation of the status of heavy metal pollution of soil and plant (Chromolaenaodorata) of Agbabu Bitumen Deposit Area, Nigeria. Am-Eur J Sci Res 5(4):241–248

[2] Fostner,U.,1995.Lead contamination by Metals: Global Scope and magnitude of Problem. In: Allen, H.E., et al.,(Eds.),Metal Speciation and contamination of Soil. Lewis Publishers, Country, pp: 1-33 Hakanson I., (1980): Ecological risk index for aquatic pollution control, a sedimentological Approach. *Water resources*, 14; 975-1001

[3] Harikumar P.S, U. P Nasir and M. P. Mujeebu Rahma, "Distribution of heavy metals in the core sediments of a tropical wetland system, "International Journal. Environmental Science Technology, Vol. 6, No. 2, 2009, pp.225-232.

[4] Knight,C. and J.kaiser. Heavy metals in surface water and stream sediments in Jamaica. Envi. Geochemistry and health, Kingston Jamiaca. Chapman and hill publishers, Kingston. 19:63-66,1997

[5] Lokeshwari H, Chandrappa GT (2006).Heavy metals content in water; hyacinth water and sediments of Lalbagh Tank, Bangalore, *India. J Environ Sci Eng* 48(3):183–188

[6] Onibokun A.G., Adedipe N.O. and Sridlier M.K.C., Affordable technology and Strategies for waste management in Africa. Lessons and Experience. Centre for African settlement studies and development CASSAD, 13,134(2000).

[7] Reference Values for Trace Elements in Soil,Monitorul Oficial al Romaniei,No,303 bis/6XII 1997 (in Romanian).

[8] Srivastava K.P. and Singh V.K., Impact of air pollution on pH of soil of Saran, Bihar, India, Res. J. Recent Sci.,1(4),9-13(2012)

[9] Stigliani,W.W., P.Doelman, W.Salomons, R.Schulin, G.R. Smidt and E.A.T.M.V.Sjoerd, 1991.Chemical Time Bomb: Predicting the unpredictable.Environ.,33:5-30.

[10] Tchobanoglous G.,Theisen H. and Vigil S., Integrated Solid waste management : Engineering Principle and Management Issue. International Ed. McGram Hill Book Co.,Singapore,825(1993)

[11] World Health Organization (WHO). World Health Organization Guidelines for drinking water quality.1996; 2nd Ed, Vol.2, *Health Criteria and Supporting Information*, WHO, Geneva.

American Journal of Engineering Research (AJER) 2016
American Journal of Engineering Research (AJER)
e-ISSN: 2320-0847 p-ISSN : 2320-0936
Volume-5, Issue-1, pp-62-72
www.ajer.org
Research Paper Open Access

Development of a Renewable Energy Integration Model for Carbon Regulation in a Developing Nigeria Grid

L.O. Uzoechi*, C.D. Okpalike, C.U. Ndukwe, O.J. Onojo
Department of Electrical/Electronic Engineering,
Federal University of Technology Owerri, Nigeria.

***ABSTRACT**: This paper carried out the development of a model for renewable energy integration as a solution to carbon regulation in the developing Nigeria power system. The integration of renewable energy resources into the power grid is driven largely by environmental regulation aimed at promoting sustainable energy resources and reducing carbon emission resulting from energy use. The Nigeria power system depends mainly on conventional sources for power generation. This obviously has increased the carbon emissions in Nigeria. This paper adopted a percentage by percentage renewable integration approach in an attempt to mitigate the rate of carbon emissions in the Nigeria electric power sector. This approach has been carried out for the various power stations operational as at 2010. Deductions and results show that as percentage of renewable integration increases, carbon emission reduces. As markedly observed, reduction in carbon emission occurs mostly for generating stations with large installed capacity. This is because the installed capacity was found to have a linear relationship with the amount of carbon emitted. Also, the relationship between the amount of renewable integrated and the reduction in carbon emissions has been represented by a linear equation. This is an invaluable tool in deductions involving renewable energy integration and carbon emission in the Nigerian power sector.*
***Keywords** − Renewable energy integration, sustainable energy, carbon regulation, carbon cap, renewable portfolio standards, carbon emission.*

I. INTRODUCTION

The integration of renewable energy resources into the power grid is as a result of environmental regulation aimed at promoting sustainable energy resources and reducing carbon emission resulting from energy use. Price and quantity controls of carbon emissions through taxation and cap and trade policies, along with renewable portfolio standards (RPS) are the primary drivers for massive penetration of renewable energy resources and for electrification of transportation. Environmental regulations, aimed at reducing carbon emissions, are setting aggressive targets that will require high levels of renewable penetration. For instance, Assembly Bill 32 in California set goals of cutting back greenhouse gas emissions to 1990 levels by 2012 and the RPS mandates 33% integration of renewable energy in California by 2020[1]. As wind penetration increases the aforementioned challenges may impact system reliability, dispatch efficiency, cost of operation and may even undermine the environmental goals that RPSs, aim to achieve, unless the adverse impact of such penetration can be mitigated through technological innovation [2].

A non-renewable resource is a resource that does not renew itself at a sufficient rate for sustainable economic extraction in meaningful human time-frames [3]. An example is carbon-based, organically-derived fuel. The original organic material, with the aid of heat and pressure, becomes a fuel such as oil or gas. Fossil fuels (such as coal, petroleum, and natural gas), and certain aquifers are all non-renewable resources.

The objective of this paper is to reduce carbon emission by integrating renewable energy of different mix in the Nigerian grid network. This can be achieved by:
(i) Reducing carbon emission of other air pollutants through increased use of renewable energy and other clean distributed generation.
(ii) Establishing a relationship between renewable energy integration and reduction between CO_2 emissions.
This paper is limited to carbon emission quantification while the technical considerations like voltage and stability analysis of integration of renewable energy systems (RES) is beyond the scope of work.

Renewable technology sources include wind, hydro, solar, biomass, etc. Air flow can be used to run wind turbines. Modern utility wind turbines ranges from about 600kW to 5MW of rated power. The power available from the wind speed increases, power output increases dramatically up to the maximum output for the particular

turbine [4]. Areas where wind are stronger are more constant such as offshore and high altitude site, are preferred locations for wind farms. As offshore wind speeds average 90% greater than that of land, so offshore resources can contribute substantially more energy than land stationed turbines [5].
Energy in water can be harnessed and used for hydro power. Since water is about 800 times denser than air, even a slow flowing stream of water or moderate sea swell can yield considerable amount of energy [6].

Solar energy is the ultimate energy source driving the earth. Though only one billionth of the energy that leaves the sun actually reaches the earth's surface, this is more than enough to meet the world's energy requirements. In fact, all other sources of energy, renewable and non-renewable, are actually stored forms of solar energy. The process of directly converting solar energy to heat or electricity is considered a renewable energy source. Solar energy represents an essentially unlimited supply of energy as the sun will long outlast human civilization on earth. The difficulties lie in harnessing the energy. Solar energy has been used for centuries to heat homes and water, and modern technology (photovoltaic cells) has provided a way to produce electricity from sunlight. There are two basic forms of radiant solar energy use: passive and active. Solar power can be 120 thousand times the total electrical energy the country's utility companies produce for the nation in 2002 and at present. It also shows that the solar energy base of the country is good enough and worth investing on [6].

Biomass energy is the oldest energy source used by humans. Biomass is the organic matter that composes the tissues of plants and animals. Until the Industrial Revolution prompted a shift to fossil fuels in the mid-18th century, it was the world's dominant fuel source. Biomass can be burned for heating and cooking, and even generating electricity. The most common source of biomass energy is from the burning of wood, but energy can also be generated by burning animal manure, herbaceous plant material, peat, or converted biomass such as charcoal. Biomass can also be converted into a liquid biofuel such as ethanol or methanol. Currently, about 15 percent of the world's energy comes from biomass. Biomass is a potentially renewable energy source. Unfortunately, trees that are cut for firewood are frequently not replanted. In order to be used sustainably, one tree must be planted for every one cut down. Biomass is most frequently used as a fuel source in developing nations, but with the decline of fossil fuel availability and the increase in fossil fuel prices, biomass is increasingly being used as a fuel source in developed nations. One example of biomass energy in developed nations is the burning of municipal solid waste. In the United States, several plants have been constructed to burn urban biomass waste and use the energy to generate electricity. The use of biomass as a fuel source has serious environmental effects. When harvested trees are not replanted, soil erosion can occur. The loss of photosynthetic activity results in increased amounts of carbon dioxide in the atmosphere and can contribute to global warming. The burning of biomass also produces carbon dioxide and deprives the soil of nutrients it normally would have received from the decomposition of the organic matter. Burning releases particulate matter (such as ash) into the air which can cause respiratory health problems.

The effects of renewable energy sources include negative net energy which is one of the biggest effects of using alternative energy sources and troublesome fact that it often requires more fossil fuel inputs than the energy source yields, space and location issues like in solar power requiring large tracts of land in order to generate the kind of power necessary for large cities, let alone a whole nation, harmful effect on environment and wildlife like wind turbines killing birds as they rotate or tidal power buoys disrupting fish migration routes, and unsightly fixtures about complaints that the installation of wind turbines would sully the view of the ocean and the horizon [7].

This work is paramount at this time due to the rising effect of global warming. The power sector has been found to be a major emitter of greenhouse gases, especially CO_2. It is in this respect that this research work focuses on reduction in carbon emissions from the power grid. The reduction in carbon emission is made possible by renewable integration into the power grid since Nigeria has a large potential of renewables.
This study only considered the Nigerian energy sector with focus on the electricity supply industry. This work will take its reference from developed countries where elaborate work has been accomplished on carbon emission regulation. Finally, the study will be limited to the next sixteen years in order to fit existing development policies such as vision 20:20:20.

The primary disadvantage of the non-renewable energy resources is that they have a very negative effect on the environment from the mining, to the processing and consumption. Coal processing plant leach toxic metals into ground water and produce tons of additional waste, while gasoline burned in combustion engines emits carbon dioxide and other pollutants, contributing to global climate change. Natural gas is mainly methane, which is twenty times more effective at trapping heat than carbon dioxide, making it twenty times more problematic as a greenhouse gas [4].

Also, non-renewable energy resources pose problems to human health. For instance, uranium, which is used in nuclear power plants, causes birth defects and abnormal heart, liver, and kidney functions with prolonged exposure.
Because unsustainable energy reserves are limited, they will become more and more expensive as they are used. Consider the state of gas prices today, and imagine how these prices will continue to rise as oil becomes rare and gasoline is no longer an easily accessible resource.

Eventually, all non-renewable energy resources will be depleted; the name itself admits this inevitability. When this happens, all technologies still running on these fuels will become obsolete, and many people may suffer in their absence. We must turn to other forms of energy production; like wind, solar, and geothermal power sources, which can be used indefinitely. With these alternatives, the process of technology conversion should begin sooner rather than later. It would be better to stop deploying fossil fuels for power generation before they completely disappeared.

II. CARBON REGULATION

Carbon regulation derives from a realization of the effects of greenhouse gas (GHG) emissions (particularly CO_2 emissions). This has been termed "global warming". The effect of this has been seen in melting of ice of the ocean which has led to unusual flooding in parts of the world and unusual increase in temperature levels [8]. Moreover, cases of asthma, heart attacks, stroke and death have been reported due to inhalation of these gases. These pollutants have been observed to affect people who live in proximity to power plants but also those who live downwind, often hundreds and even thousands of miles from the plant's actual location [8]. Coal fired power plants in the United States release enough of these gases in the atmosphere each year to cause more than thirteen thousand premature deaths and hundreds of thousands of asthma attacks [9]. The aggregate toll caused by these harmful health impacts, and the resulting medical bills and lost wages can exceed $100 billion in one year [10]. Nigeria has not been spared its own trauma. It is estimated that 79,000 deaths occur annually as a result of smoke from traditional three stone-wood stoves [10].
With these revelations, it is important to unravel ways of curbing these emissions. Carbon regulation seeks to explore ways of curbing carbon emissions into the atmosphere by establishing carbon reduction measures. One of the ways to curb these emissions is by reducing the amount of non-renewable power generation and increasing renewable energy sources. Operators of power generating stations will be restricted on the amount of carbon to be emitted. Failure to comply will attract stringent financial obligation by the power company to account for amount of carbon emitted [10].
Acceptable standards of carbon regulation now exist globally. Emission standards are requirements that set specific limits to the amount of pollutants that can be released into the atmosphere [10]. Different countries of the world have laid down standards that are effective within their domain. All these standards lay credence to two major world agreements or treaties. They are the United Nations Framework Convention on Climate Change (UNFCCC) and the Kyoto protocol.
The United Nations Framework on Climate Change (UNFCCC) is an international environmental treaty negotiated at the United Nations Conference on Environment and Development (UNCED), informally known as the Earth Summit, held in Rio de Janeiro, with the objective to stabilize greenhouse gas concentrations in the atmosphere [11]. It provided a framework for negotiating specific international treaties (called protocols) that may set binding limits on greenhouse gas [12].
The Kyoto protocol to the UNFCCC is an international treaty that sets binding obligations on industrialized countries to reduce emissions of greenhouse gases. They are those who have agreed to cap their GHG emissions at their base year levels. They are not obligated by caps that allows their emissions to expand above their base levels or countries that have not ratified the Kyoto protocol. For instance, the European Union as a whole has in accordance with the Kyoto protocol committed itself to an 8% reduction. Although not all member countries have complied, France has committed itself not to expand its emissions [13].

2.1 Carbon Regulation Experiences from Developed Countries

Carbon regulations in developed countries can be summarized as a lesson to developing countries. It is necessary to reveal carbon regulation standards in some developed countries such as China, Germany, UK, U.S.A, Canada, and Russia. The energy policy of China is a policy decided on by the Central Government with regard to energy and energy resources. The country is currently the world's largest emitter of greenhouse gases according to Dutch research energy [4]. However, China's per capita emissions are still far behind some of the developed countries. In 2011, the State Council released the Comprehensive Work Plan on Energy Conservation and Emission Reduction for a Five-Year Plan Period. China has therefore towed the path of carbon emission reduction by its conspicuous achievements in energy conservation, rapid development in non-fossil energy and strengthening energy conservation in industry.

The building sector is regarded as the key to greater energy efficiency in the German Energy Concept from 2010 [14]. In this field, the measures planned are the inclusion in the revised Energy Saving Ordinance of 2012 and the development of a renovation roadmap for existing buildings which starts in 2020 of the climate neutral building standard, to be met by new buildings by 2020.

Over the past 20 years, Russia has enacted complex and strict environmental legislation that in many cases meets or exceeds commonly accepted international standards. However, the enforcement of this legislation has been uneven [2]. Russia is continuing to develop its legislation and currently has new draft resolutions in the State Duma.

Although it ratified the Kyoto Protocol on climate change in late 2004, it has only recently enacted the legislation necessary to advance joint implementation projects and the trade of carbon credits. Carbon regulation has been carried out in the following ways - federal and regional legislation, environmental regulation, environmental permits, pay-to-pollute, etc.

III. METHODOLOGY

This paper focuses on mitigating carbon emissions from various generation stations in Nigeria through renewable energy integration. The major renewable energy resource used here is solar. This is because of its natural abundance in Nigeria. Solar is relatively mature for use in large capacities and so can have significant impact on the power grid that is likely to increase over time.

Standard emission rates have been used to obtain deductions of carbon emission rates due to each generating station. These standard emission rates have been sourced from [13]. Information from the standard rates was used to obtain the average emission rates (AER). The least value (R1) and the highest value (R2) of the AER have been summed up in a bid to obtain the average emission rate. Average emission rate for the most common conventional resources i.e. coal, natural gas and hydro have been deduced as sources of generation.

Also, AER for the target source (solar) has been obtained. This paper advocates a generation mix between the renewables and the conventional resources as a major way to curb carbon emission in our electric grid. Therefore, varying amount of renewables for integration has been considered. First, a 10% renewable integration for the various generation stations was considered. A 10% take-off is seen as ideal for meaningful achievements in a generation mix. This section continues to look at increasing amount of renewables integrated from a 10% take-off to a 20%, 30%, and 40% renewable integration respectively.

Also, the concept of a non-compliance cost was considered. This is the financial obligation for generation stations that do not comply with the renewable energy integration standard. The standard price for emitting carbon was obtained from [4]. This price has been put at €40 per ton of CO_2. This standard price will be adapted to obtain Non-Compliance Cost (NCC) for the various generation stations in Nigeria.

In addition to the AER, there is the need to obtain other parameters like the Carbon Emission Due to Installed Capacity, CEDIR (= Installed Capacity (kW) x AER), Carbon Emission Due to Generation Mix, CEDGM (= % Renewable Integration x Installed Capacity), Carbon Emission for Integrated Renewable, CEIR (= Cap(kW) x $AER_{Renewable}$), Carbon Emission for Remaining Output from Conventional Generator, CEROG (= Cap(kW) x $AER_{Non\text{-}Renewable}$).

3.1 Carbon Emission Rates

The average emission rate (AER) for the various generation resources are obtained as follows:

Coal: Emission rates for coal as a source of power generation is between 1.4pounds of CO_2 Emissions per kilowatt hour [CO_2E/kWh] and 3.6 pounds of CO_2E/kWh. Therefore, AER is obtained thus;

Average Emission Rate (AER) = (R1+R2)/2

AER (coal) = (1.4+3.6)/2

AER (coal) = 2.5pounds of CO_2E/kWh.

Natural Gas: Emission rate is between 0.6 pounds of CO_2E/kWh and 2pounds of CO_2E/kWh.

AER (Natural Gas) = (0.6+2)/2

AER (Natural Gas) = 1.3 pounds of CO_2E/kWh

Solar: Emission rate for solar is between 0.07 pounds of CO_2E/kWh and 0.2 pounds of CO_2E/kWh.

AER (Solar) = (0.07+0.2)/2

AER (Solar) = 0.135 pounds of CO_2E/kWh

Hydro: Emission rate is between 0.1 pounds of CO_2E/kWh and 0.5pounds of CO_2E/kWh

AER (Hydro) = (0.1+0.5)/2
AER (Hydro) = 0.3 pounds of CO_2E/kWh

3.2 The Power Stations and Their Deduced Emission Rates

The deduced emission rates of various power stations are obtained and presented as outlined here.

3.2.1 Generation Mix Due to 10% Renewable Integration

The 10% renewable integration into the power grid is presented as computed. Table I gives a picture of 10% generation mix with the integration of renewable energy across the power stations.

Table I: Showing a generation mix of 40% renewable energy integration to the various power stations

Power Stations	Installed Capacity (MW)	CEDIC (pounds of CO_2E/kWh) I.C×AER	CEIR (pounds of CO_2E/kWh) Cap(kw)×AER (Renewable)	CEROG (pounds of CO_2E/kWh) Cap(kw)×AER (Non Renewable)	CEDGM (pounds of CO_2E/kWh) CEIR+CEROG	NC (pounds of CO_2E/kWh)	NCC (€)
Kainji	760	760000×0.3 =228000	76000×0.135 =10260	684000×0.3 =205200	10269+205200 =215460	228000-215460 =12540	5.7×40 =228
Jebba	578.4	173520	7808.4	156168	163976.4	9543.6	173
Shiroro	600	180000	8100	162000	170100	9900	179.6
Afam	706.6	922480	9579.6	830232	839811.6	82668.4	1500
Okpai	480	624000	6480	561600	568080	55920	1014.6
Sapele	1020	1326000	13770	1193400	1207170	118830	2156
Ajeokuta	110	143000	1485	128700	130185	1215	232.5
AES	315	409500	4252.2	368550	372802.5	36697.5	665.8
Delta	912	1185600	12312	1067040	1079352	106248	1927.8
Geregu	414	528200	5589	484380	489969	48231	875
Omoku	150	195000	2025	175500	177525	17475	317
Omotosho	335	435500	4522.5	39195	391950	43550	790
Olorunsogo	335	435500	4522.5	39195	391950	43550	790
Egbin	1320	1716000	17820	1544400	1562220	153780	2790

3.2.2 Generation Mix Due to 20% Renewable Integration

Here we will obtain emission rates due to a 20% renewable integration. Table II is the calculation for 20% renewable energy integration.

Table II: Showing a generation mix of 20% renewable energy integration to the various power stations

Power Stations	Installed Capacity (MW)	CEDIC (pounds of CO_2E/kWh) I.C×AER	CEIR (pounds of CO_2E/kWh) Cap(kw)×AER (Renewable)	CEROG (pounds of CO_2E/kWh) Cap(kw)×AER (Non Renewable)	CEDGM (pounds of CO_2E/kWh) CEIR+CEROG	NC (pounds of CO_2E/kWh)	NCC (€)
Kainji	760	228000	20520	182400	202920	25080	455
Jebba	578.4	173520	115680	138816	154432.8	19087.2	346
Shiroro	600	180000	16200	144000	160200	19800	359
Afam	706.6	922480	19159.2	737984	757143.2	165336.8	3000
Okpai	480	624000	12960	499200	512160	111840	2029
Sapele	1020	1326000	27540	1060800	1088340	237660	4312
Ajeokuta	110	143000	2970	114400	117370	25630	465
AES	315	409500	8505	327600	336105	73395	1331.7
Delta	912	1185600	24624	948480	973104	212496	3855.5
Geregu	414	528200	11178	430560	441738	96462	1750
Omoku	150	195000	4050	156000	160050	34950	634
Omotosho	335	435500	9045	348400	357445	78055	1416
Olorunsogo	335	435500	9045	348400	357445	78055	1416
Egbin	1320	1716000	35640	1372800	1408440	307560	5580

3.2.3 Generation Mix Due To 30% Renewable Integration

Emission rate for a 30% renewable integration is tabulated in Table III.

Table III: Showing a generation mix of 30% renewable energy integration to the various power stations

Power Stations	Installed Capacity (MW)	CEDIC (pounds of CO_2E/kWh) I.C×AER	CEIR (pounds of CO_2E/kWh) Cap(kw)×AER (Renewable)	CEROG (pounds of CO_2E/kWh) Cap(kw)×AER (Non Renewable)	CEDGM (pounds of CO_2E/kWh) CEIR+CEROG	NC (pounds of CO_2E/kWh)	NCC (€)
Kainji	760	228000	30780	159600	190380	37620	683.6
Jebba	578.4	173520	23425.2	121464	144889.2	28630.8	519.5
Shiroro	600	180000	24300	126000	150300	29700	538.9
Afam	706.6	922480	28738.8	645736	674474.8	248005.2	4500
Okpai	480	624000	19440	436800	456240	167760	3043.8
Sapele	1020	1326000	41310	928200	960510	356490	6468
Ajeokuta	110	143000	4455	100100	104555	38445	697.5
AES	315	409500	12757.5	286650	299407.5	110092.5	1997.5
Delta	912	1185600	36936	829920	866856	318744	5793
Geregu	414	528200	16767	376740	393507	144693	2625
Omoku	150	195000	6075	136500	142575	52425	951
Omotosho	335	435500	13567.5	304850	318417.5	117082	2124
Olorunsogo	335	435500	13567.5	304850	318417.5	117082	2124
Egbin	1320	1716000	53460	1201200	1254660	461340	8370

3.2.4 Generation Mix Due to 40% Renewable Integration

Lastly, emission rates due to a 40% renewable integration is shown in Table IV.

Table IV: Showing a generation mix of 40% renewable energy integration to the various power stations

Power Stations	Installed Capacity (MW)	CEDIC (pounds of CO_2E/kWh) I.C×AER	CEIR (pounds of CO_2E/kWh) Cap(kw)×AER (Renewable)	CEROG (pounds of CO_2E/kWh) Cap(kw)×AER (Non Renewable)	CEDGM (pounds of CO_2E/kWh) CEIR+CEROG	NC (pounds of CO_2E/kWh)	NCC (€)
Kainji	760	228000	41040	136800	177840	50160	910
Jebba	578.4	173520	31233.6	104112	135345.6	38174.4	692.6
Shiroro	600	180000	32400	108000	140400	39600	718.5
Afam	706.6	922480	283840.4	553488	591806.4	330673.6	6000
Okpai	480	624000	25920	374400	313920	223680	4058
Sapele	1020	1326000	55080	795600	850680	475320	8624
Ajeokuta	110	143000	5940	85800	91740	51260	932
AES	315	409500	17010	245700	262710	146790	2663
Delta	912	1185600	49248	711360	760608	424992	7711
Geregu	414	528200	22356	322920	345276	192924	3500
Omoku	150	195000	8100	117000	125100	69900	1268
Omotosho	335	435500	18090	261300	279390	15610	2832
Olorunsogo	335	435500	18090	261300	279390	15610	2832
Egbin	1320	1716000	71280	1029600	1100880	615120	11160.6

The results obtained from these deductions for the emission rates of installed capacity of the conventional generators and emission rate due to a generation mix (i.e. 10%, 20%, 30%, and 40% renewable integration, respectively) between the renewable and the conventional sources will be analyzed. The results so obtained are that of the emission rates of the installed capacity of the conventional generators and emission rates due to a generation mix.

IV. RESULTS AND DISCUSSIONS

Having obtained carbon emission rates of the generation stations due to installed capacity and generation mix, the resulting effect is discussed. Chats, tables, and graphs have been employed to examine the outcome of various amount of renewable integration. The emission rate of the conventional generation stations due to their installed capacity (without a generation mix) is considered too. The outcome of having a generation mix between the renewables and the conventional resources is examined.

4.1 Generation Stations and Emission Rates (Without a Generation Mix)

The carbon emission rates of the various generating stations deduced Section II is shown in Figure 1. From Figure 1, it can be seen that the highest carbon emission rates is that due to the Egbin Gas Power Stations. This is followed by Sapele, Delta, and Afam Gas Power Stations, respectively. This order is consistent with the installed capacities of the stations. The highest emission rate comes from Egbin Power Station with an installed capacity of 1320MW, followed by Sapele Gas Power Station which has an installed capacity of 1020MW, Delta Gas Power Station with 912MW installed capacity, Afam Gas Power Station with an installed capacity of 709.6MW, etc. The Olorunsogo and Omotosho Gas Power plants are at par in terms of the carbon emission rate. This is because these stations have the same installed capacity and operate with the same kind of conventional source. Low emission rate have been observed to come from Kainji, Jebba, Shiroro etc. This is largely due to the fact that the AER for hydro as a source of power generation is much lower than that for natural gas. The other reason being that they have much lower installed capacity than their gas fired counterparts such as Sapele, Egbin and Afam Gas Stations, etc.

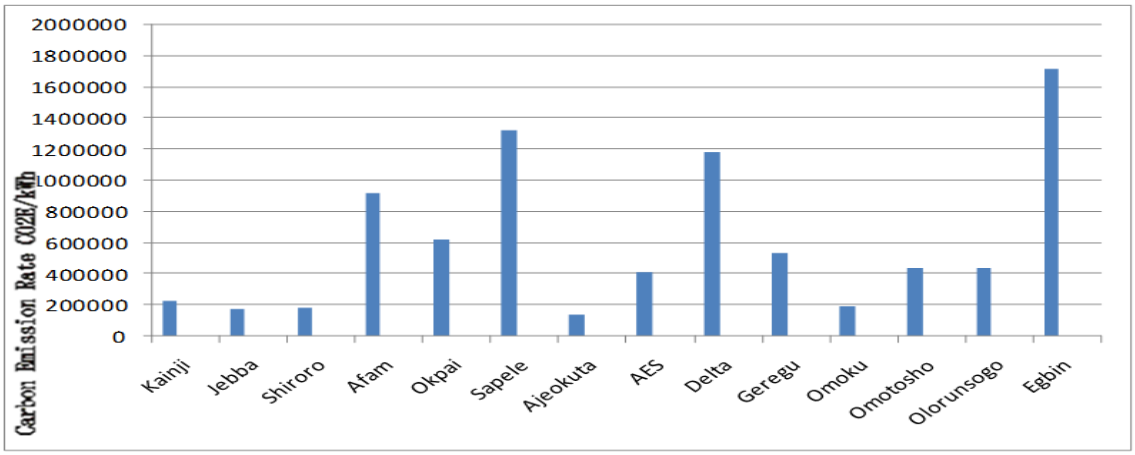

Figure 1: Chat showing the generating stations and their emission rates (without a generation mix)

4.2 Carbon Emission Due To a Generation Mix Of 10%, 20%, 30% and 40% Renewable

A chart depicting the effect of a10%, 20%, 30% and 40% renewable energy integration is shown in Figure 2.

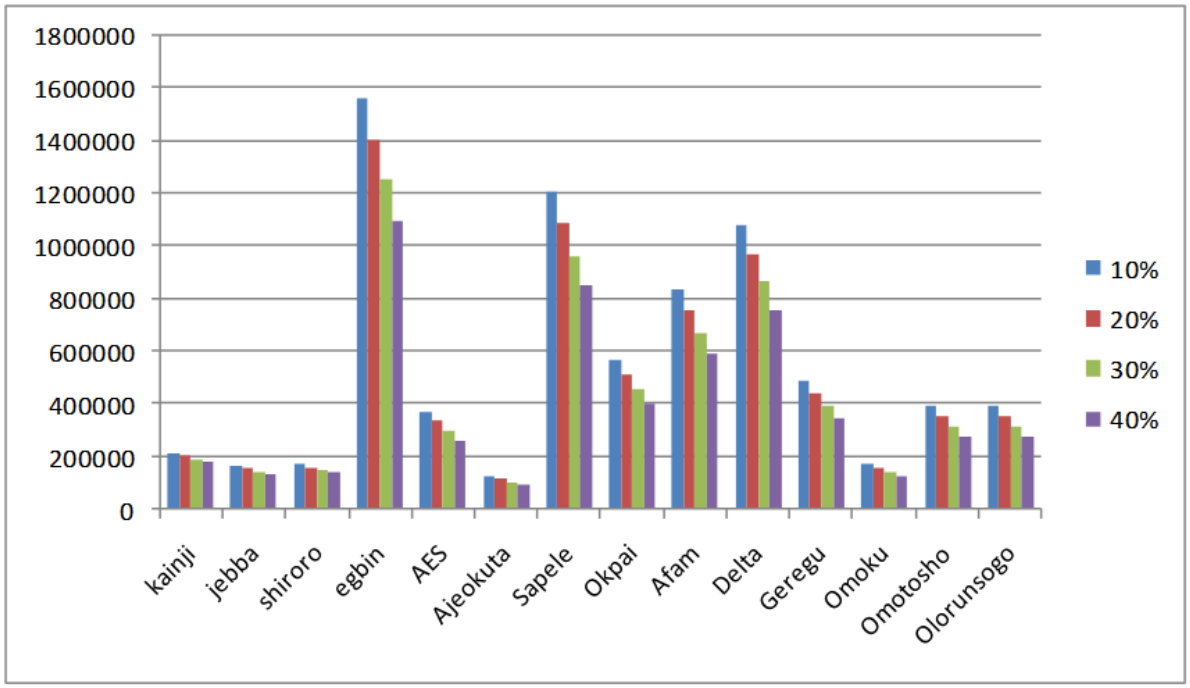

Figure 2: Chart showing the generation stations and the emission rate due to the generation mix of 10%, 20%, 30% and 40% renewable.

The minimum and the maximum reduction in carbon emission rate are obtained here for all power stations. A drastic reduction can be seen for Sapele Gas Power Station as emission rate fall from over 1,300,000pounds of CO_2E/kwh to about 850,000pounds of CO_2E/kwh. Large reductions are noticed for Okpai Gas Power station with a fall from over 600,000pounds to about 400,000pounds of CO_2E/kwh. Same goes for Ajaokuta Gas plant which achieved over 35% carbon emissions reduction. The effect of the renewable integration is further highlighted in Tables V – VIII for 10%, 20%, 30%, and 40% penetrations, respectively.

Table V: The percentage reduction in emission rate of power stations due to a generation mix of 10% renewable.

Power Stations	Carbon emission due to installed Capacity (CO_2E/kwh)	Carbon emission due to generation mix (CO_2E/kwh)	Percentage reduction (%)
Kainji	228000	215460	(228000-215460/228000)×100 =5.5
Jebba	173520	163976.4	5.5
Shiroro	180000	170100	5.5
Egbin	1716000	1562220	8.96
AES	409500	372802.5	8.96
Ajeokuta	143000	130185	8.96
Sapele	1326000	1207170	8.96
Okpai	624000	568080	8.96
Afam	922480	839811.6	8.96
Delta	1185600	1079352	8.96
Geregu	538200	489969	8.96
Omoku	195000	177525	8.96
Omotosho	435500	391950	10
Olorunsogo	435500	391950	10
Average percentage reduction=117.14/14=8.37%			

Table VI: The percentage reduction in emission rates of power stations due to a generation mix of 20% renewable.

Power Stations	Carbon emission due to installed Capacity (CO_2E/kwh)	Carbon emission due to generation mix (CO_2E/kwh)	Percentage reduction (%)
Kainji	228000	202920	11
Jebba	173520	154432.8	11
Shiroro	180000	160200	11
Egbin	1716000	1408440	17.92
AES	409500	336105	17.92
Ajeokuta	143000	117370	17.92
Sapele	1326000	1088340	17.92
Okpai	624000	512160	17.92
Afam	922480	757143.2	17.92
Delta	1185600	973104	17.92
Geregu	538200	441738	17.92
Omoku	195000	160050	17.92
Omotosho	435500	357445	17.92
Olorunsogo	435500	357445	17.92
Average percentage reduction=230.12/14=16.43%			

Table VII: The percentage reduction in emission rates of power stations due to a generation mix of 30% renewable.

Power Stations	Carbon emission due to installed Cap (CO_2E/kwh)	Carbon emission due to generation mix (CO_2E/kwh)	Percentage reduction (%)
Kainji	228000	190380	16.6

Jebba	173520	144889.2	16.5
Shiroro	180000	150300	16.5
Egbin	1716000	1254660	26.88
AES	409500	299407.5	26.88
Ajeokuta	143000	104555	26.88
Sapele	1326000	960510	26.88
Okpai	624000	456240	26.88
Afam	922480	674474.8	26.88
Delta	1185600	866856	26.88
Geregu	538200	393507	26.88
Omoku	195000	142575	26.88
Omotosho	435500	318417.5	26.88
Olorunsogo	435500	318417.5	26.88
Average percentage reduction=345.18/14=24.66%			

Table VIII: The percentage reduction in emission rate of power stations due to a generation mix of 40% renewable.

Power Stations	**Carbon emission due to installed Cap (CO_2E/kwh)**	**Carbon emission due to generation mix (CO_2E/kwh)**	**Percentage reduction (%)**
Kainji	228000	177840	22
Jebba	173520	135345.6	22
Shiroro	180000	140400	22
Egbin	1716000	1100880	35.85
AES	409500	262710	35.85
Ajeokuta	143000	91740	35.85
Sapele	1326000	850680	35.84
Okpai	624000	400320	35.85
Afam	922480	591806.4	35.85
Delta	1185600	760608	35.85
Geregu	538200	345276	35.85
Omoku	195000	125100	35.85
Omotosho	435500	279390	35.85
Olorunsogo	435500	279390	35.85
Average percentage reduction=460.35/14=32.88%			

The tables explicitly show the benefits of the various renewable integration to the grid. The average percentage reduction was evaluated accordingly.
With these results, it is obvious that renewable energy integration is a way out from the increasing carbonization of the Nigerian atmosphere due to generation of power.

4.2 Relationship between Penetration of Renewable Energy and Percentage Reduction of Carbon Emission

The graph of percentage penetration of renewables against percentage reduction in carbon emissions is presented. This is in a bid to establish the relationship between the two as shown in Table IX.

Table IX: Values for the percentage penetration of renewables and percentage reduction of carbon emission

Percentage Penetration	**Percentage CO_2 Reduction**
10%	8.37
20%	16.43
30%	24.66
40%	32.88

Figure 3 clearly shows a linear relationship between the percentage penetration of renewables and percentage reduction of carbon emission.

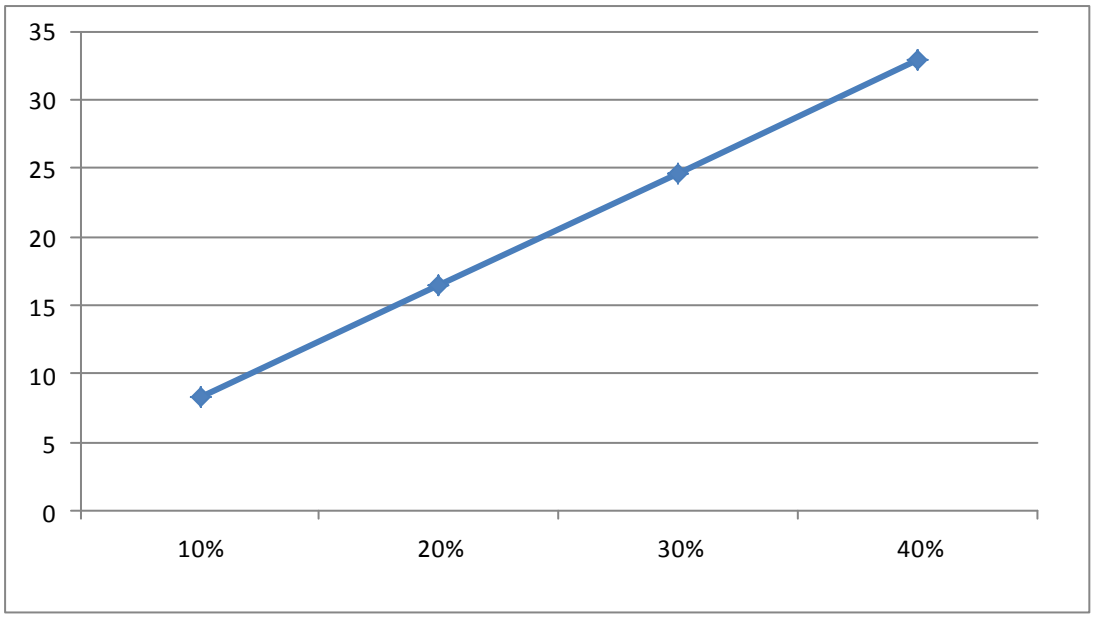

Figure 3: Graphical representation of the percentage penetration against the percentage reduction of carbon emission.

The graph so obtained shows a linear relationship between percentage penetration of renewables and percentage reduction of carbon emissions. The linear equation representing this relationship was obtained as

$$y=0.78x+0.5 \quad (1)$$

where y represents CO_2 reduction (%) and x, the renewable energy integration (%).

As the amount of renewable energy integrated is increased, so also the reduction in carbon emission. This equation is an invaluable tool in deductions involving renewable integration. It quickly tells how much carbon emission reduction can be achieved for a certain amount of renewable integration.

In order to adequately compensate for the pollution of the environment as a result of CO_2 emission, the NCC serves as a penalty for violation of carbon cap. Figure 4 shows the NCC for the power stations. Each power station will save the amount evaluated if it agrees to accomplish any of the corresponding level of integration as shown.

Table X: Showing the Non Compliance Cost (NCC) for all the power stations in each renewable integration.

Power Stations	NCC for each Percentage Renewable Integration (€)			
	10%	20%	30%	40%
Kainji	228	455	682.6	910
jebba	173	346	519.5	692.6
Shiroro	179.6	359	538.9	718.5
Afam	1500	3000	4500	6000
Okpai	1014.6	2029	3043.8	4058
Sapele	2156	4312	6468	8624
Ajeokuta	232.5	465	697.5	932
AES	665.8	1331.7	1997.5	2663
Delta	1927.8	3855.5	5793	7711
Geregu	875	1750	2625	3500
Omoku	317	634	951	1268
Omotosho	790	1416	2124	2832
Olorunsogo	790	1416	2124	2832
Egbin	2790	5580	8370	11160.6

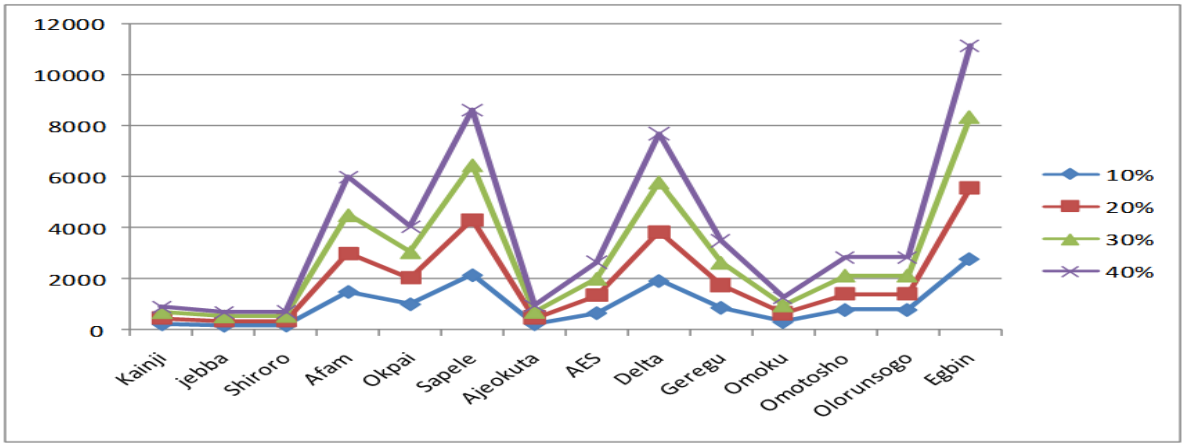

Figure 4: Graphical representation of the Non Compliance Cost (NCC) for the various renewable integration in all the power stations.

V. CONCLUSION

The quest to decarbonize our energy supply due to environmental concerns will result in massive deployment of renewable resources into the electricity supply infrastructure. The changes will normally create challenges due to the intermittent nature of renewable resources. This paper is premised on the proposition that an electric grid with carbon cap powered by mainly conventional generation resources is not sustainable and uneconomical in an environment with massive potential for renewable energy. Different penetrations of renewable energy have been proposed. A linear relationship between the percentage penetration of renewable energy and percentage reduction of CO_2 emission has been established. This model will be a handy tool for future evaluation of renewable energy penetration and government policies as it affects CO_2 emission from. Over the next years, the nation needs to make an intensive effort to deploy massive renewable technology for an effective power generation through renewables. This is supported by the non-compliance cost evaluated.

A business market has also been created due to the non-compliance cost in the event of non-compliance from power producers. Power producers will be on their toes to make sure that they do not violate the renewable integration standards. Otherwise, costs of carbon emitted will add to their operating cost.

REFERENCES

[1] Nigerian Renewable Master plan: Final Draft Report, November, 2005, [online: http://spidersolutionsnigeria.com/wp-content/uploads/2014/08/Renewable-Energy-Master-Plan-2005.pdf], Retrieved 12/03/2014.

[2] D. A. Lashof, S. Yeh, D. Doniger, S. Carter, and L. Johnson, "Closing the Power Plant Carbon Pollution Loophole: Smart Ways the Clean Air Act Can Clean Up America's Biggest Climate Polluters" *Natural Resources Defense Council (NRDC) Report, March 2013.*

[3] J.-F.K. Akinbami, M.O. Ilori, T.O. Oyebisi, I.O. Akinwumi, and O. Adeoti, "Biogas energy use in Nigeria: current status, future prospects and policy implications," *Renewable and Sustainable Energy Reviews, Elsevier (Science Direct), Volume 5, Issue 1, March 2001, Pages 97-112*

[4] A. Doig and M. Adow, "Low-carbon Africa: Leapfrogging to a green future," Christian Aid, November 11.

[5] S. O. Oyedepo, "Energy and sustainable development in Nigeria: the way forward," *Energy, Sustainability and Society*, July 2012, pp.3

[6] Famuyide O.O., Adu A.O., Ojo M.O., "Socio-Economic Impacts of Deforestation in the Sudano - Sahelian Belt of Nigeria," *Journal of Forestry Research and Management* Vol.1 (1&2), pp. 94–106, 2004

[7] Renewable Energy Master Plan: Final Draft Report, November 2005, [online: www.iceednigeria.org], Retrieved 12/03/2014

[8] C. Brahic, "China's emissions may surpass the US in 2007," New Scientist, 25 April 2007.

[9] S. Shah, "China to surpass US greenhouse gas levels by 2010". *The Independent* (UK). November 8, 2006. [online:http://www.independent.co.uk/news/world/asia/china-to-pass-us-greenhouse-gas-levels-by-2010-423407.html], Retrieved 12/03/2014

[10] "China fears disasters, grain cut from global warming," Zeenews, India, December 28, 2006. [online: http://zeenews.india.com/news/eco-news/china-fears-disasters-grain-cut-from-global-warming_344727.html], Retrieved 12/03/2014.

[11] "Energy policy of China," [online: http://www.ambpechino.esteri.it/NR/rdonlyres/54879255-E4DB-4BF3- A1B2-2C8C0D47C8CF/21586/Librobiancoenergia2012Cina.pdf], Retrieved 3/05/2014

[12] "Energy efficiency policies and measures in Germany," ODYSEE- MURE 2010, Monitoring of EU and national energy targets Report, Karlsruhe, November, 2012, [online: www.isi.fraunhofer.de], Retrieved 3/05/2014

[13] "Overview of Russian Environmental Regulation," King & Spalding Environmental Practice, May 2012. [online:http://www.kslaw.com/imageserver/KSPublic/library/publication/RussianEnvironmental.pdf], Retrieved 15/07/2014.

[14] C. Newsom, "Renewable energy potential in Nigeria: Low-carbon approaches to tackling Nigeria's energy poverty," International Institute for Environment and Development, 2012, [online: http://pubs.iied.org/pdfs/G03512.pdf], Retrieved 12/03/2014.

American Journal of Engineering Research (AJER) 2016
American Journal of Engineering Research (AJER)
e-ISSN: 2320-0847 p-ISSN : 2320-0936
Volume-5, Issue-1, pp-73-79
www.ajer.org
Research Paper Open Access

Structural optimization of a reinforced concrete building

Enea Mustafaraj[1], Denis Saliko[2],
[1](Department of Civil Engineering, Epoka University, Albania)
[2](Department, Civil Engineering, TU Dresden, Germany)

ABSTRACT : *In this study, a residential building has been designed multiple times, firstly with the initial configuration and later optimized based on different theories. Each of the optimized designs was created based on a specific idea of structural optimization. Eurocodes have been used as the design code for the models. In order to compare the designs, CSI ETABS commercial software has been used. In the design of the models, some initial conditions such as the soil type and the seismicity of the area were specified the same for the models in order for the optimization to be intended for the conditions of the real building. The main objective was to compare different design strategies and optimize to achieve the most suitable case.*

Keywords *–reinforced concrete design, structural optimization, FEM analysis, ETABS*

I. INTRODUCTION

Most of the residential structures built in Albania after 1990s are reinforced concrete structures. The planned service life for this type of building is around 50 years. The structural design of reinforced concrete buildings generally consists on finding the proper arrangement between geometrical shapes of the frame elements and materials (concrete and steel in this case). As the structure will be subjected to wide variety of loads and act predictably under different situations, the basic considerations for a structural design are: the load combinations, the soil type, the seismicity of the area and the properties of the materials. Design codes have been established to help engineers to create structures which comply with all the requirements.

In order to improve the design, optimization techniques are used. The main purpose of optimization techniques is to obtain the maximum benefit out of the resources available. To achieve an optimized design it is necessary to minimize the usage of materials and maximize the performance of the structure in various predicted situations. Most of the procedures used to achieve an optimized design consist on trying different cross sections, materials and arrangements in order to achieve the limit state parameters predicted by design codes. In cases when multiple design arrangements satisfy the code parameters, the design with the highest performance is considered as a better design compared to the others.

The performance of the building is clearly defined on various design codes as the behavior of a structure under different loading conditions. For the analysis of the models Eurocode 2 [1] was used to specify the different actions and conditions on the building.

Since the structural design of residential buildings takes a lot of time and requires a high accuracy in calculations, it is a common practice to use structural analysis software. In this study, ETABS2015 [2] has been used to analyze the models and to display various output parameters. The details of the reinforcement are an integral part of the design of any reinforced concrete structure, therefore the reinforcement details for the typical beams columns and slabs of the optimized structure generated have been designed.

II. MATERIALS AND METHODS

2.1 Structural Optimization

The idea of creating an improved design over the original one date back to 1600s when Leonardo da Vinci created multiple small scale structures and compared their performance. Structural optimization as a term and its importance was noted by Cohn and Dinovitzer in 1994, who showed the gap between structural theories and practical application on structural design and the importance of a good initial design [3].Sarma and Adeli, in 1998, pointed out that the cost of reinforced concrete structures depended on the cost of concrete, reinforcement and formwork and the combination of different materials and geometry arrangements would produce an optimized structure [4]. However, this study focused only on the economic analysis of the structure and not the optimization of its performance. Later with the development of computers and programming the field of structural optimization was separated into two main branches, the traditional approach and the heuristic

approach. The traditional approach means an implementation of trial and error techniques and comparison between the initial and the optimized structure. Fletcher, 2001[5] and Hernandez and Fontan 2002 [6] were the first to start development into this approach. The heuristic approach followed the computerized path with the development of multiple algorithms such as genetic algorithms, bee colonies, threshold accepting, stimulated annealing etc.[7-10].

As it is pointed out by Tang, 2011 performance based structural optimization is divided into 3 categories: size optimization, shape optimization and topology optimization [11]. Size optimization consists on the size of the member being the only type of variable in the structure. Shape optimization consists on the variety of shapes to be used for different structural elements. Topology optimization consists on finding the optimal layout of the structure. The initial ideas for finding the optimal layout came from Maxwell, 1890 [12] and Michell, 1904, [13] who developed the layout optimization theory for thin bar structures such as trusses. Later, the optimal layout theory was developed by Prager and Rozvany, 1977, [14]. This theory was based on Mitchell's optimization for trusses but instead it focused on the optimization of grid-like structures. The bubble-method proposed by Eschenauer et al., (1994) [15] introduced the removal of non-functional material by placing holes or bubbles in order to create a new type of structure. Xie and Steven, 1993, [16] proposed the evolutionary structural optimization (ESO) method which implied the gradual removal of the elements until an optimized design had been achieved. Nibbling ESO was a part of this theory which allowed only the removal of external boundary elements similar to a worm which nibbles the leaf. Later, the bi-directional evolutionary structural optimization (BESO) by Querin, 1998 [17] which modified the original ESO by allowing also element addition where was necessary. Over the last years several approaches have been made in the improvement of ESO and BESO methods of structural optimization.

2.2 Case study

The case study building is an-eight-story residential building located in Fier, Albania and was constructed in 2009.The first floor is intended for commercial purposes while the other stories are intended for residential purposes. The floor area is 382.4 m^2 for each of the floors. The building is characterized by the irregular shapes of the balconies (Fig.1).

Figure 1: Case study building.

The slab type used on the structure is ribbed slab with a thickness of 300 mm. The thickness of the concrete layer is 50 mm and the remaining 250 mm is composed of polystyrene. The stem width at top is 500 mm, the stem width at bottom is 100mm and the rib spacing is 400 mm. Two types of beams were used for the structure each with different sections. The perimeter beam section 250 x 650 mm and the internal beams 250x 300 mm. The concrete grade used for the slabs and the beams is C20/25 concrete. The columns are of 7 different types of sections out of which 4 are columns with rectangular sections (900 x 250; 550 x 250, 650 x 250 and 800 x 250 mm). There are two L-shaped column sections (800 x 800 x 250; 900 x 900 x 250 mm). The last type of column section is a T-section 800 x 800 x 250 mm. The concrete grade used for the columns is C25/30 concrete. The partition brick walls used for the building were 120 mm for the internal partitions, 200 mm for the balconies and 250 mm for the external walls. For the lintels on the doors and windows, C20/25 secondary beams with a section of 125 mm x 250 mm were used.

In the consideration of earthquake loads, the response spectrum has to be defined. This required various input data such as the ground acceleration, ground type and the behavior factor. This data is different for each area, and specific studies for Albania were required. The seismic hazard assessment studies by Aliaj et al. (2004) [18], Duni et al., 2010, [19] and Galasso et al., 2013, [20] were considered on the earthquake considerations during the analysis of the models in this study.

2.3 Modeling

In this study, the structure was modelled using ETABS 2015 commercial software. Since ETABS is based on Finite Element Method FEM all the shell elements have to be divided into smaller elements. This is called the meshing process and it can be done manually or automatically in ETABS. Figure 24 shows the automatic mesh settings for floors with 1m approximate mesh size.

2.3.1 Loading considerations

Dead and live loads were assigned to the shell elements of the structure according to Eurocode 1 EN1991-1-1:2002 [21]. Since this is a domestic/residential building it is included under category A of Eurocode 1. The following values to be assigned were obtained from Table 6.2 on Eurocode 1.

- Dead Loads: Gk = 2.0 kN/m^2 (includes the floor tiles, finishes and screed concrete)
- Live Loads:
  - Floors: Qk = 2.0 kN/m^2
  - Stairs: Qk = 4.0 kN/m^2
  - Balconies: Qk = 3.0 kN/m^2

Earthquake loads were also taken into consideration in the form of response spectrum with a PGA = 0.3 g and a behavior factor 4.0 inferred from the soil type "D" "deposits of loose-to-medium cohesionless soil" based on EN 1998 [22].

In order to obtain the moment envelope for the load cases different combinations of these cases are specified based on Eurocode 1 [21] were defined:

- Combination 1: 1.25 Qk + 1.5 Gk
- Combination 2: 1.25 Qk + 1.05 Gk
- Combination 3: 1.35 Qk + 1.5 Gk
- Combination 4: 1.35 Qk + 1.05 Gk
- Combination 5: 1.35 Qk + 1.5 Gk + 0.7 EQx + 1.0 EQy
- Combination 6: 1.35 Qk + 1.5 Gk + 1.0 EQx + 0.7 EQy

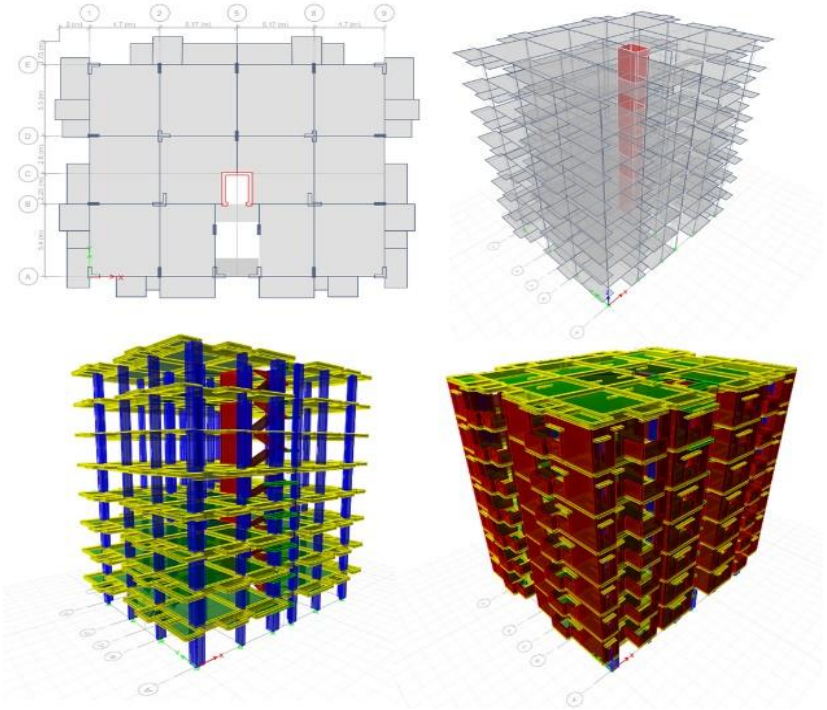

Figure 2: Stages of modelling of the structure in ETABS.

2.4 Analysis Approach

Analysis approach consists of comparing four different models of the same layout, subjected to the same type of loading conditions but having different cross-sectional characteristics, and material strengths. The comparison was made by comparing the maximum values of shell stresses and modal displacement values. The

shell stresses are generated by the FEM algorithms incorporated into ETABS and are displayed as scalar field representation with varying colors representing the variation of stresses on shell elements.

The modal analysis uses superposition to linearly add the sinusoidal oscillations in order to obtain the deformations which happen on the building during the earthquake. The technique considers both spatial and time changes evaluating both displacements and periods/frequencies. The period of the building is the time required for a full cycle of displacement until the building returns to its original position.

2.4.1 Model 1

The first model was the same as the original structure with the same materials specified on section 2.2.

2.4.2 Model 2

In the second model the concrete grade used for the elements of the frame was changed. For each element, the concrete grade was increased by one scale based on EC2. For the columns and the staircase C30/37 concrete was assigned. For the beams and the slabs C25/30 was assigned. The second model was modeled to inspect the changes in behavior of the structure with the change of the material type.

2.4.3 Model 3

In the third model the section geometry of the columns was changed. All the columns of the building were substituted with circular columns with a diameter of 400 mm and 500 mm (only for the composite column). The vertical supporting area of the columns per floor was significantly increased from 58750 cm^2 to 126228 cm^2. The third model was created to show the optimization of the structure using a different type of section geometry.

2.4.4 Model 4

For the fourth model, the slab type was changed from ribbed slab into monolithic slab with the same slab thickness 300 mm. This was done in order to increase the weight of the structure and provide it with a lower center of gravity.

III. RESULTS AND DISCUSSION

For the shell stresses, the comparisons were made for the 4 models on 3 different load combinations. The load combinations taken into consideration were:

- Combination 3: 1.35 Qk + 1.5 Gk
- Combination 5: 1.35 Qk + 1.5 Gk + 0.7 EQx + 1.0 EQy
- Combination 6: 1.35 Qk + 1.5 Gk + 1.0 EQx + 0.7 EQy

The following shell stresses were extracted from ETABS in order to be used as variables for comparison of the four models: S11, S12, S13, S22, S23, Smax, SmaxV, Smin and SVM. The scalar field representations for the abovementioned shell stresses are shown in the following figures in the abovementioned order. Figs. 3-6 show stress distribution examples using various load combinations. The values of the stress are presented in detail in the tables below.

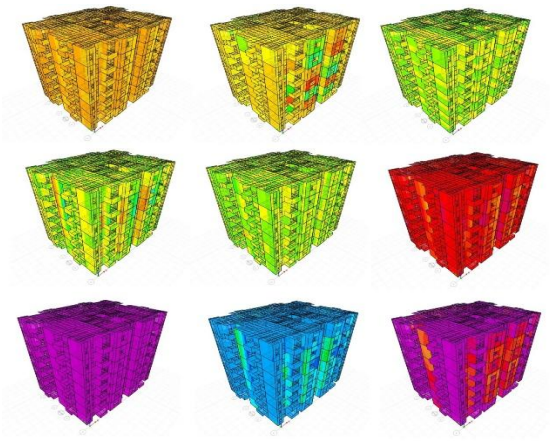

Figure 3: Shell stresses: model 1; load combination 3

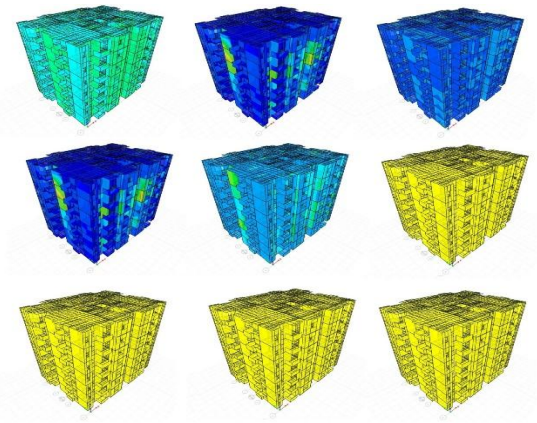

Figure 4: Shell stresses: model 1; load combination 5

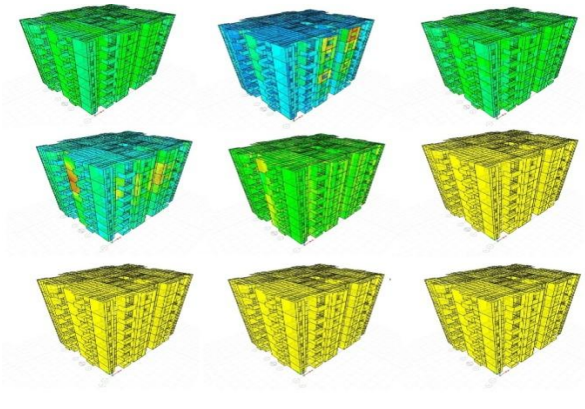

Figure 5: Shell stresses: model 2; load combination 5

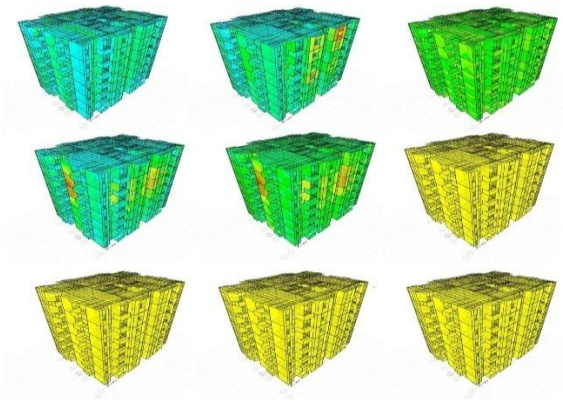

Figure 6: Shell stresses: model 2; load combination 6

The comparison between shell stresses of different models for the same load combination 1.35Qk + 1.5Gk is shown in Table 1. As it can be seen from the table, Model 2 is superior among them, as all the values are lower.

Table 1: Comparison of shell stresses on load combination 1.35 Qk + 1.5 Gk

Load Case: $1.35Q_k + 1.5G_k$					
		Model 1	**Model 2**	**Model 3**	**Model 4**
S11 (MPa)	Max	17.68	12.422	10.368	6.541
	Min	-12.351	-11.751	-12.491	-7.066
S12 (MPa)	Max	4.599	1.719	2.194	4.738
	Min	-4.609	-2.212	-1.772	-3.112
S13 (MPa)	Max	5.257	5.903	6.159	3.344
	Min	-5.603	-4.922	-4.11	-3.855
S22 (MPa)	Max	8.826	4.093	4.957	7.151
	Min	-9.428	-8.016	-8.694	-7.122
S23 (MPa)	Max	0.213	0.176	0.213	1.883
	Min	-0.311	-0.264	-0.253	-3.011
Smax (MPa)	Max	11.713	12.422	12.491	7.186
	Min	-1.79	-0.71	-0.881	-0.731
SMaxV (MPa)	Max	5.607	5.904	6.16	3.901
	Min	0	0	0	0
Smin (MPa)	Max	1.686	0.652	0.52	0.56
	Min	-17.713	-12.422	-12.491	-7.186
SVM (MPa)	Max	17.527	12.324	12.218	8.236
	Min	-4.2E-05	-5.1E-05	-2.29E-05	-8.4E-05

In Table 2, it is presented the comparison of the main stress values under combination 5. As it can be seen from the table, Model 3 is superior, followed by Model 2.

Table 2: Comparison of shell stresses on load combination 1.35 Qk + 1.5 Gk+ 0.7 EQx + 1.0 EQy

Load Case: $1.35Q_k + 1.5\ G_k + 0.7\ EQ_x + 1.0\ EQ_y$					
		Model 1	**Model 2**	**Model 3**	**Model 4**
S11 (MPa)	Max	23.51	9.653	10.526	5.809
	Min	-108.769	-34.027	-16.786	-8.803
S12 (MPa)	Max	2.509	1.297	1.145	1.868
	Min	-35.011	-6.89	-0.216	-9.663
S13 (MPa)	Max	3.261	4.266	3.571	2.752
	Min	-34.645	-10.347	-5.528	-7.911
S22 (MPa)	Max	5.035	5.422	4.221	9.871
	Min	-83.947	-18.949	-9.534	-14.822
S23 (MPa)	Max	0.384	0.278	0.162	2.204
	Min	-1.542	-0.42	-0.332	-4.005

For the modal analysis, five modes were taken into consideration. The maximum and minimum displacements and the periods were generated by ETABS for each mode. The modal analysis comparison between the models is displayed on Table 3.

Table 3: Comparison of modal displacements between the models.

		Model 1	Model 2	Model 3	Model 4
Mode 1	U_{max}(mm)	0.002089	0.00328	0.01932	0.002407
	U_{min}(mm)	-0.01832	-0.01892	-0.00228	-0.01963
	T(s)	1.82	0.344	0.069	0.514
Mode 2	U_{max}(mm)	0.02353	0.03536	0.03095	0.0239
	U_{min}(mm)	-0.031	-0.02301	-0.02421	-0.03127
	T(s)	0.105	0.093	0.108	0.08
Mode 3	U_{max}(mm)	0.7	0.1	0.8	0.8
	U_{min}(mm)	-0.8	-0.04236	-0.7	-0.7
	T(s)	0.024	0.037	0.024	0.024
Mode 4	U_{max}(mm)	0.01951	0.8	0.03048	0.0298
	U_{min}(mm)	-0.0302	-0.7	-0.01961	-0.0189
	T(s)	0.014	0.024	0.014	0.014
Mode 5	U_{max}(mm)	0.03193	0.01923	0.1	0.1
	U_{min}(mm)	-0.03328	-0.03003	-0.1	-0.1
	T(s)	0.012	0.014	0.007	0.009

IV. CONCLUSION

As it can be inferred from the comparisons, none of the models is superior to the others in every direction. While intending to optimize the structure for a specific behavior there might be "side effects" meaning that other properties might change to unexpected values.

The results obtained from the analysis of Model 2 show that an increase in the concrete grade optimizes the structure when subjected to dead and live loads in all the stress values. However after observing shell stresses and modal displacements having considered the earthquake loads, some of the values show no significant optimizations and some of them even show deterioration.

From the third model it is shown that while circular columns and the increase of column area per floor show no visible optimization on dead and live loading conditions, they decrease the shell stresses significantly when the building is subjected to earthquake loads therefore optimizing the structure. However since the beams which transmitted the loads to the columns had a smaller section compared to the column, a check on the connection between the beams and the column is required.

From the fourth model it is concluded that strength is not the only important parameter in structural design but weight is also needed to be taken into consideration. A lower weight especially on the upper floors contributes significantly in lowering the center of gravity for the entire structure as well as decreasing the stresses on many elements of the structure.

REFERENCES

[1] EN1992-1-1 – Design of reinforced concrete structures, 2005.
[2] CSI ETABS 2015, Berkeley, California (USA), *Computers and Structures Inc*., 2015.
[3] Cohn M.Z. and Dinovitzer A.S., Application of structural optimization. *ASCE Journal of Structural Engineering, 120(2)*: pp.617-649, 1994.
[4] Sarma K.C. and Adeli H., Cost optimization of concrete structures, *ASCE Journal of Structural Engineering, 124(5)*, pp.570-578, 1998.
[5] Fletcher R., Practical Methods of Optimization, Wiley: Chichester, 2001.
[6] Hernández S. and Fontan A., Practical Applications of Design Optimization, WIT Press: Southampton, 2002.
[7] Coello C.A., Christiansen A.D. and Santos F., A simple genetic algorithm for the design of reinforced concrete beams, *Engineering with Computers, 13*, pp. 185-196, 1997.
[8] Lee C. and Ahn J., Flexural design reinforced concrete frames by genetic algorithm, *ASCE Journal of Structural Engineering, 129(6)*, pp. 762-774, 2003.
[9] Camp C.V., Pezeshk S. and Hansson H., Flexural design reinforced concrete frames using a genetic algorithm, *ASCE Journal of Structural Engineering, 129(1)*, pp. 105-115, 2003.

[10] Leps M. and Sejnoha M., New approach to optimization of reinforced concrete beams, Computers and Structures, 81, pp. 1957-1966, 2003.
[11] Jiwu Tang. Developing Evolutionary Structural optimization Techniques for Civil Engineering Applications, RMIT University, 2011
[12] Maxwell JC. 1890. On reciprocal figures, frames and diagrams of forces. *Scientific Papers 2*:160-207.
[13] Michell AGM. 1904. The limits of economy of material in frame-structures. Phil Mag 8:589-597.
[14] Prager W, Rozvany GIN. 1977. Optimization of structural geometry. In Proceedings of Dynamical systems, New York, 1977, 265-293.
[15] Eschenauer HA, Kobelev VV, Schumacher A. 1994. Bubble method for topology and shape optimization of structures. *Structural Optimization. 8*:42-51.
[16] Xie YM, Steven GP. 1993. A simple evolutionary procedure for structural optimization. *Computers and Structures 49*, 885-886.
[17] Querin OM, Steven GP, Xie YM. 1998. Evolutionary structural optimization (ESO) using a bi-directional algorithm. Engineering Computations 15:1034-1048.
[18] Aliaj S., Adams, J., Halchuk S, Sulstarova S. Probabilistic Seismic Hazard Maps for Albania. 13th World Conference on Earthquake Engineering. 2004
[19] Duni Ll., Kuka N. Towards a New Seismic Hazard Assessment of Albania. *EECE*. 2010
[20] Galasso C., Gomez I., Gupta A. Probabilistic Seismic Hazard Assessment for Albania, Macedonia and Serbia. *SE-EEE*. 2013.
[21] EN 1991-1 Actions on structures - Part 1-1: General actions, 2002. Densities, self-weight, imposed loads for buildings.
[22] EN 1998-1: European seismic design code, Design of structures for earthquake resistance, Part 1: General rules, seismic actions and rules for buildings, 2004.

American Journal of Engineering Research (AJER) 2016
American Journal of Engineering Research (AJER)
e-ISSN: 2320-0847 p-ISSN : 2320-0936
Volume-5, Issue-1, pp-80-86
www.ajer.org
Research Paper Open Access

Design and Analysis of a Wheelchair Mounted Robotic Arm with Remote Actuation System

Ernest Sharp[1], Ryan Binter[2,] Yimesker Yihun[3]
[123](Mechanical Engineering, Wichita State University, USA)

ABSTRACT: *This paper presents a new design of foldable, compact and cost-effective Wheelchair-Mounted-Robotic-Arm (WMRA).The design is based on remote actuation using stepper motors placed near the wheel- chair armrest and a synchronous belt system. This design helps to shift the weight closer to the wheelchair and maintain the required speed, torque and inertia while delivering full dexterity by actively driving each joint of the robot. The robot will assist patients with different conditions of impairments to eat, drink, and move objects accurately. The lightweight structure designed from hollow PVC tubes and aluminum sheets helps to ease and facilitate port ability. The placement of the whole robot and coupled joints are taken into consideration to reduce physical and sensory interference with the user and the wheelchair. The strength and deflection of critical parts of the robot have been tested through finite element analysis (FEA) and the workspace of the robot has been studied through Kinematics analysis. The testing results indicate that the designed WMRA is strong enough to handle and manipulate objects as heavy as 4kg in a wide range of workspace.*

Keywords - ADL, Assistive Devices, Assistive Technology, WMRA

I. INTRODUCTION

Assistive technology systems are one of the highly active areas of recent robotic research. In the past few years, the demand for high performance robots for daily human activities increased rapidly due to the advancement of robotics technology. New robot technologies, acting in collaboration with humans, have the potential to increase greatly both productivity and quality of life. One such evolving co-robot technology is the WMRA. The goal of the WMRA is to augment the abilities of people with disabilities to accomplish routine day-to-day activities. In 2013, 50.7 % of Americans age 75+ were classified as having a disability, with 33% of them have ambulatory disabilities. Considering all Americans, about 20.7 million Americans potentially need wheel chairs or other mobility assistance devices [1]. Assistive technologies such as robotic arms hold a promising future in helping the elderly and people with disability. Currently, many WMRAs are proposed/designed [2–5]. However, there are still many challenges and issues that limits the advancement of the technology for instance the availability of effective controls, higher performance actuators, cost, safety, size, payload and user interface. All these considerations made the design difficult. Some of the issues that need to be addressed in the mechanical design of WMRA are range of motion, comfort, low inertia and safety. Similarly, in the control of WMRA issues like control ability, smooth motion generation and flexibility are required. Of particular interest are the ability to design, Implement, and test assistive control strategies.

People with varying degrees of disability can use the WMRA. Finding a control system that is compatible with all users is a key part to a successful WMRA. Many users have limited muscle control in their arm/hands, making switches and joysticks hard to manipulate with care. One possible solution to this might be the incorporation of visual recognition software into the arm similar to [6]. The user can then input through voice/touchpad which object in the field of view is to be picked up/moved. A nine-degree of freedom robotic arm system controlled by user brain wave is developed in [7]. The user wears a cap with sensors in it, and when a stimulus is detected, the arm moves accordingly. All users, regardless of the degree of disability can utilize this ideal interface system. Another desire is to have the ability to recognize beyond the field of view. An example of this would be checking

into a hotel and inputting room number and the WMRA will access the elevator, open the doors etc. to get into the room [8].

Another challenge to WMRA is the design of a gripper capable of doing different tasks. The gripper must be able to perform a variety of tasks, including picking up objects at different angles, opening doors, pushing buttons, etc. Some tasks, such as picking up a glass of water, are best done with two fingers. Other tasks like opening knob style doors may require three fingers in order to get a sufficient grip. Rapacki tested a three-finger arm on a variety of doorknobs [9], and the results were surprising. Even with a rubber coating on the fingers, the arm could not grip most knobs. A possible solution to this would be to increase the torque applied to the fingers. Although increasing torque means increasing quality of components, leading us back to the affordability problem.

The current market offers WMRAs in the price range of $5,000 to $40,000 [10], which is too costly to be utilized by many users. In this paper, three specific issues associated with the WMRA are explored: 1) maximizing workspace of the robotic arm, 2) reducing weight in the arm through remote-actuation system, and 3) keeping the cost of the WMRA low while maintaining a good balance of maneuver ability and functionality. It is expected that with this design many people with varying degrees of disability will be benefited.

II. MECHANICAL DESIGN

The mechanical design is approached to meet the list of requirements such as space constraints (able to be stored on the side of the wheelchair), lightweight (under 5kg weight), foldable and extendible up to 1m, ability to lift and hold a weight of 4kg object, ability to feed the user, and affordability (under $1,000). Considering these and other factors, the overall shape and size of the WMRA is outlined as shown in Fig. 1. To keep the arm lightweight, durable and low cost, the robotic arm components are made from PVC tubes and aluminum sheets. The PVC tubes also added an aesthetic value to the robot by discreetly hiding the pulleys, cables and belts. The design also provides a clear access to the motors, cables and joint pulleys for a simple maintenance without having a major disassembly.

Figure 1: The general layout of the WMRA in extended and folded position

2.1 Base Swivel

The base consists of a stationary motor mount bracket, mounted to the wheelchair, and carries the complete arm assembly as shown in Fig.2. The complete arm assembly will pivot around a single bolt ran through the fixed bracket, and supported by a thrust and axial bearings. Rotational motion will be supplied via a Nema 17 stepper motor with gearbox (capable of 3 Nm) connected via pulley and synchronous belt to a pulley that is fixed to the arm assembly. After the pulley reduction, the output torque is 8Nm.

2.2 Shoulder and Elbow Joints

A Nema 23 stepper motor with gearbox (capable of 40 Nm) mounted in the motor box will power the shoulder joint. Power will be transferred via a 2:1 pulley and belt system to a pulley that is fixed to the PVC shoulder joint of the arm (Fig.2).The final output torque of the motor after gear reduction is 80 Nm.The elbow joint will have a pulley fixed to it via brackets inside the elbow (Fig.3). A synchronous belt will run inside the PVC arm from the elbow joint to the shoulder joint. The Nema 23 stepper motor (capable of 40Nm) for the elbow joint is kept at the base in order to keep a low center of gravity in the arm. The stepper motor output shaft will run directly through the pivot point to the shoulder joint, and have a pulley fixed to the shaft on the inside of the PVC arm. The pulley configuration will yield a 60 Nm torque capability.

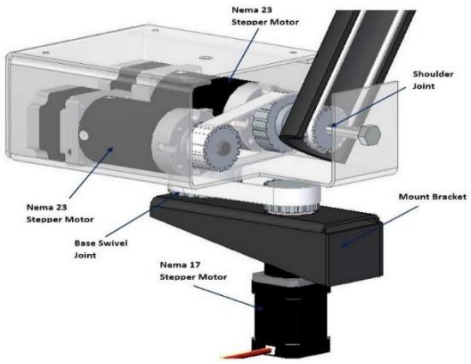

Figure 2: The motor box located at the base of the arm. The base swivel, shoulder and elbow joints are powered from these motors. (PVC arm sectioned for clarity)

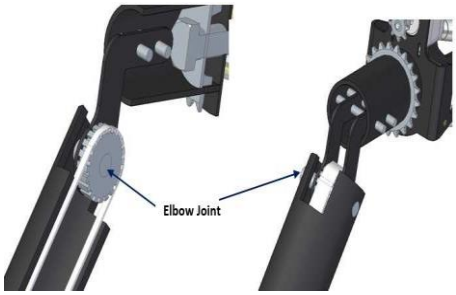

Figure 3: The elbow joint: powered via the motor located in the base and belt ran inside the PVC arm).

2.3 Gripper Assembly

The gripper assembly uses a Nema 17 stepper motor fixed to the gripper assembly, and sprocket fixed to the arm assembly to allow for wrist rotation. See Fig.4. Dual pneumatic cylinders (Bimba #021-6-DXP) power the wrist pivot, providing a lifting force capable of supporting 5.4 kg. A single pneumatic cylinder (Bimba #020.65-D) powers the dynamic gripper finger. This gripper finger has a gripping strength of 40N in the center of the palm. The wrist swivel joint is actuated using a NEMA stepper motor. The gripper wrist joint is capable of pivoting approximately 90 degrees. Coupled with the wrist joint swivel capability of 180 degrees, this will allow a full range of motion for the hand. The rounded finger base and extending fingertips will help hold bottles and other objects securely. The grippers can also be easily lined/covered with rubber to grasp different size of objects without causing any damage to the object.

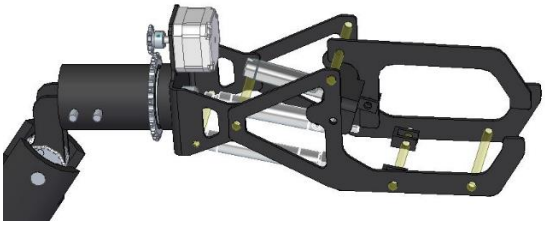

Figure 4: Gripper assembly, stepper motor and sprockets provide rot provides dual air cylinder provide wrist joint movement, and single air cylinder provides finger gripping.

2.4 Actuation System

Nema stepper motors combined with a belt system are used to actuate the main joints of the WMRA. These stepper motors provide the desired amount of torque and are also widely used, readily available and relatively inexpensive [11].The stepper motors will be powered through a Tiny GCNC controller board. The board has four stepper motor drivers and a microcontroller integrated into the board (Fig.5),the detail features of the board can be obtained in [12].To maintain a smooth motion and a constant jerk, a cubic polynomial will be used in the trajectory planning. Input from the user will be via surface electromyography (EMG) signals. This will allow users of any level of disability to control the arm.

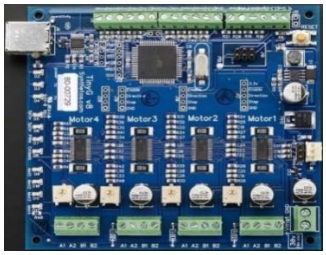

Figure 5: TinyG CNC controller board [12]

III. KINEMATICS ANALYSIS OF THE WMRA

The designed WMRA is a serial chain robot and its forward kinematics equations are defined by a transformation from the base frame to the end- effector frame. These equations provide the set of all positions reachable by the robot for the given joint inputs. The Denavit-Hartenberg convention [13– 15] is frequently used to assign reference frames to each link of the robot defined as a series of joint axes denoted by S_i, where, i= 1, ...,n (Fig.6). In this convention, link coordinate frames are attached so that the z-axis is directed along the axis S_i and its x-axis is directed along the common normal A_{ij}. Considering x=(x, y, z)^T to be coordinates in moving frame (M) and X= (X,Y,Z)^T to be coordinates measured in the fixed frame (F), the screw displacement along a joint axis, S_i, is defined by $X = [Z(\theta_i, d_i)]x$, Similarly, the screw displacement from one joint axis to another along the X-axis by the amounts a_{ij} and α_{ij}, which is defined by X = [X (α_{ij}, a_{ij})]x, where,

$$[Z(\theta_i, d_i)] = \begin{bmatrix} cos\theta_i & -\sin\theta_i & 0 & 0 \\ \sin\theta_i & cos\theta_i & 0 & 0 \\ 0 & 0 & 1 & d_i \\ 0 & 0 & 0 & 1 \end{bmatrix} \quad (1)$$

$$[X(\alpha_{ij}, a_{ij})] = \begin{bmatrix} 1 & 0 & 0 & a_{ij} \\ 0 & \cos\alpha_{ij} & -\sin\alpha_{ij} & 0 \\ 0 & \sin\alpha_{ij} & \cos\alpha_{ij} & 0 \\ 0 & 0 & 0 & 1 \end{bmatrix} \quad (2)$$

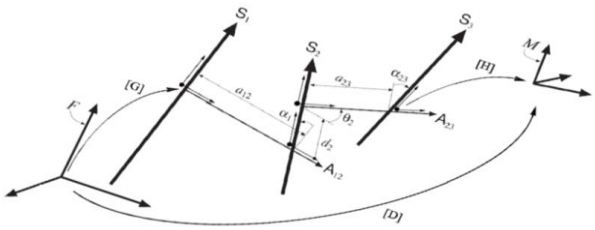

Figure 6: A serial chain with its joints

The set of all positions reachable by the robot is defined by its kinematic equations as the set of all homogenous transformation [D] from the base frame to the end-effect or frame as follows,

$$[D] = [G][Z(\theta_1, d_1)][X(\alpha_{12}, a_{12})][Z(\theta_2, d_2)] \dots [X(\alpha_{n-1,n}, a_{n-1,n})][Z(\theta_n, d_n)][H] \quad (3)$$

Where, [G] and [H] are the coordinate transformations from the base frame to the first joint axis and from the last joint axis to the end-effector frame, respectively. Equation (3) provides the work space of the robot parameterized by the joint variables, (θ_i, d_i), and the link dimensions, (α_{ij}, a_{ij}).

The DH-Parameters for the designed WMRA are shown in Table.1. Based on these parameters, the forward kinematics have been analyzed using RoboAnalyzer software [16]. The kinematic model of the robot is formulated as shown in Fig.7. For the given trajectory and range of joint angles (Fig.8), the corresponding end-effector/gripper positions are shown in Fig.9.

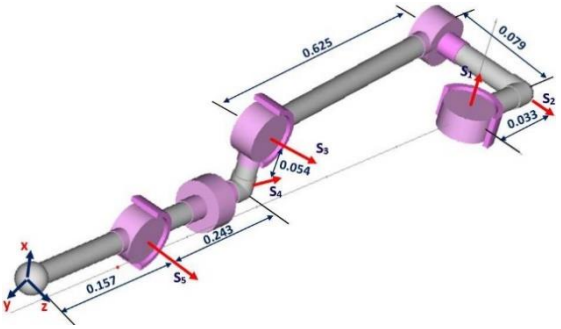

Figure 7: Kinematic Model of the WMRA: all measurements are in meters

TABLE 1: DH-Parameters of the Designed WMRA

Joint	Joint Offset (d_i) in meters	Joint Angle(θi) in degrees	Common normal Length(aij) in meters	Twist Angle(αij)
1	*0*	θ1	*0.033*	90^0
2	*0.079*	θ2	*0.625*	0^0
3	*0*	θ3	*0.054*	90^0
4	*0.243*	θ4	*0*	-90^0
5	*0*	θ5	*0.157*	0^0

The workspace of the robot is analyzed in the CAD environment. Considering physical interference with the wheelchair, the user and applying the range of motion of each joint of the arm (Table 2), the workspace of the WMRA is developed (Fig.10). This workspace of the robot arm will allow the user to perform several tasks easily.

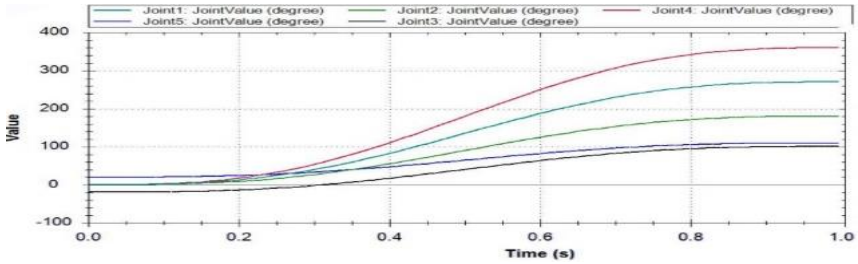

Figure 8: Trajectory of Joint angles

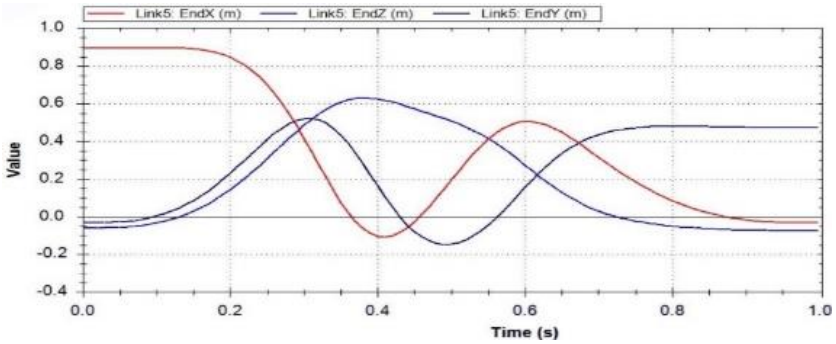

Figure 9: Gripper positions

TABLE 2: Range of motion of each joint of the WMRA

Joint	Range of Motion
The gripper wrist	Pivot 90^0
The gripper assembly	Rotate 180^0
The elbow joint	Pivot 180^0
The shoulder joint	Pivot 210^0
The base pivot	Rotate 310^0

Figure 10: Workspace of the WMRA

IV. TESTING AND SIMULATION RESULTS

An FEA static study was performed on the overall assembly using Solid Edge ST8 software with NX Nastran solver. Gravity effects are taken into consideration and the point load value of 42N is applied at the center of the gripper palm. The wheelchair mount bracket is held fixed during the analysis. The arms pivot points are constrained as rigid connection. Four node linear tetrahedral elements are used in the mesh, with mesh properties; mesh type: solid mesh, subjective mesh size: 1.85mm, total nodes: 300,400, and total elements: 166,400. The material properties assigned in the analysis are shown in Table 3.

3.1 Stress Analysis

The FEA results show that the Von Mises stress is located in the bolt that the base assembly pivots on (see Fig.11). According to the model, this bolt is subjected to a stress of 17.7 kpsi. This number is on the conservative side, considering that in the final product this bolt is supported from bending/buckling with bearings. Considering the outside edge of the bolt is under tensile load, we can use the tensile strength of a 3/8 Grade 8 bolt of 150 kpsi. This will provide a factor of safety of 8.4 for this specific scenario.

TABLE 3: Materials used and their properties

Material	Modulus of Elasticity (10^6 Psi)	Poisson's Ratio	Yield Strength (K psi)	Ultimate Strength (K psi)	Used in
PVC	0.345	0.4	8	7.5	Arm links
Aluminum 6061-T6	10	0.33	40	45	Base box, Bracket, Gripper
Steel	30	0.29	38	52	Bolts, Shafts

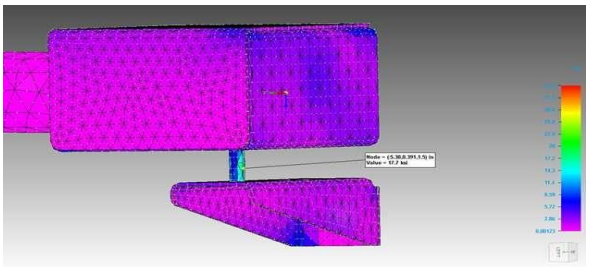

Figure 11: Von Mises Stress of 17.7 kpsi in the Main Pivot Bolt of the Base Assembly

3.2 Deflection

The deflection at the palm of the gripper, when fully loaded with 4 kg, is approximately 25 mm as shown in Fig.12.While this is the worst case scenario, it is more than we desire. The analysis shows that we can reduce a great deal of this deflection by adding a stiffening tab to the base motor box.

Figure 12: Stress and strain analysis of the arm assembly

3.3 Payload

Considering the weight of most of the common items in the home and grocery stores, the WMRA was designed with a payload of 4 kg. Based on the FEA simulation, it is confirmed that the robot arm can lift an object up to 5.4 kg.

3.4 Costs

PVC was chosen as the arm linkages due to its great strength and affordability. The gripper assembly and mounting brackets will be made of aluminum sheet metal due to its light weight and ease of manufacturability. In order to keep costs low, standard parts that are easily accessible off-the-shelf are used in the design; machining is only required for a few parts with a minimal amount of machining time. The designed WMRA has a total cost of under $800, which allows more number of people to have access to the technology. This is the lowest cost of a WMRA that we found during our research.

3.5 Prototype

A prototype was created in order to test the design parameters. The air cylinders provide an effective gripping and holding capability to the gripper (see Fig.13). Although the air hose routing could be further improved. Overall, the design strengths and range of motion were as expected. Implementing user-friendly control systems will help to conduct additional tests on the WMRA.

Figure 13: A prototype of the WMRA

V. CONCLUSIONS

The proposed WMRA is cost effective, it costs under $800 to produce. This is considered very affordable compared to other designs. Using affordable materials such as PVC pipes and aluminum sheet metals helps to lower the budget. Production and assembly of the WMRA are easy due to the use of readily available components with minimal machining required. This could allow many people to build their own WMRA. The strength and stiffness of the critical components have been tested through finite element analysis. The remote actuation system helps to minimize inertia and power requirements by keeping the load closer to the wheelchair. Similarly, the functionality of the robot arm is demonstrated through its reach of a wider workspace while holding various size and shape of objects. In the future, the control aspect of the robot will be explored through joy sticks, sEMG signals and EEG inputs toaccommodate people with various disability conditions.

VI. Acknowledgements

This work is partially supported by the Department of Mechanical Engineering, Wichita State University. The content is solely the authors' responsibility.

REFERENCES

[1] Erickson, W., Lee, C., & von Schrader, S. (2013). Disability Statistics from the 2011 American Community Survey (ACS). Ithaca, NY: Cornell University Employment and Disability Institute (EDI).

[2] Jiang, H., Zhang, T., Wachs, J. P., &Duerstock, B. S. (2014). Autonomous Performance of Multistep Activities with a Wheelchair Mounted Robotic Manipulator Using Body Dependent Positioning. In *Workshop on Assistive Robotics for Individuals with Disabilities: HRI Issues and Beyond, IEEE/RSJ Int. Conf. on Intell. Robots and Systems*.

[3] Barrett, G., Kurley, K., Brauchie, C., Morton, S., & Barrett, S. (2015). Wheelchair-Mounted Robotic Arm to Hold and Move a Communication Device-Final Design. *Biomedical sciences instrumentation*, *51*, 1-8.

[4] Schmitz, A., Bhavaraju, S., Somlor, S., Dominguez, G. A., Kamezaki, M., Wang, W., & Sugano, S. (2015, July). A Concept for a robot arm with adjustable series clutch actuators and passive gravity compensation for enhanced safety. In *Advanced Intelligent Mechatronics (AIM), 2015 IEEE International Conference on* (pp. 1322-1327). IEEE.

[5] Grindle, G. G., Wang, H., Jeannis, H., Teodorski, E., & Cooper, R. A. (2015). Design and User Evaluation of a Wheelchair Mounted Robotic Assisted Transfer Device. *BioMed research international*, *2015*.

[6] Tsui, K. M., Kim, D. J., Behal, A., Kontak, D., &Yanco, H. A. (2011). "I want that": Human-in-the-loop control of a wheelchair-mounted robotic arm. *Applied Bionics and Biomechanics*, *8*(1), 127-147.

[7] Alqasemi, R., & Dubey, R. (2010). *A 9-DoF Wheelchair-Mounted Robotic Arm System: Design, Control, Brain-Computer Interfacing, and Testing*. INTECH Open Access Publisher.

[8] Jiang, H., Wachs, J. P., &Duerstock, B. S. (2013, June). Integrated vision-based robotic arm interface for operators with upper limb mobility impairments. In *Rehabilitation Robotics (ICORR), 2013 IEEE International Conference on* (pp. 1-6). IEEE.

[9] Rapacki, E. B., Niezrecki, C., &Yanco, H. (2009, November). An under actuated gripper to unlatch door knobs and handles. In *Technologies for Practical Robot Applications, 2009. TePRA 2009. IEEE International Conference on* (pp. 135-140). IEEE.

[10] Gonzalez Sergio, N. M., and Nojoomi, M., 2014. R-arm (robotic assistive reaching mechanism). https://www.nibib.nih.gov/sites/default/files/R-ARM.pdf.[Online; accessed28-Dec-2015].

[11] Jones, M. P., and Inc., A., 2015. Nema 23 stepper motors. http://www.mpja.com/NEMA-23-Stepper-Motors/products/521/. [Online; accessed29-Dec-2015].

[12] Hart, A., 2015. Tinyg. https://github.com/ synthetos/TinyG/wiki. [Online; accessed 20-Nov- 2015].

[13] McCarthy, J. M., 2000. *Geometric Design of Linkages*, first ed. Springer-Verlag, NewYork.

[14] Craig, J. J., 1989. *Introduction to Robotics: Mechanics and Control*, second ed. PrenticeHall.

[15] Tsai, L.-W., 1999. *Robot Analysis: The Mechanics of Serial and Parallel Manipulators*. Interscience, NewYork.

[16] Rajeevlochana, C. G., &Saha, S. K. (2011, February). RoboAnalyzer: 3D model based robotic learning software. In *Proceedings of the International Conference on Multi Body Dynamics, Vijayawada, India*.

American Journal of Engineering Research (AJER) 2016
American Journal of Engineering Research (AJER)
e-ISSN: 2320-0847 p-ISSN : 2320-0936
Volume-5, Issue-1, pp-87-95
www.ajer.org
Research Paper Open Access

Analytical Effects of Torsion on Timber Beams

[1]Amulu C.P, [2]Ezeagu C. A. and [3]Obiorah S. M. O.

Abstract : *This study investigates the analytical effect of torsion on a rectangular cross-sectional timber beam. It reviewed the theoretical concept of both isotropic and anisotropic elastic behavior of the rectangular beam to torsional load. Finite difference method was used to evaluate the torsional parameters* K_1, K_2, K_3, β, K_3 *and* K_4 *for isotropic and anisotropic elastic material behavior and compared with the result obtained from the analytical values from previous research. The finite difference codes and equations together with the associated boundary conditions are employed to approximate the stress function and torsional parameter derivatives in the differential equation of analytical method. MATLAB programming was used to seek solution to the finite difference equations formulated. It was observed that the values obtained by finite difference method are approximate to the analytical values. However, the findings through ANOVA Test, revealed that there was no significant difference between the finite difference method and the analytical values* ($F_{calculated}$ (4.747) > $F_{critical}$ (0.00167) *at* 0.05 *level of significant and a strong value of correlation of* 0.998 *was obtained. The finite difference method was capable of predicting the stress functions and torsional parameters for both isotropic and anisotropic material behavior of the rectangular beam cross-section.*

Keywords: *Torsion, Finite difference method, Timber, isotropic, anisotropic, analytical*

I. Introduction

All structures are designed to satisfy the requirement of strength, rigidity and stability which is essentially for their reliability and safe operation. Structural elements can be deformed under the action of external forces, that is, their shape and dimension can change to the extent of warping and distorting. Torsional load is a load that subjects a structural member to couples or moments that twist the member spirally (Onouye and Kane, 2007) under the action of torque. . Torsion may be induced in a structural timber beam in various ways during transfer of load in a structural system. Torsion can be induced in a structural beam when the beam is subjected to external transverse load in such a manner that the resultant force acts a distance away from the shear centre axis of the beam. Torsion can also be induced in a structural timber beam due to monolithic and to satisfy the compatibility condition between members that are joined. In other words, torsion happens because of integrity and continuity of members and also under the effect of external loads in timber structures. Shear centre is defined as the point in the cross-section through which the transverse load must pass to produce bending without twisting. The determination of the torsional moment for any loading in torsion and shear requires knowledge of location of the centre of shear in addition to the geometric centroid (Ziegler, 1995). If the timber beam is subjected to two opposite turning moments, it is said to be in pure torsion (Rajput, 2004), it will exhibit the tendency of shearing off at every cross-section which is perpendicular to longitudinal axis. The induced torsional moment or torque tends to twist the beam to give a rotational displacement. When this occurs, the beam undergoes deformation by warping and distorting, that is changes in dimension, shape, or both simultaneously. If the timber beam is not properly designed against these torsional shear stresses, a sudden fragile fracture can occur, leading to failure of the beam at torsional cracking loads. The consequences of torsional effect on timber beams' cross-section and shape are; reduction in the reliability and safe operations of the structure under serviceability. Structural timber beams subjected to torsion are of different shapes such as solid saw lumber, I- shaped joists, glue laminated timber joists and open web trusses (Khokhar, 2011)

The effects of torsional loading can be classified into uniform and non-uniform. When torsional load is applied to a structural member, its cross-section may warp in addition to twisting. If the member is allowed to warp freely, then the applied torque is resisted entirely by torsional shear stresses (called St Venent's torsional shear stress). If the member is not allowed to warp freely, the applied torque is resisted by St Venant's torsional shear stress and warping torsion (Hoogenboom, 2006). This behavior is called non-uniform torsion. Warping of

the cross-section does not allow a plane section to remain as plane after twisting and this phenomenon is predominant in thin walled section. Timber beams must be designed against all induced stresses. Through the design of wooden structures, we try to avoid torsion of structural beams with different shape and constructive measures, and carry all loads through preferably bending. If we can succeed in doing that, we will have only tensile and /or compressive normal stresses to which wood corresponds better. Wood is a natural material which varies in mechanical properties. Knowledge of these properties is obtained through experimentation either in the employment of the wood in practice or by means of special testing apparatus in the laboratory. The shear modulus and shear strength are fundamental mechanical properties that are used in general timber design, compared to other engineering materials, timber has a relatively low shear stiffness and strength in comparison to its modulus of elasticity and so shear deformation contributes a more significant portion of flexural deflection (Khokhar and Zhang, 201).

Problem statement

The properties of timber can be obtained, theoretically through analytical model and numerical model. The problems of elasticity usually require solution of certain partial differential equations with a given boundary conditions. Only in simple boundary cases can these equations be treated in a rigorous manner. Very often, we cannot obtain a rigorous solution and must resort to approximate methods. It is necessary to realize that analytical solution requires quite a lot of theoretical knowledge due to its mathematical exactness and it's convenient only for the simpler cases. Analytical approach has been rarely used due to its complex procedure. Finding exact analytical solutions in general more complicated cases is usually very difficult, sometimes even impossible. However, the use of finite difference equations with the specified values of the independent variables, then lead to a system of simultaneous algebraic equation that can be solved by computer.

Aims and objectives of this study is to: understand the basic behavior of timber beams subjected to torsional loading, review the theoretical concept of torsion in timber beams, evaluate the analytical and numerical methods of determining the torsional parameters; stress functions and shear stresses in two-directions of a rectangular timber section and compare the results obtained from the two methods.

The scope and limitations of the study: This study is based on the evaluation of torsion problems in timber beams using analytical and numerical models (Finite difference) to determine the stress functions, shear stresses induced in a solid rectangular cross-section. The study also discussed the isotropic and anisotropic behavior /response of timber beams to torsional effects. The study uses MATLAB computer programming to seek for the solution of the finite difference equations derived and compared it with the analytical value

II. LITERATURE REVIEW

Wood, as a structural material is subjected to various types of loading conditions. If no external forces act upon a timber beam, its particles assume certain relative positions, and it has what is called its natural shape and size. If sufficient external force like torque is applied the natural shape and size will be changed. This distortion or deformation of the material is known as the Torsional strain. The ability of the timber beam material to withstand a twisting load, the ultimate strength of the timber material subjected to torsional loading, and the maximum torsional stress that the material sustains before rupture depends on its Torsional strength (Record, 2004). The design of a timber joists mainly depends upon its stiffness and strength properties. Stiffness is the property by means of which a body acted upon by external forces tends to retain its natural size and shape, or resists deformation.

Theory of elasticity

The classical theory of elasticity is based on an idealized 'Hookean' solid for which stress is directly proportional to strain and the deformation is completely recoverable after release of the force that produces the deformation. Furthermore, if the relationship between the applied stresses and the deformation can be assumed linear, then the material is said to be linear elastic. This is independent from any other assumption regarding the relationship between displacements and strain (Leitao, 1994). **Saint Venant,** 1855 was the first to provide the correct solution to the problem of torsion of bars subjected to moment couples at the ends. He made certain assumptions about the deformation of the twisted bar and then show that this solution satisfied the equations of equilibrium and the boundary conditions. From the uniqueness of solutions of the elasticity equations, it follows that the assumed forms for the displacements are the exact solution to the torsional problems.

Saint-Venant Torsion Theory for non-circular cross-section

In order to develop the torsional behavior of non-circular cross section, Saint-Venant made the following assumptions (Sadd, 2005 and Sadda, 1993): The member is straight, has constant cross section without taper and; The load is pure torque and produced by the shear stresses distributed over the end cross sections; Each cross section of member rotates approximately as rigid body and rotation of each cross section varies linearly

along the longitudinal direction; Angle of twist must be small for small deformation and that warping must be small and the same for each cross section; The member must be homogeneous, **isotropic** and linearly elastic.

The torsion problem for a rectangular bar can be solved in terms of either the warping function or the stress function. Later in 1903, Ludwig Prandtl suggested that τ_{xz} and τ_{yz} can be taken as a magnitude of a slope of stress function surface to their perpendicular planes and Equations can be written as:

$$\tau_{xz} = \theta \frac{\partial \emptyset}{\partial y};\ \tau_{yz} = -\theta \frac{\partial \emptyset}{\partial x} \quad (2.1)$$

The governing equation for the problem is a Poisson equation.

$$\frac{\partial^2 \emptyset}{\partial x^2} + \frac{\partial^2 \emptyset}{\partial y^2} = -2G\theta \quad (2.2)$$

Where $\emptyset$ is the stress function, represents surface over the cross-section of the torsion member. τ_{xz} And τ_{yz} represent shear stresses in relative planes to applied torque, angle of twist per unit length of member (θ).

The stress function can be determined by using an elastic membrane analogy approach (Boresi and Schmidt, 2003). Torque-rotation relationship can further be simplified by:

$$\frac{T}{\theta} = Gk_1(d)(b)^3 \quad (2.3)$$

The maximum shear stress (τ_{max}) in the cross-section can be obtained as:

$$\tau_{max} = \frac{T}{k_2(d)(b)^2} \quad (2.4)$$

Torsion Theory of Anisotropic Bars

It has long been recognized that deformation behavior of many materials depends upon orientation, that is, the stress-strain response of a sample taken from the material in one direction will be different if the sample were taken in a different direction. The term anisotropic is generally used to describe such behavior (Sadd, 2005). Wood is highly anisotropic due mainly to the elongated shapes of wood cells and the oriented structure of the cell walls. In addition, anisotropy results from the differentiation of sizes of cell throughout a growth season and in part from a preferred direction of certain cell types (August, 2008), thus, knowledge of stress distributions in anisotropic materials is very important for proper use of these high-performance materials in structural applications. Applying anisotropic theory to wooden beams of rectangular cross-section under torsion is definitely more complex than just assuming isotropic behavior. The two shear Moduli in LR and LT plane have fundamental influence on the results for shear strength. For the orthotropic rectangular member bar, the stress function or governing equation can be written as (Lekhnitskii, 1981):

$$\left(\frac{G_{LT}}{G_{LR}}\right)\frac{\partial^2 \emptyset}{\partial x^2} + \frac{\partial^2 \emptyset}{\partial y^2} = -2G_{LT}\theta \quad (2.5)$$

G_{LT} and G_{LR} are the shear modulus in longitudinal-Tangential (LT) plane (longer side) and longitudinal-Radial (LR) plane (short side), respectively of the member). The maximum shear stresses can be obtained on the centre of either the short side or long side as:

$$\tau_{max}(short\ side) = \frac{T}{(d)(b)^2} k_3; \quad (2.6)$$

$$\tau_{max}(long\ side) = \frac{T}{(d)(b)^2\left(\sqrt{\frac{G_{LT}}{G_{LR}}}\right)}; \quad (2.7)$$

$$\beta = \frac{32}{\pi^4} C^2 \sum_{K=1,3,5,\dots}^{\infty} \frac{1}{K^4}\left(1 - \frac{2}{K\pi} C\ tanh\ \frac{K\pi}{2C}\right) \quad (2.8)$$

$$K_3 = \frac{8}{\pi^2 \beta} C \sum_{k=1,3,5,\dots}^{\infty} \frac{(1)^{(K-1)/2}}{K^2} tanh\ \frac{K\pi}{2C} \quad (2.9)$$

$$k_4 = \frac{C}{\beta}\left[1 - \frac{8}{\pi^2}\sum_{K=1,3,5,\dots}^{\infty} \frac{1}{K^2 cosh\ \frac{K\pi}{2C}}\right]; \quad (2.10)$$

Where $C = \frac{d/b}{\sqrt{G_{LT}/G_{LR}}}$ (2.11)

Numerical method for Determination of Torsion effects with Finite Difference Method (FDM)

The basic idea of the finite difference method is to represent the governing differential equations and the associated boundary conditions with finite differential equations. The finite differential equations are employed to approximate the derivatives in the differential equations. Combinations of the values of unknown functions at the specified locations of the independent variable form the finite difference quotients. The finite difference equations with the specified values of the independent variables then lead to a system of simultaneous algebraic equations that can be solved by computer. The basic finite difference expression follows logically from the fundamental rules of calculus.

For the empirical study of numerical model on torsion, Stefan et al (2012) and Hsieh (2007) respectively, have researched on the numerical determination of torsional parameters and shear stresses of a rectangular timber bar using finite difference and finite element methods.

III. Research Methodology

The Numerical model will be used in this study to determine the stress function and torsional parameters of a rectangular timber beams subjected to torsional effects. Both isotropic and anisotropic nature of timber beam will be considered in the numerical model. By means of finite difference method, approximate stress function, torsional parameters and shear stresses in rectangular structural members are evaluated using **MATLAB** computer programming and checked against the analytical values.

The analyses of torsion of a rectangular bar section using finite difference technique

The torsion problem to be modeled is one with rectangular boundary. Such cross-section will be embedded in a basic rectangle of length b, in the y-direction and width a, in the x-direction. The length and width are such that b is a fraction (or multiple of a.) Then, the length of the cross-section in the x-direction is 1. The origin of the x, y coordinate system is assumed to be at the centroid of the basic rectangle.

a) The Grid: The rectangle is partitioned into a grid, uniform in the x- and y –directions respectively, but not necessarily with equal x and y increments as shown in figure 3.1 below.

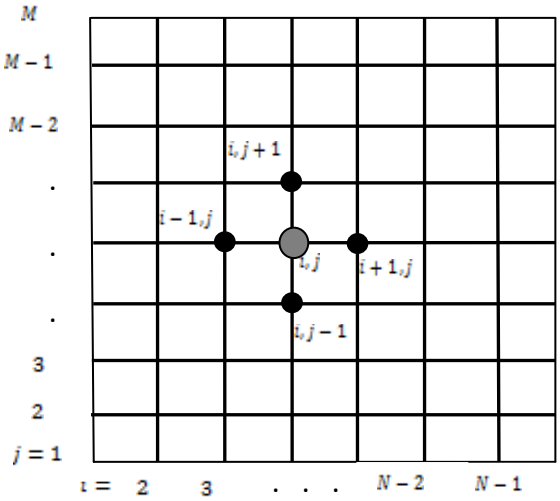

Figure 3.1, the finite difference grid for the basic rectangle R domain. The circles depict the computational molecule (of equation below).

The N grid points in x- and M grid points in y- respectively, have coordinates

$$\left[-\frac{a}{2} = x_1, x_2, x_3, \dots, x_N = \frac{a}{2}\right] \text{ with } dx = x_i - x_{i-1};\ i = 2, \dots, N.$$

$$\left[-\frac{b}{2} = y_1, y_2, \dots, y_M = \frac{b}{2}\right] \text{ with } dy = y_j - y_{j-1};\ j = 2, 3, \dots, M.$$

b) The finite difference equations: The interior constitutes all the grid points with indexes $i = 2, \dots, N-1$ and $j = 2, \dots, M-1$. the values of $\emptyset$ are specified on the boundary point $j = 1$ and M for $i \in [1, \dots, N]$ and $i = 1$ and N for $j \in [1, \dots, M]$. Let the net function $f_{i,j} = \emptyset(x_i, y_j)$ be the numerical values at the grid points of the sought after solution $\emptyset(x, y)$. The equations for $f_{i,j}$ are found by substituting the governing Poisson's equations, evaluated at each point $i, j \in R$ domain by finite difference formulae respectively.

For Isotropic nature of timber beam:

The governing equation for the problem is a Poisson equation as in (2.2): $\frac{\partial^2 \emptyset}{\partial x^2} + \frac{\partial^2 \emptyset}{\partial y^2} = -2G\theta$,

And substituting it with the finite difference equations and codes gives

$$\frac{f_{i-1,j} - 2f_{i,j} + f_{i+1,j}}{dx^2} + \frac{f_{i,j-1} - 2f_{i,j} + f_{i,j+1}}{dy^2} = -2$$

Assuming that $dx = dy$, Resulting into:

$$f_{i-1,j} + f_{i+1,j} + f_{i,j-1} + f_{i,j+1} - 4f_{i,j} = -2dx^2$$

The solution of the finite difference equation is obtained by rewriting the above equation as:

$$f_{i,j} = \frac{1}{4}(f_{i+1,j} + f_{i-1,j} + f_{i,j-1} + f_{i,j+1} + 2dx^2);$$

For Anisotropic nature of timber beam:

The governing equation for the problem is a Poisson equation as in (2.5) is: $(\frac{G_{LT}}{G_{LR}})\frac{\partial^2 \emptyset}{\partial x^2} + \frac{\partial^2 \emptyset}{\partial y^2} = -2G_{LT}\theta$.

Substituting it with the finite difference equations and codes gives:

$$\frac{g(f_{i-1,j} - 2f_{i,j} + f_{i+1,j})}{dx^2} + \frac{e(f_{i,j-1} - 2f_{i,j} + f_{i,j+1})}{dy^2} = -2$$

where $g = \frac{1}{G_{LR}}$; $e = \frac{1}{G_{LT}}$; Considering equal division points: $dx = dy$

$$f_{(i,j)} = \frac{1}{2(g+e)}[gf_{(i-1,j)} + gf_{(i+1,j)} + ef_{(i,j-1)} + ef_{(i,j+1)} + 2dx^2]$$

The iteration process:

By starting the iteration process with $f_{i,j} = 0$ everywhere, the boundary conditions are automatically satisfied. This process is considered in both isotropic and anisotropic behavior respectively.

For k=2:k
For j=2:M-1
For i=2:N-1
$f_{i,j}{}^{k} = q(i,j)[f_{i-1,j}{}^{k} + f_{i+1,j}{}^{k-1} + f_{i,j-1}{}^{k} + f_{i,j+1}{}^{k-1} + 2dx^2$
End
End
End

A fixed number of passes (K) equal to the product of number of grid points N and M in the x- and y-direction respectively, which is enough for the system to converge.

The numerical computation of the stresses and other torsional parameters are obtained from the numerical stress function $f_{(i,j)}$ using the following formulas:

The stresses are evaluated using the following:

i. For the bottom and top of the rectangle, $j = 1 \ and \ j = M; i = 1 \ to \ N \ respectively.$

$$\tau_{xz,i,1} = [\frac{\partial \emptyset}{\partial y}]_{i,1} = [\frac{-3f_{i,1}+4f_{i,2}-f_{i,3}}{2dy}]; \ \tau_{xz,i,M} = [\frac{\partial \emptyset}{\partial y}]_{i,M} = [\frac{f_{i,M-2}-4f_{i,M-1}+3f_{i,M}}{2dy}]$$

$where \ \tau_{yz,} = 0,$ On these two boundaries

ii. For the left and right ends of the rectangle; $i = 1, and \ i = N, \ \ j = 1 \ to \ M, \ respectively$

$$\tau_{yz,1,j} = -[\frac{\partial \emptyset}{\partial y}]_{1,j} = -\left[\frac{-3f_{1,jj}+4f_{2,j}-f_{3,j}}{2dx}\right]; \ \tau_{yz,N,j} = -[\frac{\partial \emptyset}{\partial y}]_{N,j} = -[\frac{f_{N-2,j}-4f_{N-1,j}+3f_{N,j}}{2dx}]$$

iii. The torsional parameters for anisotropic rectangular cross-section $K_3 \ and \ K_4$ are obtained as follows:

$$K_3 = \tau_{xz} * a * b\text{^}2; \ K_4 = \tau_{xz} * a * b\text{^}2/(\sqrt{\frac{G_{LT}}{G_{LR}}})$$

<<

IV. PRESENTATION OF RESULTS

To validate the finite difference method formulated, three examples will be evaluated for verification of the results. Analytical and numerical (finite difference method) models developed will be employed to evaluate the values on rectangular timber beam of isotropic and anisotropic material behavior of timber. In order to provide the accuracy and efficiency of the finite difference method, the results obtained from the numerical model program will be compared with those of the analytical method which is available from previous works of $(Boresi \ \& Schmidt, \ 2003)$ and (Hsiehk, 2007).

Example 1: Torsional Parameters for Isotropic material behavior of Rectangular Cross Sections. The verification example is from textbook $(Boresi \ \& Schmidt, 2003) \ and \ (Hsiehk, 2007)$. The value of the torsional parameter from the previous researcher is compared with the value obtained from the Finite difference method (FDM). The values of k_1 and k_2, depends on cross section/ aspect ratio of rectangular bar.

Table 4.1 evaluation of K_1 and K_2value between analytical and finite difference method (FDM) results for isotropic behavior which depend on the ratio of the sides of the rectangular cross-section of the beam (y-z direction)

b/a	1.0	1.5	2.0	2.5	3.0	4.0	6.0	10.0
K_1 $(Boresi \ \& Schmidt)$	0.141	0.196	0.229	0.249	0.263	0.281	0.299	0.312
K_1 (FDM)	0.1404	0.1962	0.2288	0.2493	0.2635	0.2808	0.2988	0.3055
K_2 $(Boresi \ \& Schmidt)$	0.208	0.231	0.246	0.256	0.267	0.282	0.299	0.312
K_2 (FDM)	0.2082	0.2314	0.2461	0.2557	0.2668	0.2819	0.2988	0.3124

Example 2: Torsional coefficients for anisotropic rectangular cross-section with two orthogonal shear properties in different directions of timber beam axis. The values of β, k_3 and k_4, depends on aspect ratio of the cross section and shear Modulus of rectangular bar

Table 4.2 evaluation of $\beta \ value, \ K_3 \ value \ and \ K_4 \ value$ between analytical (Lekhnitskili 1981) and finite difference method results for anisotropic behavior depending on the ratio of shear Moduli and the ratio of the sides of the rectangular cross-sectional beam

C	1.0	1.5	2.0	2.5	3.0	4.0	5.0	10	20
β $(Lekhnitskili)$	0.141	0.196	0.229	0.249	0.263	0.281	0.291	0.312	0.323
β (FDM)	0.1407	0.1968	0.2285	0.2478	0.2626	0.2812	0.2902	0.3101	0.3215

K_3 (Lekhnitskili)	4.804	4.330	4.068	3.882	3.742	3.550	3.430	3.202	3.098
K_3 (FDM)	4.8023	4.3071	4.0783	3.8819	3.7584	3.5745	3.4897	3.2128	3.0662
K_4 (Lekhnitskili)	4.804	3.767	3.234	2.975	2.538	2.644	2.548	2.379	2.274
K_4 (FDM)	4.8023	3.7948	3.2184	2.9785	2.5260	2.6249	2.5716	2.3609	2.2805

Example 3: The shear stress distribution of full-sized specimen measuring $44 * 140 * 1372\ mm^2$ under torsion for all three structural composites lumber (SCL) material; laminated veneer lumber (LVL), parallel strand lumber (PSL) and laminated strand lumber (LSL) by (Gupta and Siller, 2005) . A constant torque value of $300Nm$ was applied to each sample. Shear Moduli of the materials are: LSL (GRL = 318 Mpa, GTL = 782 Mpa), LVL (GRL = 407 Mpa, GTL = 593 Mpa) and PSL (GRL = 310 Mpa, GTL = 398 Mpa)

Table 4.3: Comparing the longitudinal tangential and radial shear stresses between Gupta and Siller (2005) experimental work, and finite difference method for both isotropic and anisotropic.

	Isotropic				anisotropic			
	(Gupta and siller)		Finite Difference Method		(Gupta and siller)		Finite Difference Method	
material	Shear stress (Mpa)				Shear stress (Mpa)			
	long τ_{LT-I}	short τ_{LR-I}	long τ_{LT-I}	short τ_{LR-I}	long τ_{LT-A}	short τ_{LR-A}	long τ_{LT-A}	short τ_{LR-A}
LSL	11.59	8.83	11.692	8.7364	12.69	6.43	12.498	6.327
LVL	7.66	5.83	7.712	5.5045	7.96	4.90	7.769	4.46
PSL	6.65	5.02	7.150	5.1637	6.82	4.55	6.787	4.775

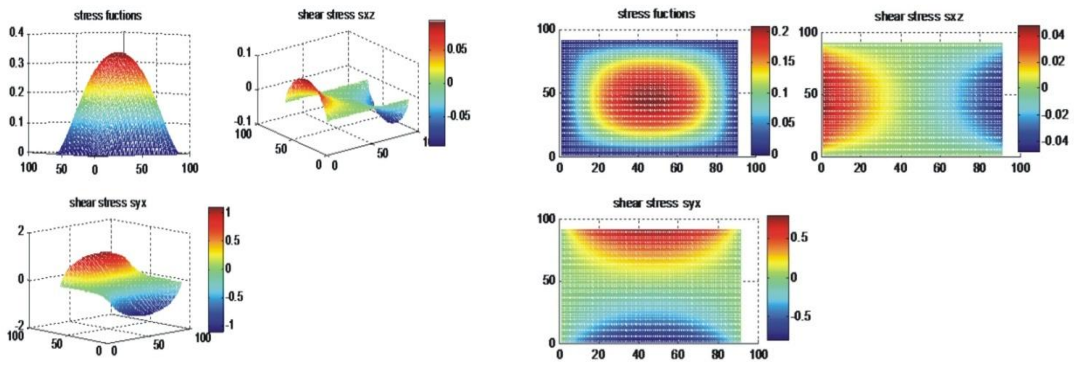

Figure 4.1 stress distribution from numerical solution for isotropic behavior: $a = 1, N = 41, M = 71$ (a) shear stress (syz) distribution in the $y - direction$ (b) shear stress (sxz) distribution in the $x - direction$ e (c) the stress function contour for rectangular section xy – view and (d) $xz\ and\ yz$ – view (from MATLAB)

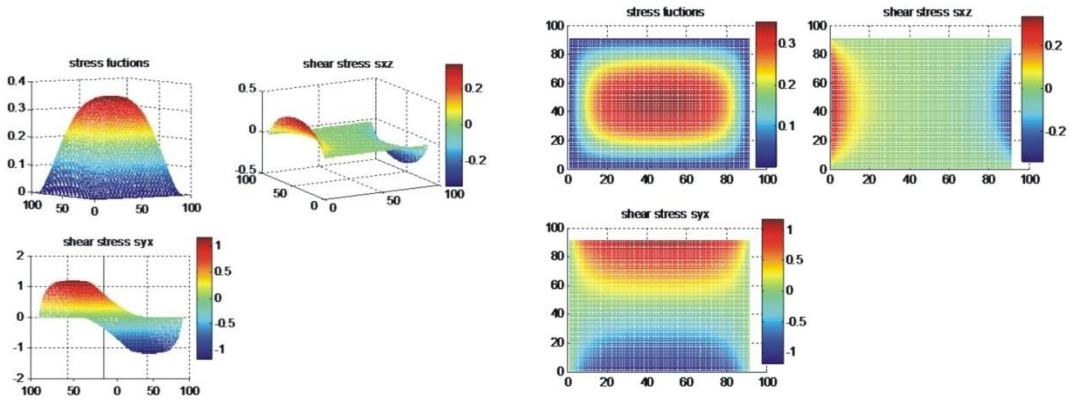

Figure 4.3 stress distribution for anisotropic material behavior of timber subjected to torsional loading, $a = 1, N = 41, M = 71$ (from MATLAB)

V. DISCUSSION ON FINDINGS

The torsional parameters for rectangular cross-sectional timber beam $K_1, K_2, \beta, K_3, K_4$ were determined using the finite difference method of numerical analysis with MATLAB programming and compared with the analytical model from previous research work for both isotropic and anisotropic material behavior of timber beam.

Tables 4.1 present the torsional parameters K_1 *and* K_2 for isotropic material behavior of rectangular cross-section for both analytical and finite difference method (FDM). The result indicates that finite difference method values are not exact, but approximately to the values obtained from analytical calculation. Observations indicated that, through ANOVA Test; there was evidence at 0.05 levels of significance that there was no significant difference between analytical and numerical values, statistically. The result shows that $F_{critical}\ (4.747) > F_{calculated}(0.00167)$ with variance of 0.00153 for K_1. $F_{critical}\ (4.747) > F_{calculated}(0.000000849)$, variance of 0.000841 for K_2.

Tables 4.2 present the torsional parameters β, K_3 *and* K_4 respectively, for anisotropic material behavior of rectangular cross-section for analytical and finite difference methods. It was observed that the values obtained by finite difference method are not exact, but approximate when compared with the analytical calculated values. From the ANOVA Test conducted, there was indication at 0.05 levels of significance that there was no significant difference between analytical and finite difference methods statistically. $F_{critical}\ (4.60) > F_{calculated}(0.0000169)$, variance of 0.001804 for β. AVOVA Test conducted for K_3, K_4 also confirmed that there was no significant difference between analytical method and finite difference method. It was found that the torsional parameters, obtained using the two methods, have a very strong correlation as R^2 was found about 0.998.

Table 4.3 presents the shear stress distribution of structural composite lumber (LVL, LSL and PSL) for both isotropic and anisotropic behavior to torsional load. Solving the problem for various materials, it was observed that some values of longitudinal tangential and radial shear stresses matched the experimental work of Gutpa and Siller (2005) for both isotropic and anisotropic material behavior, but the process is not convergence. The values obtained from finite difference method developed for tangential and radial shear stresses are approximate to that of Gupta and Siller (2005).

Comparing the isotropic and anisotropic shear stress distribution in figures 4.1 and 4.3, the shear stress distribution in isotropic timber beam behavior depends only on the ratio of the rectangular cross-sections (b/a) thereby having a uniform stress distribution with equal number of iteration (passes) on the longitudinal tangential and radial directions as shown in figure 4.1. However, in the anisotropic timber beam behavior, shear stresses are not only dependent on the rectangular side ratio, but also on the ratio of the two shear Moduli in longitudinal tangential (LT) and radial (LR) directions as shown in figure 4.2. In other words, the two shear Moduli in LT *and* LR plane have fundamental influence on the results for shear strength. The higher the aspect ratio, more anisotropic the material behaves.

Convergence of the finite difference method using MATLAB

The values of torsional parameters depend on the distance between the points laying on the boundary and the neighbor point inside the section domain ($dx\ and\ dy$). Smaller values lead to better estimation of the torsional parameters and an increase size of unknown system. The utilization of variable distance between mesh points ($dx\ and\ dy$), leads to a more accurate estimate of the torsional parameters, using smaller number of grid point. This is in line with the results gotten by **Stefan et al** in the literature review.

VI. Conclusion

The finite difference model developed in this study is capable of predicting the torsional shear stress distributions and torsional parameters of rectangular timber beam subjected to torsional load, for both isotropic and anisotropic material behavior. The finite difference method allows the study of stress distribution for sections and boundary conditions in which an analytical approach is difficult. The knowledge of stress distributions in anisotropic material behavior is very important for proper use of those high-performance materials in structural application. The isotropic material behavior neglected those effects of directional-dependent behavior of wood, thus resulting in a material that behaves the same in all directions. Good agreement was found between the finite difference method and previous results.

Recommendations

The study was limited to finite difference method. Further research needs to be conducted to evaluate the torsional parameters using finite element model or any other numerical models. Further study should be carried out on other shapes like L-shaped, I-shaped and open web trusses. Another area that needs further study is on the best way of making the finite difference method converge easily using MATLAB programming.

References

[1]. August.A. (2008). *Handbook 1: Timber Structures* (first ed.) Graz: Educational Materials for Designing and Testing of Timber Structures(TEMTIS), Leonardo da Vinci Pilot Project.

[2]. Boresi.A, P. and Schmidt.R.J. (2003). *Advanced Mechanics of Materials* (Sixth ed.). John Wiley and Sons Inc.

[3]. Brandner.R, Gehri.E, Schickhofer.G, and Bogensperger.T. (2007). *Determination of Modulus of Shear and Elasticity of Glued Laminated Timber and Related Examinations:* Project Financed by the Competence Centre holz.bau Forschungs Grubh and performed in collaboration with the Institute of Timber Engineering and Wood Technology of the Graz University of Technology and Partners from Industry.

[4]. EN 1995-1-1 (2004) *Euro code: Design of Timber structures – Part 1-1: General – common rules and rules for building European Committee for Standardization.* Brussels European Committee for Standardization

[5]. Gupta, R and Siller, T.S. (2005). *Stress Distribution in Structural Composite Lumber under Torsion.*Forest Product Journal (55) 2: 51-56

[6]. Hsiehk. (2007). *Numerical Modelling and Analysis of Composite Beams Structures Subjected toTorsional Loading.* Thesis Submitted to the Faculty of the Virginia Polytechnic Institute and State University in Partial Fulfilment of the Requirements for the Degree of Master of Scienec in Engineering Mechanics, Virginia Polytechnic Institute and State University.

[7]. Hoogenboom, P.C.J. (2006) Vlasov Torsion Theory (in Chapter 7).

[8]. Khnokhar.A, and Zhang.H. (2012, July 16-19). The Use of Torsion Test Method to Evaluate the Properties of Timber Joist. *World Conference on Timber Engineering (WCTE) .*

[9]. Khokhar.A, Zhang.H, and Ellis.D.R. (2010). *The Shear Strength and Failure Modes of Timber Joists Obtained from the Torsion Test Method. World Conference on Timber Engineering(WCTE)*

[10]. Leitato, V.M.A (1994). *Boundary Elements in Nonlinear Fracture Mechanics.* Southampton: Computational Mechanics Publications.

[11]. Lekhnitskii.S.G. (1981). *Theory of Elasticity of an Anisotropic Elastic Body.* Moscow: MIR Publisher.

[12]. Onounye, B., and Kane, K. (2007). *Statics and Strenght of Materials for Architectural and Building Construction* (third ed) New Jarsey: Pearson Prentice Hall.

[13]. Record.S.J. (2004). *The Mechanical Properties of Wood:Including a Discussion on the Factors Affecting the Mechanical Properties and Methods of Timber Testing.* India: Open Knowledge Foundation Network, Open Education Project.

[14]. Saada, A. S. (1993). Elasticity: *Theory and Applications*. Krieger Publishing Company

[15]. Sadd, M. H. (2005). *Elasticity: Theory, Applications and Numeric.* Amsterdam: Elsevier Butterworth Heinemann.

[16]. Stefan.A, Lupoae.M, Constantin.D, and Baciv.L, A. (2012). *Numerical Determinations with Finite Differences Method of Prismatic Beams Subjected to Torsion. Proceedings of the World Congress on Engineering WCE , 3*

[17]. Von Kerczek, C.H. (n. d). *Torsion of Prismatic Beams of Piecewise Rectangular Cross Section* Ziegler, F. (1995). *Mechanics of Solids and Fliuds* (Second ed.). New York: Springer-verlag.

American Journal of Engineering Research (AJER) 2016
American Journal of Engineering Research (AJER)
e-ISSN: 2320-0847 p-ISSN : 2320-0936
Volume-5, Issue-1, pp-96-99
www.ajer.org
Research Paper Open Access

Effects of Fire Outbreak, Gas Flaring, And Global Warmings on Building and Structures

[1]Ezeagu C. A, [2]Eze A.B.K, [3]Ekong F.E., [4]Iroro.O.W
[1]*Civil Engineering Department, Nnamdi Azikiwe University,P.M.B 5025, Awka.*
[2,3,4]*Civil Engineering Department, Igbinedion University Okada.*

ABSTACT: *The effect of fire outbreak, gas flaring and global warming on building and environment has been considered. Different residential, commercial and industrial buildings were considered at insitu fire gutted conditions and at perimeter distance intervals of 100m, 120m, 140m, 160m, and 180m away from the flare stack respectively. The Non-destructive tests were carried on the structural members and non structural members of these facilities to determine the integrity and strength. The observed gutted markets stanchions has a minimum steel stanchion yielding strength of 9.5N/mm^2 and a maximum yielding strength of 22.8N/mm^2 for 152 stanchion studied at a temperature range of over 200°c to 300°c of 2 to 3 hours fire intensity. The observed average room temperature for vary distance intervals were 33°c, 28°c, 26°c, 25°c , 24°c, away from the flare stack. The observed strength of other structural elements i.e. beams; columns and slabs were of minimum value 9.81N/mm^2 and maximum value of 23.05N/mm^2. The result therefore suggests that there is appreciable deterioration in the strength of both structural and non structural member due to fire outbreak, gas flaring and global warming in building.*

Keywords: *Elements, Fire, Gas, Member and Strength.*

I. Introduction

All construction materials are susceptible to change or deformation under certain conditions especially when there is an appreciable change in temperature. Temperature variation affects both the chemical and physical properties of these materials both at monolith nature and as individual material. The effect in some cases causes shrinking, melting, and charring. The associated moisture content variation and chemical decomposition affect the strength of these materials in its monolith nature as structural members and non structural members in buildings. Therefore since the strength of these member determines the strength of the buildings and by implication the safety and consequently the habitability of the facilities in an environment. Then, the investigation of the effects of fire outbreaks, gas flaring and global warning on the materials in any environment needs to be investigated to ensure safety and habitability.

Literature review: Olukotu and Akpopenamone (2010) in a thesis titled "Effects of fire outbreak on structural elements (beams, slabs, columns) and other non structural components", describes the extent of failure that took place in Agbodo market, Benin city due to fire outbreak. The study was carried out to ascertain the extent of fire damage on 152 stanchions, 3 columns and 1 external beam. Expert visual inspection result revealed several defects like exposure of part of trusses to the atmosphere, collapse of columns, spilling and peeling of paints, buckling of steel, cracks on the block walls, columns and beams. Expert experimental test result shows that the reduction in the observed yielding strength of 152 stanchions, columns, slabs was in the range of (70 – 80%) as the minimum observed shootings @ X = 0°, X = +90° and X= -90° were 15N/mm^2, 16N/mm^2 and 12N/mm^2 and the maximum observed compressive strength were 39N/mm^2 and 25N/mm^2. The engineers and architects should recognize the environment as a system, and these artefacts as sub system. Therefore structural stability, functionality, temperature variation and resistance should be encompassed. The protection of the environment and sub environment e.g building markets should go hand in hand. Under intense heat, non structural elements collapse (glass shatters, plastic melts, timber burn). Global warming and environmental changes has equally been proofed to cause failures in building. Ifekwe (2008) in a thesis titled a "Crack Monitoring and Risk Analysis in Building" a case study of some laboratory facilities, it was observed none of the cracks in the building was traced to foundation settlement. Most of the cracks are caused by roots of plant, water ingression and material separation at fracture.

A formal risk management approach was adopted to help identify dominant risk to public health safety and security propagating due to contraction and expansion because of weather change, water will infiltrate the cracks between block and thereby aid the growth of plants whose roots will equally cause more cracks and subsequent deterioration of the building. The study applied both the visual inspection technique (VIT) and the dry timber wedge (DTW) technique in analyzing the 5 (fire) sections of the laboratory building facilities and found out that the cracks are in p4 width band of (2 -5) mm. the DTW crack monitoring method shows further that for six month monitoring the increase in crack width is negligible, since the timber wedge used did not fall off and tape did not slide for more than six months of monitoring. In some portions, the crack falls within p 0 to p1 crack width range of (0.1 – 0.3) mm, structurally refers to the hairline cracks and fine cracks. In the final analysis, the crack propagates horizontally along the weak mortar joint partition joints and wall joints. Otobo (2010) carried out a progressive monitoring of structural defects and cracks, a case study of the same facility by Ifekwe (2008), two years later and agreed totally with Ifekwe (2008) findings and concluded that cracks in the roof portion was caused by water ingress into the building due to the stagnant water in the roof gutter. Iroro (2008) in a thesis titled "Effect of Fire on Building Structural Elements (using INEC Zonal Office, Okada as a case study). The study noted that the temperature of the fire gust was in the range of 300°c to 600°c. The color of affected concrete members (structural & non structural) was found to be black, greenish and gray, Iroro confirmed the very weak obtained compressive strength of the concrete members by moulding six sample specimen and purposeful subjecting these specimen to oven temperature in the range of 180°c to 200°c for 2 hours thereby simulating a fire model. The maximum compressive strength of 9.8N/mm^2 was obtain which is very small in compression with 24N/mm^2 minimum compressive strength as specified in BS 8110 (1997, 1985), ISO (1975), SFDE (2002). The study concluded that the building suffered several damages and should be rebuilt from ground zero. Therefore it has rendered that particular environment inhabitable. Okeibuno (2011) studied "the effect of temperature on the strength of concrete". The purpose of the study was to investigate the effect of temperature on the strength of concrete, the study adopted 3 mix ratio of 1:2:4, 1:1 ½ :3 and 1:3:4, a total of 192 cubes of standard specimen of (150x150x150)mm comprising of 64 cubes for each mixture were made. These cubes were oven heated at regulated temperature of 80°c, 100°c, 120°c and 140°c and four sample were each tested at different maturity days of 7, 14, 21, and 28 days. Okeibuno tested result shows that there is a progressive increase in strength from (11.1 to 21.3) N/mm^2, (8.5 to 20.5) N/mm^2 and (13.4 to 23.5) N/mm^2 for different ratio. The result further shows serious distortion in the progressive increase sequence of a naturally curing concrete cube. In the entire sample tested, the minimum compressive strength of 24N/mm^2 was not obtained in 28 days even at the maximum considered temperature of 140°c. However okeibuno's work was inconclusive because severe fire conditions were not considered at sustained fire temperature of 200°c and above. Ekong (2008) carried out a research on "Effect of Gas flaring on the Environment and Civil Engineering structures, A case study of IBENO local government area, Akwa Ibom State" and Ezeagu and Eze (2009) worked on "Effect of Gas Flaring On structural Elements in Niger Delta (A case study of IBENOEXXON MOBIL QUA IBOE TERMINAL (Q.I.T)" They noted that global warming and gas flaring both poses a serious threat to the environment, life and property. Over the past decades,based on the rapid advancement in industrialization, which has lead to the depletion of the ozone layer, by the emission of greenhouse gases into the atmosphere. This causes a corresponding rise in the average temperature of the earth. The causes and effects of global warming have been taken into consideration with particular attention to how global warming affect the environment, health, eco-system and civil engineering structures; how it affect these buildings and deteriorates them causing a reduction in the strength of the reinforced concrete members. The structural integrity (strength) of the concrete members of the tested buildings was subjected to non-destructive testing by the use of a rebound hammer (Schmidt type). The results showed that gas flaring has no immediate effect on the strength of concrete but rather this effect is time dependent.

II. Methodology

Two important approaches were used in accessing the effect of fire out break and gas flaring cum global warming. In the first part, a schmit hammer was used to carry out rebound shooting on 152stanchions in the rolls of 8 numbers. This is because the Agbado market was constructed on multibay portal frames.

On the second part, residential buildings were located at perimeter distances of 100m,120m,140m,160m and 180m, and thermometers were installed at the walls of the building to obtain the room temperature variations because of gas flaring. But generally, the standard methods of using the rebound hammer for testing elements were employed as thus. The strength of the structural elements is measured using the concrete rebound hammer usually referred to as the Schmidt hammer. According to BS1881: part 202; ASTM C805, The hammer is a hand held instrument used for testing the quality of hardeness in the structure. This is done to obtain the gained increase strength on a structure. The guiding principle is that the rebound of an elastic mass impacting on the concrete surface is a function of the hardness of the surface. Therefore the harder the surface, the greater is the rebound distance.

The procedure adopted is:

1. The surface is abraded with carborundum stone to remove irregularities.
2. The hammer is pushed firmly against the concrete until the trigger button is automatically released.
3. The hand pressure is then reduced to allow the plunger to fully emerge from the instrument.
4. Extra hand pressure is then applied to push the plunger back into the instrument, compressing the internal spring to the point the trigger mechanism overrides and causes the impact force to be applied to the surface.
5. While applying the hand pressure, the push button is pressed to the plunger in place, retaining the reading on the graduated scale.

The corresponding strength to the reading on the scale is then noted strength of these two case and the are table 1. and table 2.

III. Results

Tables 1: Average strength of 152 Stanchion Non destructively tested at Agbado Market: @ Olukotu S. and Akpopenamone P. (2010).

S/no	1st line@5m	2nd line@5m	3rd line@5m	4th line@5m	5th line@5m	6th line@5m	7th line@5m	8th line@5m
1	10N/mm^2	14.9N/mm^2	18.4N/mm^2	16.8N/mm^2	19.4N/mm^2	22.8N/mm^2	18.9N/mm^2	19.9N/mm^2
2	10N/mm^2	15.9N/mm^2	18.3N/mm^2	17.3N/mm^2	21.4N/mm^2	22.8N/mm^2	18.9N/mm^2	19.9N/mm^2
3	10.5N/mm^2	15.4N/mm^2	18.4N/mm^2	15.2N/mm^2	20.7N/mm^2	22.8N/mm^2	19.6N/mm^2	20.5N/mm^2
4	20.4N/mm^2	15.4N/mm^2	18.3N/mm^2	16.9N/mm^2	20.7N/mm^2	18.9N/mm^2	19.1N/mm^2	18.6N/mm^2
5	19.2N/mm^2	15.9N/mm^2	10N/mm^2	18.4N/mm^2	21.6N/mm^2	17.3N/mm^2	20.9N/mm^2	18.7N/mm^2
6	18.5N/mm^2	11.8N/mm^2	10.6N/mm^2	18.9N/mm^2	18.8N/mm^2	17.1N/mm^2	19.9N/mm^2	17.3N/mm^2
7	17.3N/mm^2	11.8N/mm^2	15.6N/mm^2	17.9N/mm^2	18.7N/mm^2	16.9N/mm^2	18.7N/mm^2	20.4N/mm^2
8	18.9N/mm^2	11.8N/mm^2	15.4N/mm^2	17.3N/mm^2	17.4N/mm^2	17.7N/mm^2	20.9N/mm^2	18.9N/mm^2
9	12.8N/mm^2	15.6N/mm^2	17.8N/mm^2	18.3N/mm^2	17.6N/mm^2	18.4N/mm^2	18.7N/mm^2	15.3N/mm^2
10	15.9N/mm^2	16.2N/mm^2	17.9N/mm^2	13.4N/mm^2	15.2N/mm^2	17.7N/mm^2	19.9N/mm^2	20.4N/mm^2
11	18.9N/mm^2	19.3N/mm^2	17.9N/mm^2	13.9N/mm^2	16.6N/mm^2	18.4N/mm^2	20.9N/mm^2	18.1N/mm^2
12	18.6N/mm^2	18.5N/mm^2	18.3N/mm^2	12.4N/mm^2	15.7N/mm^2	21.4N/mm^2	18.7N/mm^2	18.8N/mm^2
13	17.8N/mm^2	12.6N/mm^2	17.1N/mm^2	14.3N/mm^2	17N/mm^2	19.4N/mm^2	18.9N/mm^2	14.3N/mm^2
14	16.9N/mm^2	12.2N/mm^2	18.3N/mm^2	16.7N/mm^2	20.6N/mm^2	18.1N/mm^2	18.9N/mm^2	17.2N/mm^2
15	18.6N/mm^2	15.6N/mm^2	17.7N/mm^2	18.1N/mm^2	21.4N/mm^2	18.1N/mm^2	18.4N/mm^2	17.9N/mm^2
16	19.5N/mm^2	14.2N/mm^2	16.6N/mm^2	19N/mm^2	21.4N/mm^2	18.4N/mm^2	18.9N/mm^2	19.9N/mm^2
17	18.5N/mm^2	15.6N/mm^2	16.8N/mm^2	17.1N/mm^2	22N/mm^2	18.9N/mm^2	18.1N/mm^2	19.2N/mm^2
18	14.7N/mm^2	17.9N/mm^2	13.1N/mm^2	9.5N/mm^2	21.4N/mm^2	18.9N/mm^2	17.1N/mm^2	20.6N/mm^2
19	15.9N/mm^2	19.9N/mm^2	13N/mm^2	18.8N/mm^2	22.2N/mm^2	18.9N/mm^2	17.1N/mm^2	18.7N/mm^2

Table 2: Summary of result of effects of gas flaring and globalwarming on residential building@ Imone(2007)

S/No	Perimeter@100m	Perimeter@120m	Perimeter@140m	Perimeter@160m	Perimeter@180m
Temp	33°c	28°c	26°c	25°c	24°c
Columm	11.12 N/mm^2	10.56 N/mm^2	11.38 N/mm^2	12.66 N/mm^2	10.56 N/mm^2
slab	23.05 N/mm^2	9.81 N/mm^2	9.81 N/mm^2	13.93 N/mm^2	19.62 N/mm^2
beam	12.33 N/mm^2	12.4 N/mm^2	15.26 N/mm^2	14.84 N/mm^2	13.73 N/mm^2
wall	12.33 N/mm^2	9.8 N/mm^2	9.81 N/mm^2	9.81 N/mm^2	10.73 N/mm^2

IV. Discussion

The study has presented the effects of fire outbreaks, gas flaring and global warming in buildings. Table 1 shows the loss of yielding strength as a result of fire out break in a martket. The rate at which markets in Nigeria are burnt down is becoming alarming and these results tend to portray that there is a strength reduction. In the first two to three columns of table 1 the obtained result tends to be less than the other rolls of the columns and as the result moves down the rows, the strength increases. The value obtained confirms the oral investigation report that perhaps that the first three columns were the points where the fire started. The minimum yielding strength obtained was 10N/mm^2 and the maximum yielding strength was 22.2N/mm$^{2.}$ It was equally observed that the obtained frequently occurred strength was 18.9N/mm^2. Furthermore, the table 2 shows how structural elements stress varies with the distances of the building from the flare. The research is aware that though the buildings are not prototype buildings and are not constructed in the same standard and specifications. The observed deterioration as temperature values increase is obvious, hence the valves of the compressive strength decreases as the atmospheric temperature decrease.

Conclusion: The study has demonstrated physically that there is a reduction in structural and non structural elements especially those used by various governments to erect markets for the masses. Such reduction in strength is thus an index to suggest that the structure has failed in strength and functionality. The author has equally observed that there is reduction in strength of both structural and non structural members of building within the gas flaring perimeter. However, there is need to carry out a research which is time dependent of prototype building built of the same specification to evaluate the effects of gas flaring and global warming.

Recommendation: Fire study in buildings and facilities research has to commence in Nigeria, explosion study and Vibrational study also need to commence too. The selection of members to 2 to 3 hours of fire has not been adhering to in building and fire protection has been seriously negelected in major public buildings. This should be enforced by every end user and National Orientation Agency should enlighten the masses.

Reference

[1]. BS 8110- 1: 1997 and BS8110-2 1985 “structural use of concrete BS1 pg 42

[2]. Ekong F.E (2008) “ Effect of Gas Faring on the Environment and civil Engineering structures , A case study of IBENO Local Government Area, Akwa Ibom State unpublished B.Eng. Work Department of civil Engineering Gen. Abdusalami A. Abubakar College of Engineering, Igbenidion University okada, Supervised by Dr. C. A Ezeagu

[3]. Ezeagu C. A. and Eze A. B. K (2009) “ Effect of Gas Flaring On structural Elements In Niger Delta A case Study of IBENOEXXONMOBIL QUA IBOE TERMINAL Q. I .T IJDS vol4 N01. Pg 42-50. www.1rdionline.com

[4]. Ifekwe V. (2008), Crack Monitoring And Risk Analysis in building. A case study of civil structural Engineering laboratory building UNIBEN, an unpublished B. Eng thesis Department of civil Engineering, Faculty of Engineering, University of benin, Supervised by Dr. C. A Eeagu.

[5]. Okeeibuno N.K (2011) “ The Efffects of Temperature On The strength of Laterised concrete “ An unpublished B. Eng. Work, Department of civil Engineering, University of benin Supervised by Dr. C. A. Ezeagu.

[6]. Olukoto S. and Akpopenamone P. (2010), “Effects of Fire Outbreak on Structural Elements in Nigerian Market, a case study of Agbado market Benin City”. Unpublished B.Eng. thesis Department of civil Engineering, faculty of Engineering University of Benin, supervises by Dr C. A Ezeagu

[7]. Otobo U. R (2010) “progressive Monitoring of Structural Defects and Cracks “ A case study of civil structural Engineering laboratory building UNIBEN, An unpublished B.Eng. thesis Department of civil Engineering, faculty of Engineering, University of benin supervised by Dr. C. A Ezeagu.

[8]. Iroro O. W (2008) “Effect of fire on building structural elements (using INEC Zonal Office Okoda as a case study An unpublished B.Eng. Thesis Department of civil Engineering, General Abdusalmi Abubakar college of Engineering, Igbinedion University Okada, Edo State Supervised by Dr. C. A Ezeagu.

[9]. ISO (1975). Fire resistance Test Elements of building construction ISO 834, International Organization for standardization. Genevia 1975. Pg 19.

[10]. SFEP (2002) hand book of fire protection Engineering, 3rd national fire protection Quincy MA 2002.

American Journal of Engineering Research (AJER) 2016
American Journal of Engineering Research (AJER)
e-ISSN: 2320-0847 p-ISSN : 2320-0936
Volume-5, Issue-1, pp-100-104
www.ajer.org
Research Paper Open Access

Determination of structural behavior of a unreinforced masonry Clock Tower using FEM analysis

Enea Mustafaraj[1], Yavuz Yardım[1,2],
[1](Department of Civil Engineering, Epoka University, Albania)
[2](Department of Civil Engineering, University of Nizwa, Oman)

ABSTRACT :*In this paper it is presented the structural assessment of the Clock Tower found in the castle of Preza, an old historical landmark built during the beginning of 15th century. The structural behavior is analyzed using FEM modeling in order to examine at what extent the structural defects endanger the stability of the tower also considering the geotechnical properties of the soil under the basement of the tower. The geometrical data are acquired by means of terrestrial laser scanner (TLS). Mechanical properties of the constituents were defined through experimental tests on stone samples extracted from the tower. As a result, a better overview of the structural conditions is established and improvement techniques are suggested in order to enhance the performance under both static and dynamic loads.*

Keywords –*finite element modelling, heritage buildings, structural assessment, TSL, unreinforced masonry*

I. INTRODUCTION

Masonry is one the most used construction materials in the history of mankind used in various forms as a basic construction material for public and residential buildings, closely associated with the earliest civilization about 10 000 years ago. Unreinforced masonry (URM) buildings are the most common construction type around the world, as well as in Southern Europe and around the Mediterranean basin. Although these regions are characterized with medium-to-high levels of seismic hazard, the URM buildings are vulnerable as they have been designed (often not designed at all) to only resist gravitational loads and have been realized by rules of common practice. Many of those structures have suffered from the combined effects of inadequate construction techniques, seismic and wind loads, foundation settlements and deterioration of construction materials [1].

In Albania, there are found many cultural heritage buildings made of unreinforced masonry that carry a significant importance due to their unique, cultural, historical and architectural values. Many of those buildings due to the decay and degradation of construction material, aggressive environmental conditions, frequent seismic activity and various geological phenomena, as well as the lack of maintenance, are found to be in a very bad condition. The large number of historical structures highlights the need for preserving this cultural heritage group as one of the most immediate issues to be resolved [2].

It is believed that the suggested assessment method as well as the retrofitting strategies, could be applicable also to other similar heritage buildings that belong to the same period of construction.

II. MATERIALS AND METHODS

Assessment of seismic vulnerability of historic masonry constructions is a very challenging task due to several uncertainties regarding a material's mechanical properties and geometric characteristics of the structure. Recent earthquakes around the world have shown that most masonry towers are susceptible to structural damage and collapse. There have been many attempts from researchers all over the world to model, analyze and retrofit various heritage building structures that are prone to natural disasters. Vicarious Palace in Pescia is an example of seismic vulnerability assessment where a FEM analysis was applied. The comparison of the expected seismic demand versus capacity of that palace emphasized the insufficient resistive capacity of this building against earthquake forces [3]. Lourenço et al., 2001, with the aid of geometric simplifications, carried out an assessment seismic behavior of a basilica church defining the most vulnerable parts and identifying the possible failure mechanisms [4].

In Albania, there have not been any organized large scale attempts to assess current cultural heritage inventory. In 2012, five Ottoman mosques in Albania were analyzed and assessed based on visible "symptoms" that the structural defects or distresses had caused throughout the structures. After the analysis process, strengthening strategies were suggested [5].

2.2 Description of the structure

The Clock Tower is found in the castle of Preza located 15 km away from the capital, Tirana. It has an irregular pentagon plan which measures roughly 80 by 50 meters. The form is largely dictated by the shape of the hilltop. The eastern tower of the castle, which was turned into a Clock Tower in 1852, has a height of 14.5 meters and stands on a 4.2 x 4.2-meter-plan. It has two stories, separated by timber floors. The second story is accessible through internal ladders (Fig.1).

Figure 1. Clock tower: the past (a) and present condition (b)

The tower had a large rosette window, on the outside executed in brick work, in Ottoman style. Nowadays, the top of the tower has been modified and the clock and window are missing. However, it should be mentioned that during its existence the tower has been damaged and repaired several times, mostly due to earthquakes (Fig.1) [6].

2.2 Methodology

The methodology used for this study is based on the in-situ assessment of visible "symptoms" that structural defects and distresses had caused throughout the structure. Visual inspection was followed by a finite element model (FEM) analysis of was conducted in SAP2000 in order to examine the behavior of the tower under static and dynamic loads, as well as to identify the weak locations of potential failure in the structure. The input data related to mechanical properties of the stones were defined after conducting material tests according to ASTM, C170-90 which describes the standard test method for compressive strength of dimension stone. This test method covers the sampling, preparation of specimens, and determination of the compressive strength of dimension stone (Fig.2) [7].

Figure 2. Testing the samples in laboratory

Obtaining the geometrical data was done by using a calibrated high-resolution digital camera (Nikon D90) firmly mounted onto the terrestrial laser scanner Optech ILRIS (3D Intelligent Laser Ranging and Imaging System) together with Topcon GPT 3007 Total Station that provided a combination of scan data and image data. The laser scanner facilitates the procedure of measurements. It enables a field view of 360º along horizontal and a 60º view in vertical plane. In this way, a full panoramic view could be generated. The generated point cloud provided accurate details of the surface pattern of the structure and mapping coordinate system of the volume the structure covered. The structure surface was scanned using the laser scanner with high resolution. A laser beam is used to obtain the geometric coordinates (x,y,z) of points at regular intervals on the visible surface of the structure. Then a point cloud is obtained based on the adjustment and sensitivity of used equipment. A total of 120.000 cloud points were obtained. A color imaging device such as 3D camera used together with the scanner to projecting structure's geometric data onto obtained image for each scanned point.

The second stage of the geometric data representation with TSL is carried out in the office. Obtained data were merged using the PolyWorks commercial software. The software allows the input data to be accurately purified. The produced triangular meshes control model details. Finally, three-dimensional digital models were obtained (Fig.3).

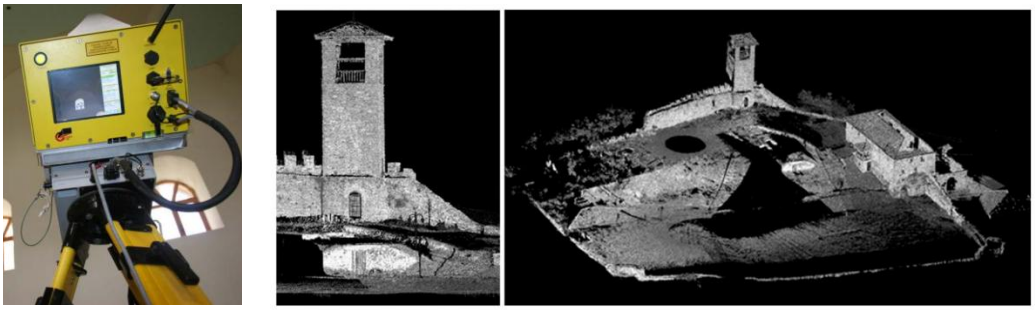

Figure 3. (a) Laser scanner used, (b) point cloud of the tower, (c) point cloud of the whole area of the castle

In order to have a better understanding of the structural behavior, the geotechnical properties of the soil under the tower have been investigated. It is composed of two layers; clayey sand and clayey gravels. The bearing capacity of the first layer, σ, is about 1.8 kg/cm^2, whereas the second one is 5 kg/cm^2. The results showed that the properties were classified as good to very good. The underground water table was found to be below 15 meters. These data clearly indicated that the soil does not have an important role in formation of the cracks in the structure.

A FEM modeling was carried out to demonstrate the behavior of the structure based on rough shapeand more accurate shape. The analysis was carried out using SAP2000 v.15.0 software [8] based on Eurocode 8 [9] (EN1998-1) with consideration of local earthquake code, KTP-N2-89 [10]. The elements and material were chosen to obtain the most realistic simulation of the structure's behavior.

The Clock Tower was modelled in SAP2000 using macro-modelling (masonry units and mortar layers are considered as a continuum, where masonry is isotropic, homogeneous and shows elastic behavior) with shell elements. The analysis would define and locate the most critical regions where the maximum stress concentrations are found. Moreover, distribution of secondary stresses and the behavior of the undamaged model under static and dynamic load was investigated.

The model consists of 2644 joints and 2568 shell elements. Material properties of the model are: unit weight, γ = 20 kN/m^3, modulus of elasticity, E = 1800 MPa, Poisson's ratioυ = 0.2[11], tensile strength, f_t = 1.42 MPa [3] and compressive strength of the stone masonry, f_c = 15 MPa.

Response spectrum analysis was conducted in order to analyze the effects of the ground motion excitations on the structure. The peak ground acceleration based on the obtained soil data and the location of the site, was taken as 0.25*g*. "Type 1" spectral acceleration curve was chosen from Eurocode 8 [9]. Response spectrum analysis predicted the maximum likely response of the structure for a possible earthquake with a magnitude of 5.5 with a 10% likelihood of occurrence and a return period of 475 years [8]. In order to validate the assumption accuracy results, the modal frequencies were compared with previous studies. The most difficult part in modeling a historical monument is obtaining the right material characteristics. Uncertainties related its construction and maintenance and obtaining required number of samples to test are the main obstacle to achieving accurate material properties.

III. RESULTS AND DISCUSSION

The results of the damage survey showed that there is a need for intervention in order to improve its structural performance under cyclic loads. There are a diffuse series of visible cracks are present in all façades of the tower (Fig.4). It is seen the propagation of cracks from top until the bottom of the tower. It is believed that seismic loads are one of the main causes of these cracks.

Moreover, from the archive, it was stated that the tower has been repaired several times. The materials used for repair might have had different properties than the original ones, thus many of the surface cracks could have been formed.

After the visual inspection, FE analysis was carried out. The laser scanner data was transferred to AutoCAD and Sap2000 software to figure out a detailed representation of the geometric model.

Figure 4. Structural cracks found on the main façade.

As expected, the tower exhibits higher displacements at the top. The stresses under dead load are seen to be below the ultimate resistive capacity of materials. In other words, maximum stress values for all the elements do not exceed the allowable limits.

The hoop stress (S11) on the walls varies from -0.274 to 0.244 MPa. S22 ranges between -1.368 to 0.34 MPa. Maximum concentrations are located at the bottom parts of the load bearing walls (Fig.6).

The response spectrum analysis results of the undamaged model have shown that the effect of the seismic loads is felt the same in both directions as the structure has a squared plan and with no irregularities. The maximum displacement is 5.4 mm at the top of the tower.

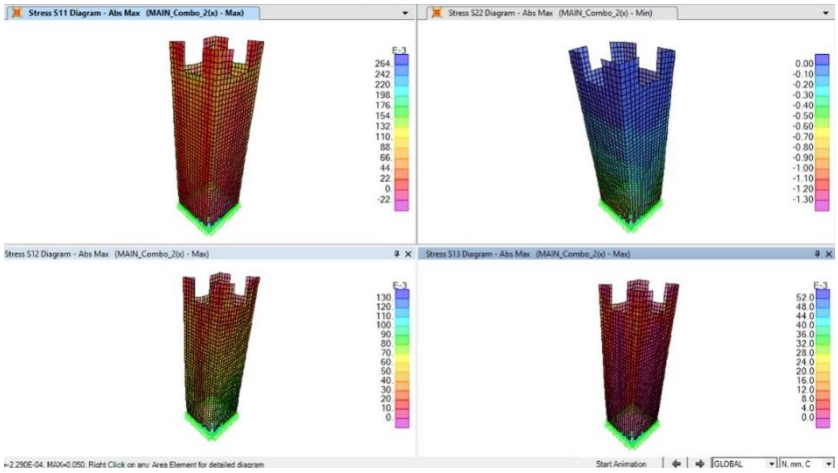

Figure 6. Example of stress distribution after analysis.

IV. CONCLUSION

As it was seen from the assessment result, this structure suffers from cracks and material deterioration. The load bearing walls of the tower exhibit both visible surface degradation as well as structural cracks. Thus, the intervention procedure should consist on reducing the shear and tensile stresses on the walls by adding additional tensile and shear resisting elements where necessary. One of the objectives to be achieved is that connections should be flexible rather than rigid to avoid stress concentrations and guarantee the durability of the structure [12].

Injection is suggested to be used in areas where non-structural cracks less than 10 mm wide are found. The most useful feature is the increase of continuity of masonry. Furthermore, neither aesthetics nor architectural features of the mosques will be altered when applied.

In order to increase ductility of the structure, it is suggested to insert longitudinal FRP bars bonded with epoxy resin or mortar at different levels. Additionally, local reconstruction “cucci scucci” technique is suggested to be used in the places sanding phenomenon is seen and where massive loss of building units is observed. The substituting units must have to the same architectural features, and should be compatible with original facades.

It is believed that the above mentioned strategies would improve the structural performance of the tower under both static and dynamic loads.

REFERENCES

[1] Faella C., Martinelli E., Nigro E., Paciello S., (2010). Shear capacity of masonry walls externally strengthened by a cement-based composite material: An experimental campaign Construction and Building Materials 24 84–93.

[2] Mustafaraj, E., Yardım, Y. (2013). Repair and Strengthening of Historical Structures: Naziresha's Mosque in Elbasan,3rd Annual International Conference on Civil Engineering, 10-13 June 2013, Athens, Greece.

[3] Betti, M., & Galano, L. (2012). Seismic analysis of historic masonry buildings: The Vicarius Palace in Pescia (Italy), Buildings.

[4] Lourenço, P.B. (2005). Assessment, diagnosis and strengthening of Outerio church, Portugal. Construction and Building Materials, 19(8) 634-645.

[5] Mustafaraj, E. (2014). Assessment of Historical Structures, A case study of five Ottoman Mosques in Albania, LAP Lambert Academic Publishing, Saarbrucken, Germany.

[6] Mustafraj, E. and Yardim, Y. Sructural assessment of Preza Clock Tower, Albania, ICESA 2014-International Civil Engineering & Architecture Symposium for Academicians 2014, 17-20 May 2014, Side, Turkey.

[7] ASTM Standard C 170 – 90, (1999). Standard Test Method for Compressive Strength of Dimension Stone, USA.

[8] CSI: SAP2000 v-15.0 (2013): Integrated finite element analysis and design of structures basic analysis reference manual, Computers and Structures Inc, Berkeley, California, USA.

[9] EN 1998-1, (2004): European seismic design code, design of structures for earthquake resistance, Part 1: General rules seismic actions and rules for buildings.

[10] KTP-N2-89: Albanian seismic design code, 1989.

[11] Faella, C., Martinelli, E., Nigro, E. & Paciello S. (2004). Tuff masonry walls strengthened with a new kind of C-FRP sheet: Experimental tests and analysis, 13thWorld Conference on Earthquake Engineering, Vancouver, Canada.

[12] Anzoni, A., Binda, L., Carpinteri, A., Invarnizzi, S. & Lacidogna, G. (2009). A multilevel approach for the damage assessment of historic masonry towers. J. of Cultural Heritage. 11, 459-470.

American Journal of Engineering Research (AJER) 2016
American Journal of Engineering Research (AJER)
e-ISSN: 2320-0847 p-ISSN : 2320-0936
Volume-5, Issue-1, pp-105-110
www.ajer.org
Research Paper Open Access

Study of harmonic contents of appliances in various combinations and their appropriateness for use in solar mini grid ac power systems.

Muhammad Riazul Hamid[1], Md. Jakaria Rahimi[1], Asma Jahan Huque[2]
[1]*Department of Electrical and Electronic Engineering, Ahsanullah University of Science & Technology, Dhaka, Bangladesh.*
[2]*ProkaushaliSangshad Ltd, Dhaka, Bangladesh*

ABSTRACT:*Solar photovoltaic (PV) based mini-grid systems have the potential to be an environmentally friendly and sustainable long term solution for electricity access in Bangladesh. However, to be a successful and cost effective solution, the longevity of these mini-grids with its expensive components is a vital issue. In this paper, we have investigated the potential problems those could hamper the performance of the ac mini-grid system using dc appliances.Specifically the problems those may arise due to harmonic injection from the load side and can eventually reduce the longevity. The investigation is based on a practical design of a solar PV-Diesel-Battery hybrid minigrid to be deployed atNoonertekisland, under Narayanganj district, Bangladesh. A miniature prototype capable of serving a single consumer has been built and measurement for different load combinations comprising of 7.5 and 9 watt LED bulbs, 25 watt DC fans and 14" ac color TV are carried out using DSO(Digital Storage Oscilloscope) and PQA(Power Quality Analyzer). The DC Fans appear to be the highest contributors of harmonic contents and recommended to be replaced by AC Fans.*

Keywords: *Harmonic distortion, Harmonic contents, Solar mini grid, Solar PV-Diesel-Battery hybridminigrid.*

I. INTRODUCTION

In recent years, Bangladesh has made a good progress in power generation sector. However, in spite of recent progress still only 74 percent of the total population of Bangladesh has access to electricity and per capita generation being 371 kWh [1]. The remaining 26 percent of the population is yet to get the benefit of electricity to improve their livelihood. In the fuel mix, major share is occupied by natural gas and imported oil. Bangladesh has a small amount of natural gas reserve which is expected to be depleted in a few years time. Under the current geo-political situation in the Middle East, oil is becoming more of a strategic product and its supply chain is becoming vulnerable. For ensuring its energy security and to reduce dependency on imported oil, Bangladesh is forced to explore the potential of renewable energy resources available in the country. Renewable Energy Policy of Bangladesh sets targets for developing renewable energy resources to meet 5 percent of the total power demand by 2015 and 10 percent by 2020 [2]. Among all other renewable resource, energy from the sun promises to be the most dependable and promising option.

The country is blessed by considerable solar radiation. Bangladesh receives an average daily solar radiation of 4-6.5 kWh/m^2 [3]. Solar photovoltaic (PV) are gaining acceptance for providing electricity to households and small businesses in rural areas. Development of off-grid solar home solutions has achieved international benchmark. According to a survey, there is an existing market size of 6 million households for Solar Home Systems (SHS) on a fee-for-service basis in the off-grid areas of Bangladesh [3]. Nearly 10,000 rural markets and commercial centres in the country is still out of grid which are excellent market for centralized solar photovoltaic plants.

Several fiscal incentives have been extended by the government to Renewable Energy project developers and investors. Dedicated funding support has also been extended through government financial institutions like Bangladesh Bank and IDCOL (Infrastructure Development Company Limited) as well as through private commercial banks. Moreover, the government has extended fiscal incentives including duty exemption or some sort of relief on certain renewable energy products, e.g. solar panels, inverters, LED light, solar operated light and wind power plant. At present, national capacity of renewable energy based power is approximately 403 MW; 165 MW is from Solar [3].

The government of Bangladesh in its "500 MW solar Program" has set the target to generate 25 MW of electricity from solar mini grid. 30 remote areas for implementations have already been identified for this purpose. Most of these projects are in planning stage. In some areas there is no viability of grid expansion in next 15-20 years. According to some literature solar mini grid can be proven as most efficient model for rural electrification[4].Considering technical and business issues, solar mini grid has been found as viable option for Bangladesh[5].

With the financial assistance from the international agencies like WB, JICA, DFID, GPOBA, USAID, ADB and KfW the government of Bangladesh through IDCOL is supporting the implementation of the solar mini grid projects in Bangladesh. IDCOL has a target to finance 50 solar mini grid projects by year 2017 [6].

Recently, a Solar Mini-grid in Noonertek island, under Narayanganj district, Bangladesh has been designed. The proposed project will cater to around 600 residential users, where the maximum load will be from lights, fans and other household appliances like TV, refrigerators, etc. The night time load contributed by lamps and fans (during most of the year) will be very high compared to day time use. It is expected that in the rainy season and summer about 500 fans will be used at any one time over 6-8 hours at least. In order to keep the total load for the system to a minimum, it was initially proposed that low power consuming 25 W DC fans shall be used by the consumers. The ordinary AC ceiling fans available in the market usually consume 65-90W, but cost nearly half of that of DC fans. Before taking any final decision, it was decided to investigate the harmonic contents from these fans and LED bulbs and its overall impact on the performance of the mini grid.
This paper presents the potential problem with non linear loads in section II. In section III the experimental setup for testing is described. The results are presented and also analyzed in section IV. Finally the conclusion is drawn in section V.

II. THE PROBLEM

On scrutinizing the power characteristics of DC fans available in the local market, which use adapters for conversion from AC to DC, it was found that there was a prominent problem of harmonic distortion. This was a concern for the design team because use of these fans would make the plant size smaller, but the impact on the quality of power could be disastrous. A similar problem was faced by Bangladesh Power Development Board's (BPDB) Design Directorate when millions of low quality CFL lamps were allowed to be used in the national grid, although the effect was not visible to all because of the thousands of MW of total supply capacity involved.
For off-grid minigrids the problem may also not be visible at first because the consumers usually take time to get the connections once a plant starts its operations. However, there seems to be a great problem at hand for which a solution is required before allowing large scale use of the DC fans.
According to the recommendations of IEEE standard 519-1992, Total Harmonic Distortion should be kept below 5% at the point of common coupling (PCC). Generally Solar PV inverters are designed to handle harmonic distortion of less than 3%.

III. EXPERIMENTAL SETUP AND THE TEST PROCEDURE.

To estimate the effect of harmonics generated by these non-linear loads, a test bed was designed using the components listed in table 1.
This combination (Package-2) is envisaged to be used by more than 300 households at the project area. Initially the harmonic contents were measured using a Digital Storage Oscilloscope with FFT capability on April 04, 2014. The observation showed the presence of prominent harmonic component.

Table 1: List of loads used for observing the harmonic distortion

Sl.	Load	Wattage	Quantity
1.	LED bulbs	7.5 W	4
2.	DC Fan	22 W	2
3.	14 Inch colour TV	65 W	1

3.1Output from Digital Storage Oscilloscope with FFT capability:

During the test, snapshots of wave forms generated by the **Digital Storage Oscilloscope** (RIGOL DS 5022M) showed a high percent of higher harmonics. However magnitude of individual harmonic contents had to be determined manually. Moreover, some of the harmonics could have been missed due to errors in measurements resulting from human interventions. So, it was decided to use a more advanced digital harmonic analyzer.

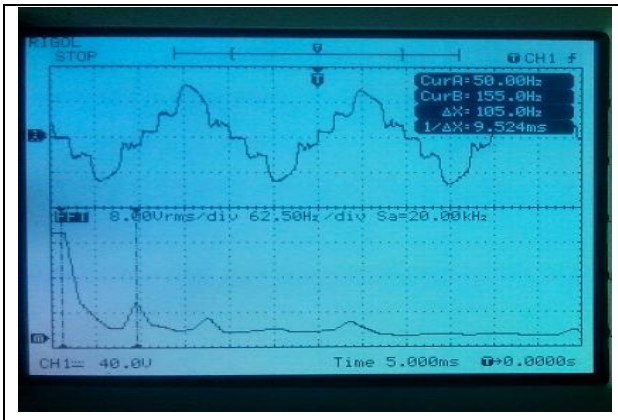

(a)

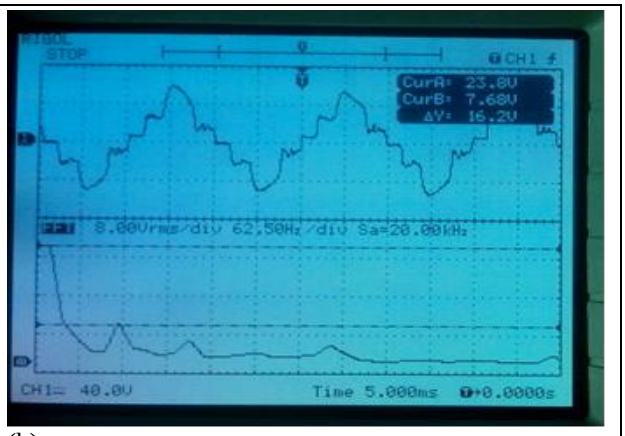

(b)

Figure 1. (a) and (b) :the upper half of these pictures show waveforms in the time domain, whereas the bottom half shows the same in the frequency domain.

In the frequency domain we can easily see the presence of a number of higher harmonics. It is obvious that measuring all the harmonics manually from this curve will be rather difficult and prone to errors. So, we decided to use Power Quality Analyzer to get accurate results.

3.2 Test results using Automatic Harmonic Analyzer:

On 13th April 2014 a set of analysis was carried out using a Power Quality Analyzer (KRYKARD ALM 35), which can pick up upto 25th harmonics automatically).This is a very sophisticated equipment which could pick up all the harmonic components which was not possible to detect manually with the digital oscilloscope. The following snapshots show the results of the experiment for 3 setups.

I. Setup 1: Appliances - 2 AC fans 80W each
II. Setup 2: Appliances - 2 DC fans 25W each
III. Setup 3: Appliances - 4 LED lamps, 2 DC fans 25W, and 1 TV 65W

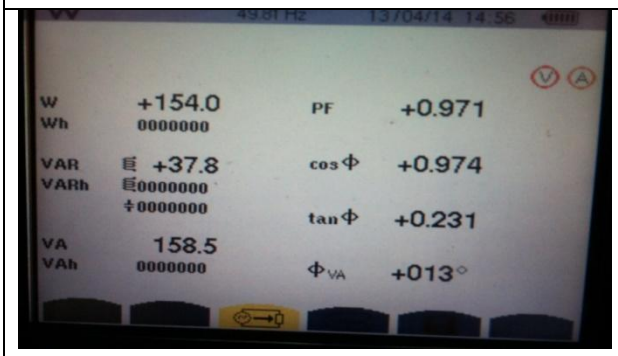

(a) 2 AC fans 80W each-PF

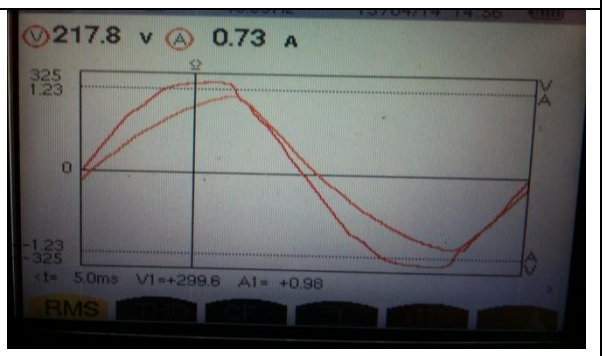

(b) 2 AC fans 80W each-RMS curves

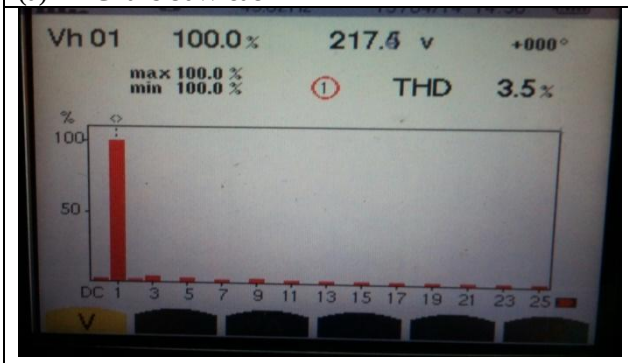

(c) 2AC fans 80W each THDv Bars

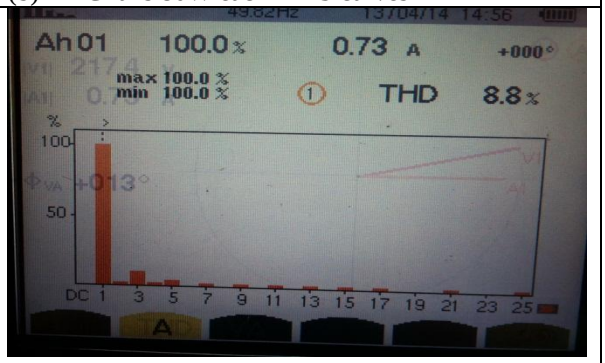

(d) 2 AC fans 80W each THDi Bars

Figure 2: Setup 1- Appliances - 2 AC fans 80W each

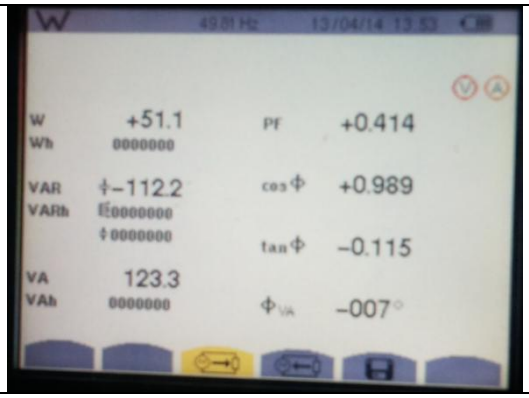

(a) 2 DC Fan: Power factor of these combined loads is +0.414

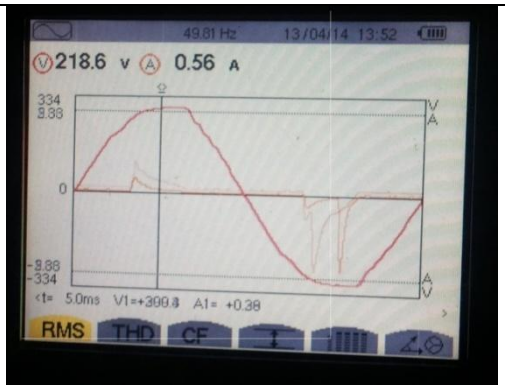

(b) 2 DC fans 80W each-RMS curves

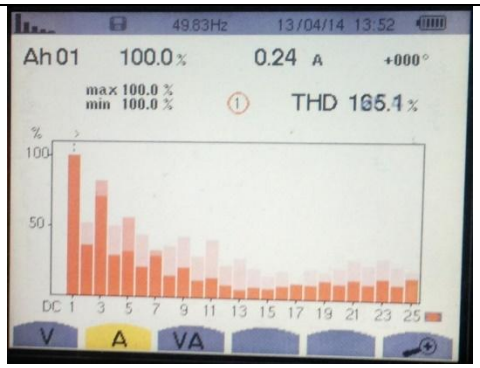

(c)2 DC fans 25W THDi bars

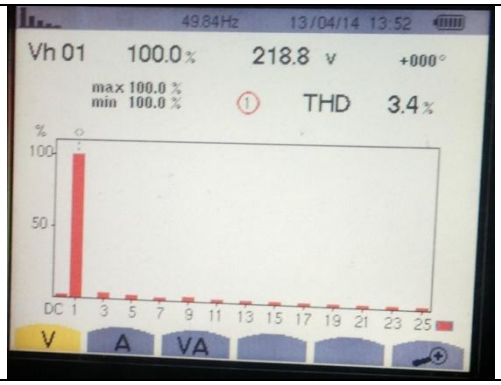

(c) 2 DC fans 25W THDv Bars

Figure3:-Setup 2 Appliances - 2 DC fans 25W each

In Figure 3 significant distortion of voltage and current is observed with a very low power factor.

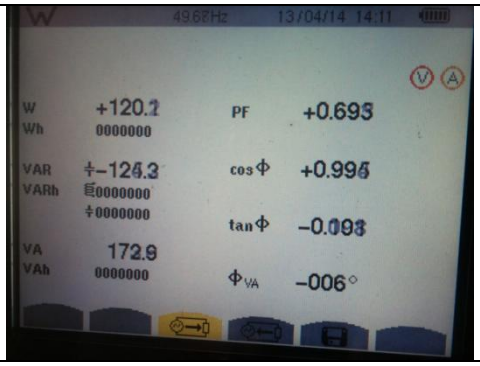

(a) 4 LED, 2 DC fans 25W, 1 TV 65W,-PF: *Power factor of these combined loads is +0.693*

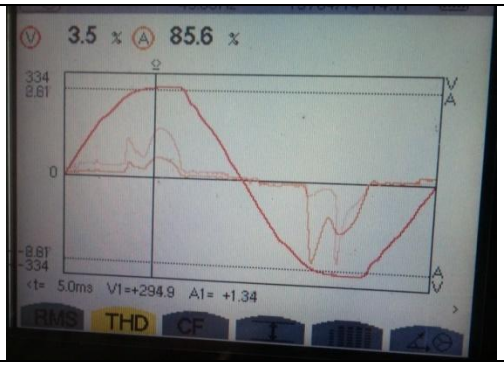

(b) 4 LED, 2 DC fans 25W, 1 TV 65W,-THD curves

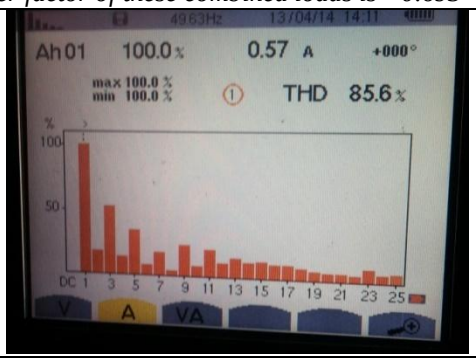

(c)4 LED, 2 DC fans 25W, 1 TV 65W,-THDi Bars

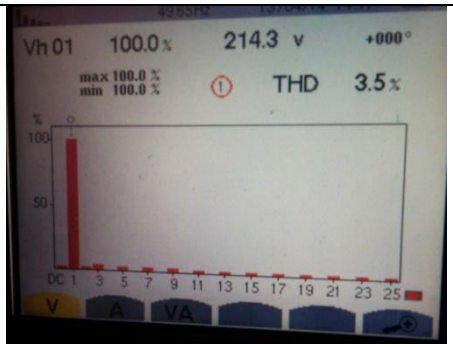

(d) 4 LED, 2 DC fans 25W, 1 TV 65W,-THDv Bars

Figure 4: Setup 3- Appliances 4 LED lamps, 2 DC fans 25W, 1 TV 65W

From observations in Figure 3 and 4 significant distortions of voltage and current is evident when the DC fans are used as loads. In both the cases the power factor is found to be very low. The data obtained from the observations are further analyzed in the foregoing section in details.

IV. ANALYSIS OF THE RESULTS

For quantitative analysis of harmonic distortion of both voltage and current, the parameter Total Harmonic Distortion (THD) has been used. It is calculated as follows:

$$THDi = \frac{\sqrt{I_2^2 + I_3^2 + I_4^2 + I_5^2 + ...}}{I_1} x\,100\ \%$$

$$THDv = \frac{\sqrt{V_2^2 + V_3^2 + V_4^2 + V_5^2 + ...}}{V_1} x\,100\ \%$$

Where,
THDi - Total Harmonic Current Distortion.
THDv – Total Harmonic Voltage Distortion.

Test results using KRYKARD ALM 35 Automatic Harmonic Analyzer

Experimental setups	Appliances	THDv	THDi	Power Factor	
Setup 1	2x80W AC Fans	3.5	8.8	+0.971	
Setup 2	2x25W DC Fans	3.4	165.1	+0.414	
Setup 3	4 x 7.5 W LED 2 x 22 W DC Fan 1 x 60 W TV	3.5	85.6	+0.693	

The DC Fans appear to be the highest contributors of harmonic contents. The most likely cause may be the presence of higher rated capacitors in their adapter circuits. Capacitors are required to get pure DC voltage wave form at the output. Power factor is also very low.

IV.I Probable effects of harmonic distortion in the proposed PV power plant at Noonertek

Harmonics in power system, especially in mini-grid system can introduce many problems [7-9]. Some of these are presented below:

- The first effect of input harmonic currents is to cause an increase in the RMS content of that current. This increase in RMS current can cause overheating of electrical distribution system wiring, and may affect the operation of sensitive electronic equipment like inverters especially in photovoltaic AC systems;
- Harmonic currents can cause false circuit breaker tripping;
- The greater the harmonic content the lower the true power factor becomes;
- Harmonic distortion in general will lower the efficiency of inverters. The issue of harmonic distortion is more important especially for smaller power systems like the mini grid under design (168 kWp);
- The inverter may malfunction and shorten equipment service life.

V. CONCLUSIONS

From the above analysis we can see that,

- The total harmonic distortion of the voltage wave form is 3.5% and the current waveform is in the range of85.6% which is far beyond the specified limit of 5% as recommended by IEEE (IEEE-519-1992). Please note that the tests were carried out with power supply from the national grid which has a huge generation capacity (above 10,000 MW). The effects of harmonics on the voltage were already around 3.5%. Besides, total harmonic distortion of the load current is 85.6%, which is also very high. We need to remember that in the power grid of Bangladesh, the share of non-linear appliances is negligibly small and hence its effects are not much reflected on the operation of the grid and the generating stations. However, in the case of Noonertek solar mini grid project, the plant capacity is very small (168kWp) and the system would be entirely loaded (almost 100%) with these types of loads (with built-in electronics in them)

generating harmonics. It should be investigated what would be the THDv and THDi when the loads are connected to the inverters and whether these inverters would be able to handle these harmonics.

- The DC Fans appear to be the highest contributors of harmonic contents.
- The low power factor (leading) is also a matter of great concern which should be properly addressed before taking decision on design capacity of a plant. Otherwise may not be possibleto utilize full power generated from PVs and generator.

The results found are quite noteworthy and alarming. If the potentialproblem due to harmonic distortionis not dealt with, and significant importance and preventive measures are not taken, it may have adverse effect on the performance and life of the mini grid. In that case it is recommended that adapters for use with DC fans available in the market are selected and properly tested before being allowed to be used in anySolar mini-grid to ensure longevityof the system and warranty requirements of the inverters.

REFERENCES

[1] Power Cell, Power Division, Ministry of Power, Energy and Mineral resources, Government of Bangladesh as accessed on 29th December 2015. http://www.powercell.gov.bd/index.php?page_id=267

[2] "Renewable Energy Policy of Bangladesh", Power Division, Ministry of Power, Energy and Mineral Resources, Government of the People's Republic of Bangladesh, 6 Nov 2008 (Policy Document)

[3] www.powerdivision.gov.bd/site/page/7cdf7d30-6656-41ec-aa8a-943193f30a61. Accessed in November, 2015

[4] http://ep-bd.com/online/details.php?cid=32&id=18691. Accessed in April, 2014.

[5] Subhes C. Bhattacharyya, "Mini-grid based electrification in Bangladesh: Technical configuration and business analysis",Elsevior, Renewable Energy,Volume 75, March 2015, Pages 745–761

[6] http://idcol.org/notice/feead32c0c458badcc023e78e18f649a.pdf. Accessed in January, 2014.

[7] Y. J. Wang, R. O'Connell, and G. Brownfield, "Modelling and Prediction of Distribution System Voltage Distortion Caused by Nonlinear Residential Loads", Power Delivery, IEEE Transactions on Volume 16, Issue 4, October 2001, Page(s): 744 – 751.

[8] R. W. Erickson and D. Maksimovic, "Fundamentals of Power Electronics", Second Edition, Springer Science & Business Media Inc, Page(s): 912.

[9] R. C. Dugan, M. F. McGranaghan, S. Santoso, H. W. Beaty, "Electrical Power Systems Quality", Second Edition, McGraw-Hill, Page(s): 528.

American Journal of Engineering Research (AJER) 2016
American Journal of Engineering Research (AJER)
e-ISSN: 2320-0847 p-ISSN : 2320-0936
Volume-5, Issue-1, pp-111-117
www.ajer.org
Research Paper Open Access

Modelling and Simulation of Load Balancing in Computer Network

[1]Gbadamosi Luqman and [2]Akanbi Lukman
[1]*Computer Science Department, Lagos State Polytechnic, Lagos State, Nigeria*
[2]*Research Scholar, Embeddedkits Technology, Osun State , Osogbo, Nigeria*

Abstract: *The overload of the servers and the resulting decrease in the Quality of Service (QoS) and performance becomes more serious as the use of Web services grows. In order to avoid this, service providers use large distributed networks of servers to attend the requests of the increasing number of visits in popular sites. OPNET (Optimum Network Performance) is used to develop a new model suitable for Osun State University, Nigeria. The model was then evaluated to measure the performance of the wireless local area network. The model was used for two types of applications (ftp and http) and found that among a set of other parameters response time and wireless media access delay were highly affected by the number of users per application with and without load balancing. OPNET simulation showed the impact of load balancing on wireless and wire-line network for two different types of applications.*

Key Words: *WLAN, Load balancing, Media Access Delay, Http response time, ftp response time.*

I. Introduction

Wireless access points are now common place on many university campuses (Bennington and Bartel, 2007) Technologies such as IEEE 802.11b wireless LANs (WLANs) have revolutionalized the way people think about networks, by offering users freedom from the constraints of physical wires. Mobile users are interested in exploiting the full functionality of the technology at their fingertips, as wireless networks bring closer the "anything, anytime, anywhere" promise of mobile networking. Wireless local area networks (WLANs) are spreading rapidly, their major advantage over wired ones being their easy installation.

Wireless communications is one of the most active areas of technology development of our time. Over the recent years it has rapidly emerged in the market providing users with network mobility, scalability and connectivity. Wireless Local Area Networks (WLANs) have been developed to provide users in a limited geographical area with high bandwidth and similar services supported by the wired Local Area Network (LAN) (George et al (2000)) Radio wave signals propagate through walls, ceilings, and even cement structures. A WLAN is a flexible data communications system that can either replace or extend a wired LAN where cost is an issue or running cables between floors or different rooms on the same floor is not feasible (GloMoSim, 2011)Examples of structures that are difficult to wire are warehouses, historic buildings, and manufacturing facilities. A WLAN basically consists of one or more wireless devices connected to each others in a peer-to-peer manner or through APs, which in turn are connected to the backbone network providing wireless connectivity to the covered area. Fig.1 shows a typical layout of a WLAN with two APs (GloMoSim, 2011)

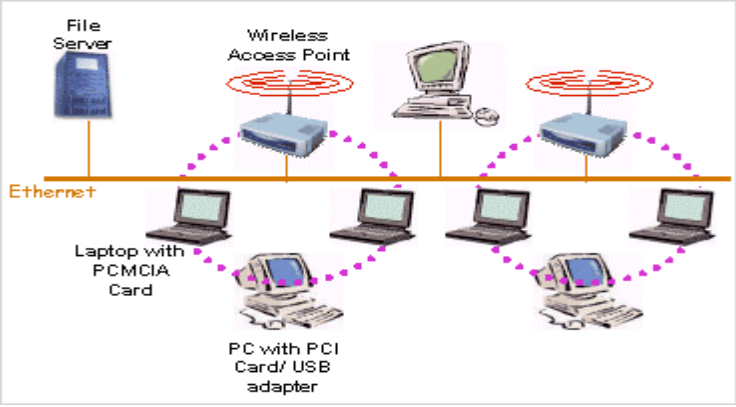

Fig. 1: WLAN with two APs

II. Review of Related Works

Nakagawa et al (2003)is a new bridge architecture proposed to address the problems associated with spanning trees in LANs. Packet forwarding in smartBridge architecture is done along the shortest paths. Although shortest path switching may provide a low latency path, it does not address the load balancing issue in the network and requires all bridges in the network to be smartBridge compliant.

Sharma *et al*. (2007)discuss a novel approach named STAR (Spanning Tree Alternate Routing) to find and forward frames over alternate paths that are probably shorter than their corresponding tree paths. Although the approach reduces latency between most of the source and destination pairs, it risks overloading of critical links.

Another approach to load balancing is Tree-Based Turn-Prohibition (TBTP) LTE load balancing problem has been investigated in the literature. Steenkiste et al (2003). presented a mathematical framework for quantitative study of self-optimizing wireless networks for LTE system, in which a self-optimizing network algorithm was proposed to adjust the cell-specific handover thresholds for load balancing

Tang *et al (2000).* proposed a handover off set based load balancing algorithm using the parameter "cell specific offset" to force users to handover from the overload eNB to the target eNB . The main goal of the proposed algorithm is to find the optimalhand over offset that allows the maximum number of users to change cell without any admission rejection at the target eNB A directional cell breathing based reactive congestion control algorithm was proposed where the coverage area of a cell can be dynamically extended towards a nearby loaded cell when it is under-loaded, or shrunk towards the cell center when it is over-loaded.

(Tarek , 2007) Has proposed a technique to balance the traffic load among the available gateways nodes in the network. In this technique, an average queue length in the gateway is used to estimate congestion over that period of time and an alert is raised by the congested gateway upon which selective active sources are sent notification messages to switch their internet attachment to an alternative less-congested gateway. This technique can reduce overloading the gateway nodes, but a technique that balance the network load across not only the gateway nodes, but also intermediate nodes in the network thus avoiding centre loading problem is also needed. Sending notification to some sources will also increase the overhead traffic in the network.

King-Shan Lui *et al*. (2009) discuss a novel approach named STAR (Spanning Tree Alternate Routing) to find and forward frames over alternate paths that are probably shorter than their corresponding tree paths. Although the approach reduces latency between most of the source and destination pairs, it risks overloading of critical links.

Another approach to load balancing is Tree-Based Turn-Prohibition (TBTP) (Mikael, 2005)TBTP constructs a less restrictive spanning tree by blocking a small number of pairs of links around nodes, called turn, so that all cycles in a network can be broken. However, TBTP is complex and did not consider the best spanning tree and switch load balancing.

MSTP or Multiple Spanning Tree Protocol (Andreolini et al, 2003) is defined in IEEE 802.1s. MSTP uses a common spanning tree that connects all of the regions in the topology. The regions in MSTP are multiple instances of the spanning tree. An instance of RSTP governs a region, where each region has its own regional root. The regional roots are in turn connected to the common root that belongs to the common spanning tree. Since MSTP runs pure RSTP as the underlying protocol, it inherits some drawbacks of RSTP as well. However, a failure in MSTP can be isolated into a separate region leaving the traffic flows in other regions untouched. In addition, the administrators can perform light load balancing manually by assigning certain flows to a specific spanning tree.

A fault tolerant multiple spanning tree protocol was proposed in Viking (2008). Viking relies on per-VLAN-spanning tree implementation of Cisco where there is a separate spanning tree running on every switch for every VLAN. This has the limitation on the number of VLANs the Metro Ethernet can support due to the maximum VLAN tag size and the number of spanning trees a switch can handle without compromising performance.

III. Methodology

3.1 IMPLEMENTING USING OPNET MODELLER

OPNET is a tool used to simulate the way networks run. In this study, comparative study is carried out on the LAN performance for Low Load Campus environment with without load balancer. We have chosen this simulation tool – OPNET IT GURU Academic Edition for our research because of the several benefits:

i. OPNET IT GURU provides the set of complete tools and a complete user interface for topology design and development.
ii. It is being extensively used and there is wide confidence in the validity of the results it produces.
iii. It enables realistic analysis of performance measures and the effectiveness of WAN design techniques.

OPNET IT Guru is very similar to an OPNET Modeler. The main differences are that it does not include a process editor, the possibilities of editing code level in C language, and various advanced modules. From that aspect, we cannot change existing communication models or create new components. Maximum network

expanse, which can be simulated, is also bounded in OPNET IT Guru. In this section, it has been considered that the campus having a LAN connected with 3 FTP Server and 3 HTTP Server with and without load balancer. All of these servers are provided to serve the load demand on the campus network. When one server is not enough then it will load the request will be routed to other servers. The simulation scenario is if the campus network had a high load demand, and all the servers serve the load request. These LANs are connected via 100 based T Ethernet wired network. Two different scenarios & setting have been considered to optimize the network

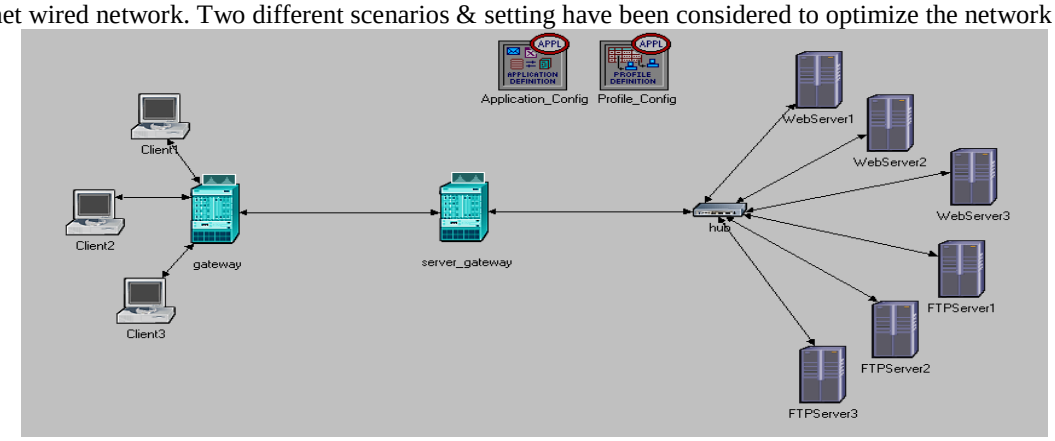

Fig. 2: Scenario I: LAN without Load Balancer

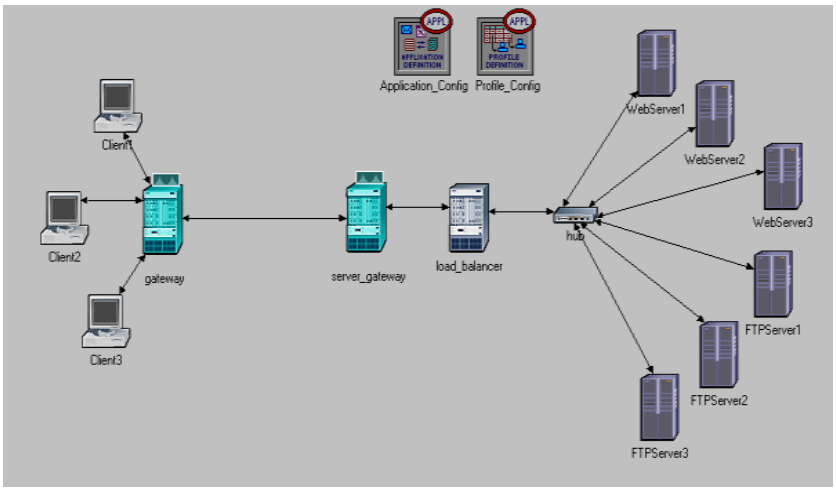

Fig. 3: Scenario II: LAN with Load Balancer

Fig. 2 and 3 show the two scenarios present a Campus Network with Local Area Networks. These scenarios are simulated each LAN with the same network and application configuration. LAN servers support all applications expect for FTP and HTTP which are supported by FTP Server and HTTP Server.

Table 1: Application Description

APPLICATIONS	ATTRIBUTE	LOAD
HTTP SERVER	HTTP	Heavy Browsing
FTP SERVER	FTTP	High Load
EMAIL	CPU UTILISATION	%
PRINT	CPU UTILISATION	%

Table 2: Simulated Parameters

APPLICATION	PARAMETER	UNIT
FTP SERVER	Download Response Time Traffic Sent Traffic Received CPU Utilization Load	Seconds packets/seconds packets/seconds percent requests/ seconds

In this network are examples of how LAN models may be used instead of explicitly modeling the entire LAN. This model represents aggregate traffic of many users on a LAN

3.2 Development of OPNET Simulation Algorithm

This project uses OPNET (Optimized Network Engineering Tool) simulation research on artificial spider routing algorithm and comparative analysis. OPNET modeling hierarchy to the network, the process model and its underlying mechanisms using state machine to simulate the network protocol, node model middle usually contain multiple process model for equipment simulation network, network model of the top, each node model are connected, forming network topology. The establishment of three levels of the model OPNET, both structure and the actual communication protocols, communication equipment and network corresponding to complete, evaluation, testing and improvement of the network routing protocol, so as to optimize the performance of the network. OPNET software provides a good experimental platform for artificial spider routing algorithm,

3.3 Development of Design Flowchart

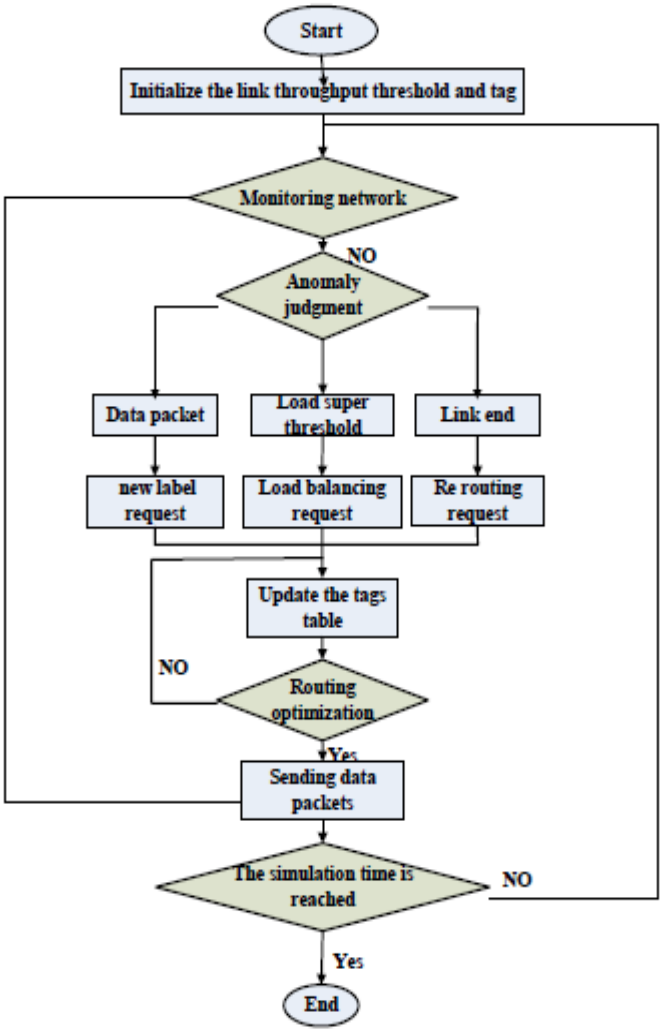

Fig. 4. Design Flowchart

The Figure 8 is the simulation of OPNET software flow chart. In the simulation the flow chart, the unit is bps, average end to end delay in seconds (s), the average packet loss rate is the ratio of overflow data packet and the total contract number, the abscissa simulation map of all are the simulation time, unit for minute (min).

3.4 Development of Load Balancing Algorithm

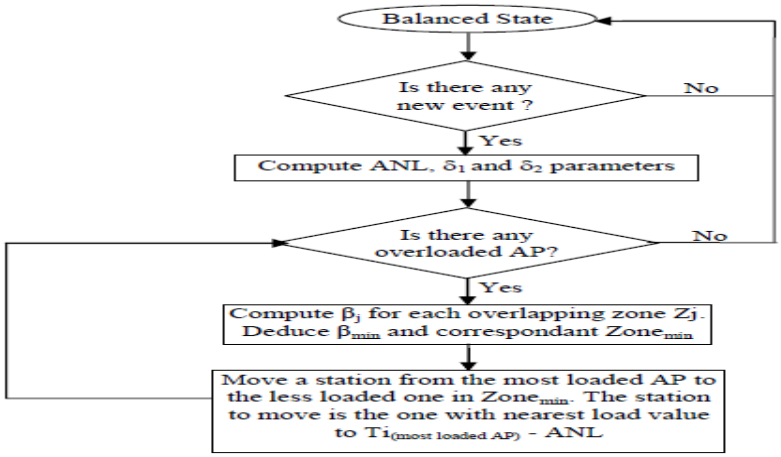

Fig.5 : the Load Balancing Algorithm

IV. Result and Discussions

In each network in both scenario there are 3 HTTP Server and 3 FTP Server. This 3 servers is provided to server the HTTP and FTP load in the campus's network. In Fig. 6, it shows that FTP Download Response Time faster at starting point in network without load balancer, but after that network with load balancer has faster Download Response Time. In Fig. 7, Traffic Received in FTP Server in network without load balancer and with load balancer is similar, but after that network with load balancer is faster, and the Traffic Sent is faster at starting point in network without load balancer, but after that network with load balancer is faster.

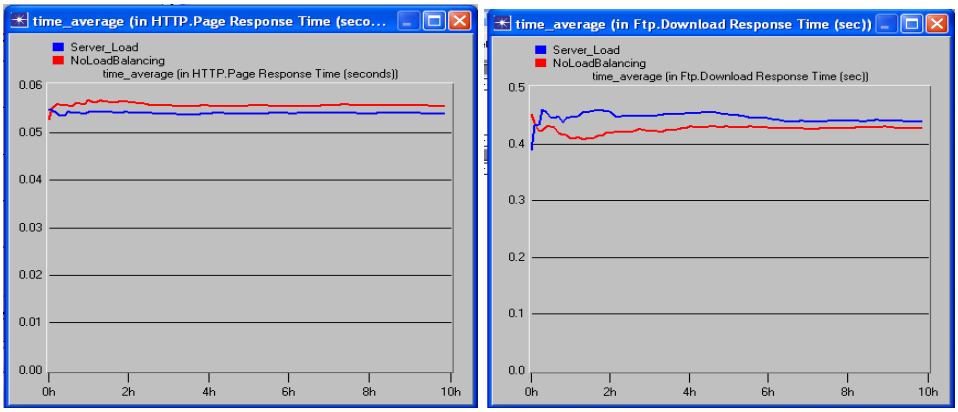

Fig. 6: FTP Download Response Time and HTTP Page Response

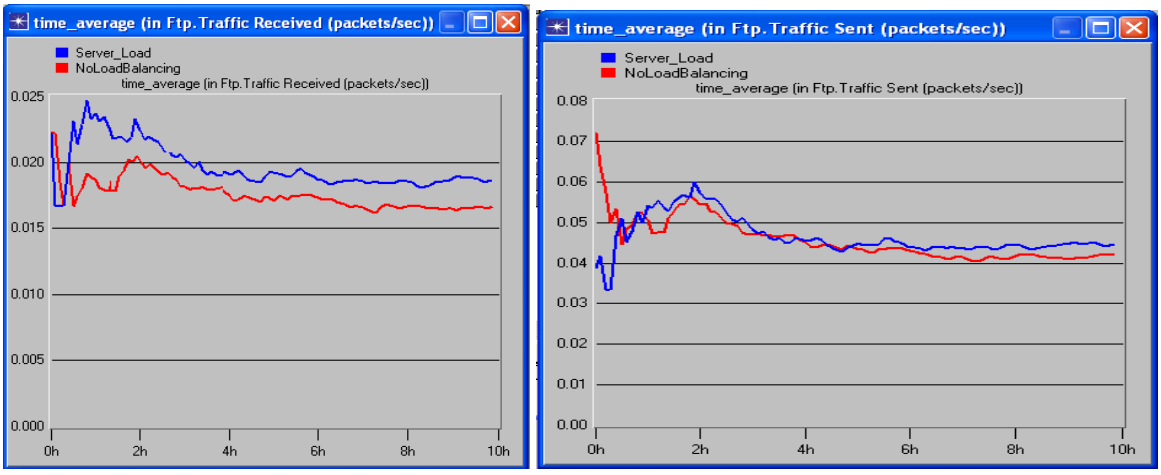

Fig. 7: FTP Server Traffic Received and Traffic Sent

Fig. 8: HTTP Server Traffic Received and Traffic Sent

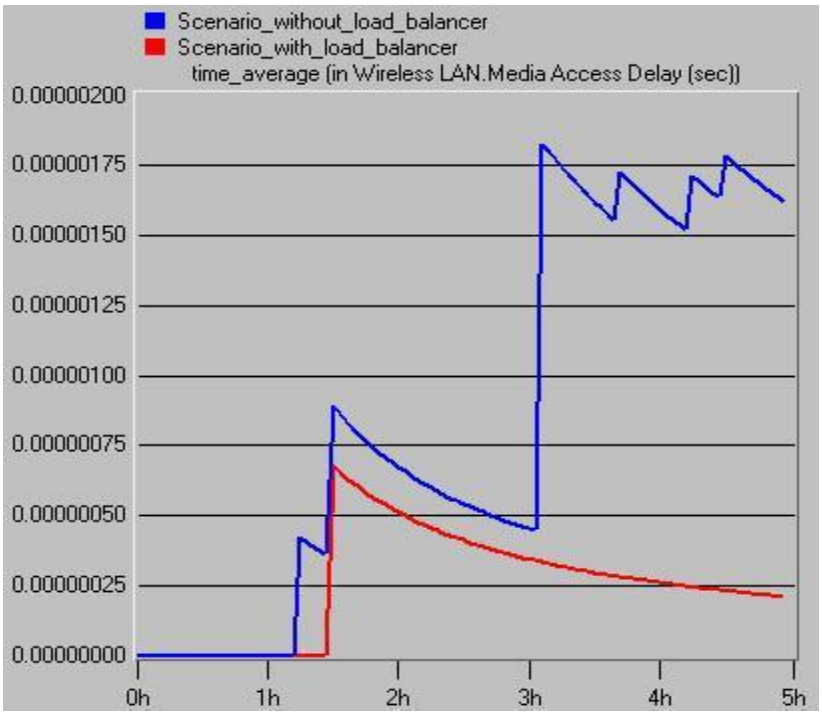

Fig. 9: Media Access Delay (sec)

V. Conclusion

This project investigates the load for Osun State University, Nigeria campus environment with and without Load Balancer. In this study we have build a model of browsing behavior for a HTTP and downloading for FTP application, and use this model in a simulation study addressing the performance of the campus area network. Our investigations reveal that load balancer is useful to increase the FTP download response time. Thus, it is evident that the use of load balancer is recommended for downloading processes. The observations indicate that FTP and HTTP traffic send and received is less in case of using load. Thus we conclude that the overall performance is better with load balancer as comparison of without load balancer.

References

[1] Bennington B. and Bartel C., (2007) 'Wireless Andrew: xperience Building a High Speed, Campus-WideWireless Data Network', Proceedings of ACM MOBICOM, Budapest, Hungary, September, pp. 55-65,

[2] Fitzhugh, S. (2012). Portable network laboratory. 32nd ASEE/IEEE Frontier in Education Conference, Boston, MA, November 2002.

[3] George Apostolopoulos, David Aubespin, Vinod G. J. Peris, Prashant Pradhan, and Debanjan Saha. Design, implementation and performance of a content-based switch. In proc. of INFOCOM, 2000

[4] GloMoSim. (2011). Global mobile information systems simulation library. Retrieved January 26, 2006, from http://pcl.cs.ucla.edu/projects/glomosim

[5] Hansen T., Yalamanchili P. and Braun H-W., (2002) 'Wireless Measurement and Analysis on HPWREN', Proceedings of Passive and Active Measurement Workshop, Fort Collins, Co, March, pp. 222-229.

[6] IT Guru Academic Edition. OPNET Technologies, (2007) http://www.opnet.com/university _program/ itguru academic_edition.

[7] Jipping, et al (2003). Using Java to teach networking concepts with a programmable network sniffer. Proceedings of the 34th SIGCSE Technical Symposium on Computer Science Education, 120-124.

[8] Jussara Almeida, Mihaela Dabu, and Pei Cao. Providing differentiated levels of service in web content hosting. In proc. of the First Workshop on Internet Server Performance, 2008.

[9] Keshav, S. (2008). REAL: A network simulator. Technical report 88/472, University of California, Berkeley.

[10] Kneale, B. & Box, L. (2003). A virtual learning environment for real-world networking. Information Science, 71.

[11] Kurose, J., Leibeherr, J., Ostermann, S., & Ott-Boisseau, T. (2002). Workshop report. ACM SIGCOMM Workshop on Computer Networking: Curriculum Designs and Educational Challenges.

[12] Kotz D. and Essein K., (2009) 'Analysis of a Campus-Wide Wireless Network', Proceedings of ACM MOBICOM, Atlanta, GA, September.

[13] Mauro Andreolini, Michele Colajanni, and Marcello Nuccio. Kernel-based web switches providing content-aware routing. In proc. of the 2nd IEEE International Symposium on Network Computing and Applications (NCA'03), 2003.

[14] Mayo, J. & Kearns, P. (1999). A secure unrestricted advanced systems laboratory. The Proceedings of the 30th SIGCSE Technical Symposium on Computer Science Education (SIGCSE'99), 165-169.

[15] Mikael Andersson, Jianhua Cao, Maria Kihl, and Christian Nyberg. Admission Control with service level agreements for a web server. In proc. of European Internet and Multimedia Systems and Applications, 2005.

[16] Nakagawa, Y., Suda, H., Ukigai, M., & Miida, Y. (2003). An innovative hands-on laboratory for teaching a networking course. 33rd ASEE/IEEE Frontier in Education Conference, Boulder, CO, November 2003.

[17] NS-2 (2006). The Network Simulator – NS2. Retrieved February 18, 2006, from http://www.isi.edu/nsnam/ns

[18] OPNET (2006). OPNET network simulator. Retrieved February 21, 2006, from http://www.opnet.com

[19] Richards, B. (2001). Rtp: a transport layer implementation project. Proceedings of the Sixth Annual CCSC Northeastern Conference on the Journal of Computing in Small Colleges, 134-141.

[20] Sharma M. and Manoj, (2007) 'Comparative Investigation on Throughput and Client Response Time for a Switched and Routed Wireless LAN based on OPNET' Proceedings of National Conference on "Emerging Trends in "Computing and Communication

[21] Soliman A. Wabie Al-, (2002) 'The New Wireless Local Area Networks (WLAN's) Standard', University of Maryland.

[22] Steenkiste, P. (2003). A network project course based on network processors. Proceedings of the 34th SIGCSE Technical Symposium on Computer Science Education, 262-266.

[23] Tang D. and Baker M., (2000) 'Analysis of a Local-Area Wireless Network', Proceedings of ACM MOBICOM, Boston, MA, August, pp. 1-10.

American Journal of Engineering Research (AJER) 2016
American Journal of Engineering Research (AJER)
e-ISSN: 2320-0847 p-ISSN : 2320-0936
Volume-5, Issue-1, pp-118-124
www.ajer.org
Research Paper Open Access

Risk Assessment and Risk Mapping

Younes BOURASS[1], Saoudi TAIBI[2]
[1,2] *Laboratory Quality, Safety and Maintenance, Mohammadia Engineering School, Mohammed 5 University, Morocco*

Abstract: *This working paper aims to emphasize the complexity of the environment in which today's business is evolving, and associated risks. We will focus on methods of analysis and assessment of these risks, particularly in the context of a project. We first introduce the concept of risk in the company, by explaining that it is considered as an inseparable parameter of any project. Then, we present the general approach of risk management methods, which are based on two key phases: risk analysis, and treatment of identified risks.*
The risk management methods can be quantitative or qualitative. The ultimate goal is to establish a risk map with a probability of occurrence and impact of risk that are real and sincere.

Keywords: *Risk project, risk mapping, uncertainty, risk assessment*

I. INTRODUCTION

Today's business world is constantly changing, it's unpredictable, volatile, and seems to become more complex everyday. Uncertainty is an inherent parameter to the life of any organization. One of the main challenges for management is the determination of an acceptable degree of uncertainty to maximize value creation, objective considered as the basic premise in the concept of risk management. The uncertainty is a source of risks and opportunities that could create or destroy value. Risk management provides the ability to respond effectively to the risks and opportunities associated with the uncertainties that the organization faces, reinforcing the organization's value creation capacity. In the current global economic environment, identifying, managing, and exploiting risk across an organization has become increasingly important to the success and longevity of any business. One of the most effective tools used by the risk management, particularly to facilitate the decision-making, is risk mapping.

A risk map helps to formalize and prioritize the key risks of the firm, contributes to create, with managers, a common language on risks and facilitates the elaboration of a plan to take immediate actions. It will promote the emergence of a shared risk culture, which is a source of improved performance and greater risk prevention.

II. THE COMPANY DEAL WITH THE COMPLEXITY, SOURCE OF THE RISK

Companies are actresses of a complex and unstable economic environment. This complexity is characterized by the globalization of markets, the development of information systems and the interdependence of business, politics, social and ecological at the global level, the sharp fluctuations in the financial markets or economic conditions [Laszlo 1998].

We can add to this, the development of new technologies, shorter product life cycle, requirements for quality and specificity of increasingly stringent, the changing nature of competition, cultural changes, new techniques communication, the changing relationship of man with the work [Grasset 1996]. Given these global developments, it is necessary for the company to constantly adapt to its environment.

To understand the complexity, it is necessary to deal with the multiplicity of the system "the complexity is a web of heterogeneous components inseparably associated: it raises the paradox of the one and the many" [Morin 1990]. According to Genelot (2001), a phenomenon is complex when it's beyond our control and our understanding. The complexity is manifested to us in the guise of uncertainty, the multiple, the tangled, and unstable.

The complexity is perceived and linked to notions of unstable and uncertain. Admittedly, as Morin emphasizes that we will never have full knowledge of the complex phenomena [Morin 1990]. We are then in an unstable world, we can not have a rational view [Braech 1995]. However, the complexity should not be perceived as a constraint. As shown Yatchinovsky, complexity is a source of richness of diversity and depth [Yatchinovsky 1999], it can be a source of opportunities.

The company must integrate this notion of uncertainty in its management and control to adapt to the external environment. At that consideration of changes in outdoor environments, the company also has to deal with the complexity of managing its own developments and internal and external uncertainties [Braesh 95]. These uncertainties are sources of risk. The mastering of uncertainty, and therefore risk, allows better control of the firm. However, it is necessary to give up control everything, because it is impossible to identify all factors to consider for controlling the uncertainty [Yatchinovsky 1999].
This is in internal company risks, specifically in project risks, that we place our research.

2.1 The Project Risk: a Parameter Inseparable from Project

The risk is a "*hazard which occurrence deprives a resource system and prevents it from achieving its objectives*" [Wybo 1998]. The project risk is defined as an "*event whose occurrence is uncertain and whose manifestation is likely to affect the project objectives*" [AFNOR 2003]. It alters the project design process, and is "*the possibility that a project does not proceed in accordance with the desired objectives and processes, the difference being considered harmful*" [AFITEP 1998]. This disruption of the project includes the loss of control of the triptych cost-quality-time. The project risk is "*the possibility that a project does not run according to the forecast completion date, cost and specifications, these differences from the forecast are considered less acceptable or even unacceptable*" [Giard 1995].
These risks should be managed by the project team, including the project manager in the project management process. A project involves an approach built vis-à-vis the risks; its prototype character (or innovation), its integration in an environment that reacts involve a number of risks different in nature, size and frequency that the project manager can not ignore [Belicar 1994]. This responsibility must be borne by the project manager. The project manager, who supports the management of the project, has to:
- Set the objectives, strategy, resources and organization,
- Coordinate the successive actions and / or concomitant,
- Control at all times and in all fields and change the strategy, means and structure if an objective is changing or if the program can not be met,
- Optimize the allocation of resources to achieve the project objectives.

It is necessary to control these risks and opportunities in project management for companies. We discuss first what are the methods and project management tools available to project managers, and how risk mapping is elaborated.

III. METHODS OF RISK MANAGEMENT: GENERAL APPROACH

In numbers of companies, the risk assessment is too often fragmented, divided between different functions, which don't take into account only the risks related to their activities, with a view to protecting them.
Since 2003, to avoid failures and widespread methods of project risk management, a standard was drafted. Based on the principle "prevention is better than cure" approach project risk management defined by the FC X50-117 standard is as follows [AFNOR 03]:

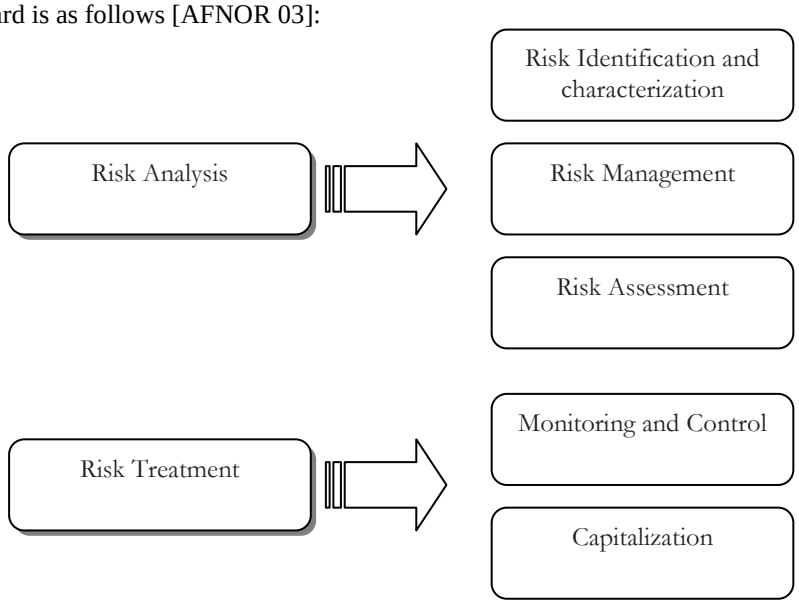

Figure 1: General approach of risk management methods

1. Risk Assessment

Desroches (2003) defines risk by its two endpoints, the occurrence and impact, "the risk is a quantity to two dimensions noted (p, g): p is a probability that gives a measure of the uncertainty that we have on the gravity effects g, in terms of damage consequential to the occurrence a dreaded event "[Desroches 2003]. Cooper, Kasenty and Navier assess the risk according to these two criteria [Cooper 1987] [Kasenty 1997] [Navier 2003].
In this evaluation phase two approaches are possible [Courtot 1998]:
- Quantitative approaches are often based on the use of the method of Monte Carlo [Kasenty 1997] [Vickoff 2000] and often require the use of a specific computer tool to decrease the importance of computing time.
- Qualitative approaches are based on the choice of a distribution according to a predefined scale of the variable and its parameters [Desroches 2003], [Navier 2003], [Chapman 2003], [Gautier 1995].
The purpose of the assessments is to allow the whole team appreciate the prioritization of risks and have a consensus on the order of actions by means of an "impartial" indicator [Chapman 2003].The precise quantification of the risk criticality is not the main purpose of risk management [Cooper 1987]. Qualitative approaches are the most common, and as Munier points out, there is no objective tool to predict risk when the feedback is low, but it is necessary to control its risk assessment scale. It should not be that the practice uses the subjective as rule of thumb that does not mention and which we do not review the operation [Munier 2003].
The assessment and prioritization of risks identified qualitatively or quantitatively are delicate and crucial. This step is essential to elaborate the risk map.

2. Typology of Risks in Project

In one project, we distinguish several types of risks depending on the chosen criterion. The major challenge is to integrate risk management and project management in a single activity. Therefore, classification of project risks must flow from the joint intervention of a domain-expert and risk-expert. This approach is based on a matrix overlap between:
- Generic risk: these are the basic families of risks apply to all projects. For example, we cite human risks, technological risks, exchange risks ... etc. ;
- Project tasks: these are the elements that make up the project. For example, we cite the supply chain task, engineering task, maintenance task ... etc.
The result of these confrontations between generic project risks and project tasks is a matrix ensuring completeness of operation. This matrix allows linking each generic risk with every component of the project description.
At the end, separate couples (generic risk / component project) emerged following the interviews of the project expert and the risk expert draft risk corresponding to real project risks which are identifiable and describable.
Risk classification is the first step to take for a better identification of project risks. However, this classification must meet two requirements:
- It must cover all potential risks. This feature guarantees the relevance and effectiveness of the adopted typology.
- It must be uniform to ensure balance in the grid and do not deprive the project risks.
That being said, it should be noted that this aspect concerning the precision and smoothness of the mesh does not condition the identification of risks itself.
The typology of the proposed generic risk is not a static model. Rather, it is a first interesting work that can be further enriched by experts and researchers of a particular technical discipline.
In the same line of ideas, a repository of risk areas was established by professionals, distinguishing between internal and external project risks.
Hereafter, we resume the typology contained in the AFNOR[1] standard.

Internal Risks:
- Human risks: organization, animation, internal communication, decision ...
- Corporate Risks: planning, monitoring, documentation, release, budget
- Technological risks: ergonomics, safety, competence, availability, adequacy
- Contractual risks: requirements, specifications

External Risks:
- Technical Risks: evolution
- Political risks: business, lobbying, social, protest
- Customer or market related risks: changing needs, competition, use
- Legal risks: safety, environment, taxation

[1] AFNOR, *Gestion du risque*,– Fascicule de documentation FD X50-117, 2003.

This typology is very exhaustive, and remains the benchmark for the professionals of project management. Several researchers have proposed risk classes to help guide the project manager and facilitate the collection of risk data incurred. In particular those of Courtot (1998) and Desroches (2003) are retained. The first one distinguishes two risk areas: organizational and human risks and risks related to project management, which are divided into 36 categories as shown in the table below.

TABLE 1: Typology of Project Risks According to Courtot (1998)

Organizational and human risks	Related to project structure	Related to principales structures		
		Related to the choice of project structure		
	Decisional risks	Related to managers behavior compared to actors		
		Related to decision making process		
	Hierarchical risks	Related to the role and activities of head office		
		Related to hierarchical relationships between actors		
	Risks related to the definition of roles and responsibilities	Related to the definition of roles		
		Related to the delegation and shared responsibility		
	Risks related to communication and information exchange	Related to behaviors of project actors		
		Related communication mechanism in place and the quality of information exchanged		
	Risks related to the capitalization and transfer of know-how	Related to capitalization		
		Related to the accessibility of expertise		
		related to the transmission of know-how		
	Conflict risks	Sources of conflict in the project		
		Evolution of sources of conflict in time		
		Evolution of sources of conflict during the project phases		
	Risks associated with management of project actors	Related to selection and recruitment of actors		
		Related to the measurement of the collective and individual performance		
		Related to training, skills management and mobilization of project actors		
		Related to the management of the project actors careers, their mobility and reconversion at the end of project		
Risks related to project management	Risks involved in project development phase	Related to the definition of work involved	Internal risks	Imprecision of tasks
				Ambiguities in objectives and priority level
				Project Inconsistency
				Technical and Technological
			External risks	policies
				commercial obsolescence
				On regulatory specifications
				Relations with partners
		Related to resources use	Definition of required resources	Regulations on resources
				Poor definition of resources
			Availability of required resources	Poor definition of the estimated production potential
				Poor management of resource use conflicts
	Risks involved in project implementation	Related to instrumentation		
		Related to late detection of problems		
		Erroneous or partial diagnosis		
		inappropriate responses		

Desroches meanwhile classifies risks into eight areas as follows:

- Development strategy
- Expression of needs and specification,
- Project organization,
- Contractual interfaces,
- Project management,
- Costs and delays,
- Technical and operational performance,
- Users and exploitation sites.

These generic checklists while very useful do not cover all risks specific to a given project.
In addition, some authors have tried to synthesize the different categories of risks the company faces. We cite particularly Pinto (2007, p. 223), who groups the risks into five categories: financial risks, technical risks, business risks, risks of execution, contractual and legal risks.

3. Risk Mapping

A risk map is a data visualization tool for communicating specific risks an organization faces.

The goal of a risk map is to improve an organization's understanding of its risk profile and appetite, clarify thinking on the nature and impact of risks, and improve the organization's risk assessment model. A risk map is often presented as a matrix. The likelihood a risk will occur may be plotted on the Y-axis while the impact of the same risk is plotted on the X-axis.

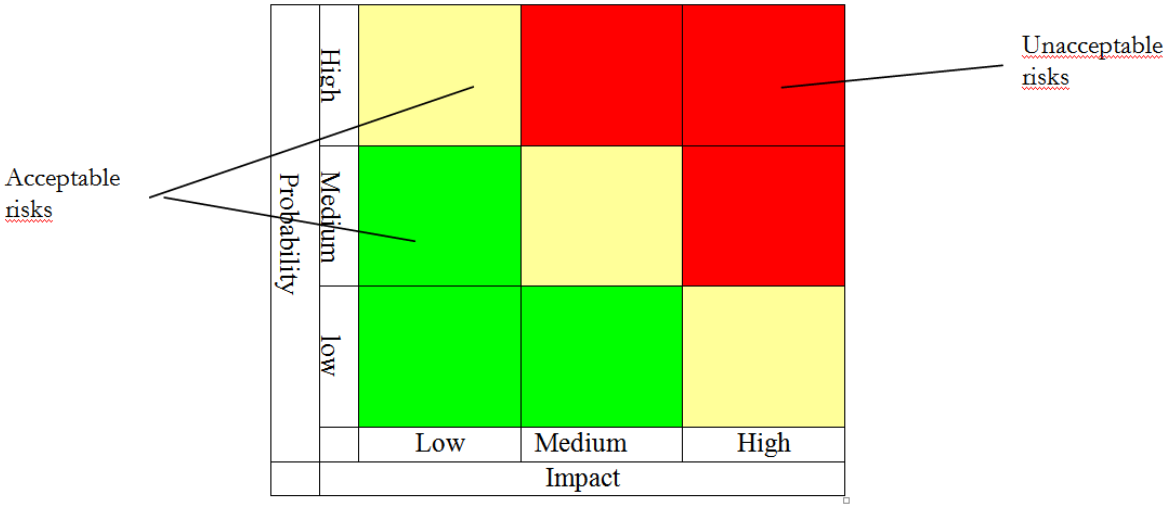

Figure 2: Example of a Risk Map

Events identified as potentially impeding the achievement of objectives are deemed to be risks and should be evaluated based on the likelihood of occurrence and the significance of their impact on the objectives. It is important to first evaluate such risks on an inherent basis-that is, without consideration of existing risk responses and control activities.

For example, an organization with headquarters on the banks of a river may seek to assess its exposure to the risk of flooding. On an inherent basis, it would consider the likelihood and impact of a flood by considering external data (such as the historical and projected frequency of floods) and internal data (such as the estimated damage to its physical assets if a flood were to occur). An impact and probability rating should then be assigned using defined risk rating scales.

These individual risk ratings should then be brought together in the form of an inherent risk map (see Fig. 2), which enables an analysis of risks not only on an individual level (e.g., high, medium, low) but also in relation to one another (e.g., a concentration of certain risks that potentially creates a greater overall risk exposure-for example, reputational damage-than the sum of the individual risk exposures). Additionally, as risk assessments are refreshed over time, a risk map can allow analysis over time (e.g., upward or downward trend of risks, and extent of positive or negative correlations between certain risks).

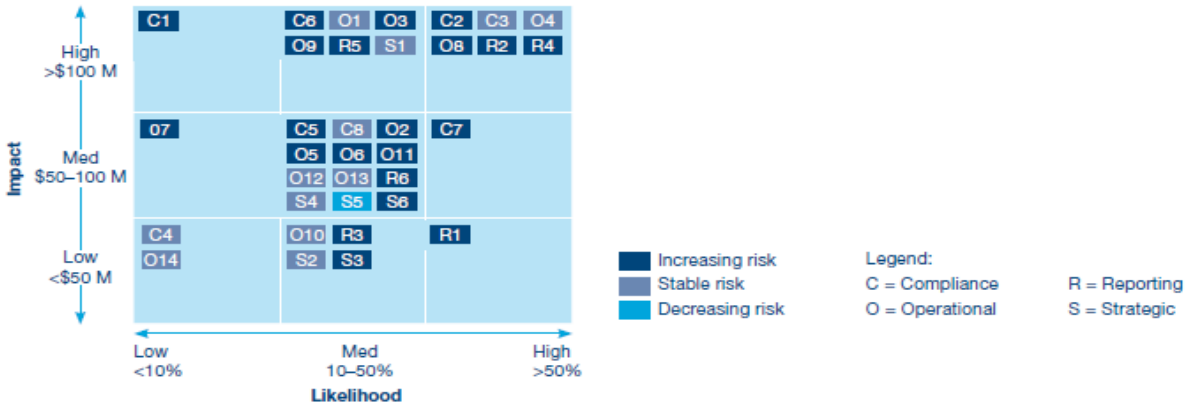

Figure 3: Risk Map[2]

TABLE 2: Risk categories

Categories	Description	Categories	Description

[2] *A practical guide to risk assessment*, Price Waterhouse Coopers, December 2008.

[C1] Compliance	Non-compliance with laws, regulations, or policies	[O10] Security	Security breaches at company sites
[C2] Ethics and integrity	Fraudulent, illegal, or unethical acts	[O11] Sourcing	Lack of access to key raw Materials, failure of supplier
[C3] Intellectual property	Inability to enforce patents and trademark, infringement	[O12] Supply chain	Failure of transportation and logistics network
[C4] Legal and disputes	Changing laws, liabilities, and commercial disputes	[O13] Technology	Development of new, potentially disruptive technologies
[C5] Product quality	Producing off-spec products	[O14] Weather	Prolonged, adverse weather conditions
[C6] Product safety	Unsafe products	[R1] Commodity	Variability and increasing trends in commodity prices
[C7] Regulatory Changing	regulations threaten competitive position	[R2] Credit	Failure of customers or counterparties to perform
[C8] Tax	Failure to adequately support tax positions	[R3] FX	Volatility in foreign exchange rates
[O1] Catastrophic loss	Major natural or manmade Disaster, terrorism	[R4] Interest rate	Variability in interest rates
[O2] Customer	Failure to follow customer preferences/needs	[R5] Investment	Financial market volatility impacts investments
[O3] Efficiency	Inefficient operations	[R6] Process design and execution	Failure in the design and execution of key management processes
[O4] Engineering	Inability to design and manage facilities projects	[S1] Alliance	Inefficient or ineffective alliance, joint venture, affiliation
[O5] Environmental	Environmental incidents or exceedances	[S2] Capital	adequacy Lack of access to capital or liquidity
[O6] Equipment	Plant equipment failure	[S3] Competitive	Actions of competitors or new market entrants
[O7] Health and safety	Health and safety incidents harm employees	[S4] Industry	Industry changes threaten industry attractiveness
[O8] IT	Failure of IT systems, cyber attack	[S5] Macroeconomic	Changes in broad economic conditions
[O9] People	Lack or loss of qualified employees	[S6] Political	Adverse actions by foreign governments

IV. CONCLUSION

The risk assessment process forms the cornerstone of an effective program to protect continuously firms. When assessments are performed systematically and consistently throughout the organization, management is empowered to focus its attention on the most significant risks and make more informed risk decisions. Organizations gain the ability to prioritize the deployment of capital and measurement of relative performance across various objectives or entities, potentially reducing the occurrence and significance of negative events, and their associated losses. Through risk mapping, organizations can better coordinate multiple risk responses, effectively addressing risks that threaten multiple business areas or functions.

REFERENCES

[1] AFITEP, "*Management de projet : principes et pratique"*, Editions AFNOR, Paris, 1998, 278 p.
[2] AFNOR, *Norme FD X50-117 : Management de projet, gestion du risque, management des risques d'un projet*, Editions AFNOR, 2003, 38 p.
[3] J.P. Belicar, "Contribution à une méthodologie d'approche risque pour les projets internationaux", *Actes de la 10ème convention Nationale du Management de projet*, 1994, p 305-317.
[4] C. Braesch , A. Haurat, "*Systemic entreprise modelling"*, Editions Hermès, Paris, 1995, 288 p.
[5] C. Chapman, S. Ward, "*Project risk management: processes, techniques and insight*", Editions Chichester, UK, 2003, 389 p.
[6] H. Courtot, "*La gestion des risques dans les projets*", Editions : Economica Gestion, 1998, 295 p.
[7] D.F. Copper, C.B. Chapman, "*Risk analysis for large projects: model, methods and cases*", Editions Chichester, New-York, 1987, 260 p.
[8] A. Desroches, "*La gestion des risques : principes et pratiques*", Editions Hermès Science Publication, Paris, 286 p.

[9] R. Gautier, "*Qualité et innovation : De la nécessité de maîtriser les risques dans les projets de Conception de Produits Nouveaux*", Mémoire d'HDR, UTC, 2004, 203 p.
[10] V. Giard, "*Project Management*", Editions Economica, Paris, 1991, 174 p.
[11] G. Heal, H. Kunreuther H., "Modeling interdependent risks", *Risk Analysis, 27*(3), 2007, p 621-634.
[12] E. Henley, H. Kumamoto, "*Probabilistic risk assessment"*, IEEE Press, New York, 1992.
[13] J. Klein, R. Cork, "An approach to technical risk assessment", *International Journal of Project Management, 16*, 1998, p 345-35.
[14] CH. Lazslo, "*Economie du Chaos : comment gérer la transformation permanente des entreprises dans des environnements complexes et instables"*, Editions d'organisation, 1998, 195 p.
[15] E. Morin, "*Introduction à la pensée complexe"*, Editions ESF, Paris, 1990, 158 p.
[16] B. Munier, "Revoir les pratiques de gestion des risques industriels - In : Conference «*maîtrise des risques d'un projet* », Association des ingénieurs Arts et Métiers, Paris, 2003, 12 p.
[17] P. Navier, "Processus de maîtrise des risques dans le cadre d'un projet", In Conference « *maîtrise des risques d'un projet* », Association des ingénieurs Arts et Métiers, Paris, 2003, 20 p.
[18] J.K Pinto, "*Project Management: Achieving Competitive Advantage*", Editions Pearson, 2007, 490 p.
[19] L.A. Vidal, F. Marle, J-C Bocquet, "Measuring project complexity using the analytic hierarchy process", *International Journal of Project Management, 29*(6), 2011, 718-727.
[20] A. Yatchinovsky, "*L'approche systémique : pour gérer l'incertitude et la complexité*", Editions ESF, Paris, 1999, 168 p.

American Journal of Engineering Research (AJER) 2016
American Journal of Engineering Research (AJER)
e-ISSN: 2320-0847 p-ISSN : 2320-0936
Volume-5, Issue-1, pp-125-136
www.ajer.org
Research Paper Open Access

An Exponent-Based Propagation Path Loss Model for Wireless System Networks at Vehicular Speed

Anyanwu Chinedu[1], Okoye Arinze Christian[2]
[1, 2] *(Department of Electrical and Electronic Engineering, Federal University of Technology Owerri, Imo State, Nigeria)*

ABSTRACT*: This work investigated and developed an exponent-based path loss model on the level of signal loss experienced on the Airtel Third Generation network within the Port-Harcourt city of Rivers State, Nigeria at vehicular speed. This was deduced by carrying out a drive test within the area, using Transmission Evaluation and monitoring system installed mobile phone, laptop, and Global Positioning System. From the data collected, a path loss model that best describe the signal loss within the area was developed via a path loss exponent for the Airtel Port-Harcourt Third Generation network. It is recommended that Airtel Communication Company should replace their directional Base Transceiver Station Antennas with a bi-sector high gain antenna that will ensure wider and Omni-directional signal coverage within the area.*

Keywords – *exponent, model, network, path loss, signal, wireless system*

I. INTRODUCTION

The era of modern wireless communication begun in the 1980's and is divided into generations. First Generation (1G) wireless communication systems could only transmit voice calls and a limited size of data, and had no roaming capability. The Second Generation (2G) systems came on board when the roaming capability was integrated into wireless communication. 2G has a high data carrying capacity compared to 1G. The emergence of cellular systems marked the beginning of the Third Generation (3G) systems which is also called International Mobile Telecommunication – 2000 (IMT-2000). 3G systems offer better voice quality, global roaming, as well as high data rate service. The Fourth Generation (4G) system is now being developed as an Internet Protocol (IP) based wireless mobile network which offers broadband data communication that is capable of transmitting voice, video, and data.

The challenges of 1G and 2G technologies were resolved when Airtel Communication Company deployed its 3G network in the city of Port-Harcourt, Rivers State, Nigeria. The 3G network carries the promise of ubiquitous broadband wireless access enabling real-time and multimedia applications [1]. Though the capacity of this network created a new ground for public surveillance, however, this technology is not without its peculiar challenges. At vehicular speed, its data rate does decrease sharply with speed for mobile applications thereby resulting to service degradation while traversing the streets in Port-Harcourt city. This challenge/drawback is traced to be as a result of multipath propagation, Doppler spread, among other factors.

This research intends to carry out a thorough investigation on the level of signal loss experienced on the Airtel 3G networks within the Port-Harcourt city by carrying out a drive test within the area. The research is expected to deduce a path loss exponent for the Airtel Port-Harcourt 3G network; compute the standard deviation that exists between the measured path losses and the predicted path losses; develop a path loss model that best describe the signal loss; compare the proposed model with the Okumura-Hata standard model, and then offer solution on how to minimize the service degradation in the Airtel 3G networks in Port-Harcourt city.

This study will be limited to the use of drive test to determine the signal loss in the AIRTEL Port-Harcourt 3G network. It will employ the use of Transmission Evaluation and Monitoring System (TEMS) software, Actix software, including the MatLab software in carrying out the analysis.

II. RELATED WORKS

2.1 Hata model

The Hata path loss prediction model is preferred since it is convenient for frequency range of 150-15000 MHz and for distance range of 1km - 20km. it demands that the base station antenna height be 30m and above while the receiving station antenna height will be 3m and above. Hata prediction model also gives room for correction factors addition.[2]
Hata model is a set of equation which is acquired from taken measurements and extrapolations acquired from curves that are developed by Okumura. [3]

The three categories of Hata prediction models, according to [4], are as enlisted below:

- Open or rural Hata pathloss,
- Suburban Hata pathloss and
- Urban Hata pathloss.

2.1.1 Rural Hata path loss

$$PL = PLUrban - 4.78(\log_{10}(f)^2) + 18.33\log_{10}(f) - 40.98 \quad (2.1)$$

Where;

For the above three categories, the correction factor for the Mobile station antenna is given thus:

$$a(hm) = 1.11\log_{10}(f) - 0.7)h_m - (1.56\log_{10}(f) - 0.8)dB \quad (2.2)$$

f is the frequency (MHz)

h_m is the height of the mobile antenna in meters

h_b is the height of the base station antenna in meters

2.1.2 Urban Hata path loss

$$PL = 69.55 + 26.16\log_{10}(f) - 13.82\log_{10}(hb) + (44.9 - 6.55\log_{10}(hb))\log_{10}(d) + s\text{-}a(hm) \quad (2.3)$$

2.1.3 Surban Hata path loss

$$PL = PLUrban - 2((\log_{10}f/28))^2 - 5.4 \quad (2.4)$$

III. DERIVATION OF THE PROPOSED MODEL

The apparatus that were used to carry out the drive test in the course of this research work include the following:

i. Laptop with an installed Transmission Evaluation and Monitoring System (TEMS) software
ii. Global positioning System (GPS)
iii. Mobile Phone with an installed TEMS software
iv. Power supply from external battery source
v. Car for mobility

The interconnections made among these materials are represented in Fig. 3.1

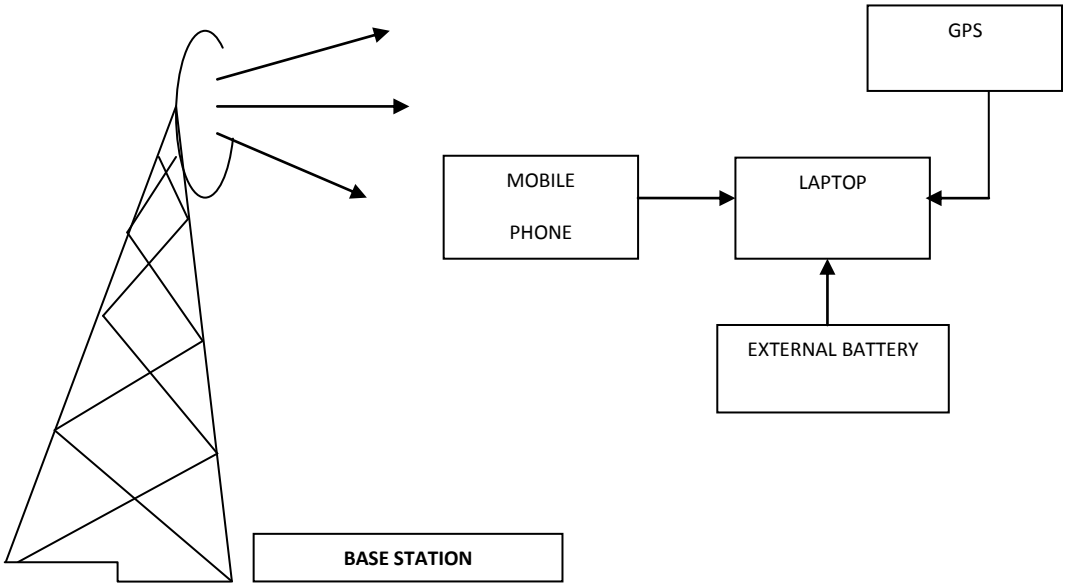

Figure 3.1: Block diagram showing the interconnections of materials used for the Drive test.

The above block diagram simplifies the essential connections made with required materials before the drive test was commenced. The service was provided by the Airtel 3G networks operating at a frequency range of 10,712MHz and 10,737MHz. The transmitter power is at the range of 20W and 30W, and was mounted on steel tower of about 30m above ground level.

An Airtel SIM card was inserted into the mobile phone installed with TEMS software, and the mobile phone is then connected to the Laptop mentioned above through a USB cord. The GPS is connected to the laptop through another USB cord and then placed firmly on top of the car. An external battery source provided an extra power source to the laptop in order to ensure continuous and constant power supply throughout the drive test.

This drive test was carried out in three sites in port-Harcourt city which altogether is about 1500m in distance. On the start of each phase, the laptop is initiated to commence readings on the site by the click of the cursor on the 'Record' button which is located at the start tab button. At this point, the radio Propagation Simulator (TEMS Phone) initiates and terminates short calls (about 15 seconds each), the GPS points coordinates (latitude and longitudes) of the environment, while the laptop records the Received Signal Strength (RSS) and displays the log video on the screen. The Average Received Signal Level along the measured routes are represented in Table 3.1

Table 3.1: Average Received Signal Level along the measured routes

Distance(km)	Average RSL (dBm)
0.10	-59
0.20	-67
0.30	-75
0.40	-71
0.50	-70
0.60	-70
0.70	-72
0.80	-85
0.90	-72
1.00	-76
1.10	-86
1.20	-71
1.30	-84
1.40	-83
1.50	-84

Table 3.1 stands for the Average Received Signal Level at various distances. From the table, the closest distance at which the signals were received is 100m. In other to calculate the average power received at this closest distance (100m), the conventional formular in (3.1) is used as shown below:

$$\text{Power Received, } P_r\ (RSS_{av}) \text{ in dBm} = 10\log P_r = -59\text{dBm} \quad (3.1)$$

$$P_r = 10^{-5.9} = 1.26X10^{-6}\text{dB}$$

The Transmitter power P_t is 30w. Thus:

$$P_t = 30\text{w} = 14.77\text{dB}$$

Using (3.2) below, the measured path loss across the Port-Harcourt city could easily be obtained thus:

$$P_m(d0) = 10\log\left(\frac{p_t}{p_r}\right) \quad (3.2)$$

Where;

P_m is the measured path loss

$P_t$is the transmitter power

P_r is the received signal strength [5]

Hence;

at d1 ,

$$P_m(d1) = 10\log\left(\frac{14.77}{1.26X10^{-6}}\right) = 70\text{dB}$$

at d2,

$$P_r = 10^{-6.7} = 2.0 \times 10^{-7}\text{dB}$$

$$P_m(d2) = 10\log\left(\frac{14.77}{2.0 \times 10^{-7}}\right) = 79\text{dB}$$

at d3,

$$Pr = 10^{-7.5} = 3.16 \times 10^{-8}\text{dB}$$

$$P_m(d3) = 10\log\left(\frac{14.77}{3.16 \times 10^{-8}}\right) = 87\text{dB}$$

at d4,

$$Pr = 10^{-7.1} = 7.9 \times 10^{-8}\text{dB}$$

$$P_m(d4) = 10\log\left(\frac{14.77}{7.9 \times 10^{-8}}\right) = 83\text{dB}$$

at d5,

$$Pr = 10^{-7} = 1.0 \times 10^{-7}\text{dB}$$

$$P_m(d5) = 10\log\left(\frac{14.77}{1.0 \times 10^{-7}}\right) = 82.dB$$

at d6,

$$Pr = 10^{-7} = 1.0 \times 10^{-7}dB$$

$$P_m(d6) = 10\log\left(\frac{14.77}{1.0 \times 10^{-7}}\right) = 82dB$$

at d7,

$$Pr = 10^{-7.2} = 6.31 \times 10^{-8}dB$$

$$P_m(d7) = 10\log\left(\frac{14.77}{6.31 \times 10^{-8}}\right) = 84dB$$

at d8,

$$Pr = 10^{-8.5} = 3.16 \times 10^{-9}dB$$

$$P_m(d8) = 10\log\left(\frac{14.77}{3.16 \times 10^{-9}}\right) = 97dB$$

at d9,

$$Pr = 10^{-7.2} = 6.31 \times 10^{-8}dB$$

$$P_m(d9) = 10\log\left(\frac{14.77}{6.31 \times 10^{-8}}\right) = 84dB$$

at d10

$$Pr = 10^{-7.6} = 2.51 \times 10^{-8}dB$$

$$P_m(d10) = 10\log\left(\frac{14.77}{2.51 \times 10^{-8}}\right) = 88dB$$

at d11,

$$Pr = 10^{-8.6} = 2.51 \times 10^{-9}dB$$

$$P_m(d11) = 10\log\left(\frac{14.77}{2.51 \times 10^{-9}}\right) = 98dB$$

at d12,

$$Pr = 10^{-7.1} = 7.90 \times 10^{-8}dB$$

$$Lp(d12) = 10\log\left(\frac{14.77}{7.90 \times 10^{-8}}\right) = 83dB$$

at d13

$$Pr = 10^{-8.4} = 3.98 \times 10^{-9}dB$$

$$P_m(d13) = 10\log\left(\frac{14.77}{3.98 \times 10^{-9}}\right) = 96dB$$

at d14

$$Pr = 10^{-8.3} = 5.01 \times 10^{-9}\,dB$$

$$P_m(d14) = 10\log\left(\frac{14.77}{5.01 \times 10^{-9}}\right) = 95dB$$

at d15

$$Pr = 10^{-8.4} = 3.98 \times 10^{-9}dB$$

$$P_m(d15) = 10\log\left(\frac{14.77}{3.98 \times 10^{-9}}\right) = 96dB$$

Table 3.2: Average Received Signal Levels and the measured path losses

Distance(km)	Average RSL (dBm)	Measured Path losses, Pm (dB)
0.10	-64	70
0.20	-67	79
0.30	-75	87
0.40	-71	83
0.50	-70	82
0.60	-70	82
0.70	-72	84
0.80	-85	97
0.90	-72	84
1.00	-76	88
1.10	-86	98
1.20	-71	83
1.30	-84	96
1.40	-83	95
1.50	-84	96

In order to generate the proposed model for the Airtel 3G network for the port-Harcourt city, (3.3) is a veritable tool. The model demands the computation of the path loss exponent and the standard deviation as shown:

$$Lp = Lp(d0) + 10nplog\left(\frac{di}{d0}\right) + X\delta \quad (3.3)$$

Where;

$Lp =$ is the proposed path loss

$Lp(do)$ is the path loss at close-in distance, do

$np =$ path loss exponent [6]

It is very vital to determine the predicted path losses along the routes concern. The values of the measured path losses and predicted path losses are essential for computing the path loss exponent along the routes under consideration. The predicted path losses are computed using (3.4):

$$Lp(di) = Lp(d0) + 10nplog\left(\frac{di}{d0}\right) \quad (3.4)$$

Where;

$Lp(di)$ is the predicted path loss at di

for i=1, 2, 3, ...

$Lp(do)$ is the path loss at close-in distance, do

np = path loss exponent [6]

From Table 3.2,

Lp(d0)= 70dB (at close- in distance (do) of 0.10km).

Generating the predicted path losses at various distances;

at $d1 = 0.10km = do$

$$Lp(d1) = 70 + 10nplog\left(\frac{0.10}{0.10}\right) = 70$$

at $d2 = 0.20km$

$$Lp(d2) = 70 + 10nplog\left(\frac{0.20}{0.10}\right) = 70 + 3.0np$$

at $d3 = 0.30km$

$$Lp(d3) = 70 + 10nplog\left(\frac{0.30}{0.10}\right) = 70 + 4.8np$$

at $d4 = 0.40km$

$$Lp(d4) = 70 + 10nplog\left(\frac{0.40}{0.10}\right) = 70 + 6.0np$$

at $d5 = 0.50km$

$$Lp(d5) = 70 + 10nplog\left(\frac{0.50}{0.10}\right) = 70 + 7.0np$$

at $d6 = 0.60km$

$$Lp(d6) = 70 + 10nplog\left(\frac{0.60}{0.10}\right) = 70 + 7.8np$$

at $d7 = 0.70km$

$$Lp(d7) = 70 + 10nplog\left(\frac{0.70}{0.10}\right) = 70 + 8.5np$$

at $d8 = 0.80km$

$$Lp(d8) = 70 + 10nplog\left(\frac{0.80}{0.10}\right) = 70 + 9.0np$$

at $d9 = 0.90km$

$$Lp(d9) = 70 + 10nplog\left(\frac{0.90}{0.10}\right) = 70 + 9.5np$$

at d10 = 1.0km

$$Lp(d10) = 70 + 10nplog\left(\frac{1.0}{0.10}\right) = 70 + 10.0np$$

at d11 = 1.10km

$$Lp(d11) = 70 + 10nplog\left(\frac{1.10}{0.10}\right) = 70 + 10.4np$$

at d12 = 1.20km

$$Lp(d12) = 70 + 10nplog\left(\frac{1.20}{0.10}\right) = 70 + 10.8np$$

at d13 = 1.30km

$$Lp(d13) = 70 + 10nplog\left(\frac{1.30}{0.10}\right) = 70 + 11.1np$$

at d14 = 1.40km

$$Lp(d14) = 70 + 10nplog\left(\frac{1.40}{0.10}\right) = 70 + 11.5np$$

at d15 = 1.15km

$$Lp(15) = 70 + 10nplog\left(\frac{1.50}{0.10}\right) = 70 + 11.8np$$

Table 3.3: Average Received Signal Levels, the measured path losses and predicted Path Losses

Distance (km)	Average RSL (dBm)	Measured Path loss, Pm (dB)	Predicted Path loss Lp (dB)
0.10	-64	70	70
0.20	-67	79	70+3.0np
0.30	-75	87	70+4.8np
0.40	-71	83	70+6.0np
0.50	-70	82	70+7.0np
0.60	-70	82	70+7.8np
0.70	-72	84	70+8.5np
0.80	-85	97	70+9.0np
0.90	-72	84	70+9.5np
1.00	-76	88	70+10.0np
1.10	-86	98	70+10.4np
1.20	-71	83	70+10.8np
1.30	-84	96	70+11.1np
1.40	-83	95	70+11.5np
1.50	-84	96	70+11.8np

Predicted path losses have been computed as represented in Table 3.3. The path loss exponent which shows the relationship between the signal loss in the Airtel 3G Network can now be calculated using (3.4) below:

$$\text{path loss exponent, np} = \sum_{i=1}^{k}\left[P_m(d_i) - L_p(d_0)\right]^2 \quad (3.4)$$

Substituting the values of Table 3.4 into (3.4) accordingly generates (3.5) below:

$$\text{Path loss exponent, np} = 1140.7(np)^2 - 4574np + 5202 \quad (3.5)$$

Differentiating both sides with respect to np:

$$\frac{\partial(np)}{\partial np} = 2[1140.7np] - 4574 = 0$$

$$2281.84np = 4574$$

$$\text{path loss exponent, } np = 2.01$$

According to [3], the value for the standard deviation, δ can be obtained using (3.6) below:

$$\delta = \sqrt{\sum \frac{[(P_m)-(L_p)]^2}{N}} \quad (3.6)$$

$$\delta = \left[\frac{[(P_m)-(L_p)]^2}{N}\right]^{\frac{1}{2}}$$

Where;

δ = Standard deviation

P_m= measured path loss values

L_p= predicted path loss value

N=Number of data points =15

$$\delta = \left[\frac{(1140.7np)^2 - 4574np + 5202)}{15}\right]^{\frac{1}{2}}$$

$$\delta = [76.05(np)^2 - 305np + 346.8]^{\frac{1}{2}}$$

$$\delta = [2]^{\frac{1}{2}}$$

$$\delta = 1.49$$

$$\delta = 1.49\text{dB}$$

Hence, standard deviation δ is computed as being equal to 1.49dB, which approximated to $\delta = 1.5$dB.

Substituting theses values for path loss, np (2.01) and standard deviation, δ (1.5dB) into (3.3); (3.7) is then obtained as shown below:

$$Lp = Lp(d_0) + 20.1 \log\left(\frac{d_i}{d_0}\right) + X\delta \quad (3.7)$$

In other words, the path loss model for the Airtel 3G network in Port-Harcourt city is written as:

$$Lp = 70\text{ dB} + 10 * 2.01 \log\left(\frac{d_i}{d_0}\right) + 1.5\text{ dB} \quad (3.8)$$

$$Lp = 71.5\text{ dB} + 20.1 \log\left(\frac{d_i}{d_0}\right) \quad (3.9)$$

$$Lp = 71.5\text{ dB} + 20.1 \log(D) \quad (3.10)$$

For,

$$D = \frac{d_c}{d_o}$$

IV. SIMULATION RESULTS & DISCUSSION

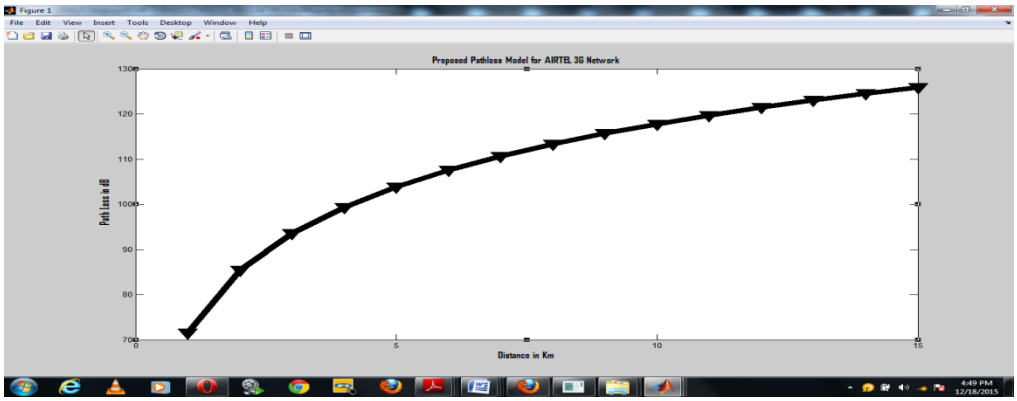

Figure 4.1: The MatLab plot of the Airtel 3G network Model for Port-Harcourt city

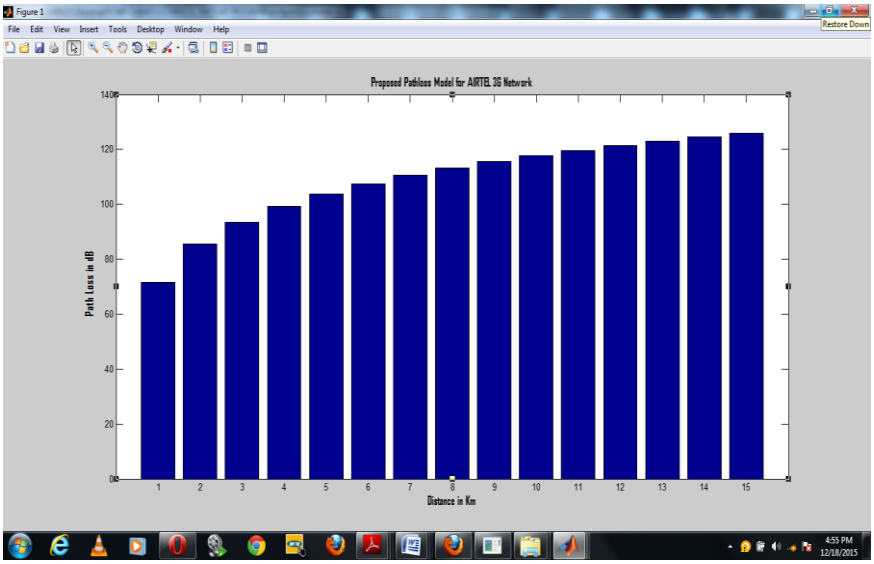

Figure 4.2: The MatLab Bar Plot of the Airtel 3G network Model for Port-Harcourt city

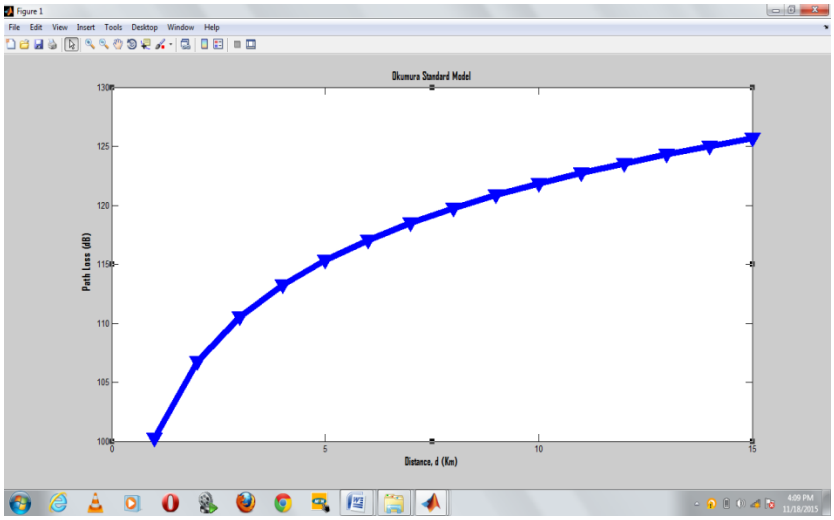

Figure 4.3: The MatLab plot of the Okumura-Hata Standard Model

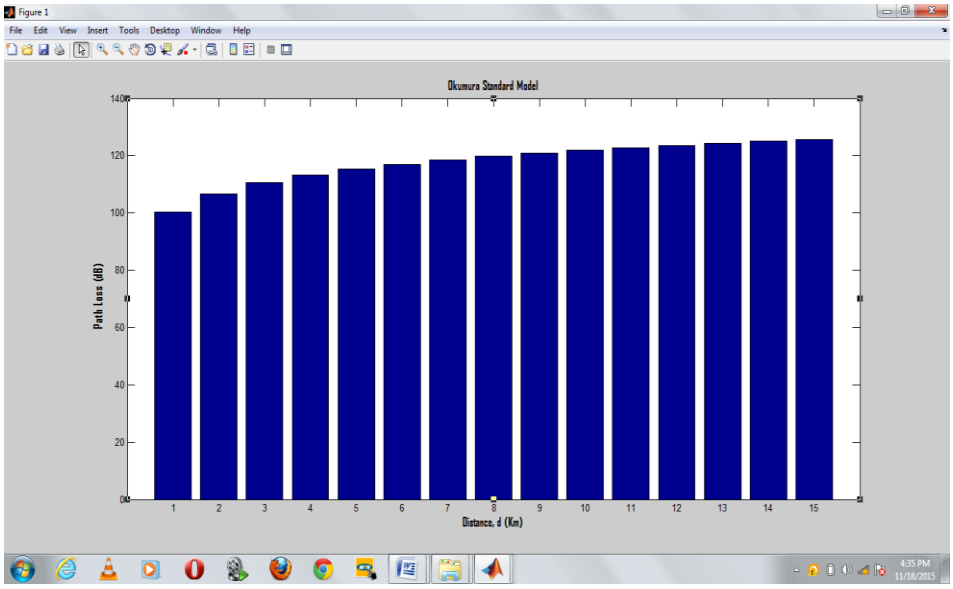

Figure 4.4: The MatLab Bar plot of the Okumura-Hata Standard Model

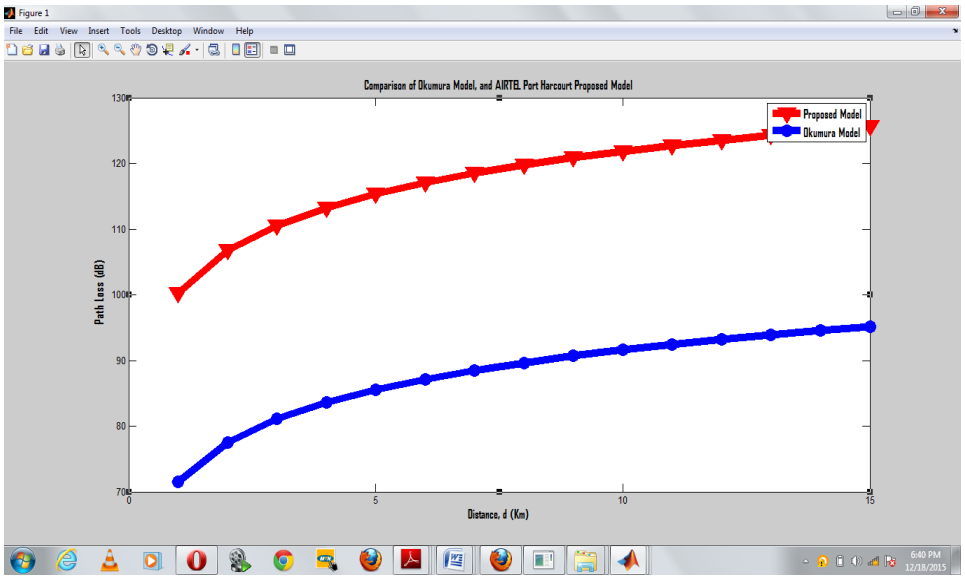

Figure 4.5: The MatLab plot of the Airtel 3G network Model for Port-Harcourt city compared with Okumura-Hata Model

4.1 Discussion

(3.10) is the Airtel 3G network Model for Port-Harcourt city. From the model, it clearly shows that the minimum signal loss experienced in the network at a close-in distance of 100m (0.1Km) is 71.5dB. At further increase of the distance, the signal loss is increased with the factor, $20.1\log(D)$. The MatLab program of this model is plotted in Figs. 4.1 and 4.2. To ascertain the authenticity of this model, it was compared with a standard model called Okumura model, and then plotted in Figs. 4.3 and 4.4. Both models (the AIRTEL 3G network Model for Port-Harcourt city and Okumura-Hata Model) were compared in Fig. 4.5.

The Okumura-Hata model is employed since it is convenient for frequency range of 150-15000 MHz and for distance range of 1km - 20km. [2] It could be seen from the plot that both curves, though are spaced a bit from each other, are similar in the rate at which the signal loss varies with distance of separation of the receiver from the transmitter. In other words, Okumura model could well be deployed to determine this variation rate whereas the proposed model will best describe the path loss at each distance. In order to ensure proper signal coverage and accurate signal handover at a vehicular speed, it is recommended that Airtel Communication Company should replace their directional BTS Antennas with a bi-sector high gain antenna that will ensure wider and Omni-directional signal coverage.

V. CONCLUSION

In this work, a drive test was carried out at a vehicular speed within the Port-Harcourt city using Transmission Evaluation and Monitoring System (TEMS) software installed mobile phone, laptop, and Global Positioning System (GPS). From the data collected, an analysis was carried out. A path loss exponent for the Airtel Port-Harcourt 3G network was deduced; the standard deviation that exists between the measured path losses and the predicted path losses in the Airtel Port-Harcourt 3G network was computed; a path loss model that best describe the signal loss was developed; the proposed model with the Okumura-Hata standard model was compared; and solution on how to minimize the service degradation in the Airtel 3G network was offered.

REFERENCES

[1] Dalela, C. (2012). Propagation path loss Modeling for Deployed WiMAX Network. International Journal of Emerging Technology and Advanced Engineering, vol.2, issue 8.

[2] Ubom, E. A, Idigo, V.E., Azubogu, A.C.O., Ohaneme, c.o., and Alumona, T.L. (2011). International Journal of computer theory and Engineering, vol.3, N03.

[3] Ayyapan, k. and dananyayan, p. (2014). PROPAGATION MODEL FOR HIGHWAY IN MOBILE COMMUNICATIONS JOUNAL, VOL. 3, N04.

[4] Alshami, M.A, Arslan, T., Thompson, J. and Erdogan, A.T.(2011). Frequency Analysis of path loss models on wimax. Computer science and Electronic Engineering conference (CEEC).

[5] Okorogu, V. N. et al., (2013). Empirical Characterization of Propagation Path Loss and Performance Evaluation for Co- Site Urban Environment. International Journal of Computer Applications: Volume 70, No.10.

[6] Nwalozie et al. (2014). PATH LOSS PREDICTION FOR GSM MOBILE NETWORKS FOR URBAN REGION OF ABA, SOUTH-EAST NIGERIA. International Journal of Computer Science and Mobile Computing, Vol.3 Issue.2, February- 2014, pg. 267-281

American Journal of Engineering Research (AJER) 2016
American Journal of Engineering Research (AJER)
e-ISSN: 2320-0847 p-ISSN : 2320-0936
Volume-5, Issue-1, pp-137-143
www.ajer.org
Research Paper Open Access

The Design and Implementation of a Workshop Reservation System

Chintan Shah, Wenbin Luo
(Engineering Department, St. Mary's University of San Antonio, USA)

ABSTRACT: *In this paper, we present the design, implementation, and testing of a workshop reservation system. It was developed for the Academic Technology Department at St. Mary's University to handle workshop registration and history recording of attendance information. After going through strict software engineering processes of specification, design, coding, and testing, we successfully developed the workshop reservation system, as will be shown in the paper. Our subsequent testing indicated that the proposed workshop reservation system met all the requirements set forth by the Academic Technology Department.*
Keywords -*MySQL,PHP, software development, software engineering,web application*

I. INTRODUCTION

The Academic Technology Department (ATS) at St. Mary's University needs a simple, fast, and reliable workshop reservation system to handle workshop registration and history recording of attendance information. The goal of the workshop reservation system is to allow workshop attendees to easily register for workshops, add or modify their sign-ups by selecting or canceling a workshop according to different available time and dates. The proposed workshop reservation system will be used for self-registration online. A well-run workshop needs to have an efficient and reliable way of handling attendance and registration. An automated system reduces the amount of paperwork, time, and effort spent by an attendee on registration. It can also reduce the errors resulted from the manual registration process. The workshop reservation system, therefore, provides benefits to both workshop attendees and workshop organizers.

After several meetings with the management team at ATS, we underwent detailed system analysis, system design, physical design, and application design procedures to design and implement the workshop reservation system [1-3]. A number of use cases were created by analyzing information offered in the requirement document. Detailed use cases were then developed to understand how some of these use cases might operate in more details. Use case diagrams were created to illustrate how these use cases might be utilized by certain actors which serve as the direct means of interaction with the system. Using the detailed use cases as a basis, sequence diagrams were developed to understand how sequential events might occur in the typical success scenario of these use cases. The deployment diagram was created to identify which physical tools and software protocols would be necessary to get the system up and running. Finally, screen flow diagrams were created to sketch out how the system's different interfaces would flow and intercommunicate with one another.

II. SYSTEM FEATURES

Below is a list of features that are currently available in the proposed workshop reservation system,for aregular user and a super administrator, respectively.

List of Features available for a regular user (Student/Staff/Faculty):

- View Workshop Information
- Register
- Login
- Add workshops to the cart
- Edit the cart
- Check attended workshops
- Print attended workshops.

List of Features available for a Super Administrator:

- View Workshop Information
- Register
- Login
- Add workshops to the cart
- Edit the cart
- Check attended workshops
- Print attended workshops
- Add, Edit and Delete workshops to the system
- Add, Edit and Delete schools to the system
- Add, Edit and Delete departments to the system
- Add, Edit and Delete major programs to the system
- Add users to the system from admin side
- Edit and Delete the user from the system
- Assign roles like Super Administrator, Administrator, Dean, and Chair to selected users
- Assign authorities to those particular users to whom the roles were assigned
- Generate Reports

The aforementioned features will be discussed in more details when we present use cases later.

III. FUNCTIONAL AND DATA REQUIREMENTS

The proposed workshop reservation system will be able to process transitions for multiple workshops. Each workshop will be defined by the following:

- Workshop ID (Event ID)
- Workshop Title (Event Title)
- Workshop Description (Event Description)
- Workshop Category (Event Category)
- Workshop Subcategory (Event Subcategory)
- User ID (people registered for workshop)
- Workshop Date and Time
- Workshop Location

The offerings for a workshop will be defined by the following data requirements:

- Workshop ID
- Workshop Title
- Workshop Instructor (Moderator)
- Workshop Description
- Workshop Category
- Workshop Subcategory
- Workshop Start Date and Time
- Workshop Duration
- Workshop Location
- Workshop Access Type (Student/Staff/Faculty)
- Workshop Last Registration Time

The workshop reservation system will track an individual's registration information. The following general registration information will be collected:

- First Name
- Last Name
- User Name (a St. Mary's email address required)
- Password (minimum 6 characters with a combination of alphabets, digits, and special characters)
- Confirm Password

- Mother's Maiden Name (for password reset)
- School (for Student or Faculty)
- Major Program (for Student)
- Department (for faculty)
- Captcha code
-

The workshop reservation system will allow a user to add a workshop to his/her cart, check history, and see workshop details along with other regular activities that a content management system usually offers to its registered users. The following features will be provided to a regular user.

- A user can sign up or login from any computing devices with a standard web browser.
- A user can cancel a workshop that he has recently signed up any time before the workshop starts. Once the workshop starts, the user cannot cancel it.
- As soon as the user signs up the workshop, that event will go to his *recently signed up* tab with the attended flag set to "NO". When an instructor or a Super Administrator marks his attendance, the flag will set to "YES" and the workshop information will be moved from recently signed up to the Past sessions tab.
- A user can print his records from the *past session* tab where the workshops attended by him will be shown.
- A user can edit his profile from the edit profile tab. A user can also change his password by going to the *change password* tab.

A super administrator will be able to do all the functionalities without any restrictions. The following are some of the actions a super administrator can perform:

- A super administrator can Add, Edit and Delete Workshops.
- A super administrator can Add, Edit and Delete the School, the Department, and the Student Major information.
- A super administrator can Add, Edit and Delete the location for a workshop.
- A super administrator can Add, Edit and Delete the existing users as well as new users.
- A super administrator can assign roles, i.e., Super Administrator, Administrator, Dean, Chair, and Director of HR to registered users, if needed.
- A super administrator can assign responsibilities, i.e., Workshop management, School, Department and Program management, and Instructor responsibility.
- A super administrator can generate a report for any workshop.
  A super administrator can mark the attendance for any workshop.

IV. SYSTEM ANALYSIS AND DESIGN

The system analysis of the proposed workshop reservation system involved the formulation of fundamental principles of the system. To properly understand and explicate out these principles, we developed a number of textual and extended use cases. All of these techniques allowed us to better articulate the demands of the system in terms of objects, classes, attributes, relationships, scenarios, and actors. A sample use case for a regular user and a super administrator is shown below.

A sample use case for a regular user (Student/Staff/Faculty):

Use Case Name	Workshop Details
Actor	User
Purpose	To see details about the workshops available.
Overview	A user can see the details regarding the various workshops from any category. The user does not need to register/login with the system for those information.

A sample use case for a super administrator:

Use Case Name	Add/Edit/Delete Workshop
Actor	Super Administrator
Purpose	To allow a super administrator to add, edit, and delete workshops
Overview	A super administrator will have the sole permissions, unless he assigns the responsibility of a super administrator to anybody else, to add, edit and delete workshops from the database.

Regarding the use cases written above, each will serve as a particular scenario or function that will fulfill the need of having a workshop reservation system. A detailed use case provides information such as preconditions, post conditions, description, exception, and frequency. A use case diagram reflects the functions performed by various actors of the system through its many modes of action.

The analysis class diagram brings the information of the use case diagram, the use case description, and extended use cases into consideration by modeling the classes of the system. These classes, though not software components, will influence later software development. The features of the analysis class diagrams are the classes and their cardinality. A sample use case diagram is shown below.

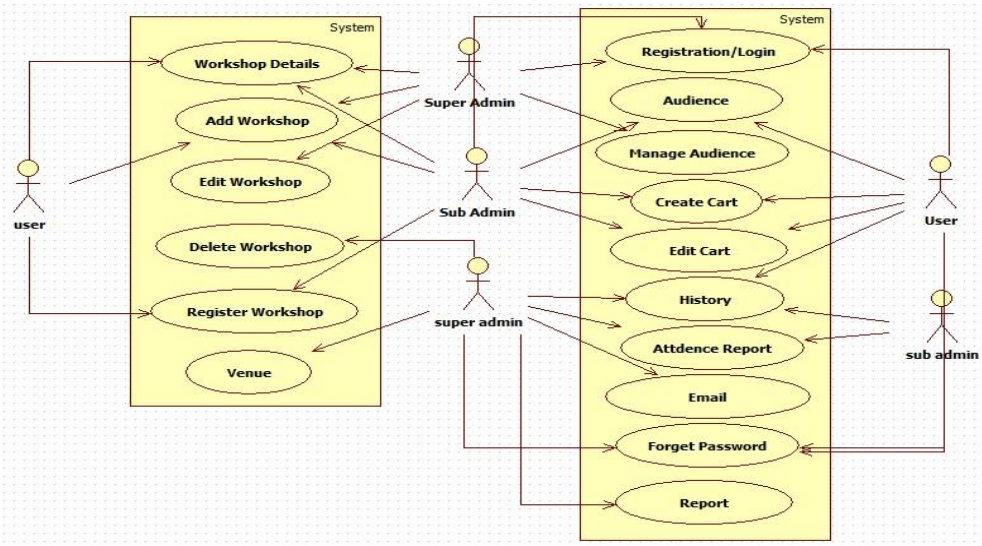

Fig. 1 use case diagram

Sequence diagrams are the interaction diagrams that show how processes operate with one another and in what order. Here, we have displayed four different sequence diagrams. The first sequence diagram is for a regular user. The sequence diagram displays the number of processes a regular user can perform within the system and the order in which a user can conduct those processes.

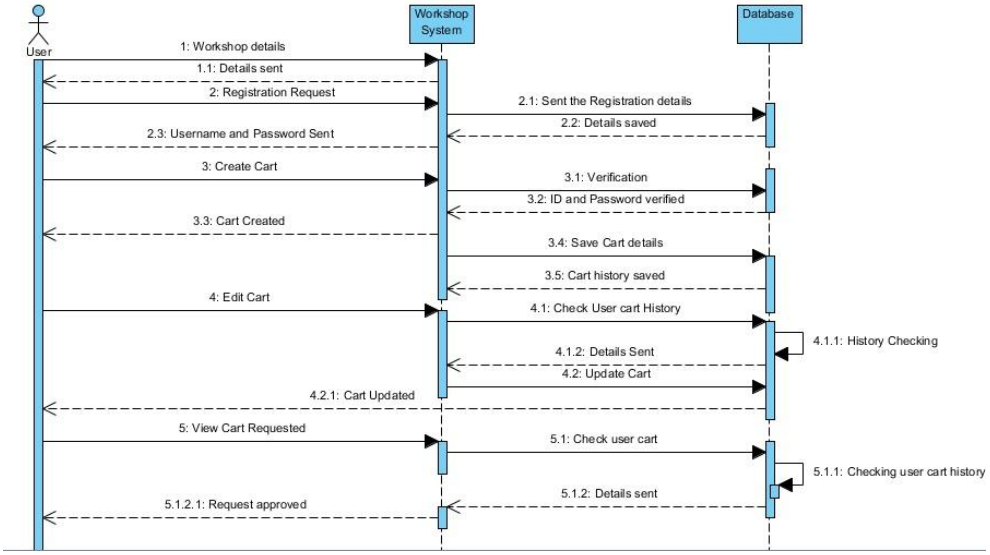

Fig. 2a sequence diagram for a regular user (User/Faculty/Staff)

Similar sequence diagrams were drawn for 1) a super administrator's workshop activity, 2) a super administrator's system activities, and 3) a super administrator's report function activity. The following state diagram shows the decision tree that is followed during the completion of a process from start to finish for a regular user.

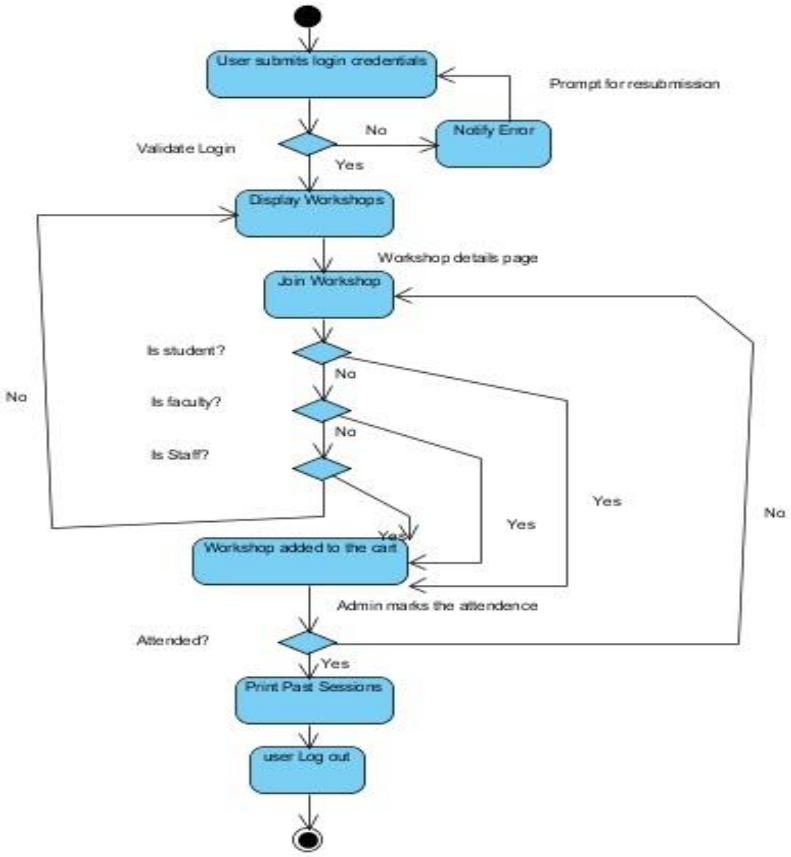

Fig. 3 a state diagram for a regular user

A second state diagram was drawn for a super administrator. A super administrator has the sole rights to conduct all activities, including all functionalities available to a regular user. Notes are provided in the state diagram to clarify the functionalities available to a super administrator.

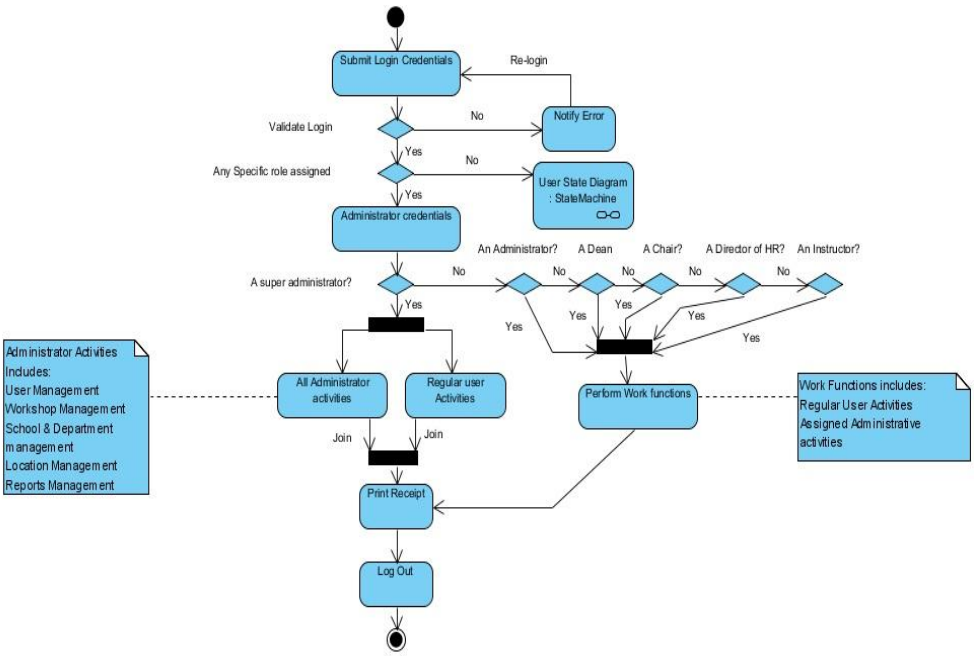

Fig. 4 state diagram for a super administrator

V. PHYSICAL AND APPLICATIONS DESIGN

The deployment diagram shows the overall system and software architecture, The workshop reservation system was designed as a web application, which can be accessed from any standard web browser available on personal computers or mobile devices. The system is hosted by an Apache web server that understands PHP scripting language [4-6] and is connected to a MySQL database.

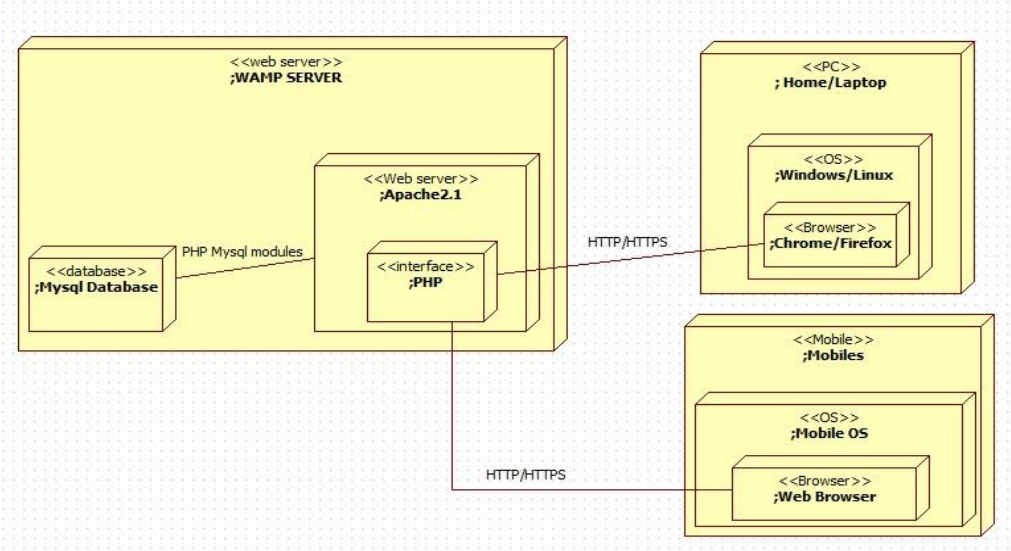

Fig. 5 deployment diagram

A screen flow diagram provides the navigation path between screens based on user actions. The home page is workshop homepage which will display all the workshops available in the system. If a user clicks on any workshop it will take him to the workshop details page. If a user wants to join the workshop, he either creates a new account or logs in using the existing account. As soon as the user logs in, he will again see the workshop home page. From there, he will be able to select the workshops according to his preferred time.

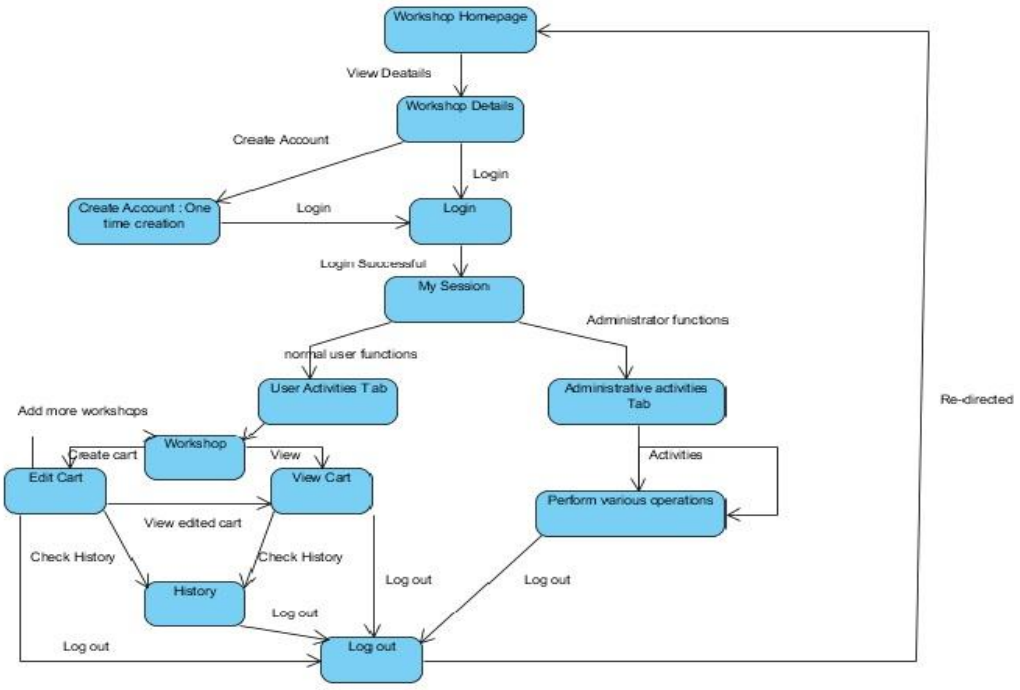

Fig. 6 screen flow diagram for super administrator

VI. CONCLUSION

In this paper, we presented a workshop reservation system that we have successfully designed and implemented for the Academic Technology Department at St. Mary's University. With the workshop reservation system, St. Mary's community can register for the different technological workshops offered by the Academic Technology Department. The workshop reservation system is a dynamic web application. As a result, a super administrator of the workshop reservation system can change its contents at any time.

Solid software engineering principles were utilized in the design and implementation of the proposed workshop reservation system. In addition, we performed extensive testing to validate different functionalities available in the system. Our testing indicated that the aforementioned workshop reservation system met all the requirements proposed by the Academic Technology Department.

REFERENCES

[1] J. Arlow and I. Neustadt,*UML 2 and the Unified Process* (Boston, MA: Addison-Wesley, 2005).
[2] C. Fox, *Introduction to Software Engineering Design*(Boston, MA: Addison-Wesley, 2006).
[3] R. Pressman,*Software Engineering*(New York City, NY: McGraw-Hill, 2005).
[4] *http://www.php.net*
[5] *http://www.phphunt.com*
[6] *http://www.github.com*

APPENDIX

A screenshot of the workshop reservation system:

American Journal of Engineering Research (AJER) 2016
American Journal of Engineering Research (AJER)
e-ISSN: 2320-0847 p-ISSN : 2320-0936
Volume-5, Issue-1, pp-144-149
www.ajer.org
Research Paper Open Access

Frequency Selective Fading in Wireless Communication using Genetic Algorithm

[1]Gbadamosi Luqman and [2]Akanbi Lukman
[1]*Computer Science Department, Lagos State Polytechnic, Lagos State, Nigeria*
[2]*Research Scholar, Embeddedkits Technology, Osun State , Osogbo, Nigeria*

Abstract: *Mobile communications and wireless network have experienced massive growth and commercial success in the recent years. With the prevalence of higher bandwidth application, such as 3G, WiFi, WiMax, UWB and other such technologies, the frequency selective fading issue becomes more important for wireless network simulation. It will be of great interest to implement more functionality support for frequency selective fading using genetic algorithm.*

The methodology implemented involves simulating a GSM carrier frequency and bandwidth, and use pilot data to estimate the channel phase. These are simulated in MATLAB environment using genetic algorithm toolbox. The model was then integrated into image processing, which will give a better environment to simulate a wireless network model. PSK, ASK and QAM modulation models are used to test the effect of different channels to the received data.
The O-MPSK schemes were compared with MPSK scheme in terms of BER for SNR values of 0 to 20 dB. The O-MPSK investigated include $\pi/2$ *-QPSK,* $\pi/4$ *-8PSK,* $\pi/8$ *-16PSK,* $\pi/16$ *-32PSK and* $\pi/32$ *-64PSK. The results reveal that the O-MPSK schemes outperform the MPSK schemes for both MIMO-SM and MIMO-BF as the O-MPSK schemes give relatively lower mean BER compared to the MPSK schemes*

1. Introduction

The goal of an ideal digital wireless communication system is to produce the exact replica of transmitted data at the receiver(Harjot, Bindiya and Amit, 2011). This has necessitated the corresponding numerous tremendous researches carried out in digital communications industry which leads to rapid growth recorded in the past two decades especially in its various applications (Gesse and Oladele, 2010). This growth, in turn, has spawned an increasing need to seek automated methods of analyzing the performance of digital modulation types using the latest mathematical software or programming language. Modulation is the process by which some characteristics, usually the amplitude, frequency or phase of a carrier is varied in accordance with instantaneous value of some other voltage, called the modulating voltage or signal (Carlson, Crilly and Rutledge, 2002). Forms of digital modulation practically in use now include Amplitude Shift Keying (ASK), Frequency Shift Keying (FSK), Phase Shift Keying (PSK) and Quadrature Amplitude Modulation (QAM) with each having their distinctive features and characteristics. In the case of ASK, the use of amplitude modulated analogue carriers to transport digital information always results in a relatively low quality output. Although it is a low cost type of digital modulation, this is seldom used except for a very low speed telemetry circuits. FSK has a poorer error performance than PSK or QAM and consequently is not used regularly for high-performance digital radio systems (Proakis and Salehi, 2002).

The demands for high data rate wireless communication in recent years have continued to increase rapidly for wireless multimedia services. Multiple-input, multiple-output (MIMO) systems are now the popular approaches to meet these demands (Foschini and Gans, 1998). The use of multiple antennas at both transmitter and receiver in wireless communication links provides a means of maximizing the system performance of wireless systems. MIMO technology provides diversity by making the receiver to receive multiple replicas of the same information-bearing signal; and this provides a more reliable signal reception (Gesbert*et al*, 2000).

II. Previous Research

2.1 BER Performance of MPSK and MQAM in 2x2 Almouti MIMO Systems

Mindaudu and Miyim (2012) investigated the error performance of the 2x2 MIMO system using the Almouti (1998) space-time coding with M-PSK and M-QAM modulation schemes of modulation orders M = 4, 8, 16, 32 and 64. The problem of increasing error rates and power consumption is associated with using the MIMO for the provision of high speed multimedia wireless services. The aim of the investigation was to develop a MIMO system that would mitigate error rates and also provide better efficiency in power and bandwidth consumption.. The simulation results show that the scheme with the M-QAM modulation gives better BER performance compared to the M-PSK modulation. The proposed scheme shows good BER performance, but it is limited to only a 2x2 MIMO antenna configuration. Also, the energy needed to achieving a given error probability increases with the modulation order.

2.2 Performance Comparison of MIMO Systems over AWGN and Rician Channels

A dense multipath fading environment stands as a bottleneck to achieving high data rate wireless transmission. Kaur and Kansal (2013) aimed at exploiting the multipath effect of the wireless communications environment for the enhancement of diversity and capacity gains. The method involved utilizing a MIMO-STBC system with zero-forcing (ZF) equalizer and higher order M-PSK modulation schemes; that is M = 32 and above. The system was simulated over a multipath Rician fading channel. Simulation results for 32-PSK, 64-PSK, 128-PSK, 256-PSK and 1024-PSK showed good BER performances due to space diversity provided by the MIMO system. However, the BER increased with increase in the value of *M* for *M*-PSK as a result of decrease in the space between different constellation points, and the energy needed to achieving a given BER increases with the modulation order *M*.

2.3 Bit Error rate Performance of MIMO Spatial Multiplexing with MPSK Modulation

The achievable data rate of the MIMO system with space-time trellis codes (STTC) is limited by the complexity of the ML decoder which grows exponentially with the number of bits per symbol. With a view to reducing the complexity of the ML decoder in a MIMO system, Vishal and Mahesh (2013) investigated the BER performance of MIMO system utilizing a layered space-time coding (LSTC) technique with MPSK modulation schemes and ZF receiver. The system was simulated over the Rayleigh fading channel. Simulation results showed significant improvement in BER for the proposed technique compared to the STTC technique. The BER of the system, however, increases with increasing modulation order.

2.4 Performance Comparison of MIMO-OFDM Transceiver Wireless Communication System

The MIMO system helps to achieve high spectral efficiency, but the system still suffers from the problem of inter-signal interference (ISI) in a frequency-selective mobile communication environment. The aim is to mitigate the problem of ISI in MIMO systems at the same time achieving high spectral efficiency in mobile communication environments. Mangla and Singh (2013) compared the BER performances of higher order M-QAM and M-PSK modulation schemes in a MIMO-OFDM system. The system was simulated for M = 16, 64, 256, 512 and 1024. The results showed that spectral efficiency increases with increasing modulation order M. Also, M-QAM gives better BER performance than M-PSK. The BER of the higher order modulations can be reduced but at the cost of increasing the SNR. Increasing the SNR is however not advisable because excessive power consumption would adversely affect system lifespan.

III. Methodology

3.1 Design of the Offset MPSK Schemes

A modulated signal consists of a combination of the carrier signal and the message (or information) signal. The *M*-ary PSK modulation is achieved by shifting the carrier in phase according to the message data. A modulated signals*(t)* in time (t) domain can be expressed as:

$$s(t) = Re\{\mathbb{g}(t)\exp[j\omega_c t)\} \quad 3.1$$

where $Re\{.\}$ denotes the real component of the complex function indicated by *j*,

$\omega_c = 2\pi f_c$,

f_c = The carrier frequency,

$\mathbb{g}(t)$ = The complex baseband envelope of $s(t)$.

This complex baseband envelope $\mathbb{g}(t)$ is a function of the message signal $m(t)$ and can be expressed as:

$$\mathbb{g}(t) = Am(t)\exp[j\theta(t)] \quad 3.2$$

where*A* is a constant amplitude

and, $\theta(t)$ = The phase of the signal

Substituting equation (3.2) into (3.1) gives:

$$s(t) = Am(t)\cos[\omega_c t + \theta(t)] \quad 3.3$$

Applying trigonometric identity to Equation 3.3, the equation can be expressed in cosine and sine forms as:

$$s(t) = Am(t)[cos\omega_c t cos\theta(t) - sin\omega_c t sin\theta(t)] \quad 3.4$$

The constant amplitude A is a function of the signal power; and it is given as:

$$A = \sqrt{2P} \quad 3.5$$

where$P$ is the signal power. Also, P is a function of the energy contained in a symbol duration; and is given as:

$$P = \frac{E}{T_s} \quad 3.6$$

whereT_s is the symbol period;

E is the energy contained in the symbol period.

Substituting Equation 3.6 into 3.5 gives:

$$A = \sqrt{\frac{2E}{T_s}} \quad 3.7$$

With‘ A ’ into equation 3.4 gives:

$$s(t) = m(t)\sqrt{\frac{2E}{T_s}}[cos\omega_c t cos\theta t - sin\omega_c t sin\theta t] \quad 3.8$$

By shifting the carrier in phase, Equation 3.8 becomes:

$$s(t) = m(t)\sqrt{\frac{2E}{T_s}}[cos\omega_c t cos(\theta_i - \theta_0)t - sin\omega_c t sin(\theta_i - \theta_0)t] \quad 3.9$$

With $\theta_i = \frac{2\pi}{M}i, \quad for\ i = 1,2,3,\dots M$ 3.10

andθ_o is the initial phase given as:

$$\theta_0 = \frac{2\pi}{M} \quad 3.11$$

where$M$ is the constellation size of the M-ary PSK; the phase takes on one of M possible values.

Equation 3.9 represents an M-ary PSK modulated signal. The phases of an MPSK constellation can be represented with a polar diagram in Inphase/Quadrature (I/Q) format. The cosine component of the modulated signal $s(t)$ takes the inphase axis while the sine component takes the quadrature axis.

The offset MPSK (OMPSK) modulation can be implemented by delaying the input bit stream of the quadrature part by one bit period T_b. The bit period is given as:

$$T_b = \frac{T_s}{k} = \frac{T_s}{\log_2 M} \quad 3.12$$

where k is the number of bits that represents a symbol. Therefore, the conventional MPSK modulation Equation 3.9 can be modified for the OMPSK as:

$$s(t) = m(t)\sqrt{\frac{2E}{T_s}}[\cos\omega_c t\cos(\theta_i - \theta_0)t - \sin\omega_c t\sin[(\theta_i - \theta_0)(t - T_b)]] \quad 3.13$$

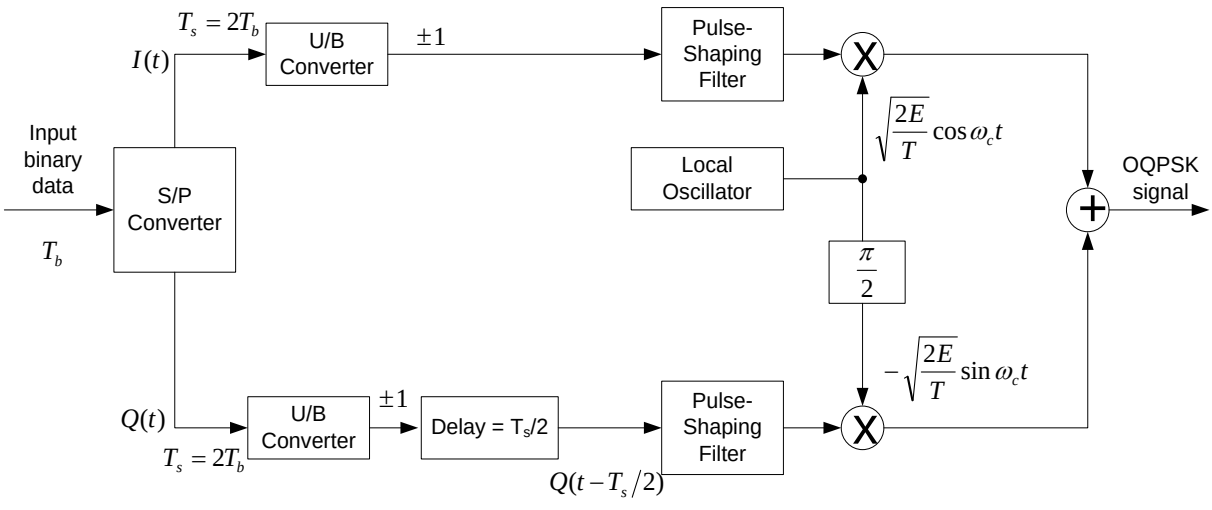

(a)

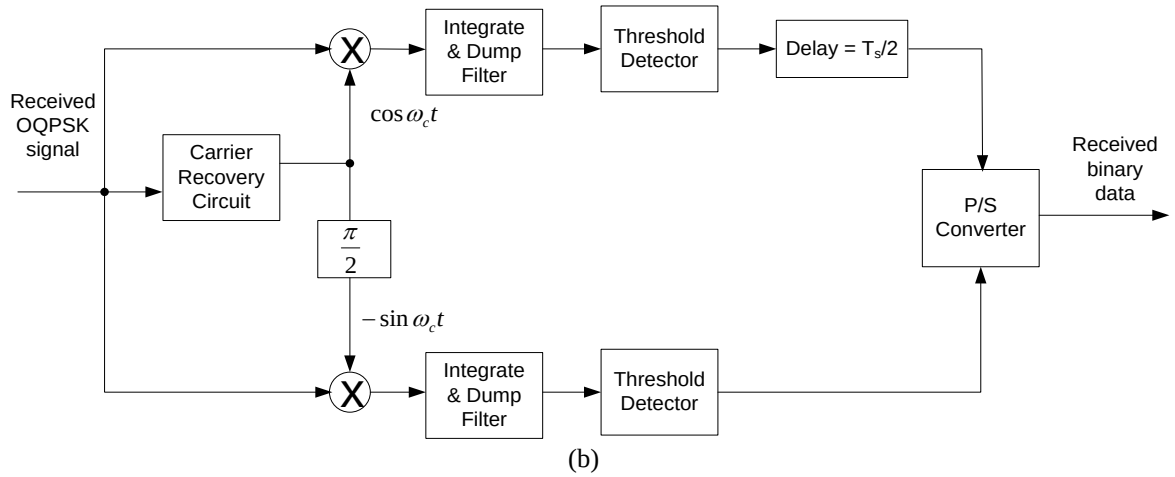

Figure 3.1: Offset QPSK Scheme (a) Modulator (b) Demodulator

IV. Result and Discussions

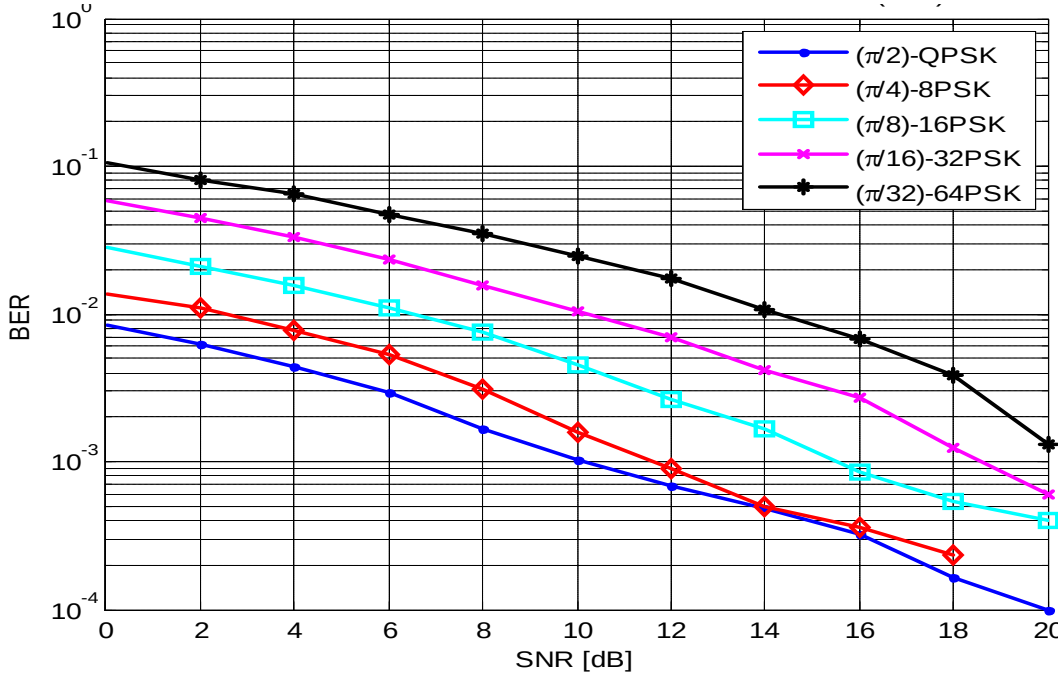

Figure1: Comparison of the O-MPSK in 2x2MIMO-SM over Rayleigh Fading Channel

The mean BER values for $\pi/2$ -QPSK, $\pi/4$ -8PSK, $\pi/8$ -16PSK, $\pi/16$ -32PSK and $\pi/32$ -64PSK in MIMO-BF are 0.0016, 0.0025, 0.0038, 0.0064 and 0.0107 respectively. Also, the mean BER values for $\pi/2$ -QPSK, $\pi/4$ -8PSK, $\pi/8$ -16PSK, $\pi/16$ -32PSK and $\pi/32$ -64PSK in MIMO-SM are 0.0024, 0.0040, 0.0085, 0.0183 and 0.0360 respectively. The results reveal that the best BER performance is obtained with $\pi/2$ -QPSK of MIMO-BF and the worst with $\pi/32$ -64PSK of MIMO-SM.

The comparison between MIMO-SM and MIMO-BF for $\pi/2$ -QPSK is illustrated graphically in Figure 1. The mean BER values obtained for MIMO-SM and MIMO-BF are 0.0024 and 0.0016 respectively; this shows that MIMO-BF gives a lower BER compared to MIMO-SM. Figure 2 shows the comparison between MIMO-SM and MIMO-BF for $\pi/8$ -16PSK. The BER values obtained for MIMO-SM and MIMO-BF are 0.0085 and 0.0038 respectively; this also shows that MIMO-BF gives a lower BER compared to MIMO-SM.

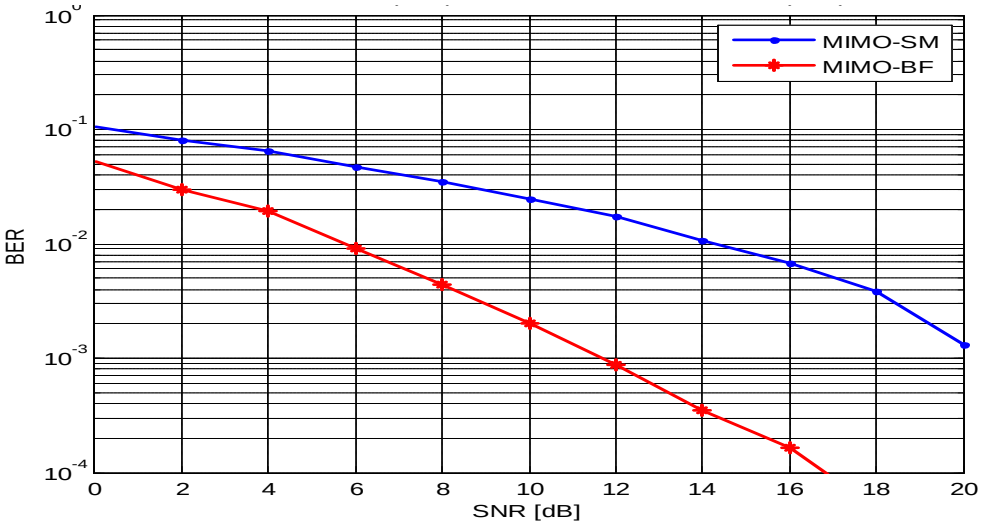

Figure 2: Comparison between 2x2 MIMO-SM and 2x2 MIMO-BF with $\pi/32$ -64PSK

V. Conclusion

In this work, offset MPSK (O-MPSK) modulation schemes in wireless communication using genetic algorithm were developed and the performances evaluated in 2x2 MIMO-SM and 2x2 MIMO-BF communication systems over Rayleigh fading channel. The O-MPSK schemes were compared with MPSK scheme in terms of BER for SNR values of 0 to 20 dB. The O-MPSK investigated include $\pi/2$ -QPSK, $\pi/4$ -8PSK, $\pi/8$ -16PSK, $\pi/16$ -32PSK and $\pi/32$ -64PSK. The results reveal that the O-MPSK schemes outperform the MPSK schemes for both MIMO-SM and MIMO-BF as the O-MPSK schemes give relatively lower mean BER compared to the MPSK schemes. Also, the results reveal that the best performance is obtained with the $\pi/2$ -QPSK scheme.

References

[1] Adeyemo, Z. K. (2009), *Performance Evaluation of Digital Mobile Communication over Fast and Frequency Non Selective Rayleigh Fading Channels*, Unpublished PhD Thesis, LadokeAkintola University of Technology, Ogbomoso, Nigeria.

[2] Adeyemo, Z. K. and Ajayi, O. O. (2011), "Effect of Subcarriers on Orthogonal Frequency Division Multiplexing at Different Mobile Speeds," Journal of Theoretical and Applied Information Technology, vol. 29, no.2, pp 61-68.

[3] Almouti, S. M. (1998), "A Simple Transmit Diversity Technique for Wireless Communications," IEEE Journal on Select Areas in Communications, vol. 16, no.8, pp 1451-1458.

[4] Antti V. R. and Arto L. (2003), "*Radio Engineering for Wireless Communication and Sensor Applications"*, Artech House, Boston, London.

[5] Amin, A. (2011), "Computation of Bit-Error Rate of Coherent and Non-Coherent Detection M-ary PSK with Gray Code in BFWA Systems," International Journal of Advancements in Computing Technology, vol. 3, no.1, pp 27-38.

[6] Asad, M., and Abas, M. (2010),"Characterization and Channel Modelling for Satellite Communication Systems,"Blekinge Institute of Technology, Sweden, pp. 134-151. Retrieved from http://www.intechopen.com/

[7] Bernard S. (1997), ''Rayleigh Fading Channels in Mobile Digital Communication Systems Part 2: Mitigation,'' *IEEE Communications Magazine*.

[8] Cao, L. and Beaulieu, N. (2004), "Bit Error Rate analysis of hybrid selection/ maximal ratio with channel estimation error," IEEE Global Telecommunications Conference, vol.1, pp 446 – 451.

[9] Carlson, A. B., Crilly, P. B and Rutledge, J. C. (2002), "*Communication Systems: An Introduction to Signals and Noise in Electrical Communication"*, 4th edition, McGraw Hill, London.

[10] Dang, X. (2009), *Offset QPSK in SISO and MIMO Environments*, PhD Dissertation, Brigham Young University, Provo, Utah.

[11] Dennis, R. (2001), *Satellite Communications*, 3rd Ed. Tsinghua University Press.

[12] Gaudenzi R. (2002), European Space Agency, American Institute of Aeronautics and Astronautics paper.

[13] Foschini G. J. and Gans M., "On Limits of Wireless Communications in a Fading Environment when using Multiple Antennas," *Wireless Personal Communications,* vol 6, pp 311-335, March 1998

[14] Frenzel L. E. (2008), "*Principles of Electronics Communication Systems"*, 3rd edition, McGraw Hill, London.

[15] Fuqin X. (2006) "Digital Modulation Techniques," 2nd edition, Artech House.

[16] Gesbert D., Bolcskei H., Gore D. and Paulraj A., (2000) "MIMO Wireless channels: Capacity and Performance Prediction," in *Proc. IEEE Globecom*, San Francisco, CA, Nov 2000, pp 1083 - 1088

[17] Gesse, M. K. and Oladele O. P. (2010) "Performance Evaluation of LTE Downlink with MIMO Techniques," M.Tech Thesis, Blekinge Institute of Technology, Karlskrona, Sweden.

[18] Goldsmith A. (2005), *"Wireless Communications"*, Cambridge University Press, Cambridge, United Kingdom

[19] Harjot K., Bindiya J. and Amit V. (2011), "Comparative Performance Analysis of M-ary PSK Modulation Schemes using Simulink" International Journal of electronic & Communication Technology, vol. 2, no. 3, pp 204 – 209.

[20] Ippolito, L.J. (2008), *Satellite Comunications Systems Engineering*, John Wiley and Sons, Ltd.

[21] Jaiswal A. K., Kumar A. and Singh A. P. (2012), "Performance Analysis of MIMO-OFDM System in Rayleigh Fading Channel," International Journal of Scientific and Research Publications, vol. 2, Issue 5, pp 1 – 5.

[22] Kaur N. and Kansal L. (2013), "Performance Comparison of MIMO Systems over AWGN and Rician Channels with Zero Forcing Receivers," International Journal of Wireless and Mobile Networks, vol. 5, no 1, pp 73 – 84.

[23] Kamilo, F. (1983), *Digital Communications: Satellite / Earth Station Engineering*, Prentice-Hall Inc.

[24] Kolimbiris H. (2000), "*Digital Communications Systems"*, Prentice Hall, USA.

[25] Krzysztof, W. (2002), *"Mobile Communication Systems",* West Sussex, England.

[26] Lou F. (2012), "Understanding Modern Digital Modulation Techniques", a tutorial on the most common digital modulation techniques Jan. 23, 2012http://electronicdesign.com/communications/

[27] Mangla R. and Singh M. (2012) "Performance Comparison of MIMO-OFDM Transceiver Wireless Communication System using QAM and QPSK Modulation Schemes," International Journal of Advances in Engineering Science and Technology, vol. 1, no 2, pp 66 – 72.

[28] Mindaudu, A. S. and Miyim, A. M. (2012), "BER Performance of MPSK and MQAM in 2x2 Almouti MIMO Systems," International Journal of Information Sciences & Techniques, vol. 2, no 5, pp 1 – 10.

[29] Nelson, T. and Rice, M. (2006), "Mimo Communications using offset modulations," Proceedings of IEEE International Waveform Diversity and Design Conference, pp 23 – 27.

[30] Pasupathy, S. (2003), ''Minimum shift keying: a spectrally efficient modulation,'' *IEEE Communications Magazine*.

[31] Peppas, K.P.; Nistazakis, and Tombras, G.S. (2011), "An Overview of the Physical Insight and the Various Performance Metrics of Fading Channels in Wireless Communication Systems," Advanced Trends in Wireless Communications. Retrieved from http://www.intechopen.com/

[32] Poongodi, C., Ramya, P. and Shanmugam A. (2010), "BER Analysis of MIMO OFDM System using M-QAM over Rayleigh Fading Channel," International Conference on Communication and Computational Intelligence, Kongu Engineering College, Perundurai, erode, T. N., India, pp. 284-288.

[33] Prasad, K. V. (2003),*Pinciples of Digital Communication Systems and Computer Networks,*Dreamtech Press, 1st Edition, Massachusetts, USA

[34] Proakis, J. G. (2001),*Digital Communications*, McGraw – Hill Companies, inc, International Edition, New York City, USA

[35] Proakis, J. G. and Salehi, M. (2002), *Communication Systems Engineering*, 2nd Ed., Prentice-Hall Inc., USA.

[36] Rappaport, T. S. (2002), *Wireless Communications – Principles and Practice*, 2nd Ed., Prentice-Hall Inc., USA.

[37] Sklar, B. (1997), "Rayleigh Fading Channels in Mobile Digital Communication Systems," IEEE Communications Magazine, July, pp. 90-100.

[38] Sklar, B. (2001), "*Digital Communications: Fundamentals and Applications"*, 2nd edition, Prentice Hall, USA.

[39] Sulyman, A. I. (2008), "Performance of MIMO Systems with Antenna Selection over Nonlinear Fading Channels," IEEE Journal of Selected Areas in Communications, vol. 2, no 2, pp 159 – 170.

[40] Sydaap Technologies Pvt. Ltd. (2010), "Multiple Input Multiple Output (MIMO)" a tutorial on Multiple Input Multiple Output (MIMO) Jan. 7, 2010http://www.sydaap.com/docs/MIMO.pdf

American Journal of Engineering Research (AJER) 2016
American Journal of Engineering Research (AJER)
e-ISSN: 2320-0847 p-ISSN : 2320-0936
Volume-5, Issue-1, pp-150-153
www.ajer.org
Research Paper Open Access

Aeration, Coagulation and Flocculation Processes in Water Treatment plant: Case Study Water Treatment Plant around Maiduguri, Borno State Nigeria.

[1]Hussaini A Abdulkareem, [2]Bitrus Auta and [1]Nuhu Abdullahi
[1]*Department of Mechanical Engineering School of Industrial Engineering College of Engineering Kaduna Polytechnic, Nigeria .*
[2]*Applied Science Department School of Science and Technical Education College of Science and Technology Kaduna Polytechnic, Nigeria*

Abstract: *The paper identify and explain three of the most commonly use processes of enhancing the quality and purity of water treatment namely aeration which is the process that provides oxygen from the atmosphere to effect beneficial changes in the raw water such as taste, odor and colour, coagulation that is the addition of chemical substances to water in order to aid settlement of the dissolved particles, by forming large floc and flocculation which is use of gentle stirring in water, which floc has formed to induce the particles to coalesce and grow into bigger and denser floc particles, for quicker increase of the rate of settlement.*

I. INTRODUCTION

Absolutely pure water is rarely found in existence in nature, and man cannot exist without water, so there has always been a demand for pure portable water. (3) Most waters have to be purified before they can be used for portable purposes. Raw water is so infinitely variable in quality, that there is no fixed starting point to the treatment process, and within much narrower limits, there is any rigidly fixed finishing point either. There is virtually no water that is impossible to purify into potable standards. To slake man's thirst, drinking water must be whole some and palatable. Accordingly it may be free from disease-producing organisms and poisonous or physiological undesirable substances[1].

The source of raw water determines its inherent quality, the quality of which is difficult to foresee, hence there is the need to collect samples of the raw water for a certain period of time and carry out some tests to ascertain the characteristic purities of the raw water and the relative quantity of each impurity. Naturally occurring water can generally be classified as; groundwater, or surface water. Each has its own characteristic, but in general, ground water is the purest form of water available, and may not require much treatment compared to its counterpart (surface water). The associated impurities of surface and ground waters can be classified as shown in table 1.

It is worthwhile to look into, what processes actually take place in these stages, and the components required for the processes. The processes, which take place, are governed by certain scientific theories relating to the behavior of the liquid particles, and the impurities associated, with them in the various purification stages.

This can generally be outlined as; screening; raw-water storage; pre-chlorination; aeration; algal control; straining; preliminary setting; mixing; coagulations; flocculation; settlement, filtration and sterilization. In this presentation we shall only look at aeration, coagulations and flocculation processes.

II. AERATION

This treatment process provides oxygen from the atmosphere to effect beneficial changes in the raw water. At the same time it may liberate undesirable gases such as carbon dioxide, hydrogen. The principle behind this is that of mixing the raw water with normal air from the atmosphere to replenish or add to the raw water quality. This trend generally improves the water taste, odor, and colour and may also affect the killing of some pathogens. This is usually done by splashing the water over trays to break up the stream into countless droplets or by reversing the effect and blowing air bubbles through the water.

Gases are absorbed or liberated front water until equilibrium is reached between the natural content of each gas in there and its content in the water [1].

Aerators are commonly found to be necessary if any of the following conditions are present in the raw water.

(a) Hydrogen sulphide (tests, odor etc.);
(b) Carbon dioxide (corrosive tendencies);
(c) Test due to algal growth (caused by volatile oils release);
(d) Iron and Manganese in solution;
(e) De-aeration
(f) Above increase oxygen content, while (a) – (b) liberate excess gas.

Types of Aeration

1. Fixed – Spray Aerators: - This are specially designed nozzles which direct thin jets of water against metal plates to produce a spray which exposes countless droplets of the water to the atmosphere. Some of the factors considered in the design of this aerator include; orifice or nozzle behavior, including ballistic principles: wind-age or wind effects, shared with spray cooling and pipe friction associated with multiple tank inlets and filter under drains. The resistance offered by calm air can usually be neglected. The time of exposure also governs the distance droplet are carried by the wind [2]. The areas where the sprays are working are often sheltered by louvers set in a surrounding wall.
2. Mechanical Aerators: - There are many kinds of mechanical aerators, but the most commonly used is those which employ the use of submerged paddies that circulate water in aerator chamber and renew its air water interface.
   Surface paddles or brushes that dip lightly into aeration chambers, but far enough to circulate their water release air bubbles and throw spray of droplets onto their water surfaces.
   Propeller blades that whirl at the bottom of a central down draft tube in an aeration chamber and aspirate air into the water.
   Turbine blades that cap a central up draft tube in aeration chamber and spray droplets over its water surface (3).
3. Cascade Aerators:- This depend on the turbulence created in a thin stream of water flowing swiftly down an incline and impinging fixed obstacles the surface area of liquid exposed is rather limited and there is a loss of efficient (1). 25-50% of carbon dioxide may be removed (2)
4. Gravity Aerators: - In this design water is allowed to fall on sheet over one or more concrete steps. Overman (1968) single arrangement with 400mm supply can de-aerate meters per day with 50% - 60% carbon dioxide removal (2).
5. Tray type Aerators: -This consists of about five perforated trays, increasing in size from top to bottom. Then waterfalls from tray through a total depth of 2-3m and splashes on through and off the trays 5-6 times. The total area of the trays in relation to the flow is generally about $0.2m^2$ per m^3/h. This type of aerator is apt to freeze in cold weather and to encourage the growth of algae and other life in warmer climates. However it is a simple and cheap method used much more widely than any of the others.
   The trays may be filled with layers of coke or gravel and this loss found to improve its carbon dioxide removal to 30%- 60%.

III. COAGULATION

Coagulation can be said to be the addition of chemical substances to water in order to aid settlement of the dissolved particles, by forming large floc. (Gelatinous precipitates). There are many substances which react suitably with water to produce such an effect and these are known collectively as coagulants, examples of these are A12 (SO4)3.18 H2O, known as alum (Aluminum sulphate), ferrous sulphate or FeSO4.7H2O sodium Aluminates etc. [l]. Use of additional chemicals, which while not themselves true coagulants, intensify and improve floc formation otherwise called coagulant aids. Coagulants should be added immediately downstream of any re-setting basin which may have been considered necessary. Their primary purpose is to assist in the removal of the more finely divided sediment and colloids. Most of the larger and heavier particles settle unaided in the pre-settling basin thus permitting the coagulants to work more efficiently on the finer particles [1].

Where floc formation is poor, or for reasons of overall economy, coagulant aids may be added. By producing a heavier faster-setting floc, this allows small basins to be used, and smaller doses of the main coagulants may also be possible. The choice of the best coagulant for any particular water is determined by experiment [1].

Immediately coagulants are introduced into the water, rapid mixing is essential. Floc starts to form and immediately after this, the water is stirred very gently for the fine particles adhere to each other and grow into settle-able floc. This gentle stirring action occurs to some degree naturally in all basins but can be greatly accentuated by methods designed to encourage the rolling action required. [1]

Certain designs of basins are multi-chambered and therefore flocculation does not infact proceed more separately than might appear to be the case at first glance. The pH of water is very vital in coagulation because, it indicates the right type of coagulant and dosage required to form the heaviest floc at the waters characteristic pH value, which can also be determined using the jar test. Acid waters i.e. those having a pH of 5-6.5 are often difficult to clarify, due to the high dosage of coagulants and alkalis required. Waters of pH between 6.2 - 7 with a reasonable degree of alkalinity reacts well with aluminum sulphate. Alkaline waters with PH values of 7 - 7.8 may again be difficult and absorb high doses of alum. [1]

Coagulants can be added to the water either as a solution, which is the commonest way or in powder or slurry form. As treatment is a continuous process, dosing must also proceed in continuous and controlled fashion. The types of feed of coagulants can generally be classified as solution feeds and dry feeders. The two essential parts of solution feed system comprise a tank in which a solution of the correct strength may be stored and closing rate or flow controller. The tank should hold 24 hours supply and be duplicated so that one tank may be in service while the other is being replenished. There should be some sort of continues stirring mechanism to reduce the risk of settlement after initial preparation. Many coagulants (particularly ferric chloride and alum) are corrosive and the tanks should be lined with acid resisting material, commonly rubber, glass or special cement.
The dosing mechanism should be capable of being controlled manually. There are two kinds of dosers: gravity-feed, and displacement pumps or tippers. The rate of flow can be altered in the former by altering the length of piston stroke of the specially made plunger pumps. The speed at which tippers operate can also be regulated. In big works of sophisticated design, dosing is automatically controlled. A dry feeder incorporates a hopper which contains the feeds measuring device; this often takes the form of a revolving table from which a scraper of adjustable length deflects a greater or lesser amount of powder into the raw water. If the powder is not very soluble it may be mixed with water and fed as slurry. In humid/tropical conditions, trouble by caking is sometimes experienced on dry feeders and for this reason solution feeders are preferred. Most mixers lend themselves to automation, with the rate of flow of coagulate dependent on the rate of flow of water through the works on a small or unsophisticated works where the rate of flow tends to be constant, the simplicity of manual regulation is much to be preferred [1]. The design considerations for coagulation are basically that of knowing the right amount or dosage of chemicals to be added and the time taken for such a treatment.

IV. FLOCCULATION

Flocculation as a means of further improvement in the water is a relatively new invention, which emerged in about the 19thcentury. This is the process whereby the water purification stage of coagulation is further enhanced by the rotating members to form large floc which become heavy and easy to settle in the bottom of the tank [5]. The use of gentle stirring in water, which floc has formed to induce the particles to coalesce and grow is known as flocculation. The bigger and denser the floc particles, the quicker are the rate of settlement. The source of power for flocculating devices are mechanical and pneumatically. Generally speaking, seldom used in large plants, even though they possess quite useful features ([2].
When the dosed water carrying floc finally passes into the flocculator through the inlet port, a certain rolling motion is inevitable, which can be accentuated by baffles in Horizontal flow basin or in an upward flow basin by the sludge blanket [1].
However in many basins there is ample evidence that better results can be obtained if mixing and flocculation can be intensified. In recent years much research has been done on both and sound theoretical rules have been laid down. There are methods of theoretical approach, the mixing and flocculation can be carried out either by mechanical means in specially built chambers or in suitable baffled channel or interconnected chambers. The latter methods requires no mechanical equipment but lacks flexibility, because the system can be designed for maximum efficiency only at one rate of flow and at one temperature, where-as the speed of mechanical paddles can be adjusted to suit the variations of flow, temperature and silt conditions. However, the cost added to the complexity of mechanical equipment introduces additional complications to be avoided in a developing country, and in practice a sinuous inlet channel preceded by violent mixing generally provides a reasonable effective solution [1]. If the pipe or channel through which the incoming water enters the basin is so dimensioned as to ensure a velocity greater than 1m/s, and if the channel or directed at an end wall so that the flow is forced to reverse abruptly through 180o, any coagulant introduced into the water before that sudden reversal will be adequately mixed and flock will form almost instantaneously.
Unlike the absolute necessity for thorough mixing, the need for flocculation as a separate process may or may not be essential much depends on the nature of the suspended solids. For rivers carrying coarse and heavy sediment the main problem is to prevent the silt settling and blocking the inlet channels before it reaches the basin [1].
Shallow depth settling may present operational difficulties in developing countries, so separate flocculators are mostly found before conventional horizontal flow basins where colloids are a problem and the complication of additional machinery may be avoided by having the flocculating action imparted to the water by the gently rolling motion resulting from passing water along a sinuous channel. In practice a channel providing a velocity of flow of about 0.3m/s with cross-walls ensuring 12-20 changes of direction though 180o (with well rounded corners), has often proved to be very effective. The emphasis must be placed on the comparative smoothness of flow required. Under no circumstances should velocity or turbulence be such as to break up the floc this can be seen in fig. 1 below. Similarly table: 1 show the recommended GT values for flocculation.

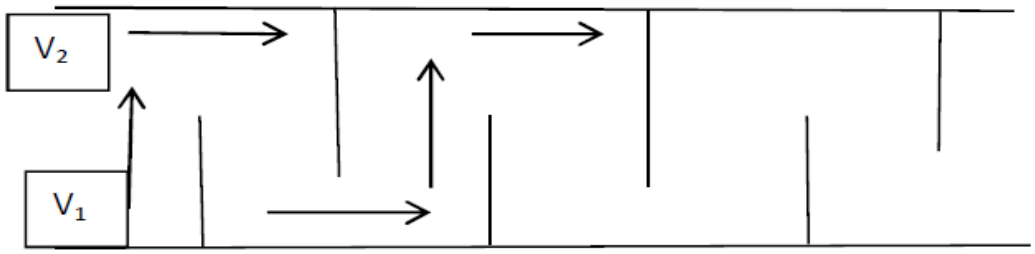

Fig: 1 Sinous Flow Channel

TABLE 1: RECOMMENDED GT VALUES FOR FLOCCULATION [1]

Type	Velocity Gradient G,s^{-1}	GT
Turbidity or colour removal (without solids recirculation	20-100	20,000-150,000
Turbidity or colour removal (with solids recirculation)	75-75	25,000-200,000
Softeners (solid contact reactors)	30-200	200,000-250,000
Softener (ultra-high solid)	250-300	300,000-400,000

V. CONCLUSION

The need for pure water for human use and consumption cannot be overemphasis. Different method and processes for water treatment to meet up with the world health organization standard (WHO) for a portable drinking water are available both in the literature and practical applications. However in this presentation three of the most widely used and the most cost effective have been identify particularly within a villages and small communities with surface water sources. That is aeration which explain the principle of pass air into the water under certain condition with a view to liberate undesirable gases such as carbon dioxide, hydrogen and also improves the water taste, odor, and colour and may also affect the killing of some pathogens. While coagulation involve the addition of chemicals such as alum to water in order to aid settlement of the dissolved particles, by forming large floc. This is followed by gentle stirring by rotating members to form large floc which become heavy and easy to settle in the bottom of the tank referred to as flocculation.

REFERENCES

[1] Smsrthurst G.: Basic Water Treatment 1997; Thomas Telford Ltd, London
[2] M. Fair, Gordon/C. Geyer, John/A. Okun, Daniel. Water and Waste water Engineering Vol.1, 1968, John Willey and Sons Inc.
[3] James G. V.: Water Treatment. Lorch: Handbook of Water Purification 1981, McGraw-Hill (UK), (London; | New York :)
[4] M. Fair, Gordon/C. Geyer, John/A. Okun, Daniel; Water and Waste water Engineer Vol. 2, 1968, John Willey and Sons Inc.
[5] Mogarr, F: Water and Waste Water Utilization in Hot Climate
[6] Dunn, P.D.: Appropriate Technology 1978, MacMillan Press Ltd
[7] Ernest, F. B, Horace W. K, James E. L, C. Y. Wei; Handbook of Hydraulics 1996, McGraw-Hill
[8] Wilcork, Dennis: Water Engineering (March 1, 1996), McGraw-Hill Education; 7 editions
[9] Maria J. Ferrua, R. Paul Singh; Understanding the fluid dynamics of gastric digestion using Computational modeling, Procedia Food Science 1 (2011) 1465 – 1472, 11th International Congress on Engineering and Food ICEF11

American Journal of Engineering Research (AJER) 2016
American Journal of Engineering Research (AJER)
e-ISSN: 2320-0847 p-ISSN : 2320-0936
Volume-5, Issue-1, pp-154-158
www.ajer.org
Research Paper Open Access

Head Determination and Pump Selection For A Water Treatment Plant In Villages Around Maiduguri, Borno State, Nigeria

[1]Hussaini A. Abdulkareem, [2]Raymond O. Ikeleji and [3]Bitrus Auta
[1,2]*Department of mechanical Engineering,School of Industrial Engineering, College of Engineering, Kaduna, Polytechnic, Nigeria*
[3]*Applied Science Department, School of Science and Technical Education, College of Science and Technology,Kaduna Polytechnic, Nigeria*

Abstract: *Water treatment plant uses pumps extensively for lifting from one level to another, for a small plant in a rural community the needed pump is selected for a total head of 9.221 m as calculated. This led to a selection of pump with flow rate of 0.0074 m/s (7.407 liters/s) and an output power of 1.894 kw(2.54 hp). The storage tank is design to cater for about 260,000 people and when the pump is shut there will be supply of about 3.7 hrs.*

Key words: *Total Head, pump, water treatment*

I. INTRODUCTION

Total head and flow are the main criteria that are used to compare one pump with another or to select a centrifugal pump for an application. In all water treatment plant pumps are used in transporting water from a low level to high level, hence the need to select a pump that can perform this function and also be able to overcome the friction within the piping system. Total head is related to the discharge pressure of the pump. For good reasons, pump manufacturers do not use discharge pressure as a criteria for pump selection. One of the reasons is that they do not know how you will use the pump. They do not know what flow rate you require and the flow rate of a centrifugal pump is not fixed. The discharge pressure depends on the pressure available on the suction side of the pump. If the source of water for the pump is below or above the pump suction, for the same flow rate you will get a different discharge pressure. Therefore to eliminate this problem, it is preferable to use the difference in pressure between the inlet and outlet of the pump. It is also known that the amount of pressure that a pump can produce will depend on the density of the fluid, for a salt water solution which is denser than pure water; the pressure will be higher for the same flow rate, so that a criteria that does not depend on density is very useful and it is called TOTAL HEAD, and it is defined as the difference in head between the inlet and outlet of the pump.

II. HEAD DETERMINATION

Consider, the raw water in the storage tank flowing under gravity to the cone shaped vortex mixer as shown in fig. 1 below.

Applying the energy equation (Bernoulli's equation), for an incompressible fluid flowing between points 1 and 2 as in fig. 1, we have

$$\frac{p_1}{pg} + \frac{v_1^2}{2g} + z_1 = \frac{p_2}{pg} + \frac{v_2^2}{2g} + z_2 + \sum hi \ldots\ldots\ldots\ldots (1)$$

For large surfaces, exposed to the atmosphere, p_1& p_2 are assumed to be at atmospheric pressure and also $v_1 \cong v_2$ thus, from equation1, $(z_1 - z_2) = \sum hi \ldots\ldots\ldots\ldots\ldots\ldots\ldots$ (2)

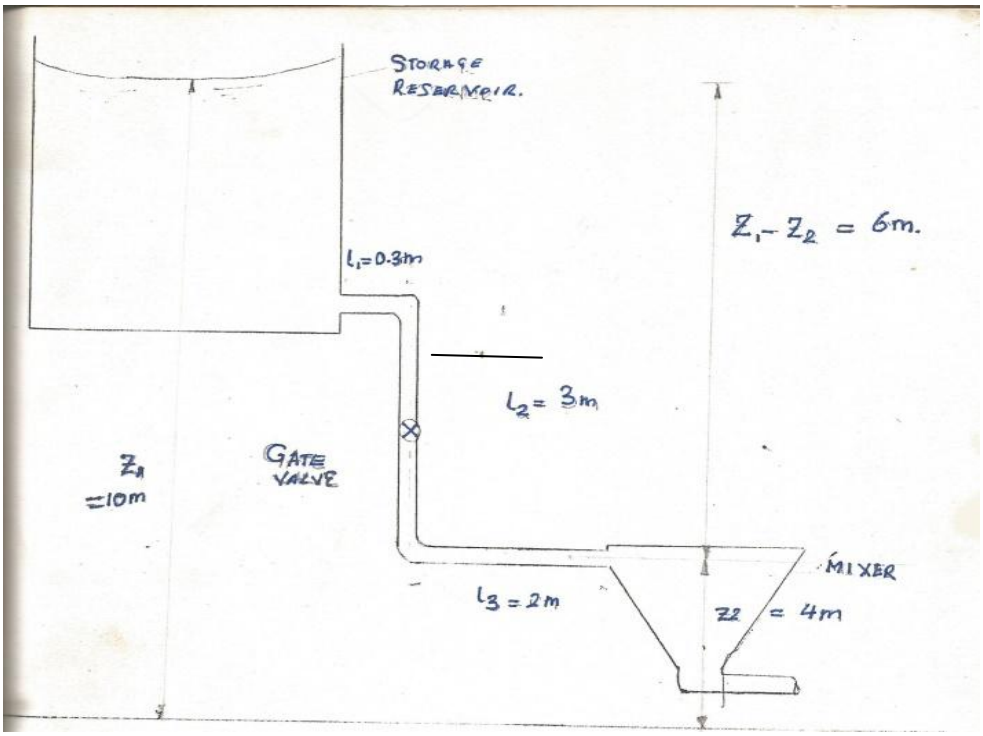

Figure 1: Total Head Determination

Where,

P_1= pressure of fluid at point (1) in N/m^2

P_2 = pressure of fluid at point (2) in N/m^2

V_1 = velocity of fluid at point (1) in m/s

V_2 = velocity of fluid at point (2) in m/s

ρ= density of fluid at that temperature in kg/m3

g= acceleration due to gravity in m/s^2

z_1= altitude above datum of fluid in tank (1) in m

z_2= altitude above datum of fluid in tank (2) in m

$\sum hi$ = summation of the losses of energy along the pipes in m

Thus, from figure 1 the height z_1 =9m, z_2=4m and the lengths l_1, l_2 and 1_3 = 300mm (0.3m), 3m and 2m respectively. The summation of the head loses is given by;

Thus, $\sum hi = k_1 v^2/2g + \frac{FIQ^2}{3d^5}\frac{FI_1 Q^2}{3d^2} + k_2 v_2/2g + \frac{FI_3 Q^2}{3d^{25}} +$

$k_3 v^2/2g$…… (3)

Where F= Friction coefficient in the Darcy back formula

Q= Discharge required in m^3/s ($0.003m^3/s$) (for the given purpose).

D= Pipe diameter in m.

v= mean velocity of fluid in pipeline in m/s

$K_{1, 2,3}$= shock loss coefficient. (k_1 = 0.5, k_2 = 0.025, k_3 = 1)

Hence,

$$\sum hi = \frac{fQ^2}{3d^5}(0.3 + 3+2) + v^2/2g(0.5 + 0.025 + 1)$$

$$= \frac{fQ^2}{3d^5}(5.3) + v^2/2g\ (1.525)\text{…….. (4)}$$

For most mixers, the entry velocity should not be more than 1m/s, to facilitate proper mixing of the coagulant and water.

Thus, from the continuity equation,

$Q=a_1v_1=a_2v_2$ = constant …… (5)

Where,

Q = discharge in m3/s (0.003 m3/s)

A = cross sectional area of pipe in m2

V = mean velocity of fluid in pipe in m/s (1.0m/s)

Hence, substituting values of Q and V in equation5;

0.003 = a x 1.00

Or, $a = \frac{0.003}{1}$

But Area, $a = \frac{\pi d^2}{4}$ …….. (6)

Where d = Diameter of pipe in m

Thus, $\frac{\pi d^2}{4} = 0.003$

And $d^2 = \frac{4 \times 0.003}{\pi}$

Or

$d = \frac{\sqrt{0.012}}{\pi}$

The most economical pipe diameter closest to this is 60mm diameter pipe [8].

For most small treatment works, Galvanized iron pipes are mostly used, which has a roughness coefficient (e) of 0.15mm (Nikuradse-moody chart).

Thus, absolute roughness = 0.15mm,

Hence,

Relative roughness $= \frac{\text{Absolute roughness}}{\text{Diameter of pipe}} = \frac{e}{d}$ …….. (7)

Thus Relative roughness $= \frac{0.15\text{mm}}{60mm}$

Relative roughness = 0.0025

The Reynolds number for this flow is given by $N_R = \frac{vd}{v}$ ……. (8)

Where, NR = Reynolds Number

v = Velocity in pipeline in m/s

v= Kinetic viscosity in m^2/s

Thus,

For the water under consideration with a highest recorded temperature of 35°C, the kinetic viscosity at 35°C is 0.729×10^{-6} m^2/s (physical properties of water table)

Hence, from equation (8)

$N_R = \frac{1.0 \times 0.06}{0.779 \times 10} - 6$

$= 82.30 \times 10^3$

The flow is seen to be laminar (Nikuradse-moody chart)thus; an approximation of the friction factor is obtained from the Nikuradse-moody chart, which is 0.024.

But a more accurate value is obtained by the use of Colebrook equation [8].

$\frac{1}{\sqrt{f}} = -2 \log_{10} [\frac{e/d}{3.57} + \frac{2.81}{R\sqrt{f}}]$ …… (9)

Thus, for f = 0.024,

$\frac{1}{\sqrt{f}} = -2\log_{10} [\frac{0.0025}{3.57} + \frac{2.81}{82.30 \times 10^3 \sqrt{0.024}}]$.

Thus, $\frac{1}{\sqrt{f}} = 6.07$

And $\frac{1}{\sqrt{0.024}} = 6.45$

Hence a better approximation is obtained by assuming f = 0.02669,

Thus, $\frac{1}{\sqrt{f}} = -2\log_{10} [\frac{0.0025}{3.57} + \frac{2.81}{82.30 \times 10^3 \sqrt{0.02669}}] = 6.08$

i.e. $\frac{1}{\sqrt{f}} = 6.08 \cong 6.10$

Thus, the friction factor for the pipes is $0.02669 \cong 0.027$

and the friction coefficient $= \frac{\text{friction factor}}{4}$ …… (10)

$= \frac{0.027}{4}$

i.e. $f = 0.0068 \cong 0.007$

Thus, substituting values of f, Q, d and V in (4) we have

$\sum hi = \frac{0.007 \times (0.003)2 \times 5.30}{3 \times (0.060)^5} + \frac{1^2}{2 \times 9.81} \times 1.525$

$= 0.143 + 0.078$

$\sum hi = 0.221\text{m}$

Thus, the head loss in the pipe line is 0.221m the total dynamic head is given as; Total dynamic Head = Head loss + static Head ……. (11).

Total dynamic Head = 0.221m + 9m = 9.221m

Thus, it is advisable to raise the head to 10m, to compensate for unforeseen losses due to static head as a percentage should not be greater than 15% [9].

i.e. $\frac{\Sigma hi}{\text{Static Head (H)}}$ x 100≤15%.....(12)

Thus, for our purpose,

$= \frac{0.221}{10}$ x 100% = 2.21%

Which is less than 15%?

Thus if the pump is shut, there would be a 3.7hr, supply of the water from the storage tank. This will suffice for a rural community.

An overflow pipe should be fitted on the 2 x 4m side, which is a 20mm diameter galvanised steel pipe, 150mm long. Part it loners should be provided to stabilise flow, and improve the strength of the tank at the same time reducing bulging effects.

III. PUMP SELECTION

The volume of storage tank as determined in (5) is $40m^3$. Thus assuming the time required to fill this tank is $1\frac{1}{2}$hr, the flow rate required of the pump to be selected as given by;

$Q = \frac{V}{T} = \frac{40m^3}{1.5hr}$

$= \frac{40m^3}{1.5 \text{ x } 3600}$

= 0.0074m3/s

= 7.407 litters/s

Hence selecting Q = 7.00 1iters/s and a 100mm diameter pipe, the pipe friction coefficient is found to be 0.618m per 100m (water friction loss chart), thus choosing a length of pipe of 100m from the pump to the storage tank (excluding the static head).

Friction head = $\frac{0.618}{100}$ x (100 + 10)

= 0.6798m

Thus, from total dynamic head = friction head + static head

= 0.6798 + 10 = 10.6798m

Also, the $\frac{\text{friction head}}{\text{static head}}$ x100% = $\frac{0.6798}{10}$ x 100

6.798% which is < 15%

The power required in kilowatt to pump the water to the storage tank is given by,

Power in kW = $\frac{\text{liter / second x metter head}}{\text{Efficiency}}$..... (13)

Kw = $\frac{Q\left(\frac{1}{s}\right) \text{x H (m)}}{\eta}$ ..... (14)

Where ɳ = hydraulic efficiency which for most practice purposes is taken to be 50%.Q and Hence as earlier defined.

Kw = $\frac{7 \text{ x } 10.6798}{50}$ = 1.495Kw

Power = 1.50Kw

Thus, power in horse power (hp) = $\frac{\text{power in Kw}}{0.746 \text{ (Kw)}}$, where 1hp = 0.746Kw

Thus, Power (hp) = $\frac{1.50}{0.746}$

= 2.01hp

Hence, power required = 2.01hp (l.50Kw)

The actual power required = power required + derating due to temperature and altitude + derating due to aging.

i. **Derating due to temperature**:- there is a 1% reduction of power for every 2 . 8°C above 29°C [9].

Hence, for the temperature of 35°C, let(x) be the power due to the temperature increase, hence,

$X = \frac{\text{power required}}{1-\frac{(35-29)}{2.8} \text{ x } \frac{1}{100}}$

$X_{temp} = \frac{1.50}{0.98}$

X_{temp} = 1.533

Thus, power required due *to* temperature increase = 1.533 - 1.50

= 0.03kw

ii. Power reduction due to altitude;- there is a 3.5% reduction of power per 300m above 15Qm[9], the altitude range for Maiduguri area is 200-500m [11], thus a choice of 500m will be suitable. For' this altitude, let Y be the power required due to the increase in altitude hence,

$Y_{alt} = \frac{\text{Power required}}{(1-\frac{500-150}{300} \text{ x } \frac{3.50}{100})}$

$= \frac{1.5}{0.959}$

Y_{alt}= 1.564kw

Thus the power required due to increase in altitude = 1.564 - 1.50

= 0.064kw.

iii. Power required due to aging: 15-25% extra is allowed for failure in performance as the unit become older [9]. Hence choosing an increase of 20% factor of safety, we have;

Increase of power due to aging = $\frac{20}{100}$ x 1.5 = 0.3kw

Hence, the actual power required is:

Actual power = 1.5 + 0.03 + 0.064 + 0.3

= 1.894kw (2.54hp)

Let the pump be placed 1.50m above the surface of the water in well. The available net positive suction head,(NPSH) is given by

Available NPSH = P_1-H_s -V_p -F_s… (15)

Where, P_1 = Open pressure on liquid surface (m)

H_s= vertical height of pump suction above open surface in (m)

V_p = vapour pressure of liquid in (m)

F_s = suction entry and friction losses in (m)

The value F_s is practically taken to be 0.75m [9] at 35^{o}C and 500m altitude; V_p and P_1 are 0.625m and 7.04m (US standard atmosphere table).

Hence,

Available NPSH = 7.04 – 1.50 – 0.75

= 6.165m, 4.17m is taken been the maximum allowed for the pump suction intake.

Thus, from the graph of velocity VS flow, (choose of suction pump diameter chart) the bore of pipe recommended for such a suction arrangement is a 76mmdiameter pipe and the suction velocity corresponding to this flow rate and pipe diameter is 1.6m/s, which is necessary as the suction velocity should be less than 2.0m/s, to avoid cavitation.

Thus, the outlet point of the pump is to have a discharge of 71litres/s, ahead of 15m and a power of 2.5hp.For the suction arrangement, a suction pipe diameter of 76mm (3in), flexible reinforced rubber hose should be used, with a net positive suction head 4.17m as mentioned above.

Two 45° elbow joints are to be installed along the delivery line -due to changes in flow direction and the delivery line should also be fitted with the reinforced rubber hose for a length of 2m and be attached with a connector to facilitate easy removal.

IV. CONCLUSION

A Great cost reduction and improvement on the efficiency is obtained by the use of a well dug before the pump intake. This is another cost reduction, when we consider building of a raw water storage tank before the pump compared to this underground storage.

Lack of extension of electricity grid or it's instability in most rural communities, certain energy sources were considered before one was chosen for this purpose. Although Maiduguri area and most parts of Northern Nigeria have abundant solar and wind the choice of old fossil fuel type of energy source, to drive a pump was used.

The overhead tank was placed at a suitable head to produce the required flow and the choice of tank material and size all made to standard.

The mixer used for this design was adopted to ease the construction of separate mixing chamber, sophisticated mechanical or flash mixer used in high tech water treatment processes which require a great deal of power.

REFERENCES

[1] Smsrthurst G.: Basic Water Treatment 1997; Thomas Telford Ltd, London

[2] M. Fair, Gordon/C. Geyer, John/A. Okun, Daniel. Water andWaste water Engineering Vol.1, 1968, John Willey and Sons Inc

[3] James G. V.: Water Treatment. Lorch: Handbook of Water Purification 1981, McGraw-Hill (UK), (London; | New York :)

[4] M. Fair, Gordon/C. Geyer, John/A. Okun, Daniel; Water and Waste water Engineer Vol. 2, 1968, John Willey and Sons Inc.

[5] Mogarr, F: Water and Waste Water Utilization in Hot Climate

[6] Dunn, P.D.: Appropriate Technology 1978, MacMillan Press Ltd

[7] Ernest, F. B, Horace W. K, James E. L, C. Y. Wei; Handbook of Hydraulics 1996, McGraw-Hill

[8] Wilcork, Dennis: Water Engineering (March 1, 1996), McGraw-Hill Education; 7 editions

[9] Maria J. Ferrua, R. Paul Singh; Understanding the fluid dynamics of gastric digestion using

[10] Computational modeling, Procedia Food Science 1 (2011) 1465 – 1472, 11th International Congress on Engineering and Food ICEF11

[11] Regional Map of Borno State.

American Journal of Engineering Research (AJER) 2016
American Journal of Engineering Research (AJER)
e-ISSN: 2320-0847 p-ISSN : 2320-0936
Volume-5, Issue-1, pp-159-168
www.ajer.org
Research Paper Open Access

Theoretical and experimental study of cavitation dispersing in "liquid-solid" system for revelation of optimum influence modes

Roman N. Golykh
Biysk Technological Institute (branch) of Altai State Technical University named after I.I. Polzunov, Russia

ABSTRACT: *The paper contains the results of the study of cavitation dispersing in "liquid-solid" system. It is known that cavitation dispersing is one of energy effective methods of "liquid-solid" interface area increasing. For evaluation of cavitation dispersing modes providing maximum interface area the model of the process was developed. The model is based on simulation of bubble collapse near solid particle surface for determination of particle destruction possibility and calculation of particulate composition evolution using of probabilistic approach. Analysis of the model has shown that cavitation dispersing provides increasing a "liquid-solid" interface area up to 2 and more times. The proposed model was confirmed by experiments.*

Keywords - *Cavitation, dispersing, multiphase medium, shock wave, solid particles*

I. INTRODUCTION

Physical and chemical processes on liquid-solid boundary are one of the essential foundations of modern productions [1]. Examples include adsorption, chemisorption processes, surface chemical reactions, dissolution of crystalline substances, a hydrocarbon cracking catalysis, etc. [1] To maximize the efficiency or speed of implementation of such processes it is primarily necessary to provide the largest possible contact surface area between liquid and solid phases [1].

Obviously, this can be accomplished by dispersing of solid particles involved in the liquid and chemically reacting with it into smaller pieces [1, 2].

Existing methods for dispersing solid particles are divided into:

– Vibratory milling [3], ball, planetary, and others mills;

– Shock compression (explosion);

– Cavitation dispersing [1, 2].

The main disadvantage of different types of mills is inability of obtaining particles smaller than 200 μm that causes a hard limited phase contact surface. A shock compression requires high energy due to the need to create high pressures in liquid dispersed medium. Thus, the most expedient way of dispersing solids to improve the efficiency of physical and chemical processes on liquid-solid boundary is the cavitation dispersion. During cavitation dispersion low dense energy (energy of primary influence, for example, hydrodynamic vacuum, high intensity acoustic waves and so on) is converted to high dense energy. This means that energy of the primary influence is stored in cavitation bubble during the bubble expansion stage. Then shock release of stored energy occurs. As a result, the shock release of energy causes the destruction of particulate matter because the amplitude of the pressure generated by the shock wave may be exceed the tensile strength of the majority of solids (more 1000 atms) [2].

The main advantages of the cavitation dispersion are:

– The possibility of dispersing of solid particles down to submicron sizes;

– Uniform distribution of particles in a liquid due to acoustic microflows.

Today one of the most profitable methods of creating cavitation is the introduction of ultrasonic vibrations into the liquid-solid suspension [1, 2]. It is known that ultrasonic vibrations lead to the formation of a plurality of cavitation bubbles which periodically expand and collapse with frequency over 20,000 times per second. However, today, despite a number of advantages, cavitation dispersion under the influence of ultrasonic vibrations (ultrasonic cavitation dispersion) is not widespread distributed in the industry. This is due to absence of system theoretical and experimental researches which explain the mechanism of destruction of solid particles under the influence of ultrasonic vibrations and allow determining the best modes of action depending on the physical properties and characteristics of the two-phase liquid-solid system.

Therefore, the goal of presented research is the evaluation of optimum modes of ultrasonic cavitation dispersion which allows providing maximum surface area between liquid and solid.

To achieve this goal it is necessary to solve the following tasks:

– To develop physical and mathematical model of the cavitation influence on a single solid particle to detect possible destruction of the particle (the emergence of the elementary act of dispersion) depending on the exposure mode and location of cavitation bubbles with respect to the particles;

– To develop probabilistic model of the evolution of disperse composition of particulate solids in a cavitating liquid based on the evaluated influence modes and the cavitation bubbles locations with respect to the particles at which the elementary act of dispersion occurs;

– To evaluate the intensities of influence providing maximum surface area contact between the phases depending on the viscosity of liquid phase and the initial particle size;

– To experimental study ultrasonic cavitation dispersing solid particles to confirm the theoretical results.

The following topics devoted to solve the tasks.

II. PHYSICAL AND MATHEMATICAL MODEL OF INTERACTION OF A SINGLE CAVITATION BUBBLE WITH INTERFACIAL BOUNDARY "LIQUID-SOLID"

To identify the modes of the cavitation influence providing high degree of dispersion of solid particles, analysis of cavitation influence on individual particles is primarily needed.

The developed model of cavitation influence on a single particle is based on the following assumptions:

1-1. During bubbles expanding liquid with particles flowing around cavitation bubbles moves as a continuous medium. This is due to the fact that the maximum size of the bubble achieved during expansion stage is much more than the size of the particles used in practice.

1-2. Minimum size of cavitation bubbles (at collapse) is much less than the linear dimensions of the particle surface.

1-3. The influence of shock waves on the particle displacement or rotation is absent due to short time of collapse that is not enough for the change of momentum or angular momentum of a particle.

1-4. Since the start of the expansion to the point at which the radius of a cavitation bubble will be 1/3 from the nominal diameter of the particle (in the stage of collapse), it retains the vial spherical. The above assumption partly follows from 1-1 and confirmed by modeling of the interaction of a cavitation bubble with a solid surface [1, 4].

A theoretical analysis of the cavitation impact on the single particle consists the following stages.

1) Cavitation bubble expansion.

2) Cavitation bubble collapse.

3) Shock wave generation and propagation.

4) Interaction of a shock wave with a solid particle.

Further consideration of each step is described in more detail.

2.1. Cavitation bubble expansion

Consideration of the expansion stage of cavitation bubble is aimed at determining the maximum radius R_{MAX}.

Maximum bubble radius R_{MAX} is determined by the Nolting-Nepayres equation:

$$\rho\left(\frac{3}{2}\left(\frac{\partial R}{\partial t}\right)^2 + R\frac{\partial^2 R}{\partial t^2}\right) = -4\mu\frac{\frac{\partial R}{\partial t}}{R} + p_v + \left(p_0 + \frac{2\sigma}{R_0}\right)\left(\frac{R_0}{R}\right)^{3\gamma} - p_0 + \sqrt{2\rho cI}\sin(2\pi ft)\ ; \qquad (1)$$

where R is momentum radius of a cavitation bubble, m; R_0 is the radius of a cavitation nuclei, m; ρ is density of a suspension as a continuum, kg/m^3; μ is viscosity of a suspension as a continuum, Pa·s; σ is surface tension of a liquid phase, N/m; p_v is pressure of a liquid phase vapor, Pa; p_0 is static pressure in a suspension, Pa; c is sound speed in a suspension, m/s; I is intensity of a ultrasonic oscillations (primary influence), W/m^2; f is frequency of a ultrasonic oscillations, Hz; t is time, s. The maximum radius calculated by equation (1) will be used for following analysis bubble collapse and its acting on interphase boundary "liquid-solid" (surface of dispersible particles).

2.2. Cavitation bubble collapse

It is known that during the collapse of the bubble its radius decreases from the maximum being much more than the dimensions of the dispersed particles to the minimum being much less than the size of the particles, i.e. less than 1 μm. Thus, cavitation bubble during collapse stage can be in different conditions of around flow by liquid-dispersed suspension. In depending on around flow conditions the bubble collapse stage can be divided into two periods – the initial period and the final period.

During the initial period size of a bubble is still much more than the size of the particles. In this case, liquid dispersed suspension flow around the bubble can be seen as a continuum with equivalent physical properties that are viscosity and density, as well as in the expansion stage.

When the bubble size becomes comparable to the particle size and then continues to decrease to the minimum size forming pulse of a high-amplitude shock wave, the end period of collapse is realized. Obviously, during the final period the cavitation bubble is flowed by liquid continuous phase and interacts with the surface of one of the particles due to Bjerknes forces leading to the convergence of the bubbles to the particles. This cavitation bubble undergoes deformation caused by the reflection of microflows of fluid flowing around the cavitation bubble from surface of a particle. Deformation of the cavitation bubble narrows the directivity pattern of the shock wave and thus provides high concentration of pressure amplitude in a narrow beam that actually leads to destruction particle (dispersing particle).

In the initial period of the collapse of the bubble, his behavior is described by Nolting-Nepayres equation as well as on the expansion stage.

However during the final period a bubble undergoes deformation due to the interaction between shock wave and particle surface as already mentioned.

While the velocity of the bubble wall is not comparable to the speed of sound in the liquid, form of the cavitation bubble can be accurately described by the integral equation (3) with the boundary condition (4) on the wall of the cavitation bubble for the fluid velocity potential [4]:

$$\frac{\varphi(\mathbf{r}_0)}{2} = \int_{S_A \cup S_B} \left(E_{\mathbf{r}_0}(\mathbf{r}) V_{\mathbf{n}}(\mathbf{r}) - \frac{\partial E_{\mathbf{r}_0}}{\partial \mathbf{n}}(\mathbf{r}) \varphi(\mathbf{r}) \right) \partial S(\mathbf{r}) ; \quad (3)$$

$$\frac{\partial \varphi}{\partial t} + \frac{|V_{\mathbf{n}}|^2 + |V_{\tau}|^2}{2} = \frac{2\sigma K}{\rho} - \frac{p_v}{\rho} \left(\frac{3V}{4\pi R_{MAX}^3} \right)^{\gamma} ; \quad (4)$$

where $\mathbf{r}_0$, $\mathbf{r}$ are vectors of coordinates of points of cavitation bubble wall or solid surface, m; φ is the potential of liquid velocity on cavitation bubble wall or solid surface, m^2/s; $V_{\mathbf{n}}$ and V_{τ} are normal and tangential of liquid velocity components, m/s; $E_{r_0}(\mathbf{r})$ is basic solution of Laplace equation; S_A is surface of cavitation bubble wall; S_B is surface of solid particle; σ is surface tension of liquid phase, N/m; ρ is density of liquid phase, kg/m^3; p_v is liquid phase vapor pressure, Pa; V is volume of cavitation bubble, m^3; R_{MAX} is maximum radius of cavitation bubble determined in subsection 1.1, m.

The system of equations (3-4) is used for calculation cavitation bubble wall deformation during time. Equation (3) for evaluation liquid velocity potential distribution is solved by boundary element method [4].

When the speed of the bubble wall becomes comparable to the speed of sound in the fluid, equation (1) can not be used. In this case, the calculation of the evolution of the bubble shape is performed by using the asymptotic decomposition of bubble shape by cosine of the azimuth angle (see equation (5) and Fig. 1).

$$\begin{pmatrix} r(\theta) \\ z(\theta) \end{pmatrix} = \begin{pmatrix} R(\theta)\sin\theta \\ R(\theta)\cos\theta \end{pmatrix} = \left(\sum_{n=0}^{\infty} R_n \cos^n \theta \right) \begin{pmatrix} R(\theta)\sin\theta \\ R(\theta)\cos\theta \end{pmatrix} ; \quad (5)$$

where $\begin{pmatrix} r(\theta) \\ z(\theta) \end{pmatrix}$ are cylindrical coordinates of point of bubble wall, m; θ is azimuth angle, rad.

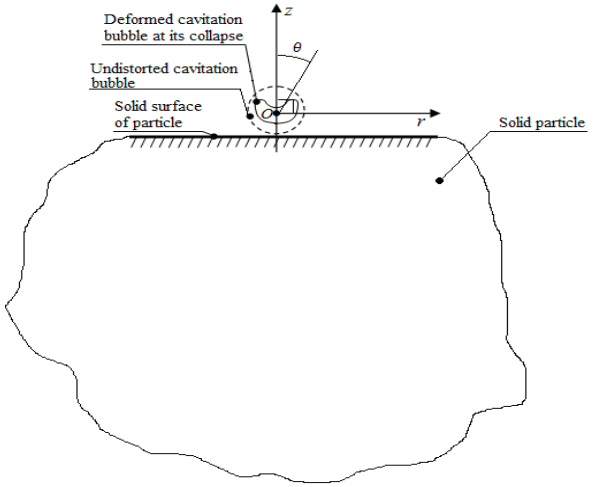

Fig. 1. Diagram of bubble collapsing near solid particle (θ is azimuth angle)

For numerical calculations it must be limited by a finite number N of terms in the decomposition:

$$\begin{pmatrix} r(\theta) \\ z(\theta) \end{pmatrix} \approx \left(\sum_{n=0}^{N-1} R_n \cos^n \theta \right) \begin{pmatrix} R(\theta)\sin\theta \\ R(\theta)\cos\theta \end{pmatrix}; \quad (6)$$

When $N = 1$ the Navier-Stokes equations [5] taking into account liquid compressibility and allowing describing bubble shape at collapse can be reduced to Gilmore equation (7):

$$R_0 \frac{\partial^2 R_0}{\partial t^2}\left(1 - \frac{\frac{\partial R_0}{\partial t}}{C}\right) + \frac{3}{2}\left(\frac{\partial R_0}{\partial t}\right)^2\left(1 - \frac{\frac{\partial R_0}{\partial t}}{3C}\right) = H\left(1 + \frac{\frac{\partial R_0}{\partial t}}{C}\right) + \frac{\partial H}{\partial t}\frac{R_0}{C}\left(1 - \frac{\frac{\partial R_0}{\partial t}}{C}\right); \quad (7)$$

where H is enthalpy of liquid, m^2/s^2; C is local sound speed in liquid, m/s; t is time.

Thus, the proposed model allows calculating the shape of the bubble near the particle surface which is during bubble collapse. Further the resulting shape of the bubble will be used to calculate the generation and propagation of the shock wave.

2.3. Shock wave generation and propagation

In the analysis of shock waves in the fluid acoustic approximation can be considered as valid, because shock wave near the particle surface has fluid velocity that is small in comparison to sound speed.

Therefore shock wave propagation can be described by the wave equation (8)

$$\frac{\partial^2 p}{\partial t^2} - c^2 \Delta p = 0; \quad (8)$$

where t is time, s; p is shock wave pressure, Pa; c is sound speed in suspension, m/s;

At the consideration of stage of shock wave generation and propagation it allows to approximate profile of wave pressure near interface "liquid-solid" by the following expression (9) obtained by the spectral decomposition and the Green formula for the Helmholtz equation.

$$p(\mathbf{r},t) = \frac{\omega}{2\pi}\sum_{n=-\infty}^{\infty} e^{-in\omega t}\int_S iG_{\mathbf{r}_0, n\frac{\omega}{c}}(\mathbf{r})\frac{n\omega}{c}\int_0^{\frac{2\pi}{\omega}} p_c(t_1)e^{in\omega t_1}\partial t_1 \partial S_0; \quad (9)$$

where $\mathbf{r}=(x;y;z)$ are the coordinates of the point of the interphase boundary "liquid-solid", m; ω is the angular frequency of the ultrasonic oscillations (primary influence), s^{-1}; t and t_1 are the moments of time, s; η is the viscosity of suspension, Pa·s; ρ and c are the density and the sound speed of the liquid phase, respectively, m/s; $p_c(t_1)$ is the pressure in the nucleus of the cavitation bubble, Pa; S is the surface of the cavitation bubble at the achievement of maximum pressure in its nucleus, m; $G_{\mathbf{r}_0, n\frac{\omega}{c}}$ is the Green's function [6] at wave number is $n\frac{\omega}{c}$.

Appearing in the expression (9) function of the shock wave pressure in the core of the cavitation bubble is determined based on its shape obtained at each time according to the following relationship:

$$p_c(t_1) = p_V\left(\frac{2R_{MAX}^3}{\int_0^{\pi} r(\theta)\left[z(\theta)\frac{\partial r}{\partial\theta}(\theta) - r(\theta)\frac{\partial z}{\partial\theta}(\theta)\right]\partial\theta}\right)^{\gamma}; \quad (10)$$

where p_V is vapor pressure in liquid phase, Pa; R_{MAX} is the maximum bubble radius determined in section 1.1, m; θ is azimuth angle (see Fig. 1), rad; $(r(\theta); z(\theta))$ is cylindrical coordinates of bubble wall point that were founded in section 1.2, m.

Further founded pressure profile of shock wave will be used to analyze the possibility of the destruction of the solid particles as a result of the elementary act of dispersion and, ultimately, to identify the optimal cavitation influence modes providing maximum surface area "liquid-solid".

Further the interaction of a shock wave with the solid particle will be analyzed to detect the possibility of dispersing the latter.

2.4. Interaction of shock wave with solid particle

Analysis of the interaction of a shock wave with the solid particles is aimed at detecting possibility destruction of the last depending on the distance between a collapse core of a cavitation bubble and a particle. The act of destruction (dispersing) of particle occurs if and only if the mechanical stresses in it exceed threshold of strength of the particle near surface area opposed surface are near the bubble collapse core.

Determination of the mechanical stresses in the material of the solid particles is based on the linear theory of elasticity using the Laplace equation for the components of the stress tensor (11) with the boundary condition (12):

$$\Delta \sigma_{33} = 0 \; ; \tag{11}$$

$$\sigma_{33}\big|_S = p \; ; \tag{12}$$

where σ_{33} is component of the stress tensor of solid particle material, Pa; p is shock wave pressure near the boundary of "liquid-solid" calculated at some distance between bubble and particle surface by expression (9) (see section 1.3), Pa.

Due to decreasing shock wave pressure with increasing distance between cavitation bubble collapse core and surface of particle this distance providing particle destruction is limited by some value calculated by (11,12).

This distance is used to analyze the evolution of the particulate composition of the solid particle. Probabilistic model of dispersing solid particles allowing determining the evolution of the particulate composition is as follows.

III. PROBABILISTIC MODEL OF EVOLUTION OF PARTICULATE COMPOSITION IN CAVITATING LIQUID

Obviously, probability of an elementary act of particles dispersing is proportional to the probability of occurrence and collapse of cavitation bubble in a neighborhood of the particle (breakdown neighborhood) that is a limited by distance at which shock wave passing it keeps pressure amplitude greater than the tensile strength of the particles. This distance (the size of the particles breakdown neighborhood) was determined at the previous stage of consideration of the model (see section 1.4). The breakdown neighborhood is schematically shown in Fig. 2.

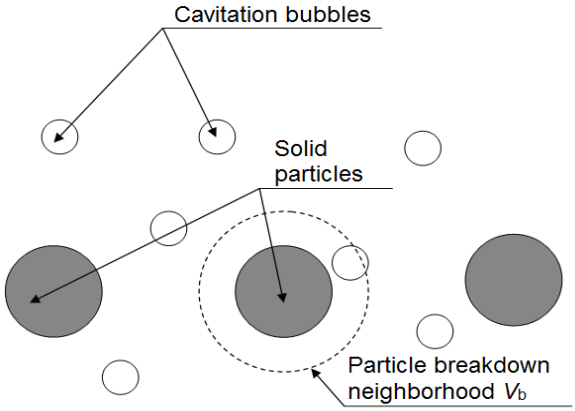

Fig. 2. Cavitation bubbles, solid particles and particle breakdown neighborhood

When concentration of bubbles n_{bub} [7] is known, probability of an elementary act of particle breakdown over small time Δt is defined as:

$$P(\Delta t) = 1 - \left(1 - \frac{N V_b}{(V - N V_p)}\right)^{f \Delta t n_{bub} (V - N V_p)} \; ; \tag{13}$$

where $P(\Delta t)$ is probability of an elementary act of particle breakdown over small time Δt(s); V is local volume of suspension, m^3; N is number of solid particles in volume V; V_b is volume of neighborhood of single particle, m^3; V_p is volume of single particle, m^3.

For a small time Δt and a small volume content of particles probability of single particle breakdown is defined as (14):

$$P(\Delta t) \approx V_b \, f \Delta t n_{bub} \; . \tag{14}$$

The obtained expression (14) for the probability of dispersible particles breakdown allows us to derive the kinetic equation of evolution of the particulate composition of the suspension "liquid-solid" under the ultrasonic cavitation influence. To do this, we take into account the assumption that during the elementary act of breakdown each particle breaks into two identical. This allows to approximate the particulate composition by discrete model by entering the value n_k that is the concentration of particles with a nominal diameter $d_0/2^{k/3}$ (d_0 is initial nominal diameter), V_{bk} is the volume of breakdown neighborhood of a particle with diameter $d_0/2^{k/3}$, $P_k(\Delta t)$ is particle breakdown probability during a small period of time Δt.

Then changing of the concentration n_k during Δt can be determined by the expression (15):

$$\Delta n_k = 2P_{k-1}(\Delta t)n_{k-1} - P_k(\Delta t)n_k = f\Delta t n_{bub}\left(2V_{b(k-1)}n_{k-1} - V_{bk}n_k\right); \quad (15)$$

where $2P_{k-1}(\Delta t)n_{k-1}$ is an increase of particles with a nominal diameter $d_0/2^{k/3}$ due to breakdown of particles with larger diameter $d_0/2^{(k-1)/3}$ in two identical; $P_k(\Delta t)n_k$ is decrease of particles with nominal diameter $d_0/2^{k/3}$ due to the collapse of their own.

In expression (15) it assumes that $n_{-1}=0$.

When Δt tends to zero, from the expression (15) the kinetic equation of particulate composition evolution follows:

$$\frac{\partial n_k}{\partial t} = fn_{bub}\left(2V_{b(k-1)}n_{k-1} - V_{bk}n_k\right). \quad (16)$$

This equation was solved by Runge-Kutta method and allowed evaluating the evolution of particulate composition of suspension over time.

Histograms of particulate composition at different time points are presented in Fig. 3, 4 (frequency of ultrasonic oscillations is 22 kHz).

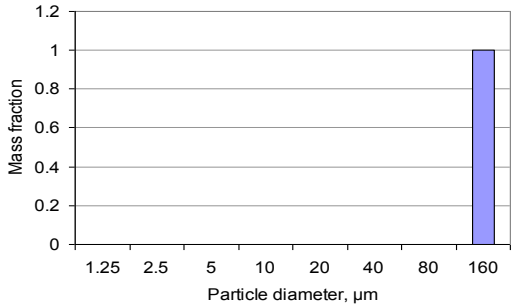

a) 0 min

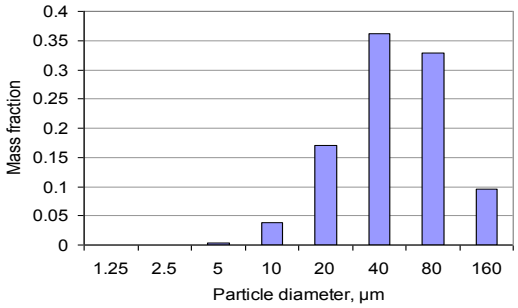

b) 20 min

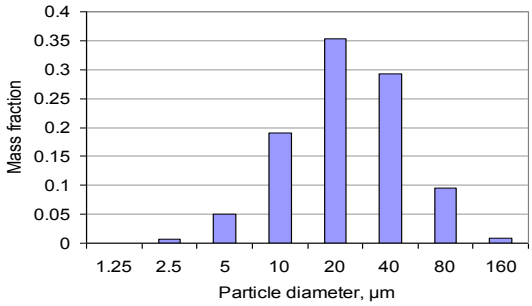

c) 40 min

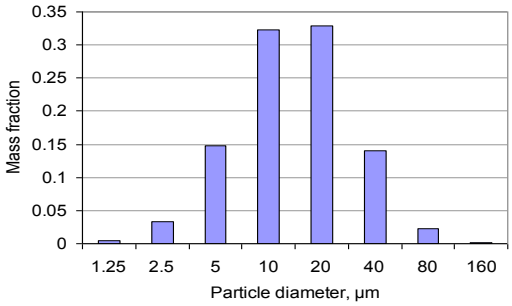

d) 60 min

Fig. 3. Histogram of particulate compositions at different time points (initial diameter is 160 μm; viscosity of liquid phase is 1 mPa·s – liquid phase is water; ultrasonic cavitation influence intensity is 10 W/cm^2)

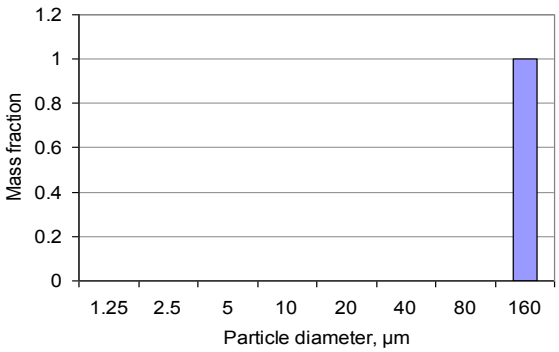

a) 0 min

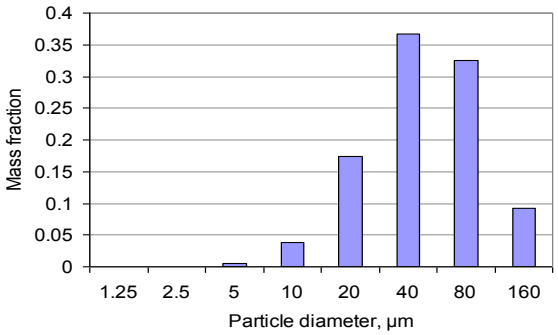

b) 20 min

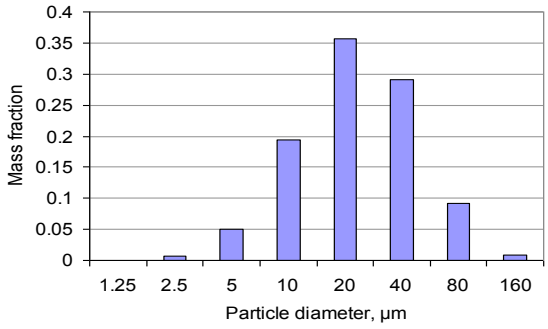

c) 40 min

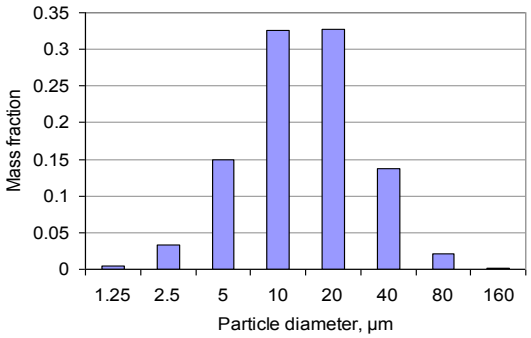

d) 60 min

Fig. 4. Histogram of particulate compositions at different time points (initial diameter is 160 μm; viscosity of liquid phase is 100 mPa·s – liquid phase is machine oil; ultrasonic cavitation influence intensity is 20 W/cm^2)

As follows from the histogram over time the share of fines increases and the proportion of large are reduced. This indicates the effect of cavitation dispersion and hence the increase the surface of contact between the phases.

The obtained evolution of the particulate composition allows the degree of the increase the phases contact surface (relative increase the interface area) according to the expression (17):

$$\frac{S(t)}{S_0} = \frac{\sum_{k=0}^{\infty} n_k(t) \frac{d_0^{\,2}}{4^{\frac{k}{3}}}}{\sum_{k=0}^{\infty} n_k(0) \frac{d_0^{\,2}}{4^{\frac{k}{3}}}}. \qquad (17)$$

The dependences of relative increase the interface area on physical properties and characteristics of suspension (viscosity and initial diameter of particles) are shown in Fig. 5, 6.

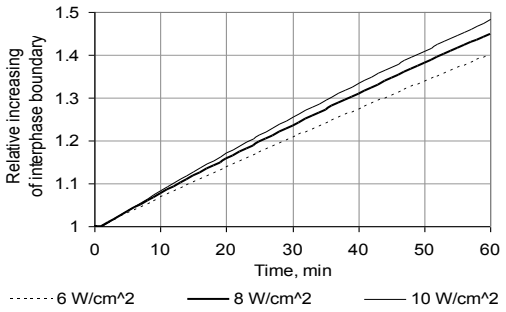

a) Initial diameter is 80 μm

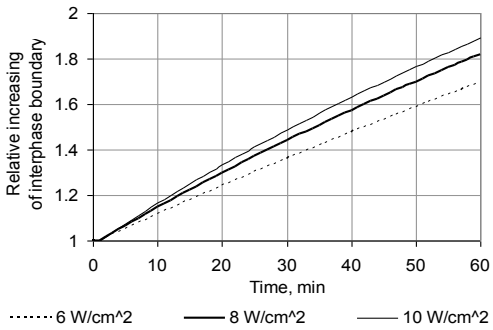

b) Initial diameter is 120 μm

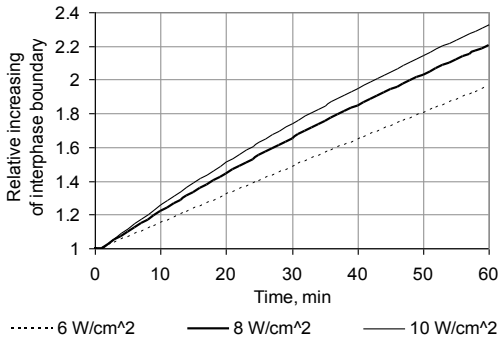

c) Initial diameter is 160 μm

Fig. 5. The dependences of relative increase the interface area on time at various intensities (W/cm^2), initial diameters (μm) and viscosity of liquid phase 1 mPa·s

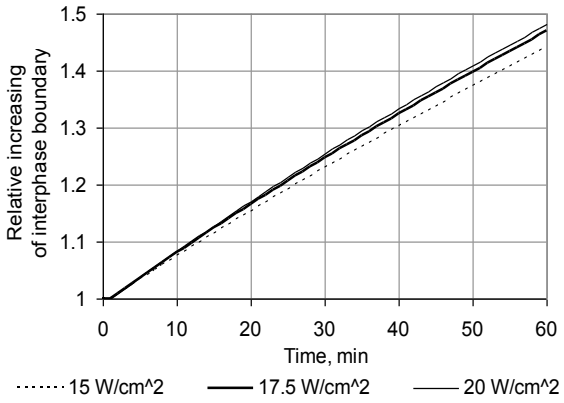

a) Initial diameter is 80 μm

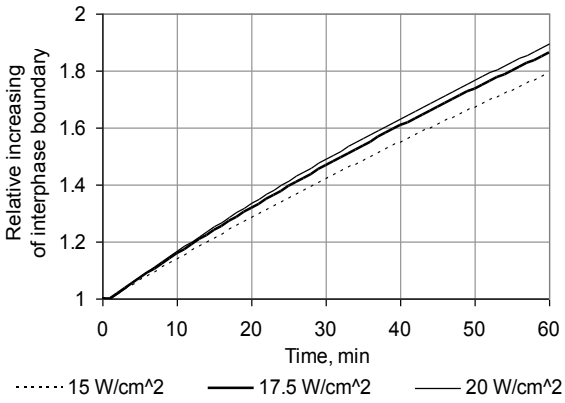

b) Initial diameter is 120 μm

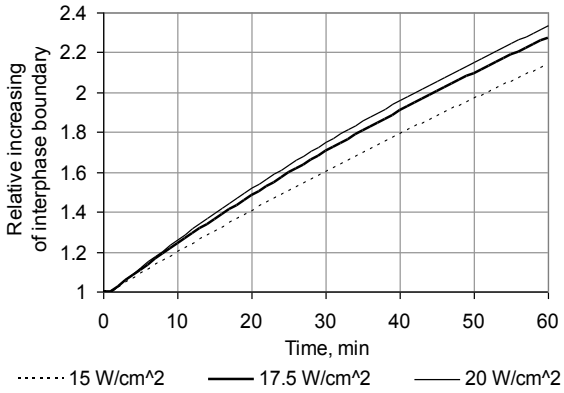

c) Initial diameter is 160 μm

Fig. 6. The dependences of relative increase the interface area on time at various intensities (W/cm^2), initial diameters (μm) and viscosity of liquid phase 100 mPa·s

Dependencies presented in Fig. 5, 6 allow determining intensity that is necessary for the required interphase boundary relative increasing depending on properties and characteristics of suspension (viscosity and initial diameter of particles).

For example, at intensity 10 W/cm^2 and liquid phase viscosity 1 mPa·s (initial diameter 160 μm) liquid-solid interface area has been increased up to 1.95 times during 40 minutes (or up to more than 2 times during 60 minutes). And at intensity 6 W/cm^2 interface area of the suspension has been increased up to 1.65 times during 40 minutes.

At greater viscosity 100 mPa·s the dispersing requires significantly more intensity of ultrasonic cavitation influence than at viscosity 1 mPa·s to achieve same interface area. For liquid phase with viscosity 100 mPa·s and initial diameter 160 μm, the interface area increasing more than 1.9 times during 40 minutes is achieved at intensity 17.5 W/cm^2 and more (for comparison, at viscosity 1 mPa·s the necessary intensity is 10 W/cm^2).

Obviously, it can be explained lower degree of cavitation intensity. The obtained dependencies can be used to recommend ultrasonic cavitation influence modes depending on physical properties and characteristics of liquid-solid suspension.

However, at smaller initial diameters the interface area increasing is less because reducing of breakdown neighborhood volume that causes reducing of particle breakdown probability. For example, at diameter 80 μm, liquid phase viscosity 100 mPa·s and intensity 17.5 W/cm^2 the increasing of the interface area is not exceed 1.5 even during 60 min.

The obtained theoretical results were confirmed by experiments. Performed experiments are described in next section.

IV. Experimental Studies of Cavitation Dispersing

Experimental studies of ultrasonic dispersion were performed to confirm the adequacy of the proposed model.

During the experiments aluminum particles with an initial size of 100 ... 400 μm mixed with the water is dispersed by ultrasonic device of series "Volna-M", created by a team of "Center of ultrasonic technologies", Ltd. (Russia, Altay, Biysk) [8].

Dispersing was carried out during 41…43 min at the exposure intensities that are 6 and 10 W/cm^2. The particle size is determined by the sampling and analysis of collected particulate samples using a set of imaging based on optical microscope "MIKMED" (Russia) and high-resolution digital camera.

Microscopic picture and particulate composition of samples taken at various time points is shown in Fig. 7, 8.

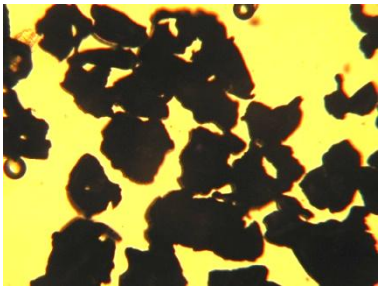

a) 0 min

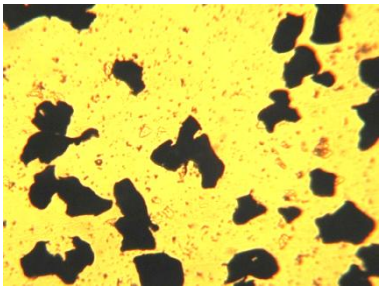

b) 18 min

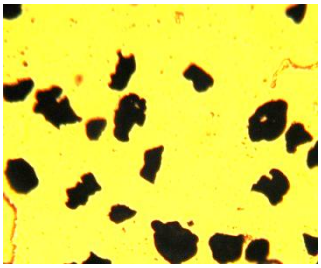

c) 41 min

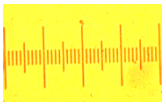

d) Object micrometer (Value of division is 10 μm)

Fig. 7. Microscopic pictures of aluminum particles dispersed at different times (intensity of influence is 10 W/cm^2)

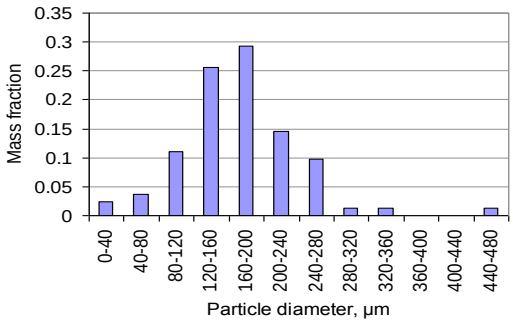

a) 0 min

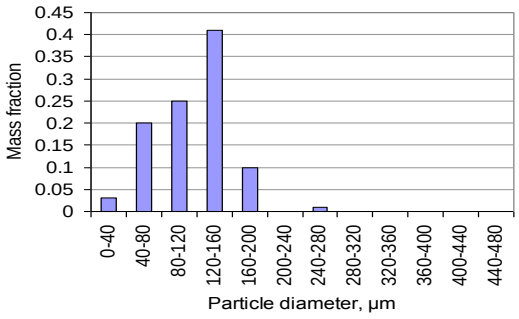

b) 5 min

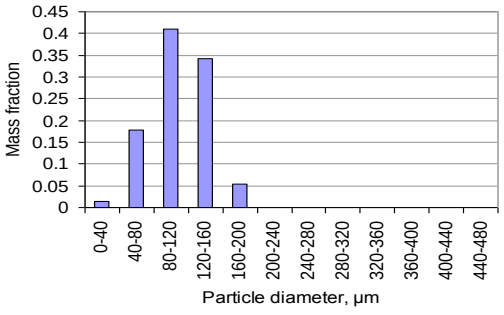

c) 18 min

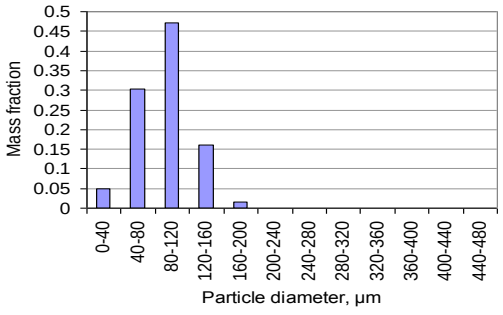

d) 41 min

Fig. 8. Particulate composition of the samples of aluminum particles at different times (intensity of influence is 10 W/cm^2)

These pictures and histograms confirm the theoretical increase in the proportion of fine particles during ultrasonic dispersion.

As has been repeatedly noted, the particulate composition is determined by a specific surface area of contact of phases "liquid-solid body." The experimental dependence in their comparison with the theoretical is shown in Fig. 9.

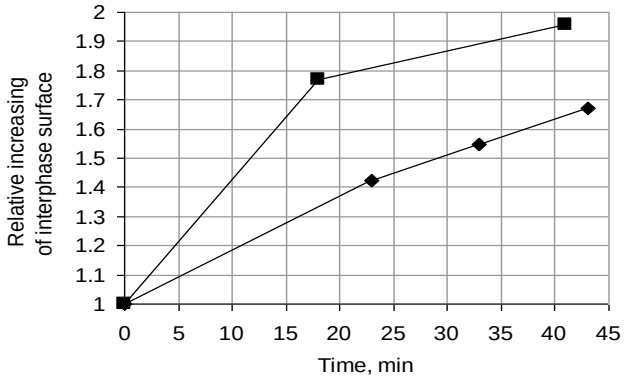

Fig. 9. Theoretical and experimental dependence of the specific surface area of contact between the phases “liquid-solid” on time at different intensities of ultrasonic cavitation influence

According to the given dependences, the experimental curves are different from theoretical curves (See Fig. 5) in less than 20 %. However the difference causes by used assumptions. Thus, the model of ultrasonic cavitation dispersing is adequately.

V. CONCLUSION

Thus in a result of the work the cavitation dispersion model was proposed. It allows evaluating the optimal ultrasonic cavitation influence modes for maximum surface contact between the phases. It was found that the impact of the intensity of 10 W/cm^2 on liquid-solid suspension with viscosity 1 mPa·s (initial diameter 160 μm) causes increase the phase interface area up to the 1.95 times during 40 minutes. And at intensity 6 W/cm^2 interface area of the suspension has been increased up to 1.65 times during 40 minutes.

At greater viscosity 100 mPa·s and at initial diameter 160 μm the necessary intensity of ultrasonic cavitation influence is significantly more than at viscosity 1 mPa·s.

For liquid phase with viscosity 100 mPa·s and initial diameter 160 μm, the interface area increasing more than 1.9 times during 40 minutes is achieved at intensity 17.5 W/cm^2 and more. However, at smaller initial diameters the interface area increasing is less because reducing of breakdown neighborhood volume that causes reducing of particle breakdown probability. For example, at diameter 80 μm, liquid phase viscosity 100 mPa·s and intensity 17.5 W/cm^2 the increasing of the interface area is not exceed 1.5 even during 60 min.

Conducted experimental studies have confirmed the adequacy of the developed model. And evaluated modes of action can be recommended for the design of ultrasonic cavitation devices for dispersing.

VI. Acknowledgements

The reported study was financially supported by Russian Foundation for Basic Research (RFBR), project no. 14-08-31716 mol_a.

REFERENCES

[1] R.N. Golykh, V.N. Khmelev, and A.V. Shalunov, The study of cavitation area formation near interphase boundary for evaluation of modes providing maximum increasing of interacting substances contact interface, *Proc. VIII International conference dedicated to the 115th anniversary of academician M.A. Lavrentyev*, Novosibirsk, RU, 2015, 98. In Russian.

[2] X. Li, Y. Yang, and D. Weiss, Theoretical and experimental study on ultrasonic dispersion of nanoparticles for strengthening cast Aluminum Alloy A356, *Metallurgical Science and Technology*, *Vol. 26-2*, 2008, 12-20.

[3] J. Sidor, Mechanical layered model of a vibratory mill, *Mechanics and control*, *29 (3)*, 2010, 138-148.

[4] R N. Golykh, V.A. Nesterov, A.V. Shalunova, and E.V. Ilchenko, Theoretical Study Of The Interaction of Cavitation Bubbles With The Interface “Liquid-Gas” Determining Optimum Modes Of Ultrasonic Effect To Increase The Surface Of The Phase Contact, *AJER*, *3(12)*, 2014, 139-149.

[5] V.K. Kedrinsky, *Hydrodynamics of explosion. Experiment and models* (Novosibirsk, RU: Publisher of SB RAS, 2000). In Russian.

[6] L. Kärkkäinen, *Course of acoustics* (Helsinki, FI: Nokia Research Center).

[7] M.A. Margulis, I.M. Margulis, Dynamics of bubbles ensemble in cavitating liquid, *Physical chemistry journal*, *Vol. 81*, *12*, 2007, 2290-2295. In Russian.

[8] V.N. Khmelev, A.N. Slivin, R.V. Barsukov, S.N. Tsyganok, and A.V. Shalunov. *Application of high-intensity ultrasound in industry* (Biysk, RU: Publisher of AltSTU, 2010). In Russian.